Title

The Conformation-Activity Relationship of Soluble Guanylate Cyclase

ISBN

9798293892419

Author

Houghton, Kimberly Anne

Publication Date

2025-08-01

Peer reviewed|Thesis/dissertation

The Conformation-Activity Relationship of Soluble Guanylate Cyclase

By

Kimberly A. Houghton

A dissertation submitted in partial satisfaction of the

requirements for the degree of

Doctor of Philosophy

in

Chemistry

in the

Graduate Division

of the

University of California, Berkeley

Committee in charge:
Professor Michael A. Marletta, Chair
Professor Daniel Nomura
Professor Sabeeha Merchant

Summer 2025

The Conformation-Activity Relationship of Soluble Guanylate Cyclase

by Kimberly A. Houghton

Abstract

The Conformation-Activity Relationship of Soluble Guanylate Cyclase

by

Kimberly A. Houghton

Doctor of Philosophy in Chemistry

University of California, Berkeley

Professor Michael A. Marletta, Chair

Soluble guanylate cyclase (sGC) is a heme-containing heterodimeric protein which is a specific sensor of nitric oxide (NO). When stimulated by NO, sGC catalyzes the formation of 3',5'-cyclic guanosine monophosphate (cGMP) from guanosine 5'triphosphate (GTP). The cGMP formed by sGC serves as a secondary messenger molecule which modulates numerous physiological responses including cardiovascular regulation and neurotransmission. Disruption of the NO-sGC-cGMP signaling pathway has been implicated in numerous pathologies of the cardiovascular and pulmonary systems, leading to intense research to both better understand the physiological activation of sGC and to develop small molecule therapeutics, stimulators, capable of increasing sGC activity without increasing circulating concentrations of NO.

sGC is composed of two homologous α and β subunits. Each subunit contains an N-terminal heme nitric oxide oxygen binding (H-NOX) domain, Per/Arnt/Sim (PAS) and coiled-coil (CC) domains, and a C-terminal catalytic (CAT) domain. When no NO is bound at the heme (U), sGC has a low, basal level of activity. NO-binding to the heme (1-NO) increases the activity of the enzyme roughly five-fold. When concentrations of NO are in excess to the heme in sGC (xsNO), activity increases 100-fold above basal activity. Despite intense research, the mechanisms behind the excess NO activation of sGC remain unsolved. Recently solved full-length cryo-electron microscopy (cryo-EM) structures for sGC in the U and xsNO states have revealed that the CC domain plays a significant role in signal transduction in sGC. In the absence of NO, a short region of the CC domain in each subunit is bent, leading to an overall contracted conformation of the enzyme. In the presence of xsNO, the bent regions of the CC domains straighten, leading to an extension of the enzyme which is believed to contribute to the increased catalytic activity of sGC in the xsNO state. Additional cryo-EM structures soon revealed that small molecule stimulators, including FDA-approved Adempas®, bind sGC in regions which facilitate the straightening of the bent region of the CC domains. Thus, these cryo-EM structures provided the first evidence for a conformation-activity relationship in sGC.

Observations of conformational change in the bent regions of the CC domains of sGC led to direct interrogation of the role of the CC domains in allosteric communication in sGC. Structure-guided mutagenesis was used to engineer two CC domain variants of sGC, one with a

constitutively bent CC domain and another with a constitutively straightened CC domain. When the catalytic activities of these variant proteins were characterized, the constitutively bent protein displayed low activity even in the presence of excess NO, and the constitutively extended protein exhibited maximal activity even in the complete absence of NO. These results revealed that conformational change in the CC domains is necessary and sufficient for determining the level of sGC activity.

Initial cryo-EM structures characterizing stimulator binding to sGC were performed using stimulators which shared extensive structural similarities. A structurally unique stimulator, CYR715, was found to be a potent stimulator of wild type and βC122 variants of sGC, even in the complete absence of NO. Cryo-EM structures were solved for CYR715 bound to sGC, revealing that the stimulator bound to the same sites as previously characterized stimulators, but with additional binding interactions at crucial residues in sGC which could contribute to straightening of the CC domains in NO-free conditions. Small-angle X-ray scattering data were also collected for sGC under various activating conditions, revealing that conformational extension following ligand binding in sGC is complex and cannot be directly correlated to catalytic activity.

In excess NO conditions, sGC undergoes full conformational extension following a non-heme interaction with NO. Current data support a role for a reversible cysteine-NO adduct in the excess NO activation of sGC, but the exact site for this interaction has yet to be determined. Cysteine-labeling reagents were used to attempt to determine which cysteines could be responsible for this excess NO interaction, but these methods resulted in the labeling of a crucial catalytic cysteine in sGC. Bioinformatic approaches were used to investigate patterns of cysteine conservation across thousands of sGC sequences, revealing cysteines which could serve as the non-heme second site for the full activation of sGC by NO.

sGC is a conformationally dynamic protein, and those conformational movements result in significant changes in catalytic activity. Conformations correlating to the basal and maximal activity states have been characterized, but the conformation(s) of the intermediate activity 1-NO state have yet to be determined. How sGC samples these conformations or how these conformations might be differentially populated during activating steps is also unknown. A model for the sGC conformational landscape, built upon structural and biochemical characterizations, is necessary to answer the remaining questions regarding sGC activation by both NO and small molecule therapeutics.

TABLE OF CONTENTS

LIST OF ABBREVIATIONS

1-NO	one equivalent of nitric oxide, stoichiometric nitric oxide
5c	5-coordinate, five coordinate
6c	6-coordinate, six coordinate
AEBSF	4-(2-aminoethyl)benzenesulfonyl fluoride hydrochloride
ATP	adenosine 5'-triphosphate
BIC	n-butyl isocyanide
BLAST	Basic Local Alignment Search Tool
BSA	bovine serum albumin
Bt	*Bos taurus,* bovine
CAT	catalytic
CC	coiled-coil
Cf	*Choanoeca flexa*
cGMP	3',5'-cyclic guanosine monophosphate, cyclic guanosine monophosphate
CO	carbon monoxide
Coot	Crystallographic Object-Oriented Toolkit
cryoDRGN	Deep Reconstructing Generative Networks
Cryo-EM	cryo-electron microscopy
CV	column volume
Cα	alpha carbon
DEA NONOate	diethylammonium (Z)-1-(N,N-diethylamino)diazen-1-ium-1,2-diolate
DENSS	DENsity from Solution Scattering
DETA NONOate	(Z)-1-[N-(2-aminoethyl)-N-(2-ammonioethyl)amino]diazen-1-ium-1,2-diolate
DMSO	dimethyl sulfoxide
DTT	dithiothreitol
E. coli	*Escherichia coli*
EDRF	endothelium derived relaxing factor
EDTA	ethylene diamine tetraacetatic acid
ELISA	enzyme-linked immunosorbent assay
EM	electron microscopy
EMDB	Electron Microscopy Data Bank (https://www.ebi.ac.uk/emdb/)
EPR	electron paramagnetic resonance
GpCpp	guanosine-5'-[(α,β)-methyleno]triphosphate
GTP	guanosine 5'-triphosphate
H/D	hydrogen/deuterium
HDX-MS	hydrogen/deuterium exchange mass spectrometry
HEPES	4-(2-hydroxyethyl)piperazine-1-ethanesulfonic acid
HNOB	heme nitric oxide binding
H-NOX	heme nitric oxide oxygen binding

Hs	*Homo sapiens*, human
IAM	iodoacetamide
LN2	liquid nitrogen
MMTS	*S*-methyl methanethiosulfonate
Ms	*Manduca sexta*, tobacco hawk moth
MS	mass spectrometer, mass spectrometry
MWCO	molecular weight cut off
NO	nitric oxide
NU	non-uniform refinement
O_2	oxygen
P(r)	pair distance function
PAS	Per/Arnt/Sim
PCR	polymerase chain reaction
PDB	Protein Data Bank (http://www.rcsb.org/)
PROLI NONOate	1-(hydroxy-NNO-azoxy)-L-proline
R_g	radius of gyration
Rn	*Rattus norvegicus*, rat
RNR	ribonucleotide reductase
ROS	reactive oxygen species
SAXS	small-angle X-ray scattering
SDS-PAGE	sodium dodecyl sulfate polyacrylamide gel electrophoresis
Sf9	*Spodoptera frugiperda* clonal isolate
sGC	soluble guanylate cyclase
So	*Shewanella oneidensis*
SONO	sensor of nitric oxide
SSN	sequence similarity network
TEA	triethanolamine
TFA	trifluoroacetic acid
U	unliganded, nitric oxide-free, 5-coordinate His-Fe heme
UV-Vis	ultraviolet visible
WT	wild type
xsNO	excess nitric oxide, stoichiometric excess nitric oxide

LIST OF FIGURES

LIST OF TABLES

ACKNOWLEDGEMENTS

Science is a collaborative process, where many minds make progress in addressing the world's numerous unsolved problems. The making of a scientist is likewise a community effort.

I would like to thank Michael A. Marletta, my principal investigator and mentor during my PhD at Berkeley. Your understanding of biochemistry is vast, and it has been an absolute honor to learn and complete my PhD under your guidance. Truth be told, sGCs and PMOs did not spark any fires of scientific interest while I was choosing rotation labs, but hearing the stories you told about your research during the ChemBio Supergroup and Chem271 both ignited and stoked a desire to work on such an… obstinate… research question. You are a consummate storyteller, weaving research narratives that make the audience stay engaged – all the way through to the last page of their PhD dissertation.

But above all, you have been exceedingly patient and compassionate. COVID introduced significant disruptions to my ability to work and progress on multiple facets of my project simultaneously. In an act of compassion I will never be able to fully articulate, you allowed me to stay in your lab while I spent 18 months recovering from a TBI that, in all honesty, should have marked the end of my PhD. But you believed in me, and you allowed me to focus on my recovery and rehabilitation so I could eventually return to lab and resume my projects. It took longer than both of us wanted, but as I stand at the finish line of my PhD (and at the starting line of my next career), I know that I am here because you never gave up on me.

To the members of the Marletta Lab, past and present, thank you for sharing your experiences and perspectives, both personal and scientific, over these many years. To those who were PhD students alongside me – Allie Batka, Dr. Ben Guthrie, Dr. Tyler Detomasi, and Dr. Yang Wu – growing and learning together has been a pleasure. To the amazing postdocs – Dr. John Hangasky III, Dr. Christopher Lemon, Dr. Elizabeth Wittenborn, Dr. Richard Sayler, Dr. Alejandra Martinez, and Dr. William Thomas – thank you for your guidance, mentorship, and training in areas involving both theory and practice. To our undergrads – Skylar Henry, Molly Hydorn, Dr. Ericka Wirachman, Emma McRae, Deirdre Hanley, Lulu Wu, Kristian Bolanos Ibarra, Chinoros Ruttanasupagid, Alexander Rose, Zachary Green, Lillian Hiraoka, Tracy Lian, and Aneesh Bhat – you all are the creative, chaotic forces that keep lab interesting and keep the rest of us on our toes and on our best behavior.

I would like to thank the members of my qualifying and dissertation committees: Prof. Michelle Chang, Prof. Alanna Schepartz, Prof. Dan Nomura, and Prof. Sabeeha Merchant. No one really wanted to hold or go through a qualifying exam over Zoom, but the guidance and advice (overwhelming at the time) that you all provided during my exam proved valuable throughout many points during my PhD.

I would also like to thank Prof. Anne Baranger, PI of the Chemical Education research group (and Interim Dean of the College of Chemistry) for her mentorship and invitation to participate in her ChemEd Supergroup. Weekly meetings to learn and discuss ongoing research into student learning and best practices were a welcome distraction from my own experimental failures and confusing data. To the members of the ChemEd Supergroup, thank you for sharing your data, experiences, and conclusions with me. I will be a better educator because of your work.

I would like to thank the lecturing faculty in the College of Chemistry with whom I have worked or studied alongside: Dr. MaryAnn Robak, Dr. Michelle Douskey, Dr. Pete Marsden, Dr. Katie Blackford, and Dr. Alexis Shusterman. You all bring a level of excellence to the teaching mission of UC Berkeley, and your contributions to undergraduate education cannot be overstated. Thank you for the years of mentorship and friendship you have provided and be warned that I will likely be asking for copies of your lesson plans soon!

To my many mentors at San Jose State University – thank you for your guidance and advice over the years. To Dr. Annalise Van Wyngarden, my first PI, thank you for encouraging me to think bigger than the small goals I had for myself. Thank you for being that first, strong woman in science that I could gravitate towards and draw inspiration from to eventually dare believe in myself. To Dr. Karen Singmaster, thank you for throwing so many teaching opportunities in my direction as an undergrad. To Drs. Ningkun Wang and Madalyn Radlauer, thank you for your emotional and psychological support as I set off for grad school as an older, married student. Your advice was invaluable to help me establish routines that would protect both myself and my marriage. I will see you all again in the Fall!

Thank you to the Stanley Hall administration and staff who have made my time in Stanley Hall safe, clean, and well air-conditioned. Thanks to Cherry Chung for your tireless efforts to keep Stanley Hall functioning despite deferred maintenance and budget cuts. Thanks to Thom Opal for coordinating building chemical and workplace safety. Thanks to Kris Thompson for your general "I can get that done" attitude and always knowing how to fix a problem. Thanks to Mike Bentley and Emily Rodriguez for your immense support behind the scenes.

I would also like to thank the many medical professionals who worked with me during my rehabilitation and recovery from my TBI. To Dr. Karen Kaufman, you provided psychological support and cognitive bandwidth when I had none. You helped track the progress of my recovery, reminding me that small setbacks were temporary while keeping me focused on my larger trajectory. You helped me learn how to speak again. To Dr. Jennifer Fisher and the other staff at the Sports Vision Clinic, you led me through hundreds of hours of pencil pushups, prism dips, and saccades exercises to retrain one part of my brain on how to interpret the data coming in from the other parts of my brain. You helped me learn how to see and read again. To Dr. Selena Ellis, you believed me when I told you how certain cognitive tasks caused migraines that crippled me with their intensity. You helped me navigate the onerous process of trying all the medications that did not work so we could get insurance to finally pay for the ones that did work. You helped my brain

work pain-free again. To Marcela Larrondo, when my brain decided that the straight hallways of Stanely Hall were spinning tunnels inside a fall festival fun house, you showed me exercises and grounding techniques that would override the bad sensory data coming from my vestibular system. You helped me to walk again.

To Nathan, my husband and chosen life partner, thank you for putting up with… whatever the last ten years have been. Our lives were turned upside-down when we moved to California, and I have been in school every season and semester since. You have supported me and my ever-changing ambitions throughout this entire journey, and I never could have made it without you by my side. I apologize that, when all is said and done, I will still be in school (though at least at the front of the class now). I look forward to us growing even older together, and I hope that you do not have too much fun when mail eventually starts arriving for Dr. and Mrs. Houghton.

To our "fur babies" Annie and Klaus – you two are the best listeners one could ask for. Whether I was practicing a lesson plan or presentation for the first or fifth time, you always looked at me with the same, thoroughly dumbfounded look during each attempt. You both greet me when I return at the end of the day and keep me on track with the various meals, treats, and medicines you need to keep yourselves happy and healthy. I know that you both understand that finishing this degree will not make me any smarter, and I will always be the dumb human that never understands what you are saying.

Chapter 1

Introduction

Summary

Soluble guanylate cyclase (sGC) is a heme-containing biological sensor of diatomic gases which increases its catalytic formation of cyclic guanosine monophosphate (cGMP) in response to ligand binding. cGMP then serves as a secondary messenger molecule which participates in various physiological responses including cardiovascular regulation and neurotransmission. In humans, sGC is an exquisitely sensitive and specific receptor of nitric oxide (NO), capable of selectively responding to NO at non-toxic concentrations. In response to NO binding, sGC undergoes significant conformational change, with concentrations of NO in stoichiometric excess to the heme in sGC leading to an extension of the enzyme into a maximally active conformation. This chapter discusses the activation of sGC in response to gaseous ligands as well as small molecule therapeutic agents which work to increase sGC activity in the presence or absence of endogenous NO.

Introduction

Nitric oxide (NO) is a small, membrane diffusible diatomic gas which participates in host response to infection and as an endogenous signaling molecule within animals.[1–6] As part of the innate immune system, NO, often in conjunction with reactive oxygen species, exerts toxic effects which facilitate antibacterial, antifungal, and anti-cancer responses.[4,6–8] As an endogenous signaling molecule, NO leads to vasodilation, decreases platelet aggregation, regulates mitochondrial respiration, and contributes to neuronal excitability, processing, and plasticity.[9–13] The vasodilatory role of NO, as the previously termed Endothelium-Derived Relaxing Factor, was only well-characterized in the 1980s; and other physiological roles for NO are still being discovered. Continuing research has implicated NO signaling in insect development,[14] while dysregulation in NO-signaling has been implicated in human pathologies such as primary ciliary dyskinesia, cancer proliferation, and a wide range of cardiovascular diseases.[15–17]

Soluble guanylate cyclases (sGCs) are physiological sensors for gaseous ligands such as NO and oxygen (O_2). In mammals, sGCs are exquisitely specific and sensitive sensors for NO which play a central role in NO-signaling. sGC catalyzes the cyclization of guanosine 5'-triphosphate (GTP) into guanosine 3',5'-cyclic monophosphate (cGMP).[18] In the presence of stoichiometric excess NO, sGC increases catalytic activity by over one hundredfold, amplifying and converting the potentially toxic NO signal into the ubiquitous secondary messenger cGMP.[18,19] Despite decades of intense study, the molecular interactions leading to the stimulation of sGC activity by NO in the maximally active state are still poorly understood.

Significant research and therapeutic efforts have been dedicated to targeting pathologies related to dysregulation of NO-signaling. Conditions such as glaucoma or neonate hypertension can be treated through supplementation of NO or NO donors[20–22], while treatments for cardiovascular diseases such as hypertension and heart failure have utilized a different therapeutic

approach by directly targeting the activity of sGC. One class of therapeutics, known as sGC stimulators, works cooperatively with endogenous NO to increase sGC function to maximum activity. Two such compounds have received FDA approval: riociguat (Adempas®, 2013)[23–25] and vericiguat (VERQUVO®, 2021).[26,27] Recent research has revealed the mechanism of sGC activation by these small molecule stimulators[28,29], providing an opportunity for rational design of targeted, potent sGC therapeutics.

This chapter will introduce the high-level organization of sGC structure, discuss sGC activation by varying concentrations of NO and therapeutic ligands, and explore the conformational changes observed in sGC when physiological or therapeutic ligands are present.

Soluble Guanylate Cyclase Structure

Soluble guanylate cyclases are dimeric proteins with domain architecture which is well-conserved across a wide variety of organisms. While recent research has investigated homodimeric sGCs from algal or colonial organisms[30,31], the most well-studied sGCs are from mammals and insects and are obligate heterodimeric proteins composed of an α and β subunit (Figure 1.1). The most prevalent human sGC isoform is formed from an $\alpha_1\beta_1$ heterodimer.[32] Each subunit of sGC contains the same high level domain architecture: a heme nitric oxide oxygen binding (H-NOX[33,34]) domain, a signal transduction region composed of Per/Arnt/Sim (PAS) and coiled-coil (CC) domains[28,35], and one subunit of the obligate heterodimeric catalytic domain (CAT).[36]

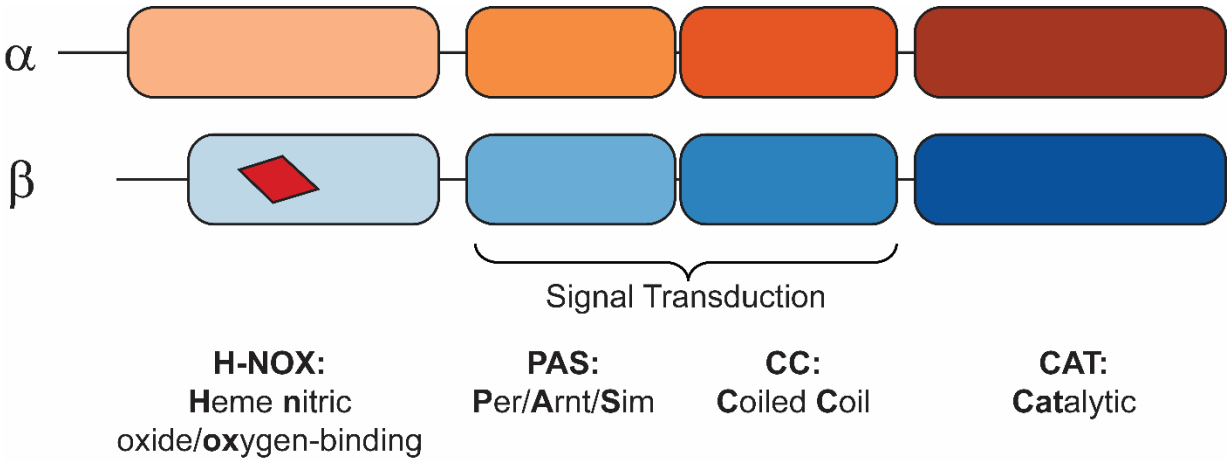

Figure 1.1. Domain architecture of a canonical α/β-type sGC. Domains of the α (orange) and β (blue) subunits share the same global domain organization: a heme nitric oxide/oxygen-binding (H-NOX) domain, a signal transduction region consisting of the Per/Arnt/Sim (PAS) and coiled-coil (CC) domains, and a catalytic (CAT) domain. Heme, which binds to βH105, is indicated by the red rhombus. Figure adapted from ref[37].

Each subunit features an N-terminal regulatory H-NOX domain, also known as heme nitric oxide binding (HNOB[38]) or sensor of nitric oxide (SONO[39]) domains. H-NOX domains are formed from an N-terminal region containing seven α-helices and a C-terminal region consisting of a four-stranded anti-parallel beta sheet. These secondary structures form a central pocket capable of binding a single heme cofactor. This pocket is further divided into distal and proximal sides, with the proximal side containing the heme-ligating histidine located on the αF helix. Although

homology analysis predicts both subunits capable of heme binding, only the β subunit binds heme in the full-length sGC α/β-type heterodimer.[34] Heme binding in α/β-type sGCs is thought to be facilitated via several unique features of the β subunit (Figure 1.2A). First, a highly conserved histidine binds reduced heme, forming a 5-coordinate (5c) His-Fe^{2+} complex.[40,41] Second, the β subunit contains a heme-stabilizing YxSxR motif in which tyrosine, serine, and arginine residues are positioned to facilitate hydrogen bonding to the propionate chains of the heme cofactor (Figure 1.2B).[42] These heme-binding features are not universally conserved within the α subunit of α/β-type sGCs. Gaseous ligand discrimination arises from the identity of an amino acid in the distal heme-binding pocket: NO-binding H-NOX domains contain an aliphatic amino acid, frequently isoleucine, at this position, while oxygen-binding H-NOX domains possess a tyrosine which can stabilize an O_2 adduct via hydrogen bonding.[33,42] Ligand binding at the heme can be characterized using ultra violet visible (UV-Vis) spectroscopy to observe shifts in the Soret band absorbance for heme in various ligation and coordination states (Figure 1.2C). Recently solved cryo-electron microscopy (cryo-EM) structures for full-length *Homo sapiens* (*Hs*, human)[29,35,43] and *Manduca sexta* (*Ms*, tobacco hawk moth)[37] sGCs have suggested a structural contribution to the lack of heme binding by the α subunit. The α subunit contains a large N-terminal extension relative to the β subunit, and while much of this region is disordered, a portion of this extension (α69 – 84, *Hs* sGC) passes through the putative heme-binding pocket of the α subunit, preventing heme access (Figure 1.2A).[44]

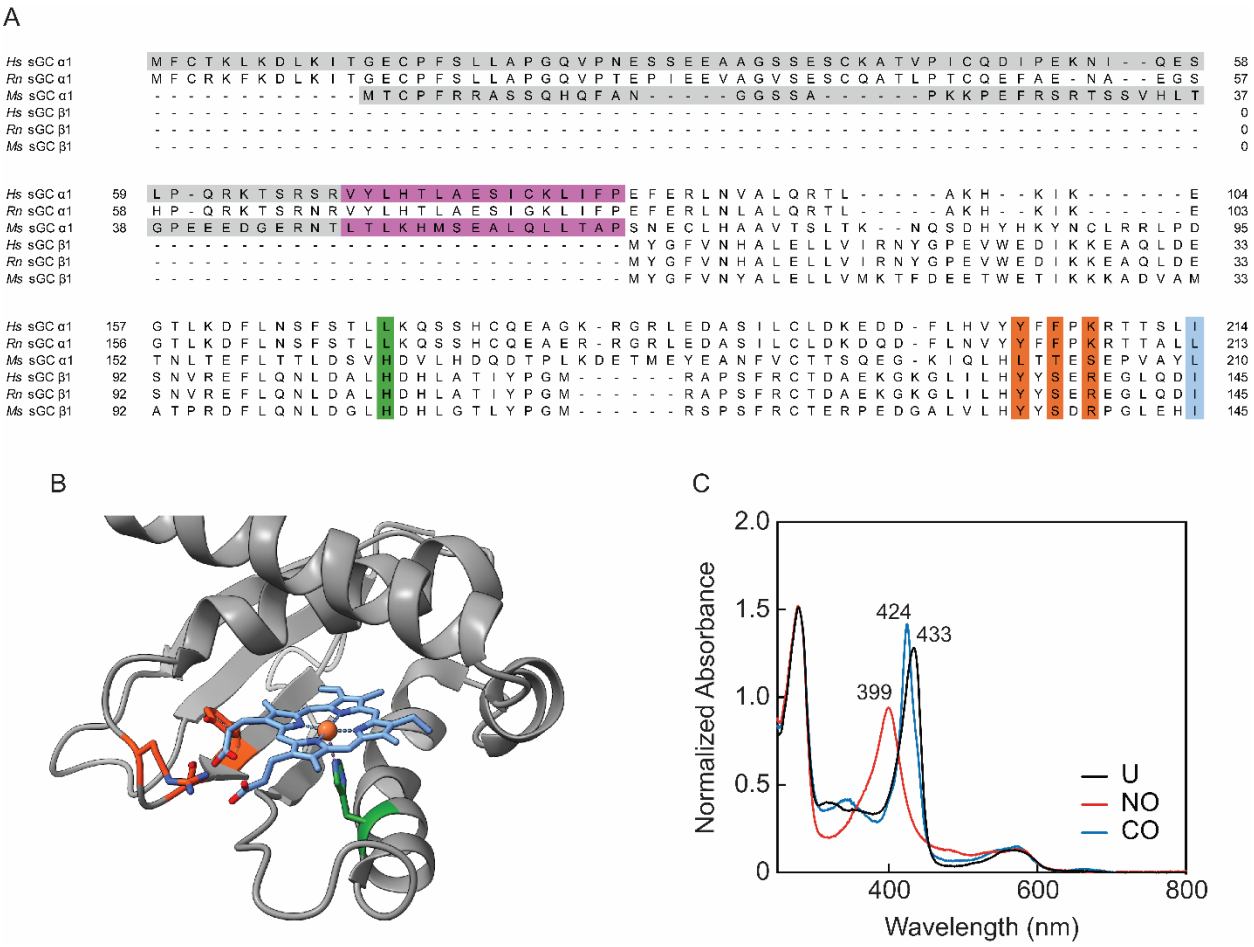

Figure 1.2. Characteristics of H-NOX domains in sGC. (A) Sequence alignments of the H-NOX domains of the α and β subunits of three α/β-type sGCs: human (*Hs*), brown rat (*Rn*) and moth (*Ms*). The disordered N-terminal extensions observed in the solved structures of *Hs* and *Ms* sGC are highlighted in gray, and the region responsible for precluding heme binding in the α subunit is highlighted in purple. The heme-binding histidine at βH105 is highlighted in green. Residues of the YxSxR motif are shown in orange. The ligand discriminating residue at β145 is highlighted in blue. Figure adapted from refs[42,44]. (B) Structure of the β H-NOX domain of *Hs* sGC (PDB 8HBE[43]). The heme is shown in blue, the heme-ligating residue βH105 is shown in green, and the residues composing the YxSxR motif (βY135, S137, and R139) are shown in orange. (C) UV-vis characterization of heme Soret absorbance following gaseous ligand binding in *Ms* sGC, an NO-sensitive sGC. When no ligands are bound at the heme (U, black), the Soret maximum is observed at 433 nm. Nitric oxide (NO) binding to the heme (NO, red) shifts the Soret maximum to 399 nm. Carbon monoxide (CO) binding to the heme (CO, blue) shifts the Soret maximum to 424 nm. Figure adapted from ref[30].

Signal transduction occurs via the PAS and CC domains. PAS domains, a ubiquitous motif found throughout many domains of life, perform a variety of physiological functions. PAS domains have been implicated in ligand binding, signal transduction, and formation and stabilization of quaternary structure.[45–47] Studies on PAS domains within sGCs have shown PAS domain involvement in Hsp90-mediated heme insertion[48], dimerization[34], and gas ligand binding.[49] The CC domains of sGC are C-terminal to the PAS domains and undergo significant conformational change to facilitate signal transduction from the regulatory H-NOX domains to the effector CAT domains.[46] Prior to solved cryo-EM structures, studies of the PAS and CC domains of *Rattus norvegicus* (*Rn*) sGC using hydrogen/deuterium exchange mass spectrometry (HDX-MS) showed

significant changes in rates of H/D exchange following the addition of NO, suggesting significant conformational changes in this region as a result of NO-induced activation (Figure 1.3).[50]

Figure 1.3. Changes in H/D exchange rates in full-length brown rat (*Rn*) $\alpha_1\beta_1$ sGC following the addition of NO. Sequence regions corresponding to the PAS and CC domains are shown in gray. Regions found to undergo increased H/D exchange after NO addition are shown in orange, while regions undergoing decreased H/D exchange upon NO addition are shown in blue. Figure adapted from ref[50].

The CAT domains of sGC belong to the Class III nucleotide cyclase domain family which contains both adenylyl and guanylyl cyclases.[36,51,52] The CAT domains of sGC form a heterodimer which contains a non-catalytically active pseudosymmetric site and a catalytically competent active site. The pseudosymmetric site is proposed to be involved in inhibition of sGC activity by ATP.[53–55] Purine nucleotide discrimination for GTP in sGCs is conferred by highly conserved glutamate and cysteine residues (βE473 and βC541, *Hs* sGC) in the catalytic pocket which stabilize the guanine ring.[36,56]

Activation and Activity States of Soluble Guanylate Cyclase

Understanding of the steps of sGC activation by NO and other ligands (Figure 1.4) has advanced significantly over decades of intense and sometimes contentious[57,58] study. These studies have led to the development a model where sGC demonstrates “three state activity” or a “two-step activation profile” in response to its physiological ligand, NO. When NO is absent (U), the enzyme has a low level of basal activity. When excess NO (xsNO) is present, the enzyme has a high, maximal level of activity. Addition of one stoichiometric equivalent of NO relative to the heme (1-NO) increases enzyme activity to ~15% of maximal activity. Small molecules targeting sGC signaling for therapeutic benefit interact with either heme-free sGC or stimulate the 1-NO form of the enzyme resulting in increased sGC catalytic function.

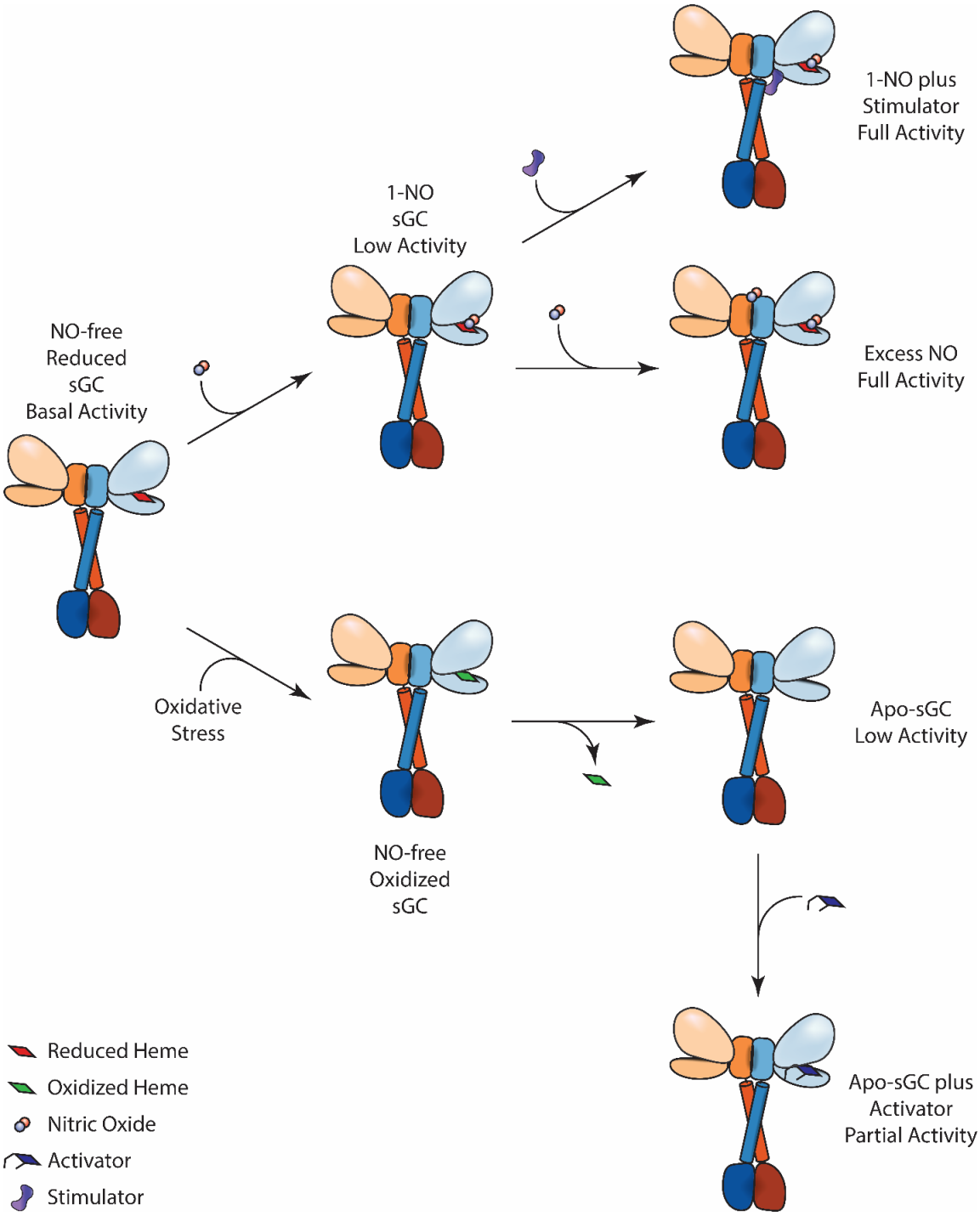

Figure 1.4. Scheme for the characterized physiological and therapeutic activation conditions for sGC. When in the NO-free state, sGC exhibits a basal level of activity. Addition of stoichiometric NO increases sGC activity to partial activity, and additional NO brings the enzyme to full activity. Alternatively, stimulators can be added to 1-NO sGC to increase activity of the 1-NO enzyme to the maximum state. Conditions of oxidative stress can oxidize the heme of sGC which then dissociates from the enzyme, leading to the formation of apo-sGC. Activators can then bind to the empty heme-binding pocket of apo-sGC, restoring partial activity to the enzyme.

Activation of sGC by NO-binding at the Heme

Initial characterizations of sGC activity and activation led to a simple NO-binding model which proposed that sGC could be fully activated by the addition of stoichiometric NO to the heme.[59–61] In this model, NO binds to the distal side of the initial 5c His-Fe^{2+} complex leading to the formation of a short-lived 6-coordinate (6c) complex[19,57,62,63] which quickly forms a 5c Fe^{2+}-NO complex following rupture of the Fe^{2+}-His bond via the strong σ trans effect of the NO ligand.[64] Rupture of the His-Fe^{2+} bond was thought to be the only step required to fully activate the enzyme.[19,59,61] However, early biochemical experiments characterizing sGC activity were performed using sGC isolated from animal tissue which had been expressed under physiological NO concentrations. Studies have determined that *in vivo* concentrations of NO under physiological signaling conditions range from 20 pM to 5 nM[65–70], which is several orders of magnitude higher than the dissociation constant for NO bound to heme in the H-NOX domain of sGC (K_d < 1.2 x 10^{-12} M).[62] Given these values, it is likely that sGC expressed or assayed under normal physiological conditions likely exists in the NO-bound state, and assays which add NO to proteins purified under these conditions are characterizing sGC in a state with a stoichiometric excess of NO.

The first studies suggesting a more complex process for the activation of sGC by NO came via spectrographic studies investigating the kinetics of Fe^{2+}-NO complex formation using heterologously expressed sGC which could be purified without NO bound at the heme. These investigations found that the presence of a stoichiometric excess of NO resulted in enhanced rates of His-Fe^{2+} bond rupture of the transient 6c His-Fe^{2+}-NO complex formed upon NO binding to heme (Figure 1.5).[57,71,62] Biochemical evidence for full sGC activity requiring stoichiometric excess NO soon followed. Studies of sGC using clamped NO concentrations revealed that sGC is fully activated by NO at nM concentrations, while the concentration-response curves for NO on sGC best fit a Hill Coefficient of 2.1, suggesting that cooperative binding of more than one molecule of NO is required for full sGC activation.[72]

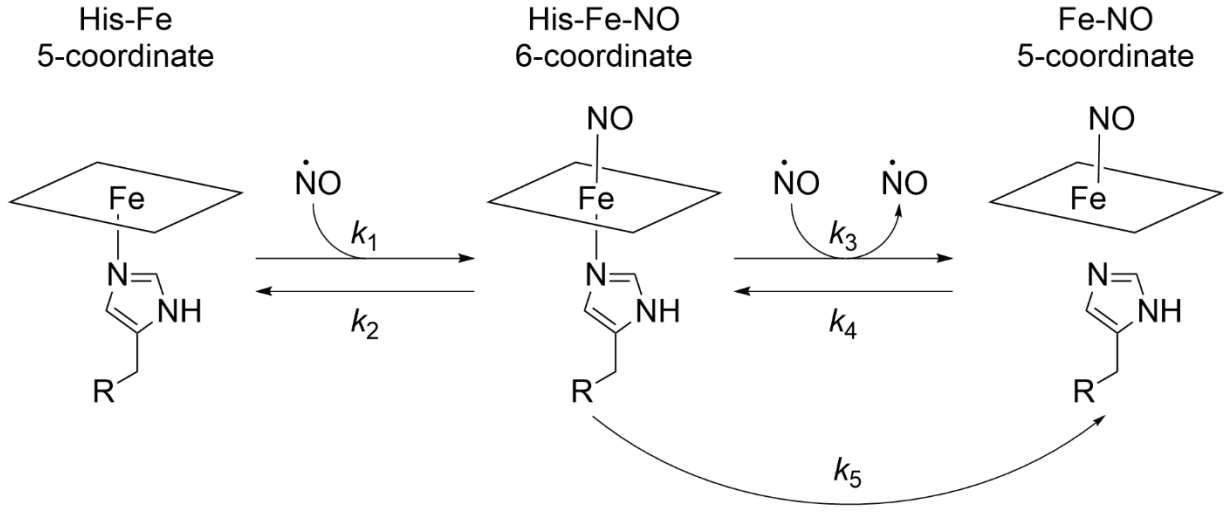

Figure 1.5. Schematic depicting NO binding and His-Fe^{2+} bond rupture in sGC. NO first binds to the 5c His-Fe^{2+} complex with k_1 > 1.4 x 10^8 $M^{-1}s^{-1}$. The resulting 6c complex can then rupture to the 5c Fe^{2+}-NO complex via two

pathways: one dependent on stoichiometric excess NO with $k_3 = 2.4 \times 10^5$ $M^{-1}s^{-1}$ and another independent of additional NO at the much slower $k_5 = 0.0087$ s^{-1}.[62] Figure adapted from ref[57].

Additional support for this hypothesis was obtained via direct interrogation of the activity of sGC at substoichiometric and stoichiometric excess NO concentrations. Researchers found that incubation of NO-free sGC with substoichiometric NO, or removal of excess non-heme NO via gel filtration, resulted in the formation of an intermediate activity state for sGC above that of the NO-free enzyme and well below that of the fully activated enzyme.[73] Additionally, it was found that while heme occupancy by NO trended linearly with %NO saturation, NO-stimulated activity of sGC deviated strongly from linearity with 70% NO saturation only yielding 20% of maximal activity. Additional experiments studying the deactivation of sGC from maximal activity using NO scavengers found that maximally active sGC deactivates to the intermediate activity state over 150 times faster than the rate of NO dissociation from heme, suggesting that sGC deactivation to the intermediate activity state is not due to NO loss at the heme.[53] Together, these results suggest that full sGC activation by NO requires a second site NO interaction.

Activation of sGC by Excess NO

Two mechanisms have been proposed for the activation of sGC in the presence of excess NO. The first involves a second addition of NO to the proximal side of the heme yielding a transient heme-dinitrosyl species which ultimately converts to a 5c proximal NO-Fe^{2+} species. Crystallography[74] and rapid freeze quench electron paramagnetic resonance (EPR)[75] experiments revealed that NO, when in vast stoichiometric excess, could bind to the proximal side of the heme in isolated H-NOX domains and sGCs, respectively. The proximal NO-Fe^{2+} hypothesis was examined via several experiments. Researchers probed whether formation of a proximal NO-ligand on the heme was necessary for full activity by using n-butyl isocyanide (BIC) as a distal ligand for the heme in sGC.[76] BIC binding forms a stable 6c His-Fe^{2+}-BIC complex which can be monitored via UV-Vis spectroscopy and persists even in the presence of excess NO. In the absence of NO, BIC binding stimulated *Rn* sGC activity 5-fold while the addition of excess NO stimulated BIC-sGC an additional 16-fold without the formation of a 5c NO-Fe^{2+} complex, indicating that formation of a proximal NO species was not necessary for the maximal activity observed in the presence of excess NO. Further experiments utilized double electron-electron resonance EPR spectroscopy to differentiate between distal and proximal heme-NO complexes in sGC. This study revealed that, in both substoichiometric and excess NO conditions, the distal 5c Fe^{2+}-NO complex was the major species formed; and following the removal of excess NO, only the distal 5c Fe^{2+}-NO complex was observed.[77] Together, these results support the hypothesis that proximal NO binding is not relevant to physiological sGC activation.

The second proposed mechanism for sGC activation by excess NO involves a non-heme interaction. Gas sensing proteins can interact with ligands via non-heme metal centers and hydrophobic binding pockets or tunnels.[78–80] However, sGC contains no metal centers other than the heme, and diatomic gasses which can access the same tunnels and binding pockets as NO, such as O_2, carbon monoxide (CO), or dinitrogen, do not fully activate sGC.[19,81,82] Consequently, the interactions necessary to fully stimulate sGC activity must occur at sites which are specific for NO. Protein and NO interactions via cysteine modification are well-established in biology and

serve to facilitate signaling and modulate enzyme function.[83–88] These interactions can form covalent additions of NO via oxidative addition, or reversible adducts via nucleophilic addition to form a transient RSNO●⁻ species. An important consideration for sGC, however, is that NO can activate sGC in anaerobic conditions, without the presence of any oxidant capable of performing a one-electron oxidation to form a covalent *S*-nitrosocysteine species.[89] Additionally, NO-activated sGC deactivates within seconds once excess NO is removed via gel filtration[62], while the half-life of *S*-nitrosocysteine is measured on the order of hours.[90] This suggests that if NO is interacting with sGC via a cysteine adduct, that interaction is most likely forming a transient, rapidly reversible RSNO●⁻ species.

Studies began to explore the possibility that the second site activation of sGC by NO occurs via a cysteine-NO interaction. Researchers labeled *Rn* sGC with *S*-methyl methanethiosulfonate (MMTS), a small hydrophobic molecule capable of reversibly transferring an *S*-methyl to thiols (Figure 1.6). When characterizing the activity of MMTS-labeled sGC, researchers found that even in the presence of excess NO, the enzyme could only reach ~15% of maximal activity, which is comparable to the activity of unlabeled sGC in the presence of stoichiometric NO.[89] When the *S*-methyl label was removed by the addition of the reducing agent dithiothreitol (DTT), the protein was again able to reach full activity following the addition of excess NO. Researchers also determined that MMTS labeling did not alter the basal (U) activity of the enzyme, did not impact NO binding at the heme, and did not fully restrict conformational flexibility of the enzyme.

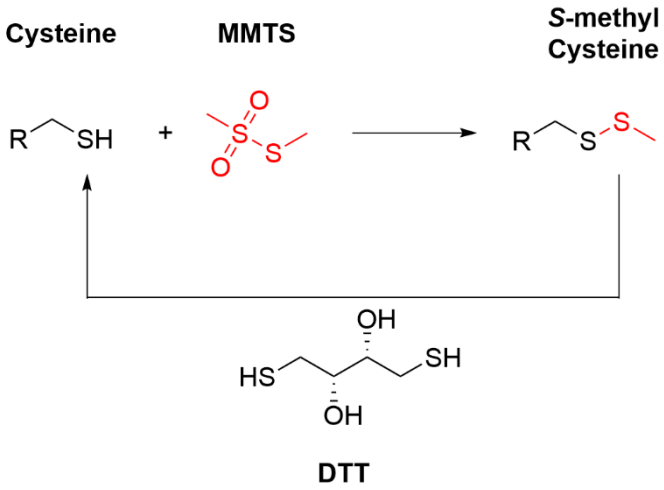

Figure 1.6. Schematic for MMTS labeling of sGC using MMTS. Upon reaction with a cysteine in sGC, MMTS transfers an *S*-methyl to the cysteine, forming a disulfide bond. This bond is easily reversible by the addition of reducing agents such as DTT which regenerate the starting thiol.

Taken together, characterizations of sGC treated either with BIC to prohibit NO addition to the proximal side of the heme or with MMTS to prevent the formation of a cysteine-NO intermediate build a compelling argument that full sGC activation occurs at a non-heme site via interaction with at least one cysteine in sGC. However, despite intense efforts, the cysteine(s) involved in the secondary site interactions necessary for full activation of sGC by NO remain unidentified.

Therapeutic Targeting of sGC Activity

The therapeutic potential for treating NO-signaling pathologies by modulating sGC activity has driven research to develop small molecules capable of increasing sGC activity. As previously discussed, under normal physiological conditions, sGC is expected to be in the 1-NO state with NO bound to the heme. Many cardiovascular diseases, however, contribute to oxidative stress[91], leading to oxidation of the heme iron culminating in the loss of heme from sGC and generating heme-free or apo-sGC which is insensitive to NO.[92–95] Other diseases lead to decreased NO biosynthesis[15,17,96,97] contributing to low physiological concentrations of NO. Small molecules, known as activators and stimulators, have been developed which act upon apo-sGC or 1-NO sGC, respectively, to increase cGMP formation *in vivo*.

Activators are heme-independent small molecule effectors of sGC activity that interact with sGC which has either undergone oxidation at the heme site or has lost the heme cofactor completely.[98,99] While no activators have received FDA approval, the best characterized sGC activator is Bayer's BAY 58-2667 (cinaciguat), a small molecule which features two carboxylic acids which branch off from a conformationally flexible tail (Figure 1.7A). sGC containing ferric heme loses its cofactor more readily than the ferrous form of the enzyme[100,101], and cinaciguat is able to both facilitate the loss of ferric heme and bind to the empty heme binding pocket of apo-sGC via interactions between its carboxylic acid moieties and the YxSxR motif.[101–103] While apo-sGC has been shown to exhibit some activity *in vitro*[104–106], it is rapidly targeted for ubiquitination and degradation *in vivo.*[107] Activator binding to apo-sGC confers protection against this biodegradation.[105] Activator-bound sGC exhibits a partial level of activity, and remains insensitive to NO.[98,103,108] Thus, activators such as cinaciguat rescue apo-sGC activity in two ways: activity is increased via the binding of the activator to the heme pocket, and degradation is inhibited ensuring that concentrations of sGC are not depleted.

Stimulators are heme-dependent small molecules which increase sGC activity in a manner dependent on the concentration of NO present.[98,109,110] When endogenous NO concentrations are low and sGC is in the reduced but NO-free state, stimulators increase the activity of sGC to approximately that of the 1-NO state.[28,98,99] When physiological concentrations of NO are sufficient for sGC to be in the 1-NO state, stimulators increase sGC activity to maximal activity.[28,29,98,99] YC-1, a benzylindazol derivative (Figure 1.7B), was the first discovered stimulator of sGC[111], however this compound was only weakly stimulating and not specific for sGC, precluding use as a therapeutic.[98,110] Subsequent optimization screens for improved sGC stimulators used YC-1 as the lead structure, culminating in a diverse array of small molecules featuring fused ring systems at the core of the molecule.[109] Two such derivative compounds have received FDA approval for the treatment of sGC-related pathologies: Bayer's riociguat (Adempas®) in 2013 for the treatment of pulmonary arterial hypertension and chronic thromboembolic pulmonary hypertension[23,25,112], and vericiguat (VERQUVO®) in 2021 for the treatment of heart failure with reduced ejection fraction.[26,27,113] These two molecules share much of their structure, with several modifications in vericiguat which significantly increase the half-life of the compound *in vivo* (Figure 1.7B). The structural details of how these stimulators interact with sGC to increase activity will be discussed in the following section.

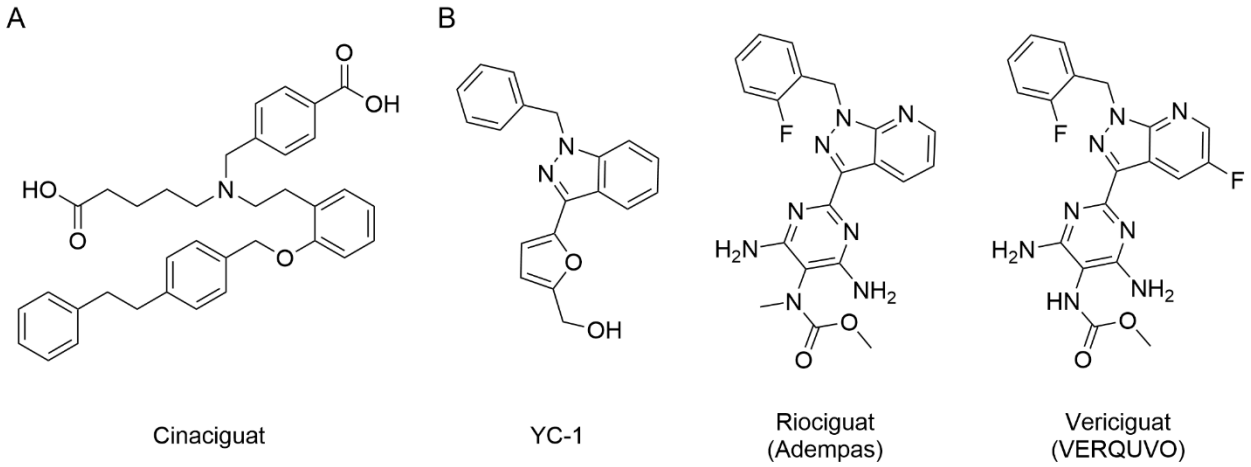

Figure 1.7. Chemical structures for small molecule sGC therapeutics. (A) Structure of sGC activator cinaciguat. (B) Structures of sGC stimulators YC-1, riociguat, and vericiguat.

Activation and Conformational Change in Soluble Guanylate Cyclase

The first steps of sGC activation by NO occur at the heme.[19,62,63] The earliest models of NO-binding and activation of sGCs were obtained through the study and characterization of isolated H-NOX proteins expressed by prokaryotic organisms.[38,102,103,114,115] In solved crystal structures of an H-NOX protein from *Shewanella oneidensis* (*So*)[74], rupture of the Fe^{2+}-His bond leads to significant perturbation of the αF helix, leading to a ~2 Å lateral shift of the Cα atom of the heme-ligating histidine as well as a change in rotamer conformation resulting in an apparent 90° rotation of the heme-ligating histidine between the NO-free and NO-bound states.[44] This conformational change has been hypothesized as a crucial component of signal transduction following NO binding in sGC (Figure 1.8A).[74]

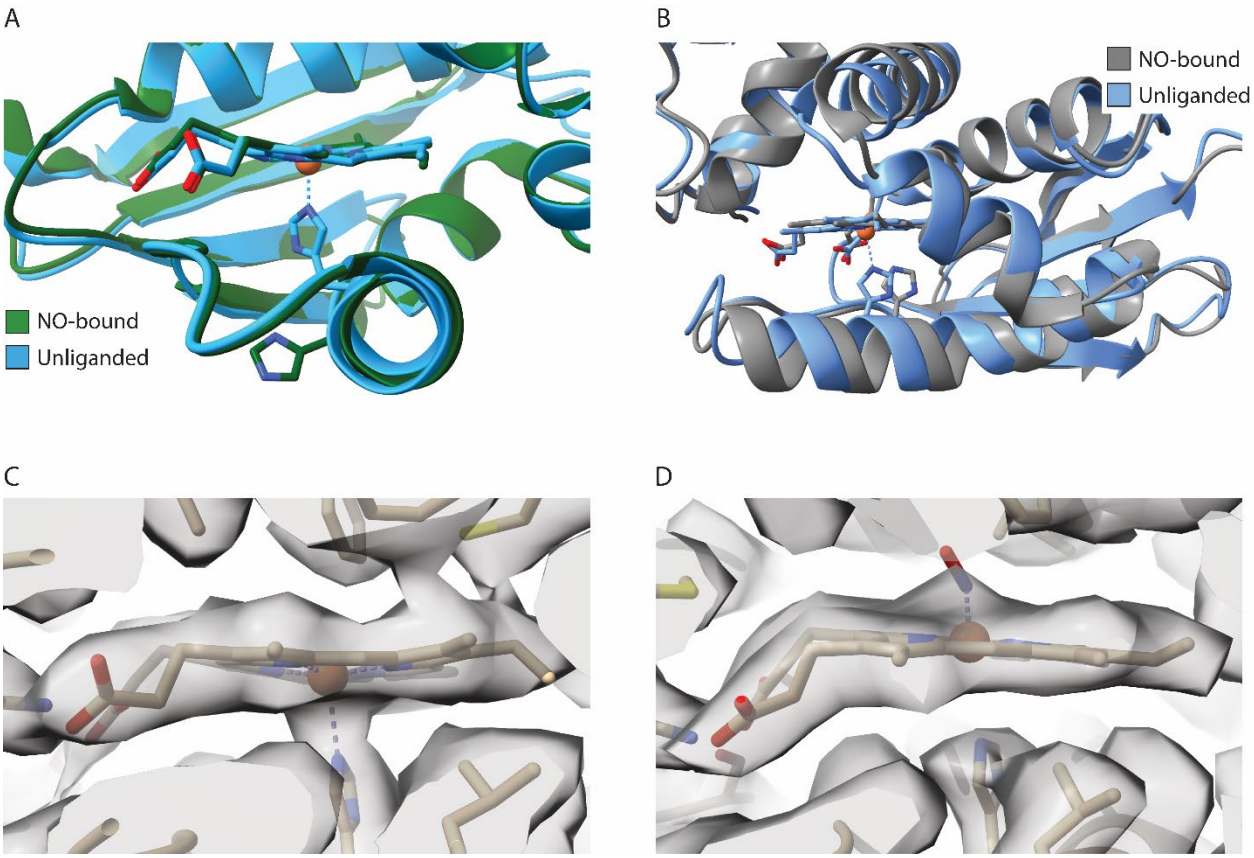

Figure 1.8. NO binding in isolated H-NOX domains and full-length sGCs. (A) Aligned structures of *So* H-NOX in the unliganded (blue, PDB ID 4U99[74]) and NO-bound (green, PDB ID 4U9B[74]) states. NO binding ruptures the His-Fe^{2+} bond, leading to a lateral shift and apparent 90° rotation of the heme-ligating histidine. (B) Aligned structures of *Hs* sGC in the unliganded (blue, PDB ID 8HBE[43]) and NO-bound (gray, PDB ID 8HBH[43]) states. NO binding ruptures the His-Fe^{2+} bond, leading to a lateral shift of the heme-ligating histidine while maintaining the rotamer conformation. (C) Structure and electron density map of unliganded *Hs* sGC (PDB ID 8HBE[43]) showing clear electron density for the His-Fe^{2+} bond. (D) Structure and electron density map for NO-bound *Hs* sGC (PDB ID 8HBH[43]) revealing an observed density for NO bound on the distal side of the heme.

The first structural observations of full-length sGC were obtained via negative stain electron microscopy of *Rn* sGC.[116] These maps revealed that sGC adopted a dumbbell-like structure, with two large lobes connected by a thin region of electron density. The larger lobe was attributed to the H-NOX/PAS domains, the thin connecting density was assigned to the CC domain, and the smaller lobe was attributed to the CAT domain. Reconstructions revealed that sGC displayed significant conformational flexibility, with extreme conformations ranging from a fully extended state with the terminal lobes separated by over 40 Å to a contracted conformation where the H-NOX/PAS domains appeared to form regulatory contacts with the CAT domain (Figure 1.9A). This range of conformational flexibility was observed for sGC both in the presence and absence of NO, suggesting that sGC can sample a full range of conformations regardless of gaseous ligand binding.

Structural Studies Using Cryo-Electron Microscopy

Recent advances in cryo-EM have allowed for the determination of full-length *Hs*[29,35,43] and *Ms*[28] sGC structures at near atomic-level resolution. In these studies, both proteins were found to adopt one of two conformations depending on the presence or absence of certain ligands. *Ms* sGC was found to adopt a contracted conformation in the absence of NO, while the protein adopted an extended, dumbbell-like conformation when prepared for EM with both NO and the small molecule sGC stimulator YC-1.[28] Correlating the freezing conditions for these samples to previous *in vitro* biochemical characterizations, the contracted form of the enzyme represents the conformation of sGC in the NO-free, basal activity state while the extended conformation represents sGC in the full activity state. Likewise, *Hs* sGC was solved in an extended conformation in the presence of NO and the sGC stimulators YC-1 or riociguat while adopting the contracted conformation in the absence of those ligands (Figure 1.9B).[29,35,43] These higher resolution structures allowed for determination of the molecular mechanisms for signal transduction and activation in full-length sGCs.

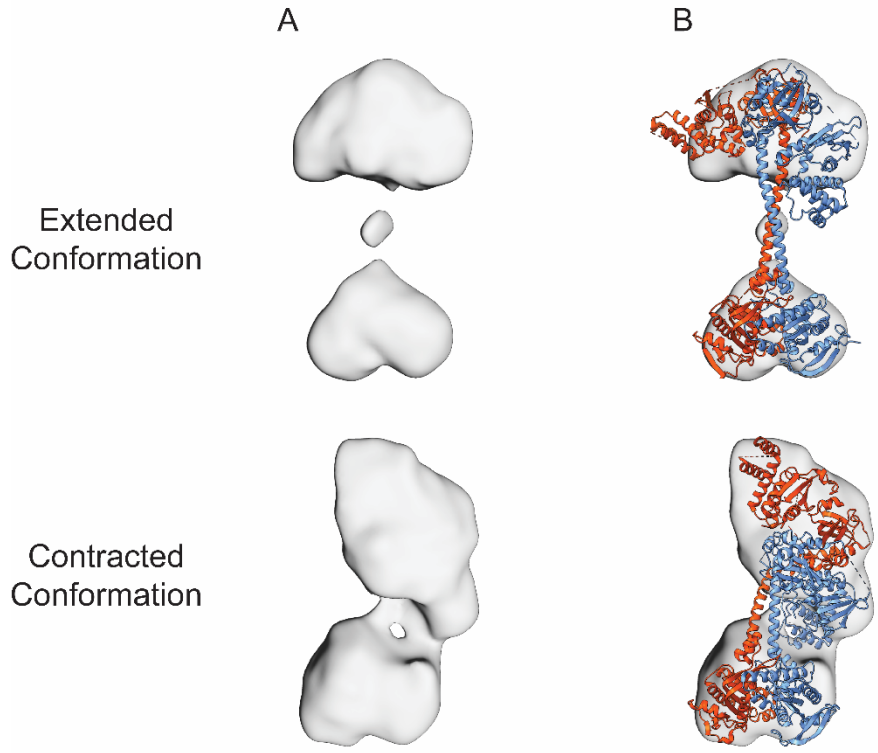

Figure 1.9. Conformational extremes in sGC. (A) Representative electron map constructions of full-length *Rn* sGC using negative stain cryo-EM data from ref[116]. (B) Solved cryo-EM structures for *Hs* sGC in the NO-activated, extended (PDB ID 8HBH[43]) or unliganded, contracted (PDB ID 8HBE[43]) conformations fit to the electron densities observed for *Rn* sGC. Figure adapted from ref[37].

As observed in isolated H-NOX domains, NO binds at the distal side of the heme leading to rupture of the His-Fe^{2+} bond and formation of a 5c Fe^{2+}-NO complex (Figure 1.8C and D).[43] The observed conformational changes at the β H-NOX domain upon NO binding in full-length

sGCs are more subtle than those observed for isolated H-NOX domains. The Cα position for the heme-ligated histidine is shifted laterally by 2 Å while the rotamer conformation is maintained (Figure 1.8B).[44] These shifts introduced by His-Fe^{2+} bond rupture disrupt hydrogen bonding interactions between the αF helix and the α CC domain but do not match the magnitude of NO-induced conformational changes observed in isolated H-NOX domains.[44] This suggests that full-length sGCs utilize mechanisms of signal transduction beyond conformational changes occurring via His-Fe^{2+} bond rupture. Indeed, studies of bovine (*Bt*) sGC provided additional clues towards the activation mechanism of sGC. In this study[82], sGC was incubated with carbon monoxide creating a 6c His-Fe^{2+}-CO complex enzyme which showed only moderate cyclase activity. When the sGC stimulator YC-1 was added to this 6c sGC, cyclase activity reached the maximum observed for the enzyme in the excess NO state, indicating that rupture of the His-Fe^{2+} bond is not necessary for full sGC activity. These observations highlighted the need for full-length sGC structures to better understand activation and signal transduction in sGCs.

The global-scale conformational changes observed in sGC are propagated via conformational toggling in the CC domain. In the contracted conformation, a region of the CC domains (α421 – 426 and β355 – 362 in *Hs* sGC, α420 – 426 and β346 – 350 in *Ms* sGC) does not form a coiled-coil and is instead present as a disordered loop (Figure 1.10A).[28,35] In the extended conformation, this region adopts the structure required for the formation of a canonical coiled-coil (Figure 1.10B). The straightened coils form a new plane ~90° from the initial bend, with the α and β coils rotating ~70°, driving significant conformational change throughout the enzyme without significant disruption to the domain arrangement of the protein (Figure 1.10C).[28,35,44] The H-NOX domains extend away from the catalytic domains, with the α H-NOX subunit undergoing slight translational movement while the β H-NOX domain undergoes both significant translation and rotation relative to the catalytic domains leading to an apparent 70° rotation about the CC bend (Figure 1.10D).[28,35,44] These movements in the CC domain ultimately facilitate an opening of the catalytic domain allowing for substrate binding. In the contracted conformation, key helices within the β CAT domain are positioned such that substrate cannot access the binding pocket.[28,35] Movement from the CC domains drives open the N-termini of the CAT domains, shifting the α4 helix of the β CAT domain away from the α CAT domain, opening the binding pocket to accommodate substrate in the active site, as demonstrated by the presence of guanosine-5'-[(α,β)-methyleno]triphosphate (GpCpp), a non-hydrolyzable substrate analog, which was bound in the catalytic pocket of the extended conformation enzyme solved via cryo-EM.[28,35,44]

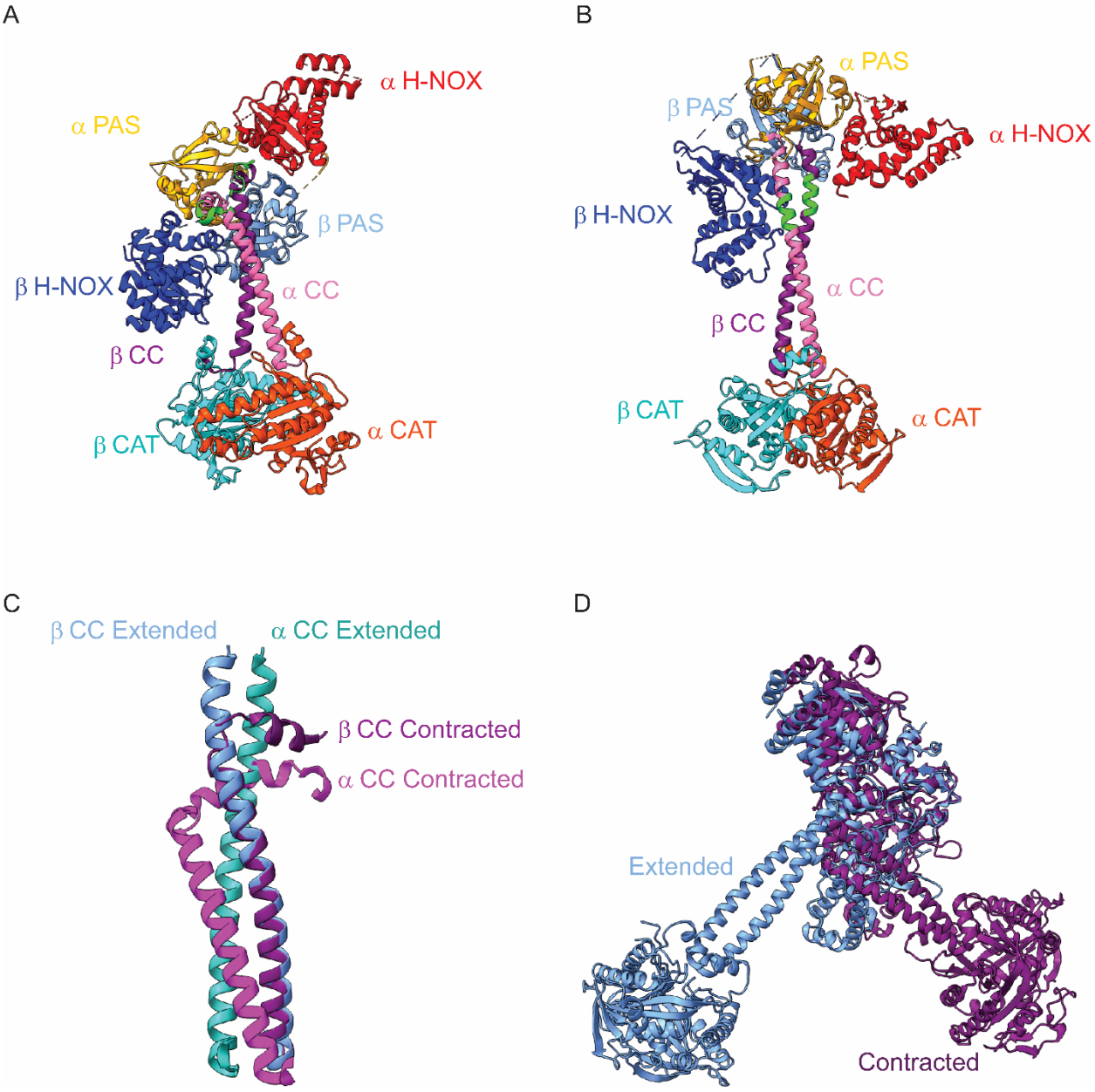

Figure 1.10. Global sGC conformational changes propagated by secondary structure in the CC domain. (A) Model of *Hs* sGC (PDB ID 8HBE[43]) in the contracted conformation, with a region of the CC domains forming a disordered bend (colored green). (B) Model of *Hs* sGC (PDB ID 8HBH[43]) in the extended conformation, with the previously bent region of the CC domains in the canonical CC motif (colored green). (C) Comparison of the CC domain in the contracted (purple shades) and extended (blue-green shades) conformations revealing the 90° change of plane for the protein and the rotation of the helices during extension. Structures were aligned by the β CC domain subunits. (D) Depiction of the global conformational rotation of sGC from the contracted (purple) to the extended (blue) states. Structures were aligned by the PAS domain dimer. Figure adapted from ref[35].

These full-length sGC structures have also revealed the binding site for the small molecule sGC stimulators YC-1 and riociguat. Prior attempts to determine the binding site for YC-1 were inconclusive and contradictory, suggesting potential binding sites at the α H-NOX domain[117,118],

the β H-NOX domain[119–121], or the CAT domain.[122–125] The first cryo-EM evidence for the binding site of YC-1 was obtained when the structure for *Ms* sGC was solved in conditions containing both NO and YC-1. After assigning density for the protein, a region of density between the CC and β H-NOX domains remained unassigned; this density was postulated to belong to YC-1.[28] However, the resolution of the structure was insufficient to determine the binding orientation of YC-1 or which residues in sGC were interacting with the stimulator. Subsequent work[29] with *Hs* sGC solved full-length structures for the enzyme bound to either YC-1 or riociguat. Both stimulators were found to engage sGC via numerous interactions with the β H-NOX domain as well as with the α and β CC domains. Crucially, these small molecules interact with sGC adjacent to the bent region of the CC domain, suggesting that stimulators increase sGC activity by stabilizing the extended conformation of the protein.

Despite intense effort, attempts to use higher resolution full-length cryo-EM structures to determine the location of the non-heme NO activation site in sGC have been unsuccessful. Comparisons of electron density maps at 3.08 Å (NO-free), 3.13 Å (excess NO), 3.07 Å (excess NO + riociguat) resolution for *Hs* sGC[43] were unable to find electron density corresponding to RSNO●$^{-}$ at positions suggested to be involved in NO-desensitization of sGC by oxidative *S*-nitrosation.[126–128] However, no electron density was observed for NO bound to the proximal side of the heme (Figure 1.8D), supporting the model that non-heme NO interactions are still responsible for inducing the conformational changes and activities observed in excess NO conditions.

Structural Studies Using Small-Angle X-Ray Scattering

While the previously discussed cryo-EM structures provide valuable insight into the extremes of conformational flexibility in sGC, they represent a rigid, two-state interpretation for the conformational sampling of sGC. While these two conformations were also observed in the negative stain electron microscopy experiments using *Rn* sGC, that study revealed that sGC could adopt a wide array of intermediate conformations with or without the presence of NO or GpCpp (Figure 1.11).[116] Additionally, all conformationally extreme cryo-EM structures were solved for sGCs in either NO-free or highly activating conditions utilizing NO and small molecule stimulators. As mentioned previously, considering non-signaling physiological concentrations of NO, the 1-NO state is the most likely resting state for sGC *in vivo*. The previously discussed biochemical characterizations of sGC have determined that sGC exhibits an “in-between” activity level in the 1-NO state, yet no cryo-EM structures have been solved for sGC in a corresponding “in-between” conformation.

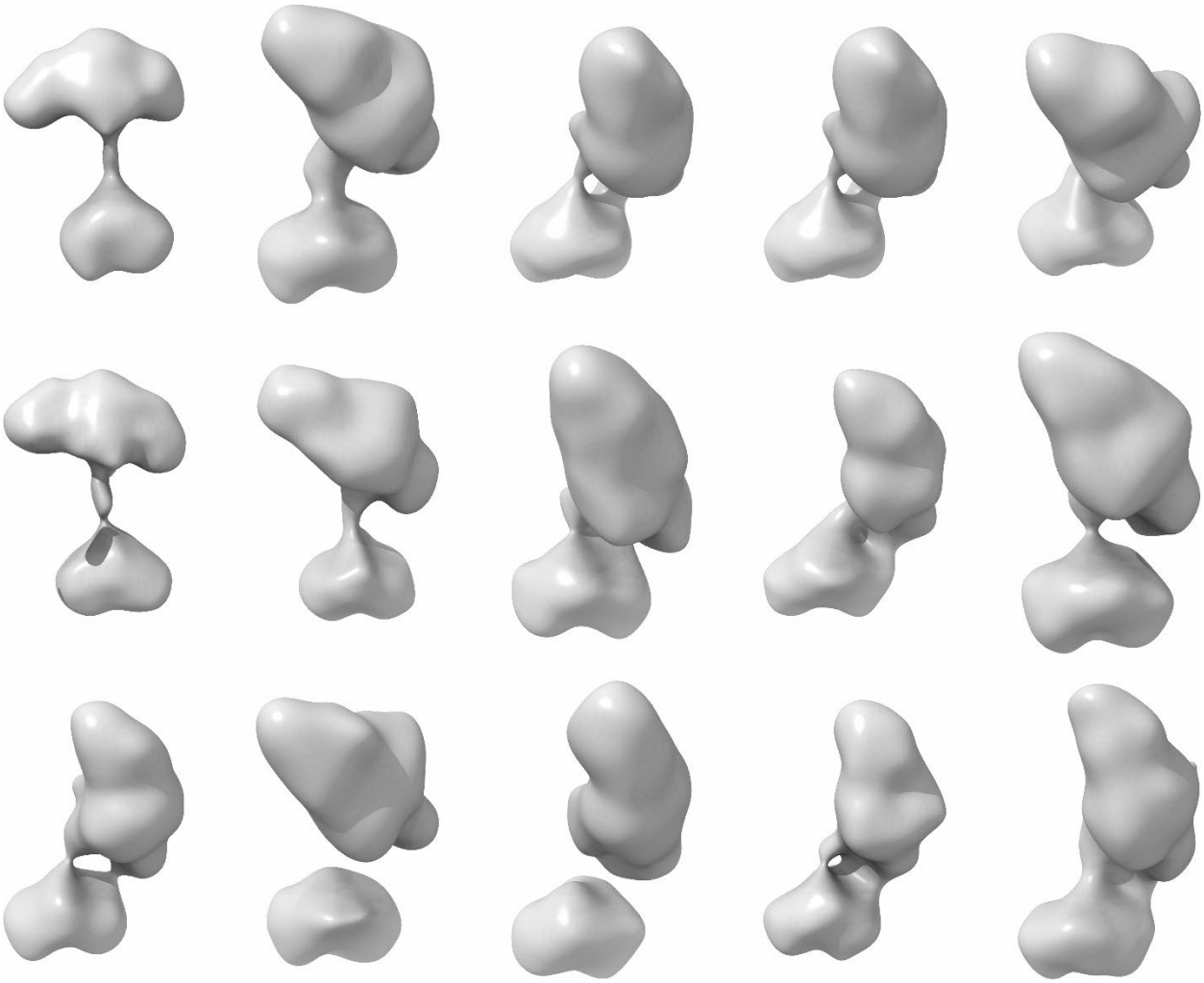

Figure 1.11. Three-dimensional reconstructions demonstrating the range of conformational flexibility observed for *Rn* sGC. *Rn* sGC was observed to access the full range of conformations, from contracted to extended, even in the absence of NO. Reconstructions capturing contracted forms of the enzyme also reveal the out-of-plane rotation arising from the conformational toggling of the CC domains of the structure. Figure adapted from ref[116].

While techniques such as X-ray crystallography and cryo-EM have provided "snapshots"[129] of molecules in static states, many proteins are dynamic, flexible molecules which have evolved to function in aqueous solution. Small-angle X-ray scattering (SAXS) provides an opportunity to collect quantitative data for proteins which undergo large conformational changes by interpreting X-ray scattering patterns of those proteins in solution.[129,130] Although SAXS is a low-resolution technique (~10 – 50 Å), it can provide unique insight to the conformational landscape of proteins in different experimental conditions.[129,130] The first SAXS investigations of conformational flexibility in sGC were performed using *Ms* sGC. Utilizing predicted scattering curves for numerous sGC conformations, researchers found that sGC in 1-NO experimental conditions best fit a model with 72% of the sample in the contracted conformation with the remaining 28% in a partially extended conformation in-between the contracted and extended conformations solved via cryo-EM.[28] These results suggest that binding of NO to the heme shifts

the conformational equilibrium of sGC towards the extended state, potentially explaining the increased activity observed in the 1-NO state.

Thesis Research

This dissertation focuses on deeper investigations of the conformational flexibility of sGCs, concentrating on the effects these conformational changes have on sGC activity and the role of NO and small molecule stimulators in forcing conformational change in sGCs. Recent cryo-EM structures have provided insight into the end states of sGC conformational change but do not confirm the necessity of these changes to increase sGC activity or provide information on potential intermediate conformations or activating steps. Small molecule stimulators, designed and characterized before full-length sGC structures were first solved, largely mimic the chemical structure of the first discovered sGC stimulator and iterate upon themselves primarily based on pharmacokinetic concerns. Biochemical and structural biology techniques, applied in tandem, can provide comprehensive insights towards answering outstanding questions regarding sGC activation and therapeutic targeting.

Chapter 2 describes work investigating the role of the CC domain in activity regulation in *Ms* sGC. Using previously solved structures for both *Ms* and *Hs* sGC, CC domain variants were engineered to produce either constitutively contracted or extended sGC by eliminating or forcing, respectively, straightening in the bent region of the coiled coil. These variants were predicted to display catalytic activity matching the expected activity conditions for the solved full-length structures, with the contracted enzyme possessing basal activity and the extended enzyme displaying maximal activity. Both variants were predicted to be unresponsive to the addition of NO or small molecule stimulators. Indeed, sGC variants which were unable to extend beyond the contracted state displayed basal activity and variants which were trapped in the extended conformation exhibited maximal activity in all experimental conditions, suggesting that straightening of the bent CC region of sGC is both necessary and sufficient for full sGC activation.

Chapter 3 details research characterizing a chemically novel sGC stimulator CYR715. YC-1 derivative stimulators have been well-characterized biochemically and structurally, however CYR715 belongs to a new class of stimulators which are structurally unique in regions found to be essential for the function of YC-1 and derivative stimulators. CYR715 stimulation was determined for WT *Ms* sGC as well as two point variants with a mutation at position βC122. CYR715 was found to be uniquely potent at stimulating WT protein in the complete absence of NO, while each variant revealed that mutagenesis at βC122 changed the extent of stimulation by either CYR715 and/or YC-1. Structural work using cryo-EM revealed that CYR715 shares the same binding pocket as YC-1 and riociguat while accessing additional binding interactions due to its unique structure. SAXS analyses were performed to further investigate the conformational flexibility and activation response of sGC, revealing differences in sGC extension following ligand or substrate binding.

Chapter 4 details additional efforts made towards determining the mechanism of sGC activation by non-heme NO. Previous experimental work has linked excess NO-based sGC activation to thiol-based modification via transient RSNO●⁻ adducts. Cysteines can be modified using a variety of small molecule conjugates, yet only certain chemical modifications result in

disruptions to excess NO-stimulated activity in sGC. The excess NO-response of *Ms* sGC was characterized following labeling by two cysteine-reactive agents, and labeled proteins were further characterized via mass spectrometry to determine which sites were chemically modified. These results were then compared to solved sGC structures to potentially determine the molecular mechanism behind the loss of NO-stimulation following thiol modification. Bioinformatics approaches were also used to investigate crucial point variation in sGC β H-NOX subunits for potential future directions in pursuit of characterizing the non-heme site(s) responsible for excess NO stimulation of sGC activity.

Chapter 5 provides a reexamination of our current understanding of sGC conformation and activation, with special emphasis on developing a coherent framework for the sGC conformational landscape. The conformational "end states" of sGC have been determined, but potential intermediate conformations have yet to be characterized. Additionally, how those conformations are sampled or accessed in various ligation states remains poorly understood. Synthesis of biochemical and structural studies suggests a model where independent conformational sampling of the H-NOX and CAT domains is increased by the addition of NO, providing increased opportunities for the formation of interactions necessary to stabilize the extended conformation of sGC. Finally, a cysteine which stabilizes the β H-NOX domain in the contracted conformation is discussed as a potential second-site cysteine for the excess NO activation of sGC. The role of sGC and NO-signaling in human health and disease necessitates continued exploration into the mechanisms of both physiological and therapeutic modulation of sGC activity, and future efforts must build upon a modern foundation informed by recent discoveries of sGC structure, conformational landscape, and function.

References

(1) Furchgott, R. F.; Zawadzki, J. V. The Obligatory Role of Endothelial Cells in the Relaxation of Arterial Smooth Muscle by Acetylcholine. *Nature* **1980**, *288* (5789), 373–376. https://doi.org/10.1038/288373a0.

(2) Palmer, R. M. J.; Ferrige, A. G.; Moncada, S. Nitric Oxide Release Accounts for the Biological Activity of Endothelium-Derived Relaxing Factor. *Nature* **1987**, *327* (6122), 524–526. https://doi.org/10.1038/327524a0.

(3) Ignarro, L. J.; Byrns, R. E.; Buga, G. M.; Wood, K. S. Endothelium-Derived Relaxing Factor from Pulmonary Artery and Vein Possesses Pharmacologic and Chemical Properties Identical to Those of Nitric Oxide Radical. **1987**. https://doi.org/10.1161/01.RES.61.6.866.

(4) Marletta, M. A.; Yoon, P. S.; Iyengar, R.; Leaf, C. D.; Wishnok, J. S. Macrophage Oxidation of L-Arginine to Nitrite and Nitrate: Nitric Oxide Is an Intermediate. *Biochemistry* 1988, *27* (24), 8706–8711. https://doi.org/10.1021/bi00424a003.

(5) Knowles, R. G.; Palacios, M.; Palmer, R. M.; Moncada, S. Formation of Nitric Oxide from L-Arginine in the Central Nervous System: A Transduction Mechanism for Stimulation of the Soluble Guanylate Cyclase. *Proc. Natl. Acad. Sci.* **1989**, *86* (13), 5159–5162. https://doi.org/10.1073/pnas.86.13.5159.

(6) Bogdan, C. Nitric Oxide and the Immune Response. *Nat. Immunol.* **2001**, *2* (10), 907–916. https://doi.org/10.1038/ni1001-907.

(7) Bogdan, C.; Röllinghoff, M.; Diefenbach, A. Reactive Oxygen and Reactive Nitrogen Intermediates in Innate and Specific Immunity. *Curr. Opin. Immunol.* **2000**, *12* (1), 64–76. https://doi.org/10.1016/S0952-7915(99)00052-7.
(8) Hibbs, J. B.; Vavrin, Z.; Taintor, R. R. L-Arginine Is Required for Expression of the Activated Macrophage Effector Mechanism Causing Selective Metabolic Inhibition in Target Cells. *J. Immunol. Baltim. Md 1950* **1987**, *138* (2), 550–565.
(9) Bredt, D. S. Endogenous Nitric Oxide Synthesis: Biological Functions and Pathophysiology. *Free Radic. Res.* **1999**, *31* (6), 577–596. https://doi.org/10.1080/10715769900301161.
(10) Steinert, J. R.; Chernova, T.; Forsythe, I. D. Nitric Oxide Signaling in Brain Function, Dysfunction, and Dementia. *Neurosci. Rev. J. Bringing Neurobiol. Neurol. Psychiatry* **2010**, *16* (4), 435–452. https://doi.org/10.1177/1073858410366481.
(11) Moncada, S.; Palmer, R. M.; Higgs, E. A. Nitric Oxide: Physiology, Pathophysiology, and Pharmacology. *Pharmacol. Rev.* **1991**, *43* (2), 109–142.
(12) Brown, G. C.; Cooper, Chris. E. Nanomolar Concentrations of Nitric Oxide Reversibly Inhibit Synaptosomal Respiration by Competing with Oxygen at Cytochrome Oxidase. *FEBS Lett.* **1994**, *356* (2), 295–298. https://doi.org/10.1016/0014-5793(94)01290-3.
(13) Cleeter, M. W. J.; Cooper, J. M.; Darley-Usmar, V. M.; Moncada, S.; Schapira, A. H. V. Reversible Inhibition of Cytochrome c Oxidase, the Terminal Enzyme of the Mitochondrial Respiratory Chain, by Nitric Oxide: Implications for Neurodegenerative Diseases. *FEBS Lett.* **1994**, *345* (1), 50–54. https://doi.org/10.1016/0014-5793(94)00424-2.
(14) Gibson, N. J.; Nighorn, A. Expression of Nitric Oxide Synthase and Soluble Guanylyl Cyclase in the Developing Olfactory System of Manduca Sexta. *J. Comp. Neurol.* **2000**, *422* (2), 191–205. https://doi.org/10.1002/(SICI)1096-9861(20000626)422:2<191::AID-CNE4>3.0.CO;2-C.
(15) Walker, W. T.; Jackson, C. L.; Lackie, P. M.; Hogg, C.; Lucas, J. S. Nitric Oxide in Primary Ciliary Dyskinesia. *Eur. Respir. J.* **2012**, *40* (4), 1024–1032. https://doi.org/10.1183/09031936.00176111.
(16) Wen, H.-C.; Chuu, C.-P.; Chen, C.-Y.; Shiah, S.-G.; Kung, H.-J.; King, K.-L.; Su, L.-C.; Chang, S.-C.; Chang, C.-H. Elevation of Soluble Guanylate Cyclase Suppresses Proliferation and Survival of Human Breast Cancer Cells. *PloS One* **2015**, *10* (4), e0125518. https://doi.org/10.1371/journal.pone.0125518.
(17) Lundberg, J. O.; Weitzberg, E. Nitric Oxide Signaling in Health and Disease. *Cell* **2022**, *185* (16), 2853–2878. https://doi.org/10.1016/j.cell.2022.06.010.
(18) Arnold, W. P.; Mittal, C. K.; Katsuki, S.; Murad, F. Nitric Oxide Activates Guanylate Cyclase and Increases Guanosine 3':5'-Cyclic Monophosphate Levels in Various Tissue Preparations. *Proc. Natl. Acad. Sci. U. S. A.* **1977**, *74* (8), 3203–3207. https://doi.org/10.1073/pnas.74.8.3203.
(19) Stone, J. R.; Marletta, M. A. Soluble Guanylate Cyclase from Bovine Lung: Activation with Nitric Oxide and Carbon Monoxide and Spectral Characterization of the Ferrous and Ferric States. *Biochemistry* **1994**, *33* (18), 5636–5640. https://doi.org/10.1021/bi00184a036.
(20) Aliancy, J.; Stamer, W. D.; Wirostko, B. A Review of Nitric Oxide for the Treatment of Glaucomatous Disease. *Ophthalmol. Ther.* **2017**, *6* (2), 221–232. https://doi.org/10.1007/s40123-017-0094-6.

(21) Kinsella, J. P.; Neish, S. R.; Shaffer, E.; Abman, S. H. Low-Dose Inhalational Nitric Oxide in Persistent Pulmonary Hypertension of the Newborn. *The Lancet* **1992**, *340* (8823), 819–820. https://doi.org/10.1016/0140-6736(92)92687-B.

(22) Roberts, J. D.; Polaner, D. M.; Zapol, W. M.; Lang, P. Inhaled Nitric Oxide in Persistent Pulmonary Hypertension of the Newborn. *The Lancet* **1992**, *340* (8823), 818–819. https://doi.org/10.1016/0140-6736(92)92686-A.

(23) Mittendorf, J.; Weigand, S.; Alonso-Alija, C.; Bischoff, E.; Feurer, A.; Gerisch, M.; Kern, A.; Knorr, A.; Lang, D.; Muenter, K.; Radtke, M.; Schirok, H.; Schlemmer, K.-H.; Stahl, E.; Straub, A.; Wunder, F.; Stasch, J.-P. Discovery of Riociguat (BAY 63-2521): A Potent, Oral Stimulator of Soluble Guanylate Cyclase for the Treatment of Pulmonary Hypertension. *ChemMedChem* **2009**, *4* (5), 853–865. https://doi.org/10.1002/cmdc.200900014.

(24) Stasch, J.-P.; Evgenov, O. V. *Pharmacotherapy of Pulmonary Hypertension*; Humbert, M., Ed.; Handbook of experimental pharmacology, volume 218; Springer: Heildelberg, 2013.

(25) Conole, D.; Scott, L. J. Riociguat: First Global Approval. *Drugs* **2013**, *73* (17), 1967–1975. https://doi.org/10.1007/s40265-013-0149-5.

(26) Follmann, M.; Ackerstaff, J.; Redlich, G.; Wunder, F.; Lang, D.; Kern, A.; Fey, P.; Griebenow, N.; Kroh, W.; Becker-Pelster, E.-M.; Kretschmer, A.; Geiss, V.; Li, V.; Straub, A.; Mittendorf, J.; Jautelat, R.; Schirok, H.; Schlemmer, K.-H.; Lustig, K.; Gerisch, M.; Knorr, A.; Tinel, H.; Mondritzki, T.; Trübel, H.; Sandner, P.; Stasch, J.-P. Discovery of the Soluble Guanylate Cyclase Stimulator Vericiguat (BAY 1021189) for the Treatment of Chronic Heart Failure. *J. Med. Chem.* **2017**, *60* (12), 5146–5161. https://doi.org/10.1021/acs.jmedchem.7b00449.

(27) Xia, J.; Hui, N.; Tian, L.; Liang, C.; Zhang, J.; Liu, J.; Wang, J.; Ren, X.; Xie, X.; Wang, K. Development of Vericiguat: The First Soluble Guanylate Cyclase (sGC) Stimulator Launched for Heart Failure with Reduced Ejection Fraction (HFrEF). *Biomed. Pharmacother.* **2022**, *149*, 112894. https://doi.org/10.1016/j.biopha.2022.112894.

(28) Horst, B. G.; Yokom, A. L.; Rosenberg, D. J.; Morris, K. L.; Hammel, M.; Hurley, J. H.; Marletta, M. A. Allosteric Activation of the Nitric Oxide Receptor Soluble Guanylate Cyclase Mapped by Cryo-Electron Microscopy. *eLife* **2019**, *8*, e50634. https://doi.org/10.7554/eLife.50634.

(29) Liu, R.; Kang, Y.; Chen, L. Activation Mechanism of Human Soluble Guanylate Cyclase by Stimulators and Activators. *Nat. Commun.* **2021**, *12* (1), 5492. https://doi.org/10.1038/s41467-021-25617-0.

(30) Horst, B. G.; Stewart, E. M.; Nazarian, A. A.; Marletta, M. A. Characterization of a Carbon Monoxide-Activated Soluble Guanylate Cyclase from Chlamydomonas Reinhardtii. *Biochemistry* **2019**, *58* (17), 2250–2259. https://doi.org/10.1021/acs.biochem.9b00190.

(31) Wu, Y.; Thomas, W. C.; Green, Z. B.; Marletta, M. A. Characterization of a NO-Activated Homodimeric Soluble Guanylate Cyclase from a Choanoflagellate. *Biochemistry* **2025**. https:// doi.org/10.1021/acs.biochem.5c00228. Epub ahead of print. PMID: 40658828.

(32) Budworth, J.; Meillerais, S.; Charles, I.; Powell, K. Tissue Distribution of the Human Soluble Guanylate Cyclases. *Biochem. Biophys. Res. Commun.* **1999**, *263* (3), 696–701. https://doi.org/10.1006/bbrc.1999.1444.

(33) Pellicena, P.; Karow, D. S.; Boon, E. M.; Marletta, M. A.; Kuriyan, J. Crystal Structure of an Oxygen-Binding Heme Domain Related to Soluble Guanylate Cyclases. *Proc. Natl. Acad. Sci.* **2004**, *101* (35), 12854–12859. https://doi.org/10.1073/pnas.0405188101.

(34) Zhao, Y.; Marletta, M. A. Localization of the Heme Binding Region in Soluble Guanylate Cyclase†. *Biochemistry* **1997**, *36* (50), 15959–15964. https://doi.org/10.1021/bi971825x.
(35) Kang, Y.; Liu, R.; Wu, J.-X.; Chen, L. Structural Insights into the Mechanism of Human Soluble Guanylate Cyclase. *Nature* **2019**, *574* (7777), 206–210. https://doi.org/10.1038/s41586-019-1584-6.
(36) Allerston, C. K.; von Delft, F.; Gileadi, O. Crystal Structures of the Catalytic Domain of Human Soluble Guanylate Cyclase. *PLoS ONE* **2013**, *8* (3), e57644. https://doi.org/10.1371/journal.pone.0057644.
(37) Horst, B. G.; Marletta, M. A. Physiological Activation and Deactivation of Soluble Guanylate Cyclase. *Nitric Oxide Biol. Chem.* **2018**, *77*, 65–74. https://doi.org/10.1016/j.niox.2018.04.011.
(38) Iyer, L. M.; Anantharaman, V.; Aravind, L. Ancient Conserved Domains Shared by Animal Soluble Guanylyl Cyclases and Bacterial Signaling Proteins. *BMC Genomics* **2003**, *4* (1), 5. https://doi.org/10.1186/1471-2164-4-5.
(39) Nioche, P.; Berka, V.; Vipond, J.; Minton, N.; Tsai, A.-L.; Raman, C. S. Femtomolar Sensitivity of a NO Sensor from Clostridium Botulinum. *Science* **2004**, *306* (5701), 1550–1553. https://doi.org/10.1126/science.1103596.
(40) Zhao, Y.; Schelvis, J. P. M.; Babcock, G. T.; Marletta, M. A. Identification of Histidine 105 in the B1 Subunit of Soluble Guanylate Cyclase as the Heme Proximal Ligand. *Biochemistry* **1998**, *37* (13), 4502–4509. https://doi.org/10.1021/bi972686m.
(41) Wedel, B.; Humbert, P.; Harteneck, C.; Foerster, J.; Malkewitz, J.; Böhme, E.; Schultz, G.; Koesling, D. Mutation of His-105 in the Beta 1 Subunit Yields a Nitric Oxide-Insensitive Form of Soluble Guanylyl Cyclase. *Proc. Natl. Acad. Sci. U. S. A.* **1994**, *91* (7), 2592–2596. https://doi.org/10.1073/pnas.91.7.2592.
(42) Boon, E. M.; Huang, S. H.; Marletta, M. A. A Molecular Basis for NO Selectivity in Soluble Guanylate Cyclase. *Nat. Chem. Biol.* **2005**, *1* (1), 53–59. https://doi.org/10.1038/nchembio704.
(43) Liu, R.; Kang, Y.; Chen, L. NO Binds to the Distal Site of Haem in the Fully Activated Soluble Guanylate Cyclase. *Nitric Oxide* **2023**, *134–135*, 17–22. https://doi.org/10.1016/j.niox.2023.03.002.
(44) Wittenborn, E. C.; Marletta, M. A. Structural Perspectives on the Mechanism of Soluble Guanylate Cyclase Activation. *Int. J. Mol. Sci.* **2021**, *22* (11), 5439. https://doi.org/10.3390/ijms22115439.
(45) Henry, J. T.; Crosson, S. Ligand-Binding PAS Domains in a Genomic, Cellular, and Structural Context. *Annu. Rev. Microbiol.* **2011**, *65*, 261–286. https://doi.org/10.1146/annurev-micro-121809-151631.
(46) Möglich, A.; Ayers, R. A.; Moffat, K. Structure and Signaling Mechanism of Per-ARNT-Sim Domains. *Struct. Lond. Engl. 1993* **2009**, *17* (10), 1282–1294. https://doi.org/10.1016/j.str.2009.08.011.
(47) Ma, X.; Sayed, N.; Baskaran, P.; Beuve, A.; van den Akker, F. PAS-mediated dimerization of soluble guanylyl cyclase revealed by signal transduction histidine kinase domain crystal structure. *J. Biol. Chem.* **2008**, *283* (2), 1167–1178. https://doi.org/10.1074/jbc.M706218200.
(48) Sarkar, A.; Dai, Y.; Haque, M. M.; Seeger, F.; Ghosh, A.; Garcin, E. D.; Montfort, W. R.; Hazen, S. L.; Misra, S.; Stuehr, D. J. Heat Shock Protein 90 Associates with the Per-Arnt-

Sim Domain of Heme-Free Soluble Guanylate Cyclase. *J. Biol. Chem.* **2015**, *290* (35), 21615–21628. https://doi.org/10.1074/jbc.M115.645515.

(49) Fritz, B. G.; Roberts, S. A.; Ahmed, A.; Breci, L.; Li, W.; Weichsel, A.; Brailey, J. L.; Wysocki, V. H.; Tama, F.; Montfort, W. R. Molecular Model of a Soluble Guanylyl Cyclase Fragment Determined by Small-Angle X-Ray Scattering and Chemical Cross-Linking. *Biochemistry* **2013**, *52* (9), 1568–1582. https://doi.org/10.1021/bi301570m.

(50) Underbakke, E. S.; Iavarone, A. T.; Chalmers, M. J.; Pascal, B. D.; Novick, S.; Griffin, P. R.; Marletta, M. A. Nitric Oxide-Induced Conformational Changes in Soluble Guanylate Cyclase. *Structure* **2014**, *22* (4), 602–611. https://doi.org/10.1016/j.str.2014.01.008.

(51) Linder, J. U. Class III Adenylyl Cyclases: Molecular Mechanisms of Catalysis and Regulation. *Cell. Mol. Life Sci.* **2006**, *63* (15), 1736. https://doi.org/10.1007/s00018-006-6072-0.

(52) Winger, J. A.; Derbyshire, E. R.; Lamers, M. H.; Marletta, M. A.; Kuriyan, J. The Crystal Structure of the Catalytic Domain of a Eukaryotic Guanylate Cyclase. *BMC Struct. Biol.* **2008**, *8* (1), 42. https://doi.org/10.1186/1472-6807-8-42.

(53) Cary, S. P. L.; Winger, J. A.; Marletta, M. A. Tonic and Acute Nitric Oxide Signaling through Soluble Guanylate Cyclase Is Mediated by Nonheme Nitric Oxide, ATP, and GTP. *Proc. Natl. Acad. Sci.* **2005**, *102* (37), 13064–13069. https://doi.org/10.1073/pnas.0506289102.

(54) Derbyshire, E. R.; Fernhoff, N. B.; Deng, S.; Marletta, M. A. Nucleotide Regulation of Soluble Guanylate Cyclase Substrate Specificity. *Biochemistry* **2009**, *48* (31), 7519–7524. https://doi.org/10.1021/bi900696x.

(55) Sürmeli, N. B.; Müskens, F. M.; Marletta, M. A. The Influence of Nitric Oxide on Soluble Guanylate Cyclase Regulation by Nucleotides. *J. Biol. Chem.* **2015**, *290* (25), 15570–15580. https://doi.org/10.1074/jbc.M115.641431.

(56) Sunahara, R. K.; Beuve, A.; Tesmer, J. J.; Sprang, S. R.; Garbers, D. L.; Gilman, A. G. Exchange of Substrate and Inhibitor Specificities between Adenylyl and Guanylyl Cyclases. *J. Biol. Chem.* **1998**, *273* (26), 16332–16338. https://doi.org/10.1074/jbc.273.26.16332.

(57) Ballou, D. P.; Zhao, Y.; Brandish, P. E.; Marletta, M. A. Revisiting the Kinetics of Nitric Oxide (NO) Binding to Soluble Guanylate Cyclase: The Simple NO-Binding Model Is Incorrect. *Proc. Natl. Acad. Sci. U. S. A.* **2002**, *99* (19), 12097–12101. https://doi.org/10.1073/pnas.192209799.

(58) Bellamy, T. C.; Wood, J.; Garthwaite, J. On the Activation of Soluble Guanylyl Cyclase by Nitric Oxide. *Proc. Natl. Acad. Sci. U. S. A.* **2002**, *99* (1), 507–510. https://doi.org/10.1073/pnas.012368499.

(59) Ignarro, L. J.; Degnan, J. N.; Baricos, W. H.; Kadowitz, P. J.; Wolin, M. S. Activation of Purified Guanylate Cyclase by Nitric Oxide Requires Heme Comparison of Heme-Deficient, Heme-Reconstituted and Heme-Containing Forms of Soluble Enzyme from Bovine Lung. *Biochim. Biophys. Acta BBA - Gen. Subj.* **1982**, *718* (1), 49–59. https://doi.org/10.1016/0304-4165(82)90008-3.

(60) Ignarro, L. J.; Wood, K. S.; Wolin, M. S. Activation of Purified Soluble Guanylate Cyclase by Protoporphyrin IX. *Proc. Natl. Acad. Sci. U. S. A.* **1982**, *79* (9), 2870–2873.

(61) Ignarro, L. J.; Wood, K. S.; Wolin, M. S. Regulation of Purified Soluble Guanylate Cyclase by Porphyrins and Metalloporphyrins: A Unifying Concept. *Adv. Cyclic Nucleotide Protein Phosphorylation Res.* **1984**, *17*, 267–274.

(62) Zhao, Y.; Brandish, P. E.; Ballou, D. P.; Marletta, M. A. A Molecular Basis for Nitric Oxide Sensing by Soluble Guanylate Cyclase. *Proc. Natl. Acad. Sci.* **1999**, *96* (26), 14753–14758. https://doi.org/10.1073/pnas.96.26.14753.
(63) Yoo, B.-K.; Lamarre, I.; Martin, J.-L.; Rappaport, F.; Negrerie, M. Motion of Proximal Histidine and Structural Allosteric Transition in Soluble Guanylate Cyclase. *Proc. Natl. Acad. Sci. U. S. A.* **2015**, *112* (14), E1697-1704. https://doi.org/10.1073/pnas.1423098112.
(64) Hunt, A. P.; Lehnert, N. Heme-Nitrosyls: Electronic Structure Implications for Function in Biology. *Acc. Chem. Res.* **2015**, *48* (7), 2117–2125. https://doi.org/10.1021/acs.accounts.5b00167.
(65) Roy, B.; Garthwaite, J. Nitric Oxide Activation of Guanylyl Cyclase in Cells Revisited. *Proc. Natl. Acad. Sci. U. S. A.* **2006**, *103* (32), 12185–12190. https://doi.org/10.1073/pnas.0602544103.
(66) Sato, M.; Nakajima, T.; Goto, M.; Umezawa, Y. Cell-Based Indicator to Visualize Picomolar Dynamics of Nitric Oxide Release from Living Cells. *Anal. Chem.* **2006**, *78* (24), 8175–8182. https://doi.org/10.1021/ac061791b.
(67) Roy, B.; Halvey, E. J.; Garthwaite, J. An Enzyme-Linked Receptor Mechanism for Nitric Oxide-Activated Guanylyl Cyclase. *J. Biol. Chem.* **2008**, *283* (27), 18841–18851. https://doi.org/10.1074/jbc.M801712200.
(68) Hall, C. N.; Garthwaite, J. What Is the Real Physiological NO Concentration in Vivo? *Nitric Oxide* **2009**, *21* (2), 92–103. https://doi.org/10.1016/j.niox.2009.07.002.
(69) Batchelor, A. M.; Bartus, K.; Reynell, C.; Constantinou, S.; Halvey, E. J.; Held, K. F.; Dostmann, W. R.; Vernon, J.; Garthwaite, J. Exquisite Sensitivity to Subsecond, Picomolar Nitric Oxide Transients Conferred on Cells by Guanylyl Cyclase-Coupled Receptors. *Proc. Natl. Acad. Sci. U. S. A.* **2010**, *107* (51), 22060–22065. https://doi.org/10.1073/pnas.1013147107.
(70) Wood, K. C.; Batchelor, A. M.; Bartus, K.; Harris, K. L.; Garthwaite, G.; Vernon, J.; Garthwaite, J. Picomolar Nitric Oxide Signals from Central Neurons Recorded Using Ultrasensitive Detector Cells. *J. Biol. Chem.* **2011**, *286* (50), 43172–43181. https://doi.org/10.1074/jbc.M111.289777.
(71) Stone, J. R.; Marletta, M. A. Spectral and Kinetic Studies on the Activation of Soluble Guanylate Cyclase by Nitric Oxide. *Biochemistry* **1996**, *35* (4), 1093–1099. https://doi.org/10.1021/bi9519718.
(72) Bellamy, T. C.; Griffiths, C.; Garthwaite, J. Differential Sensitivity of Guanylyl Cyclase and Mitochondrial Respiration to Nitric Oxide Measured Using Clamped Concentrations. *J. Biol. Chem.* **2002**, *277* (35), 31801–31807. https://doi.org/10.1074/jbc.M205936200.
(73) Russwurm, M.; Koesling, D. NO Activation of Guanylyl Cyclase. *EMBO J.* **2004**, *23* (22), 4443–4450. https://doi.org/10.1038/sj.emboj.7600422.
(74) Herzik, M. A.; Jonnalagadda, R.; Kuriyan, J.; Marletta, M. A. Structural Insights into the Role of Iron-Histidine Bond Cleavage in Nitric Oxide-Induced Activation of H-NOX Gas Sensor Proteins. *Proc. Natl. Acad. Sci. U. S. A.* **2014**, *111* (40), E4156-4164. https://doi.org/10.1073/pnas.1416936111.
(75) Martin, E.; Berka, V.; Sharina, I.; Tsai, A.-L. Mechanism of Binding of NO to Soluble Guanylyl Cyclase: Implication for the Second NO Binding to the Heme Proximal Site. *Biochemistry* **2012**, *51* (13), 2737–2746. https://doi.org/10.1021/bi300105s.
(76) Derbyshire, E. R.; Marletta, M. A. Butyl Isocyanide as a Probe of the Activation Mechanism of Soluble Guanylate Cyclase: INVESTIGATING THE ROLE OF NON-HEME NITRIC

OXIDE. *J. Biol. Chem.* **2007**, *282* (49), 35741–35748. https://doi.org/10.1074/jbc.M705557200.
(77) Guo, Y.; Suess, D. L. M.; Herzik, M. A.; Iavarone, A. T.; Britt, R. D.; Marletta, M. A. Regulation of Nitric Oxide Signaling by Formation of a Distal Receptor–Ligand Complex. *Nat. Chem. Biol.* **2017**, *13* (12), 1216–1221. https://doi.org/10.1038/nchembio.2488.
(78) Aono, S. Metal-Containing Sensor Proteins Sensing Diatomic Gas Molecules. *Dalton Trans.* **2008**, No. 24, 3137–3146. https://doi.org/10.1039/B802070C.
(79) Chen, L.; Lyubimov, A. Y.; Brammer, L.; Vrielink, A.; Sampson, N. S. The Binding and Release of Oxygen and Hydrogen Peroxide Are Directed by a Hydrophobic Tunnel in Cholesterol Oxidase. *Biochemistry* **2008**, *47* (19), 5368–5377. https://doi.org/10.1021/bi800228w.
(80) Winter, M. B.; Herzik, M. A.; Kuriyan, J.; Marletta, M. A. Tunnels Modulate Ligand Flux in a Heme Nitric Oxide/Oxygen Binding (H-NOX) Domain. *Proc. Natl. Acad. Sci. U. S. A.* **2011**, *108* (43), E881–E889. https://doi.org/10.1073/pnas.1114038108.
(81) Stone, J. R.; Marletta, M. A. The Ferrous Heme of Soluble Guanylate Cyclase: Formation of Hexacoordinate Complexes with Carbon Monoxide and Nitrosomethane. *Biochemistry* **1995**, *34* (50), 16397–16403. https://doi.org/10.1021/bi00050a021.
(82) Stone, J. R.; Marletta, M. A. Synergistic Activation of Soluble Guanylate Cyclase by YC-1 and Carbon Monoxide: Implications for the Role of Cleavage of the Iron-Histidine Bond during Activation by Nitric Oxide. *Chem. Biol.* **1998**, *5* (5), 255–261. https://doi.org/10.1016/S1074-5521(98)90618-4.
(83) Gow, A. J.; Chen, Q.; Hess, D. T.; Day, B. J.; Ischiropoulos, H.; Stamler, J. S. Basal and Stimulated Protein S-Nitrosylation in Multiple Cell Types and Tissues. *J. Biol. Chem.* **2002**, *277* (12), 9637–9640. https://doi.org/10.1074/jbc.C100746200.
(84) Gaston, B.; Singel, D.; Doctor, A.; Stamler, J. S. S-Nitrosothiol Signaling in Respiratory Biology. *Am. J. Respir. Crit. Care Med.* **2006**, *173* (11), 1186–1193. https://doi.org/10.1164/rccm.200510-1584PP.
(85) Paige, J. S.; Xu, G.; Stancevic, B.; Jaffrey, S. R. Nitrosothiol Reactivity Profiling Identifies S-Nitrosylated Proteins with Unexpected Stability. *Chem. Biol.* **2008**, *15* (12), 1307–1316. https://doi.org/10.1016/j.chembiol.2008.10.013.
(86) Foster, M. W.; Hess, D. T.; Stamler, J. S. Protein S-Nitrosylation in Health and Disease: A Current Perspective. *Trends Mol. Med.* **2009**, *15* (9), 391–404. https://doi.org/10.1016/j.molmed.2009.06.007.
(87) Marozkina, N. V.; Gaston, B. S-Nitrosylation Signaling Regulates Cellular Protein Interactions. *Biochim. Biophys. Acta* **2012**, *1820* (6), 722–729. https://doi.org/10.1016/j.bbagen.2011.06.017.
(88) Dent, M. R.; DeMartino, A. W. Nitric Oxide and Thiols: Chemical Biology, Signalling Paradigms and Vascular Therapeutic Potential. *Br. J. Pharmacol.* **2023**, 10.1111/bph.16274. https://doi.org/10.1111/bph.16274.
(89) Fernhoff, N. B.; Derbyshire, E. R.; Marletta, M. A. A Nitric Oxide/Cysteine Interaction Mediates the Activation of Soluble Guanylate Cyclase. *Proc. Natl. Acad. Sci.* **2009**, *106* (51), 21602–21607. https://doi.org/10.1073/pnas.0911083106.
(90) Peterson, L. A.; Wagener, T.; Sies, H.; Stahl, W. Decomposition of S-Nitrosocysteine via S- to N-Transnitrosation. *Chem. Res. Toxicol.* **2007**, *20* (5), 721–723. https://doi.org/10.1021/tx700095u.

(91) Dubois-Deruy, E.; Peugnet, V.; Turkieh, A.; Pinet, F. Oxidative Stress in Cardiovascular Diseases. *Antioxidants* **2020**, *9* (9), 864. https://doi.org/10.3390/antiox9090864.
(92) Fritz, B. G.; Hu, X.; Brailey, J. L.; Berry, R. E.; Walker, F. A.; Montfort, W. R. Oxidation and Loss of Heme in Soluble Guanylyl Cyclase from Manduca Sexta. *Biochemistry* **2011**, *50* (26), 5813–5815. https://doi.org/10.1021/bi200794c.
(93) Hoffmann, L. S.; Schmidt, P. M.; Keim, Y.; Hoffmann, C.; Schmidt, H. H. H. W.; Stasch, J.-P. Fluorescence Dequenching Makes Haem-Free Soluble Guanylate Cyclase Detectable in Living Cells. *PLOS ONE* **2011**, *6* (8), e23596. https://doi.org/10.1371/journal.pone.0023596.
(94) Pan, J.; Zhang, X.; Yuan, H.; Xu, Q.; Zhang, H.; Zhou, Y.; Huang, Z.-X.; Tan, X. The Molecular Mechanism of Heme Loss from Oxidized Soluble Guanylate Cyclase Induced by Conformational Change. *Biochim. Biophys. Acta BBA - Proteins Proteomics* **2016**, *1864* (5), 488–500. https://doi.org/10.1016/j.bbapap.2016.02.012.
(95) Stuehr, D. J.; Misra, S.; Dai, Y.; Ghosh, A. Maturation, Inactivation, and Recovery Mechanisms of Soluble Guanylyl Cyclase. *J. Biol. Chem.* **2021**, *296*, 100336. https://doi.org/10.1016/j.jbc.2021.100336.
(96) Bertinat, R.; Villalobos-Labra, R.; Hofmann, L.; Blauensteiner, J.; Sepúlveda, N.; Westermeier, F. Decreased NO Production in Endothelial Cells Exposed to Plasma from ME/CFS Patients. *Vascul. Pharmacol.* **2022**, *143*, 106953. https://doi.org/10.1016/j.vph.2022.106953.
(97) Nagasaka, H.; Komatsu, H.; Ohura, T.; Sogo, T.; Inui, A.; Yorifuji, T.; Murayama, K.; Takayanagi, M.; Kikuta, H.; Kobayashi, K. Nitric Oxide Synthesis in Ornithine Transcarbamylase Deficiency: Possible Involvement of Low No Synthesis in Clinical Manifestations of Urea Cycle Defect. *J. Pediatr.* **2004**, *145* (2), 259–262. https://doi.org/10.1016/j.jpeds.2004.05.033.
(98) Follmann, M.; Griebenow, N.; Hahn, M. G.; Hartung, I.; Mais, F.; Mittendorf, J.; Schäfer, M.; Schirok, H.; Stasch, J.; Stoll, F.; Straub, A. The Chemistry and Biology of Soluble Guanylate Cyclase Stimulators and Activators. *Angew. Chem. Int. Ed.* **2013**, *52* (36), 9442–9462. https://doi.org/10.1002/anie.201302588.
(99) Sandner, P.; Follmann, M.; Becker-Pelster, E.; Hahn, M. G.; Meier, C.; Freitas, C.; Roessig, L.; Stasch, J.-P. Soluble GC Stimulators and Activators: Past, Present and Future. *Br. J. Pharmacol.* **2024**, *181* (21), 4130–4151. https://doi.org/10.1111/bph.15698.
(100) Fritz, B. G.; Hu, X.; Brailey, J. L.; Berry, R. E.; Walker, F. A.; Montfort, W. R. Oxidation and Loss of Heme in Soluble Guanylyl Cyclase from Manduca Sexta. *Biochemistry* **2011**, *50* (26), 5813–5815. https://doi.org/10.1021/bi200794c.
(101) Surmeli, N. B.; Marletta, M. A. Insight into the Rescue of Oxidized Soluble Guanylate Cyclase by the Activator Cinaciguat. *ChemBioChem* **2012**, *13* (7), 977–981. https://doi.org/10.1002/cbic.201100809.
(102) Ma, X.; Sayed, N.; Beuve, A.; van den Akker, F. NO and CO Differentially Activate Soluble Guanylyl Cyclase via a Heme Pivot-bend Mechanism. *EMBO J.* **2007**, *26* (2), 578–588. https://doi.org/10.1038/sj.emboj.7601521.
(103) Martin, F.; Baskaran, P.; Ma, X.; Dunten, P. W.; Schaefer, M.; Stasch, J.-P.; Beuve, A.; van den Akker, F. Structure of Cinaciguat (BAY 58–2667) Bound to *Nostoc* H-NOX Domain Reveals Insights into Heme-Mimetic Activation of the Soluble Guanylyl Cyclase. *J. Biol. Chem.* **2010**, *285* (29), 22651–22657. https://doi.org/10.1074/jbc.M110.111559.

(104) Schmidt, P. M.; Schramm, M.; Schröder, H.; Wunder, F.; Stasch, J.-P. Identification of Residues Crucially Involved in the Binding of the Heme Moiety of Soluble Guanylate Cyclase. *J. Biol. Chem.* **2004**, *279* (4), 3025–3032. https://doi.org/10.1074/jbc.M310141200.

(105) Hoffmann, L.; Schmidt, P.; Keim, Y.; Schaefer, S.; Schmidt, H.; Stasch, J. Distinct Molecular Requirements for Activation or Stabilization of Soluble Guanylyl Cyclase upon Haem Oxidation-Induced Degradation. *Br. J. Pharmacol.* **2009**, *157* (5), 781–795. https://doi.org/10.1111/j.1476-5381.2009.00263.x.

(106) Thoonen, R.; Cauwels, A.; Decaluwe, K.; Geschka, S.; Tainsh, R. E.; Delanghe, J.; Hochepied, T.; De Cauwer, L.; Rogge, E.; Voet, S.; Sips, P.; Karas, R. H.; Bloch, K. D.; Vuylsteke, M.; Stasch, J.-P.; Van de Voorde, J.; Buys, E. S.; Brouckaert, P. Cardiovascular and Pharmacological Implications of Haem-Deficient NO-Unresponsive Soluble Guanylate Cyclase Knock-in Mice. *Nat. Commun.* **2015**, *6* (1), 8482. https://doi.org/10.1038/ncomms9482.

(107) Xia, T.; Dimitropoulou, C.; Zeng, J.; Antonova, G. N.; Snead, C.; Venema, R. C.; Fulton, D.; Qian, S.; Patterson, C.; Papapetropoulos, A.; Catravas, J. D. Chaperone-Dependent E3 Ligase CHIP Ubiquitinates and Mediates Proteasomal Degradation of Soluble Guanylyl Cyclase. *Am. J. Physiol.-Heart Circ. Physiol.* **2007**, *293* (5), H3080–H3087. https://doi.org/10.1152/ajpheart.00579.2007.

(108) Stasch, J.-P.; Schlossmann, J.; Hocher, B. Renal Effects of Soluble Guanylate Cyclase Stimulators and Activators: A Review of the Preclinical Evidence. *Curr. Opin. Pharmacol.* **2015**, *21*, 95–104. https://doi.org/10.1016/j.coph.2014.12.014.

(109) Sandner, P.; Vakalopoulos, A.; Hahn, M. G.; Stasch, J.-P.; Follmann, M. Soluble Guanylate Cyclase Stimulators and Their Potential Use: A Patent Review. *Expert Opin. Ther. Pat.* **2021**, *31* (3), 203–222. https://doi.org/10.1080/13543776.2021.1866538.

(110) Stasch, J.-P.; Hobbs, A. J. NO-Independent, Haem-Dependent Soluble Guanylate Cyclase Stimulators. In *cGMP: Generators, Effectors and Therapeutic Implications*; Schmidt, H. H. H. W., Hofmann, F., Stasch, J.-P., Eds.; Springer: Berlin, Heidelberg, **2009**; pp 277–308. https://doi.org/10.1007/978-3-540-68964-5_13.

(111) Ko, F.-N.; Wu, C.-C.; Kuo, S.-C.; Lee, F.-Y.; Teng, C.-M. YC-1, a Novel Activator of Platelet Guanylate Cyclase. *Blood* **1994**, *84* (12), 4226–4233. https://doi.org/10.1182/blood.V84.12.4226.bloodjournal84124226.

(112) Ghofrani, H.-A.; Galiè, N.; Grimminger, F.; Grünig, E.; Humbert, M.; Jing, Z.-C.; Keogh, A. M.; Langleben, D.; Kilama, M. O.; Fritsch, A.; Neuser, D.; Rubin, L. J. Riociguat for the Treatment of Pulmonary Arterial Hypertension. *N. Engl. J. Med.* **2013**, *369* (4), 330–340. https://doi.org/10.1056/NEJMoa1209655.

(113) Armstrong, P. W.; Pieske, B.; Anstrom, K. J.; Ezekowitz, J.; Hernandez, A. F.; Butler, J.; Lam, C. S. P.; Ponikowski, P.; Voors, A. A.; Jia, G.; McNulty, S. E.; Patel, M. J.; Roessig, L.; Koglin, J.; O'Connor, C. M. Vericiguat in Patients with Heart Failure and Reduced Ejection Fraction. *N. Engl. J. Med.* **2020**, *382* (20), 1883–1893. https://doi.org/10.1056/NEJMoa1915928.

(114) Karow, D. S.; Pan, D.; Tran, R.; Pellicena, P.; Presley, A.; Mathies, R. A.; Marletta, M. A. Spectroscopic Characterization of the Soluble Guanylate Cyclase-like Heme Domains from Vibrio Cholerae and Thermoanaerobacter Tengcongensis. *Biochemistry* **2004**, *43* (31), 10203–10211. https://doi.org/10.1021/bi049374l.

(115) Rao, M.; Herzik, M. A. Jr.; Iavarone, A. T.; Marletta, M. A. Nitric Oxide-Induced Conformational Changes Govern H-NOX and Histidine Kinase Interaction and Regulation in Shewanella Oneidensis. *Biochemistry* **2017**, *56* (9), 1274–1284. https://doi.org/10.1021/acs.biochem.6b01133.
(116) Campbell, M. G.; Underbakke, E. S.; Potter, C. S.; Carragher, B.; Marletta, M. A. Single-Particle EM Reveals the Higher-Order Domain Architecture of Soluble Guanylate Cyclase. *Proc. Natl. Acad. Sci.* **2014**, *111* (8), 2960–2965. https://doi.org/10.1073/pnas.1400711111.
(117) Becker, E. M.; Alonso-Alija, C.; Apeler, H.; Gerzer, R.; Minuth, T.; Pleiss, U.; Schmidt, P.; Schramm, M.; Schröder, H.; Schroeder, W.; Steinke, W.; Straub, A.; Stasch, J. P. NO-Independent Regulatory Site of Direct sGC Stimulators like YC-1 and BAY 41-2272. *BMC Pharmacol.* **2001**, *1*, 13. https://doi.org/10.1186/1471-2210-1-13.
(118) Stasch, J. P.; Becker, E. M.; Alonso-Alija, C.; Apeler, H.; Dembowsky, K.; Feurer, A.; Gerzer, R.; Minuth, T.; Perzborn, E.; Pleiss, U.; Schröder, H.; Schroeder, W.; Stahl, E.; Steinke, W.; Straub, A.; Schramm, M. NO-Independent Regulatory Site on Soluble Guanylate Cyclase. *Nature* **2001**, *410* (6825), 212–215. https://doi.org/10.1038/35065611.
(119) Denninger, J. W.; Schelvis, J. P. M.; Brandish, P. E.; Zhao, Y.; Babcock, G. T.; Marletta, M. A. Interaction of Soluble Guanylate Cyclase with YC-1: Kinetic and Resonance Raman Studies. *Biochemistry* **2000**, *39* (14), 4191–4198. https://doi.org/10.1021/bi992332q.
(120) Purohit, R.; Fritz, B. G.; The, J.; Issaian, A.; Weichsel, A.; David, C. L.; Campbell, E.; Hausrath, A. C.; Rassouli-Taylor, L.; Garcin, E. D.; Gage, M. J.; Montfort, W. R. YC-1 Binding to the β Subunit of Soluble Guanylyl Cyclase Overcomes Allosteric Inhibition by the α Subunit. *Biochemistry* **2014**, *53* (1), 101–114. https://doi.org/10.1021/bi4015133.
(121) Wales, J. A.; Chen, C.-Y.; Breci, L.; Weichsel, A.; Bernier, S. G.; Sheppeck, J. E.; Solinga, R.; Nakai, T.; Renhowe, P. A.; Jung, J.; Montfort, W. R. Discovery of Stimulator Binding to a Conserved Pocket in the Heme Domain of Soluble Guanylyl Cyclase. *J. Biol. Chem.* **2018**, *293* (5), 1850–1864. https://doi.org/10.1074/jbc.RA117.000457.
(122) Lamothe, M.; Chang, F.-J.; Balashova, N.; Shirokov, R.; Beuve, A. Functional Characterization of Nitric Oxide and YC-1 Activation of Soluble Guanylyl Cyclase: Structural Implication for the YC-1 Binding Site? *Biochemistry* **2004**, *43* (11), 3039–3048. https://doi.org/10.1021/bi0360051.
(123) Yazawa, S.; Tsuchiya, H.; Hori, H.; Makino, R. Functional Characterization of Two Nucleotide-Binding Sites in Soluble Guanylate Cyclase*. *J. Biol. Chem.* **2006**, *281* (31), 21763–21770. https://doi.org/10.1074/jbc.M508983200.
(124) Mota, F.; Allerston, C. K.; Hampden-Smith, K.; Garthwaite, J.; Selwood, D. L. Surface Plasmon Resonance Using the Catalytic Domain of Soluble Guanylate Cyclase Allows the Detection of Enzyme Activators. *Bioorg. Med. Chem. Lett.* **2014**, *24* (4), 1075–1079. https://doi.org/10.1016/j.bmcl.2014.01.015.
(125) Agulló, L.; Buch, I.; Gutiérrez-de-Terán, H.; Garcia-Dorado, D.; Villà-Freixa, J. Computational Exploration of the Binding Mode of Heme-Dependent Stimulators into the Active Catalytic Domain of Soluble Guanylate Cyclase. *Proteins* **2016**, *84* (10), 1534–1548. https://doi.org/10.1002/prot.25096.
(126) Sayed, N.; Baskaran, P.; Ma, X.; van den Akker, F.; Beuve, A. Desensitization of Soluble Guanylyl Cyclase, the NO Receptor, by S-Nitrosylation. *Proc. Natl. Acad. Sci.* **2007**, *104* (30), 12312–12317. https://doi.org/10.1073/pnas.0703944104.

(127) Fernhoff, N. B.; Derbyshire, E. R.; Underbakke, E. S.; Marletta, M. A. Heme-Assisted *S*-Nitrosation Desensitizes Ferric Soluble Guanylate Cyclase to Nitric Oxide. *J. Biol. Chem.* **2012**, *287* (51), 43053–43062. https://doi.org/10.1074/jbc.M112.393892.
(128) Crassous, P.-A.; Couloubaly, S.; Huang, C.; Zhou, Z.; Baskaran, P.; Kim, D. D.; Papapetropoulos, A.; Fioramonti, X.; Durán, W. N.; Beuve, A. Soluble Guanylyl Cyclase Is a Target of Angiotensin II-Induced Nitrosative Stress in a Hypertensive Rat Model. *Am. J. Physiol.-Heart Circ. Physiol.* **2012**, *303* (5), H597–H604. https://doi.org/10.1152/ajpheart.00138.2012.
(129) Meisburger, S. P.; Thomas, W. C.; Watkins, M. B.; Ando, N. X-Ray Scattering Studies of Protein Structural Dynamics. *Chem. Rev.* **2017**, *117* (12), 7615–7672. https://doi.org/10.1021/acs.chemrev.6b00790.
(130) Skou, S.; Gillilan, R. E.; Ando, N. Synchrotron-Based Small-Angle X-Ray Scattering of Proteins in Solution. *Nat. Protoc.* **2014**, *9* (7), 1727–1739. https://doi.org/10.1038/nprot.2014.116.

Chapter 2

Role of the Coiled-Coil Domain in Allosteric Activity Regulation in Soluble Guanylate Cyclase

Summary

Soluble guanylate cyclase (sGC) is the primary nitric oxide (NO) receptor in higher eukaryotes, including humans. NO-dependent signaling via sGC is associated with important physiological effects in the vascular, pulmonary, and neurological systems; and sGC itself is an established drug target for the treatment of pulmonary hypertension due to its central role in vasodilation. Despite isolation in the late 1970s, high-resolution structural information on full-length sGC remained elusive until recent cryo-electron microscopy structures were determined of the protein in both the basal unactivated state and the NO-activated state. These structures revealed large-scale conformational changes upon activation that appear to be centered on rearrangements within the coiled-coil (CC) domains in the enzyme. Here, a structure-guided approach was used to engineer constitutively unactivated and constitutively activated sGC variants through mutagenesis of the CC domains. These results demonstrate that the activation-induced conformational change in the CC domains is necessary and sufficient for determining the level of sGC activity.

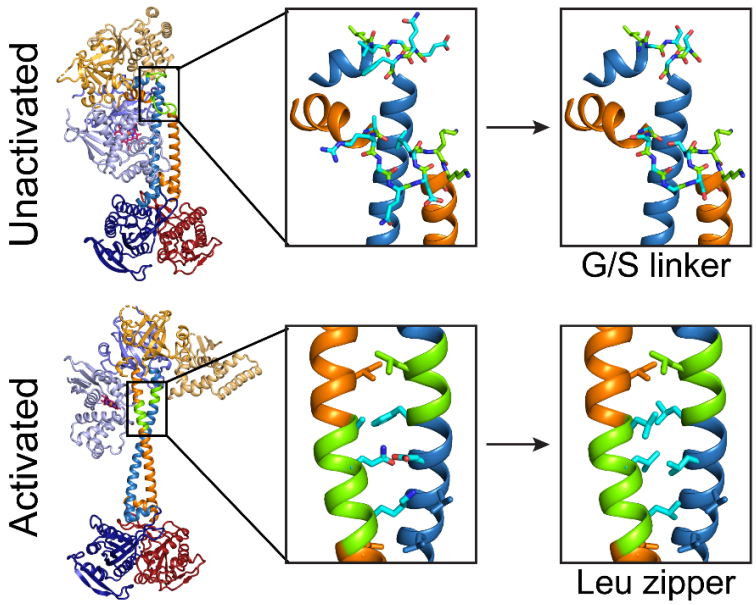

This work was carried out in collaboration with Dr. Elizabeth C. Wittenborn, Dr. William C. Thomas, Erika S. Wirachman, and Dr. Yang Wu in the lab of Prof. Michael A. Marletta. E.C.W., W.C.T., and K.A.H. designed research. E.C.W., K.A.H., and E.S.W. cloned, expressed, and purified proteins. E.C.W., W.C.T., K.A.H., and Y.W. performed research. E.C.W. and W.C.T. performed data analysis. This work led to the following publication: Wittenborn, E. C.; Thomas, W. C.; Houghton, K. A.; Wirachman, E. S.; Wu, Y.; Marletta, M. A. Role of the Coiled-Coil Domain in Allosteric Activity Regulation in Soluble Guanylate Cyclase. *Biochemistry* 2023, *62* (10), 1568–1576. https://doi.org/10.1021/acs.biochem.3c00052.

Introduction

Nitric oxide (NO) is a freely diffusible, biological signaling molecule that plays a variety of physiological roles across domains of life; and in humans and other higher eukaryotes NO is involved in regulating vasodilation, platelet aggregation, and neurotransmission.[1–7] The central NO receptor in these processes is the enzyme soluble guanylate cyclase (sGC), which catalyzes the conversion of guanosine triphosphate (GTP) to the secondary messenger cyclic guanosine monophosphate (cGMP).[8] cGMP regulates the activity of downstream effectors, including kinases, ion channels, and phosphodiesterases, leading to the physiological responses mentioned above. Defects in this NO-dependent signaling pathway are associated with several disease pathologies, and sGC has proven to be a successful drug target for the treatment of pulmonary hypertension through the action of small molecular stimulators such as the drug riociguat (Adempas®), which was approved by the US FDA in 2013.[9]

sGC is a heme-containing enzyme that exhibits an NO-dependent increase in specific activity. Most studies report on the increase in activity from the unliganded (basal) state to that observed after treatment of the enzyme with an excess of NO (xsNO). Others have investigated the changes in activity observed between 1) the unliganded state, 2) a state containing a single molar equivalent of NO relative to the heme concentration (1-NO), and 3) the excess NO state.[10–12] Of further note, the activity observed between the 1-NO state and the excess NO state is freely reversible, leading us to speculate that these two forms are important physiological contributors to activity.[11,12] A single molar equivalent of NO (1-NO) leads to a relatively modest ~4 – 5-fold increase in activity, while the presence of a molar excess of NO (xsNO) results in an additional ~5-50-fold increase over the 1-NO activity level.[10–13] In the 1-NO state, NO binds to the heme cofactor forming a five-coordinate Fe^{2+}-NO adduct,[14,15] and this ligation state is maintained upon addition of excess NO. The mechanism of further activation is unknown, although it has been suggested that cysteine residues may play a role in conferring maximal activity in the excess NO state.[12,16] Notably, the 1-NO state has been suggested to be the physiological resting state of sGC based on estimates of the K_d for NO from the heme (low pM range)[17] and the intracellular NO concentration (100–5000 pM).[18] Thus, in cells, sGC likely cycles between the 1-NO and excess NO states. In addition to the presence of excess NO, high activity can also be attained, both *in vitro* and *in vivo*, by addition of small molecule stimulators such as the benzylindazol derivative YC-1 to the 1-NO state of sGC.[12,19,20] Indeed, YC-1 has served as the starting point for development of sGC-targeted drugs, including riociguat.[9,21–24]

sGC is heterodimeric and composed of homologous α and β subunits that each contain four distinct domains: an N-terminal heme nitric oxide/oxygen binding (H-NOX) domain, a Per-Arnt-Sim (PAS) domain, a coiled-coil (CC) domain, and a C-terminal catalytic (CAT) domain. Despite this homology, only the β H-NOX domain binds a heme cofactor and is the site which binds the first equivalent of NO.[25–28] The α H-NOX domain contains an N-terminal extension that partially occupies the heme binding site, prohibiting heme incorporation.[29] The overall structure and domain arrangement of sGC has been revealed by single-particle cryo-electron microscopy (cryo-EM).[29–31] The protein is an elongated particle consisting of two distinct lobes connected by a stalk-like density. The larger of the two lobes contains a central α/β PAS dimer flanked by the two H-NOX domains and has been termed the regulatory lobe.[29–31] The stalk-like connector region contains the CC domains and connects to the smaller globular lobe, which contains the α/β CAT

dimer and has thus been termed the catalytic lobe.[29–31] Recent, high-resolution cryo-EM structures of sGC from *Homo sapiens* (*Hs*, human) and *Manduca sexta* (*Ms*, tobacco hawk moth) revealed dramatic conformational changes that take place upon enzyme activation (Figure 2.1).[29,30] In the unliganded, unactivated state, sGC adopts a contracted conformation that appears to be achieved through an unexpected bending of the CC domains (highlighted in green in Figure 2.1). Upon activation, the protein extends, and the regulatory lobe rotates ~70° relative to the catalytic lobe (Figure 2.1). In the activated state, the portions of the CC domains that were bent in the unactivated state straighten to form two long helices that extend from the PAS dimer to the CAT dimer (Figure 2.1). This large-scale conformational change is coupled to rearrangements in the CAT domains that open up the active site to allow for GTP binding.[29,30]

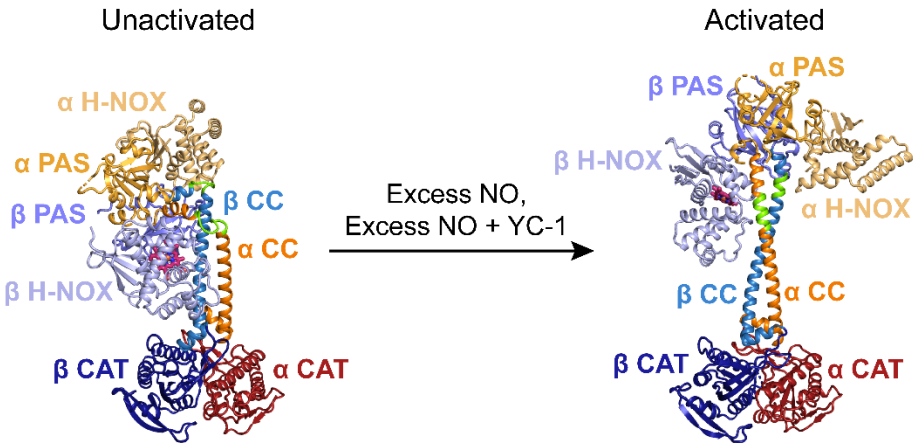

Figure 2.1. sGC undergoes a large-scale conformational change upon activation. Protein is shown in ribbon representation and colored by domain. The regions of the CC domains that straighten upon activation are highlighted in green. Heme is shown as sticks with C in pink, N in blue, O in red, and Fe in orange. PDB IDs: 6JT0 (unactivated) and 6JT2 (activated).[29]

Given that there is no direct contact between the N-terminal regulatory lobe and the C-terminal catalytic lobe, straightening of the CC domains appears to be a critical contributor to allosteric communication through the protein. In one of the cryo-EM studies, constitutive breaks in one or the other of the CC helices were engineered by the introduction of proline residues (α-D423P or β-G356P) in the bent region of the unactivated *Hs* sGC CCs.[29] NO-dependent activation was severely impaired in both variants, although the activity of the α-D423P variant in the activated, excess NO state still more than doubled relative to the unliganded, unactivated state.[29] These observations are consistent with independent mutagenesis and molecular dynamics simulations, which had suggested crosstalk between the CC domains and both the β H-NOX and CAT domains, respectively.[32,33]

The cryo-EM analysis of *Ms* sGC revealed an interesting connection between the CC conformation and the sGC stimulator YC-1. YC-1 was included in the cryo-EM sample along with excess NO to stabilize the fully activated conformation of the protein.[30] Electron density consistent with the size and shape of YC-1 was observed between the β H-NOX and α CC domains in the structure of activated *Ms* sGC.[30] This structure and ensuing higher resolution structures of *Hs* sGC with YC-1[34] revealed that the YC-1 density is adjacent to the region of the α CC domain that is

bent in the unactivated state.[34,35] This observation underscores the importance of the CC domains in sGC activity, and it has been proposed that the mechanism of YC-1 and related stimulators might be to stabilize the straightened conformation of the CC domains.[34,35] Indeed, YC-1 has been shown to have only a minimal effect on the unliganded, unactivated state of sGC, whereas it stimulates the 1-NO state to a high level of activity.[12,20,30] The 1-NO state is thought to exist as an equilibrium between the bent, unactivated conformation of sGC and a partially extended conformation,[30] and YC-1 may serve to shift this equilibrium by initially binding to the partially extended state and stabilizing it in the fully extended state.

To provide further insight into the role of the CC domains in the activation mechanism of sGC, we have used structure-guided mutagenesis within these domains of *Ms* sGC to generate 1) sGC variants with constitutively unstraightened CC domains, and 2) an sGC variant with constitutively straight CC domains. The activity profiles of these variants have been measured under different ligation states – unliganded, 1-NO, xsNO, and 1-NO + YC-1 – to determine the effect of CC conformation on sGC activity.

Materials and Methods

Materials

All chemicals were purchased from commercial vendors and used without further purification. Primers were purchased from Integrated DNA Technologies (Coralville, IA). Gibson-like Master Mix was purchased from the QB3 MacroLab (Berkeley, CA). PrimeSTAR Max Premix was purchased from Takara Bio USA (Mountain View, CA). DNA purification kits were purchased from Qiagen (Germantown, MD). Sf9 cells were purchased from Novagen (Madison, WI). ExCell-420 media, DNAase 1 from bovine pancreas, β-mercaptoethanol, sodium phosphate dibasic (Na_2HPO_4), potassium phosphate (K_2HPO_4), sodium dithionite ($Na_2S_2O_4$), guanosine 5'-triphosphate sodium salt (GTP) (>95%, HPLC), sodium carbonate (Na_2CO_3), and zinc acetate ($Zn(CH_3CO_2)_2$) were purchased from Merck (Darmstadt, Germany). 4-(2-hydroxyethyl)piperazine-1-ethanesulfonic acid (HEPES) and Zeba spin desalting columns were purchased from ThermoFisher Scientific (Waltham, MA). 4-(2-aminoethyl)benzenesulfonyl fluoride hydrochloride (AEBSF) was purchased from Research Products International (Mount Prospect, IL). Benzamidine, glycerol, sodium chloride (NaCl), and magnesium chloride ($MgCl_2$) were purchased from VWR Life Science (Visalia, CA). Dithiothreitol (DTT) was purchased from Bachem (Bubendorf, Switzerland). Imidazole was purchased from Oakwood Chemical (West Columbia, SC). Triethanolamine (TEA) was purchased from Spectrum Chemical (Gardena, CA). TALON Superflow resin was purchased from Cytiva (Marlborough, MA). Vivaspin 500 (30,000 MWCO) spin concentrators were purchased from Sartorius (Fremont, CA). PROLI NONOate was purchased from Cayman Chemical Company (Ann Arbor, MI).

Mutagenesis and Generation of Expression Constructs

Wild type (WT) *Ms* sGC constructs were generated previously in the pFastBac vector (Bac-to-Bac Baculovirus Expression System) and were termed pFastBac_Ms_sGC_α1_His6 and pFastBac_Ms_sGC_β1 for the α and β subunits, respectively.[30] The α subunit gene was appended with the sequence for a C-terminal hexa-histidine tag. In the present work, mutagenesis was performed by PCR to generate mutant gene fragments, which were then re-cloned into the

linearized pFastBac vector using Gibson assembly. Constructs were validated by Sanger sequencing at the UC Berkeley DNA Sequencing Facility.

Plasmids were transformed into DH10Bac-GFP E. coli cells to allow for transposition into baculovirus bacmids. Bacmids were isolated from successful transposants and the sGC genes were amplified by PCR and sequenced for validation. Bacmids were then transfected into Sf9 insect cells to generate recombinant baculoviruses. Baculoviruses containing the α and β subunits were amplified separately on 300-mL scales prior to co-infection for protein expression cultures.

Variant Structure Prediction

For all three constructs, structural prediction was performed using AlphaFold2[36] via ColabFold.[37] 5-rank default model parameters were used with a template date cutoff of July 7, 2022. No major differences were observed between models of different rank in structured regions, and so unrelaxed rank 1 models were subsequently analyzed for each variant. Prediction confidence (pLDDT score) was used as a tool for assessing potential structural stabilization or destabilization.

Protein Expression and Purification

Protein was expressed in Sf9 insect cells at 27 °C with shaking at 130 rpm. Sf9 cultures were infected with 50 mL/L of amplified α and β viruses (100 mL of total virus per L) and grown for 72 h. Cells were harvested by centrifugation at 4,300 g for 20 min, flash frozen in liquid nitrogen, and stored at −80 °C.

Protein was purified as described previously.[30] All steps were performed at 4 °C, unless otherwise noted. Briefly, cell pellets were thawed in a room temperature water bath and resuspended in Buffer A (50 mM K_2HPO_4, 200 mM NaCl, 1 mM imidazole, 1 mM benzamidine, 5% (v/v) glycerol, 5 mM β-mercaptoethanol, pH 8) supplemented with 10 mM benzamidine, 1 mM AEBSF, 0.5 mM DNase I. Cells were lysed by 3 rounds of bead beating for 20 s intervals with 1 min rests in between. Beads were removed by centrifugation at 2,800 g for 5 min. Lysate was clarified by centrifugation at 158,000 g for 2 h. Lysate was applied to a 2 mL TALON superflow column at 0.5 mL/min using a BioLogic LP low-pressure chromatography system. The column was washed with 20 column volumes (CV) Buffer A. Protein was eluted with 10 CV Buffer B (50 mM K_2HPO_4, 200 mM NaCl, 125 mM imidazole, 1 mM benzamidine, 5% (v/v) glycerol, 5 mM β-mercaptoethanol, pH 8) and 2 mL fractions were collected. Fractions containing sGC were concentrated to < 1 mL, supplemented with 5 mM DTT and 1 mM EDTA, and stored on ice at 4 °C overnight. The sample was then diluted to 10 mL with Buffer C (25 mM TEA, 25 mM NaCl, 5% (v/v) glycerol, 5 mM DTT, pH 7.4) and applied to a POROS HQ2 anion exchange column at 0.5 mL/min using an ÄKTA pure chromatography system. The column was washed with 3 CV Buffer C and then a gradient up to 50% Buffer D (25 mM TEA, 750 mM NaCl, 5% (v/v) glycerol, 5 mM DTT, pH 7.4) was developed over 17 CV. Fractions were analyzed by SDS-PAGE and those containing purified sGC were concentrated before drop freezing and storage in liquid nitrogen.

Activity Assays and cGMP Quantification.

Samples were handled inside of a Coy anaerobic chamber. Protein was thawed at 4 °C, incubated with 10 mM sodium dithionite for 15 min to fully reduce the heme cofactor, and then desalted over a Zeba spin desalting column pre-equilibrated with Buffer E (50 mM HEPES, 150 mM NaCl, 5% glycerol, pH 7.5). Ultraviolet-visible (UV-Vis) absorption spectra of the unliganded sample were

recorded using a NanoDrop 2000c microvolume spectrophotometer. The protein concentration was determined using the Soret peak of the reduced heme (λ_{max} = 433 nm, ε_{434} = 149,000 $M^{-1}cm^{-1}$).[30,38] An aliquot of unliganded protein was reserved for the activity assay. To the remaining protein, PROLI NONOate was spiked in (0.75 µL 30 mM PROLI NONOate added to ~30 µL samples; ~1 mM PROLI NONOate working concentration) to generate the xsNO state and UV-Vis spectra were recorded. The concentration of the xsNO state was assumed to be nominally the same as the unliganded state. Protein was then desalted into Buffer E to obtain the 1-NO state and UV-Vis spectra were recorded. The concentration of the 1-NO state was determined by comparison of the A_{399} Soret peak of the Fe^{2+}–NO species to that of the xsNO sample.

Activity assays were conducted at 25 °C in Buffer E supplemented with 5 mM DTT and 3 mM $MgCl_2$. Assays were conducted at enzyme concentrations of 20, 30, or 10 nM holo protein for the WT, GSG, and Leu zipper variants, respectively. YC-1 (150 µM) or PROLI NONOate (150 µM) were added as necessary to generate the 1-NO + YC-1 and xsNO states, respectively. Reactions were initiated by addition of 1.5 mM GTP and timepoints were quenched 1:4 (v:v) into 125 mM zinc acetate. The pH of the quenched reaction samples was then adjusted by addition of an equal volume of 125 mM sodium carbonate. Samples were stored at −80 °C.

Quenched assay samples were thawed at room temperature and the zinc precipitate was removed by centrifugation at 30,130 g for 5 minutes at room temperature. Samples were diluted and cGMP was quantified using a cGMP enzyme-linked immunosorbent assay (ELISA) following the manufacturer's instructions (Enzo Life Sciences). Initial rates were calculated from the linear regions of the time course where <10% of the GTP substrate was consumed.

Small-angle X-ray Scattering

Small-angle X-ray scattering (SAXS) was performed under anaerobic conditions on *Ms* sGC(GSG2) at the MacChess BioSAXS beamline (Sector 7B) at the Cornell High-Energy Synchrotron Source, Ithaca, New York.[39,40] 30 µL of sGC was reduced in an anaerobic glovebox, then exchanged into SAXS assay buffer (50 mM HEPES pH 7.5, 150 mM NaCl, 1% glycerol, 1 mM TCEP). After confirming heme reduction via UV/vis spectrophotometry, 40 µL of 3.9 µM sample was injected directly into an anaerobic flow cell operating in batch mode. Data were collected using a Dectris PILATUS3 × 2M detector at 4 °C. 20 x 1s X-ray exposures were collected. Scattering images were integrated about the beam center and normalized by transmitted intensities measured on a photodiode beamstop. The integrated protein scattering profile, $I(q)$, was produced by subtraction of background buffer scattering from the protein solution scattering using an exact buffer match. The X-ray wavelength was set at λ = 1.1018 Å and the sample-to-detector distance was 1713 mm, as determined by silver behenate calibration. Scattering was collected over a range of q = 0.01 $Å^{-1}$ to 0.48 $Å^{-1}$, where q is the scattering vector $q = 4\pi\sin\theta/\lambda$ and 2θ is the scattering angle. Data processing, analysis, and comparison to published WT *Ms* sGC[31] were performed in BioXTAS RAW using established protocol.[41] Radii of gyration (R_g) were estimated with Guinier analysis, and pair distance distribution analysis was performed in GNOM.[42] Error bars associated with R_g values are curve-fitting uncertainties from Guinier analysis. The predicted scattering of unactivated WT *Ms* sGC was calculated from the experimental unactivated structure PDB ID 6PAS using Crysol.[42] Difference scattering was calculated in Primus.[42]

Results and Discussion

Constitutively Unactivated sGC Variants.

The bent regions of the CC domains in *Ms* sGC are residues α-420–426 (sequence: ARAQDGL) and β-346–350 (sequence: MSEQF). To generate sGC variants with constitutively unstraightened CC domains these residues were replaced with glycine-serine (GS) repeats. Such GS repeats are widely used as linkers in recombinant protein engineering to spatially separate functional regions of a protein construct, and are chosen due to their inherent conformational flexibility.[43–45] Thus, we hypothesized that substitution of the native sequences in the bent regions of the CCs with GS repeats would prevent secondary structure formation and straightening of the CCs. Two *Ms* sGC α constructs were made, one in which the entire bent region was replaced (ARAQDGL → GSGGSGS) and the other, a more conservative construct, in which only part of this region was altered (AR<u>AQD</u>GL → AR<u>GSG</u>GL, changes underlined). A single *Ms* sGC β construct was used in which the entire region was changed (MSEQF → GSGSG). Two final protein variants were made using these constructs: the variant containing α-GSGGSGS/β-GSGSG will be referred to as *Ms* sGC(GSG1), and that containing α-GSG/β-GSGSG is termed *Ms* sGC(GSG2). AlphaFold2 models were determined for WT *Ms* sGC and both GSG variants to help predict structural characteristics.[36,37] Although a WT experimental structure exists,[30] a prediction was produced for comparative analysis. For WT and both variants, AlphaFold2 predicts an activated, straightened CC conformation that is similar to experimental structures (Figure A.1A-C). For the GSG variants, however, the residues in and around the mutated region exhibit decreased predictive confidence scores (pLDDT), particularly for the GSG1 variant, suggesting a lower propensity for the predicted secondary structure (Figure A.1A-C, Table A.1). While AlphaFold2 is not designed to be predictive of structural changes induced by site-directed mutagenesis,[46] the lower pLDDT in the GSG variants suggests a shift away from structural elements found in stable CC domains in the AlphaFold2 training dataset, i.e., in experimental structures of CC domains. Thus, the results of this prediction support the destabilizing effect expected from engineering GS repeats into the CC domain.

Both GSG variants co-purify as two bands of relatively equal intensity by SDS-PAGE, indicative of heterodimer formation (Figure A.2A,B). They also exhibit UV-Vis absorption spectra with Soret maxima at 433 nm for the Fe^{2+} unliganded species, as reported previously for WT *Ms* sGC (Figure 2.2A,B).[30,38] Unlike the WT protein, a shoulder on the Soret band centered at ~426 nm is also apparent in both spectra (Figure 2.2A,B). The cause of this shoulder is unknown, although a Soret band at 426 nm has been previously reported for reconstituted human sGC[47] and for truncations of rat sGC[27]. The ratio of absorbances at 433 nm and 280 nm was used to estimate the heme incorporation for each variant relative to that observed for the WT enzyme. For typical preparations of WT *Ms* sGC, $A_{433}/A_{280} = 0.85$.[30] This ratio is 0.47 and 0.64 for *Ms* sGC(GSG1) and *Ms* sGC(GSG2), respectively, reflecting heme incorporations of ~55% and 75% of WT levels, respectively. The Soret maxima of the variants shift to 399 nm upon NO binding, consistent with formation of the five-coordinate Fe^{2+}–NO species (Figure 2.2A,B).[14,15,30,38]

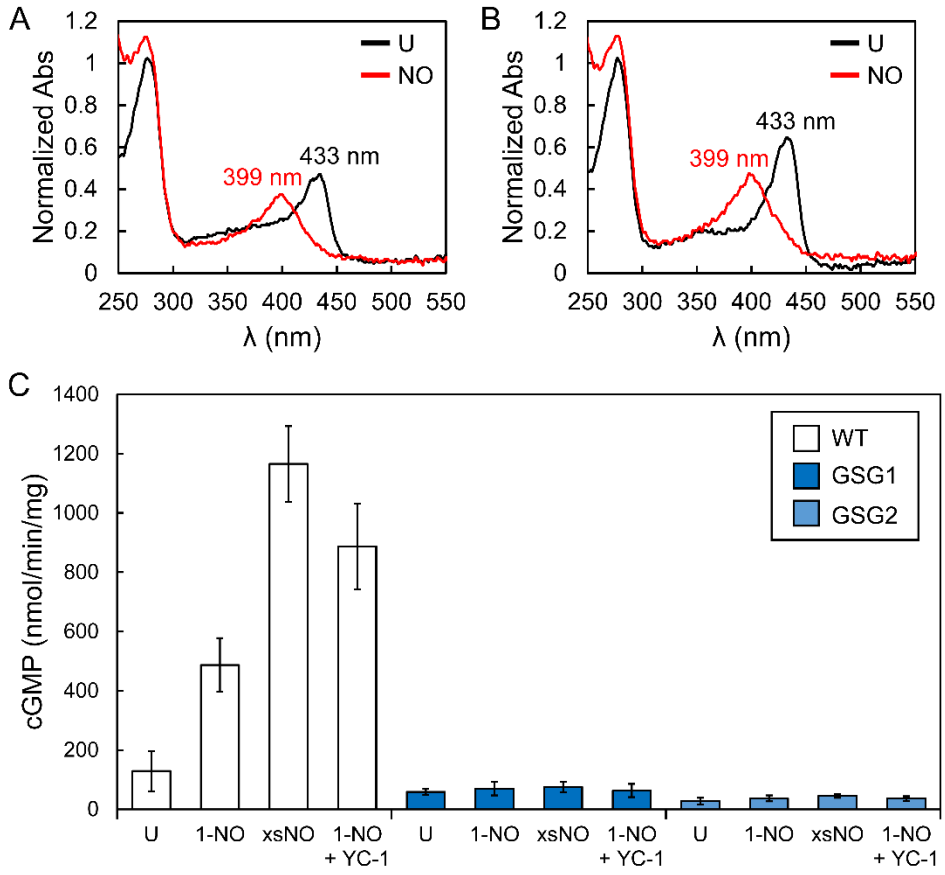

Figure 2.2. Characterization of *Ms* sGC(GSG1) and *Ms* sGC(GSG2). (A) UV-Vis absorption spectra of *Ms* sGC(GSG1). A_{433}/A_{280} = 0.47, ~55% holo protein. (B) UV-Vis absorption spectra of *Ms* sGC(GSG2). A_{433}/A_{280} = 0.64, ~75% holo protein. (C) Activity profiles of the two variants compared to WT. Average specific activities were calculated per mg of holo protein and error bars reflect one standard deviation (n = 3–4).

The activity of both variants is low (Figure 2.2C, Figure A.3). Importantly, no increase in activity is observed with any amount of added NO, suggesting that even the activity of the 1-NO state is dependent on straightening of the CC domains. This idea is consistent with previous analysis of the 1-NO state by small angle X-ray scattering (SAXS), which suggested that the 1-NO state exists as a conformational equilibrium that is best described as a mixture of the bent, unactivated conformation (72% of the population) and a partially extended conformation (28% of the population).[30] In this scenario, the activity of the 1-NO state would arise from the fraction of the sample that adopts the partially extended conformation, and when this conformation cannot be accessed, as in the *Ms* sGC(GSG1) and *Ms* sGC(GSG2) variants, the activity of the protein remains low. These results are also consistent with the previously reported activities of the α-D423P and β-G356P variants of *Hs* sGC.[29] Also notable is that YC-1 does not stimulate activity in the variants. Though it is possible that the mutations made abolish YC-1 binding entirely, there is no structural evidence that the mutated residues are directly associated with YC-1 binding.[30,34] Instead, lack of YC-1 stimulation is more consistent with the hypothesis that YC-1 interacts with and stabilizes the already straightened conformation of the α CC and that the CC domains in the variants are incapable of sampling an unbent conformation.

An alternative explanation for the low activity of *Ms* sGC(GSG1) and *Ms* sGC(GSG2) is that these variants are improperly folded or cannot dimerize properly. To test this possibility, SAXS was performed on *Ms* sGC(GSG2). SAXS is a structural technique that can be performed on a protein in solution and provides information about folding, oligomeric state, and conformational state. Sample quality and quantity limitations prevented a similar experiment on *Ms* sGC(GSG1). SAXS was performed anaerobically after the protein was reduced to the ferrous oxidation state of the heme. The SAXS profile of *Ms* sGC(GSG2) was collected without ligand bound and directly compared to that of WT *Ms* sGC reported in a previous study[30] (Figure 2.3A-B). Sample quantity prevented the use of size-exclusion-coupled chromatography SAXS (SEC-SAXS) as was previously performed for WT *Ms* sGC, and so the experimental profile shows a lower signal-to-noise scattering ratio. There is also evidence of aggregation at low *q*-value as compared to the previous study, a characteristic similarly observed in handling of WT *Ms* sGC. The aggregation component of the solution contributes to an inflated radius of gyration (R_g) for sGC(GSG2) of 54.5 ± 0.3 Å compared with 43.1 ± 0.4 for WT sGC.[30] Nonetheless, when normalized by their overall scattering intensity, the scattering of *Ms* sGC(GSG2) and WT *Ms* sGC without NO present are close matches in the mid-*q* and high-*q* regimes (Figure 2.3C). Likewise, the scattering of *Ms* sGC(GSG2) matches the calculated scattering of the unactivated WT *Ms* sGC (PDB ID 6PAS, Figure 2.3A-B, black dotted). The similarity of the scattering profiles is strong evidence that most *Ms* sGC(GSG2) in solution is folded and forms a heterodimer of a similar conformation to unactivated WT sGC. By contrast, 1-NO sGC in a partially extended conformational state was previously found to display a pronounced increase in mid-*q* scattering at ~0.07 $Å^{-1}$ not seen in *Ms* sGC(GSG2) (Figure 2.3B-C, pink). Thus, the SAXS experiment supports the conclusion that *Ms* sGC GS-linker mutants are properly folded but trapped in an unactivated conformation of the protein.

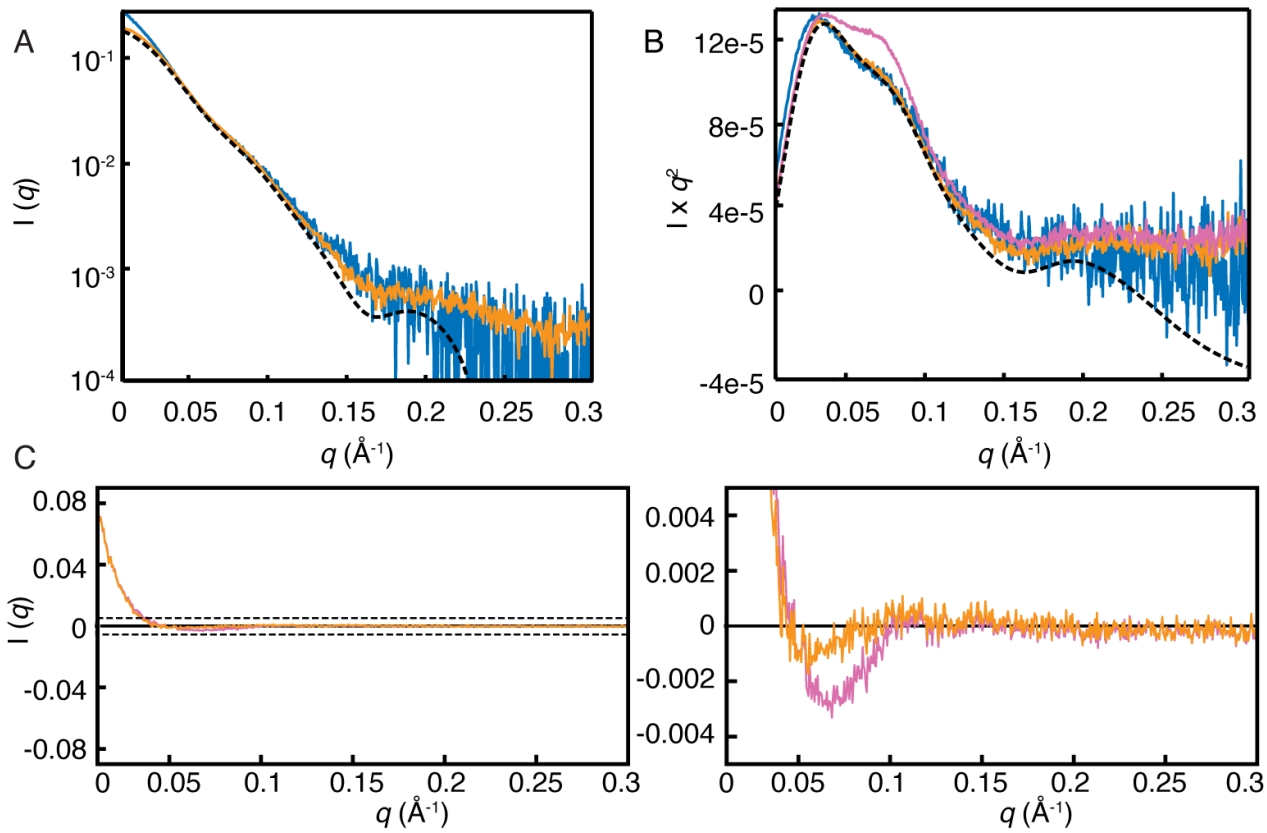

Figure 2.3. SAXS results with *Ms* sGC(GSG2). Results are consistent with a well-folded protein in an unactivated, bent conformation. (A) Semi-log SAXS profiles of *Ms* sGC(GSG2) unliganded (blue), WT unliganded *Ms* sGC (orange, from ref[30]), and the calculated scattering of the unactivated WT *Ms* sGC cryo-EM structure (black dotted, 6PAS from ref[30]). Differences in scattering at low-*q* are due to aggregation of sample. (B) The same profiles are shown in a Kratky plot to better emphasize shared mid-*q* features (blue and orange solid, black dotted). Additionally, the SAXS profile of sGC with 1-NO bound is shown with a pronounced increase in mid-*q* scattering (pink, from ref[30]). (C) Difference scattering between *Ms* sGC(GSG2) unliganded and either WT unliganded sGC (orange) or WT NO sGC (pink). The difference scattering is dominated by low-*q* aggregation (left panel), but a zoomed view (right panel) reveals that WT unliganded sGC is a better match at *q*~0.075 Å.

Constitutively Activated sGC Variant

Recent cryo-EM analysis of sGC revealed an NO-dependent conformational change centered on straightening of the CC domains. This straightening of the CCs leads to repacking of the two CC helices such that the CAT domains open to allow for GTP binding and subsequent hydrolysis.[29,30,34] Thus, to generate a constitutively activated sGC variant, we sought to stabilize the straightened conformation of the CCs. Residues along the dimer interface of the activated, straightened portion of the CC domains were changed to leucine residues to generate a leucine zipper-like motif. Leucine zippers are common structural motifs in proteins in which amphipathic α-helices dimerize via hydrophobic interactions.[48,49] Sequences of leucine zippers are typified by heptads in which every seventh residue is a leucine. These leucine residues then form the hydrophobic core of the coiled coil "zipper". We hypothesized that we could stabilize the secondary structure of the sGC CC domains in a straightened conformation by the selective introduction of leucine residues. The residue substitutions made are: α-A420L, α-Q423L, α-

R427L, β-F350L, and β-D353L; this variant will be referred to as *Ms* sGC(Leu zipper). An AlphaFold2 model was also determined for the Leu zipper variant. AlphaFold2 predicts the activated, straightened CC conformation and has an increased confidence score (pLDDT) for residues in and around the mutated CC-domain interface relative to WT, suggesting a higher likelihood for the straightened conformation (Figure A.1D, Table A.1).

Ms sGC(Leu zipper) co-purifies as two bands by SDS-PAGE, indicative of heterodimer formation (Figure A.2C). It was isolated with ~41% heme incorporation relative to WT, based on an A_{433}/A_{280} ratio of 0.35 (Figure 2.4A). The reduced variant exhibits a UV-Vis Soret maximum at 433 nm, with a slight shoulder at 426 nm, that shifts to 399 nm upon NO binding (Figure 2.4A). The activity of the variant is constitutively high and independent of ligation state (Figure 2.4B). The lack of activation by YC-1 suggests that the protein is already stabilized in the fully activated state through the introduction of the leucine zipper motif. Interestingly, when the specific activity of *Ms* sGC(Leu zipper) is calculated per milligram of holo protein, with the protein concentration estimated from the Soret absorbance at 433 nm, the activity appears unusually high (~4000 nmol cGMP/min/mg sGC) (Figure A.4). One explanation for this observation may be that the heme-containing variant, even under basal conditions, supports higher activity than the heme-containing WT under excess NO conditions due to the increased rigidity of the straightened CC domains. Alternatively, the apo variant may itself have high activity. When the total protein concentration, accounting for the 59% apo protein in the sample, is used to calculate the specific activity, the values are similar to those observed for the WT protein (~1500 nmol cGMP/min/mg sGC) (Figure 2.4B, Figure A.4). Thus, introduction of the leucine zipper motif may also exert an effect on the apo protein, rendering it constitutively active, as well.

We were unable to obtain quantities of *Ms* sGC(Leu zipper) sufficient to determine its structure by SAXS. However, heightened constitutive activity is challenging to explain by misfolding or mis-oligomerization. Instead, the combination of our biochemical data suggests that the most likely explanation for activity increase is that the mutations to the CC-domain stabilize the active conformation.

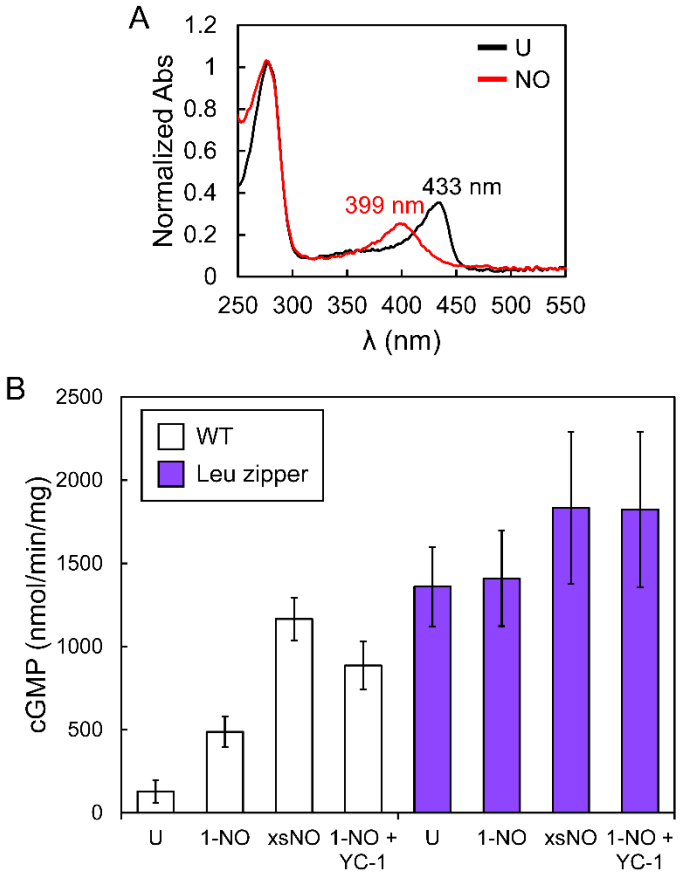

Figure 2.4. Characterization of *Ms* sGC(Leu zipper). (A) UV-Vis absorption spectra. A_{433}/A_{280} = 0.35, ~41% holo protein. (B) Activity profile of the variant compared to WT. Average specific activities were calculated per mg of total protein and error bars reflect one standard deviation (n = 3).

Heme-deficient WT Ms sGC

The three *Ms* sGC CC variants described here were found to have a lower heme content than typical preparations of the WT enzyme. To determine whether the presence of apo protein in the samples affected the observed activity profiles of the variants, we sought to obtain samples of WT *Ms* sGC with low heme incorporation. It is well known that the sGC heme dissociates more readily in the Fe^{3+} oxidized state than in the Fe^{2+} reduced state.[50,51] Therefore, to promote oxidation and subsequent heme loss, less reducing agent was used during the course of the purification. In particular, DTT was not added to the sample between the affinity and anion exchange chromatography steps, allowing for oxidation to occur during the overnight storage period between the two columns (see Methods). Following purification, the protein was reduced with sodium dithionite and the UV-Vis spectrum was recorded to assess the resulting heme content (Figure 2.5A). The A_{433}/A_{280} ratio of the reduced protein was 0.33, in contrast to the typical ratio of 0.85 for WT *Ms* sGC,[30] indicating a heme content of ~39%, relative to typical preparations of WT. The 39% holo WT protein exhibits a standard three-state activity profile, confirming that the background of apo protein does not measurably affect the relative, ligation state–dependent activity states of sGC (Figure 2.5B). Additionally, the specific activities obtained for this protein are comparable to those of typical, heme-replete WT *Ms* sGC,[30] further suggesting that the

presence of apo protein in our variant samples should not have a significant effect on the interpretation of the data.

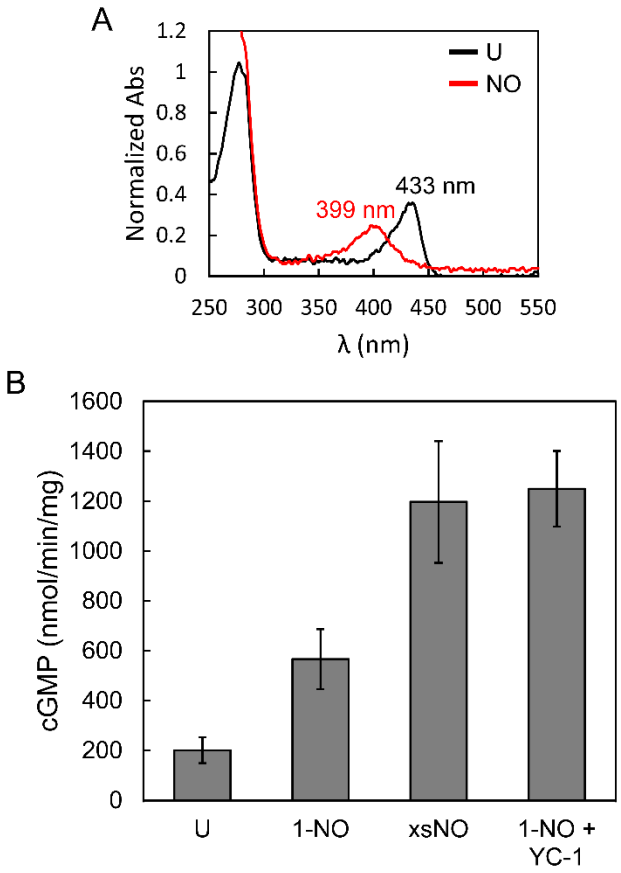

Figure 2.5. Characterization of heme-deficient WT *Ms* sGC. (A) UV-Vis absorption spectra. A_{433}/A_{280} = 0.33. (B) Activity profile of the sample. Average specific activities were calculated per mg of holo protein and error bars reflect one standard deviation (n = 3).

Conclusions

Recent high-resolution cryo-EM structures of sGC in the unactivated and activated states revealed large-scale, ligand-induced conformational changes, providing an initial structural basis for understanding allostery in this important enzyme.[29,30,34] In particular, the structures indicate that rearrangements in the CC domains may play an important role in intramolecular signal transduction: the CC domains are bent in the unactivated state and then straighten to form two long, continuous helices upon activation. Furthermore, the structures reveal an association between the straightened α CC domain and the small molecule stimulator YC-1, suggesting that this class of molecules might function by stabilizing the straightened, activated conformation of sGC. To provide insight into the significance of the sGC conformational change, structure-guided protein engineering within the CC domains has been used to generate variants with constitutively unstraightened CCs and constitutively straight CCs. To prevent CC straightening, flexible GS linker-like regions were incorporated into the bent portion of the unactivated CCs. These variants

retain a basal level of activity regardless of ligation state, highlighting the functional relevance of these domains in activation. A SAXS experiment provides further evidence that this basal activity is a result of folded, dimeric protein trapped in a conformation that closely resembles that of unactivated WT sGC.

To promote formation of constitutively straight CCs, a leucine zipper motif was engineered into the CC dimer interface of the activated conformation. The leucine zipper variant exhibits constitutively high levels of activity, indicating that stabilization of the straightened CCs does indeed promote activation. Throughout our investigations, sGC activity variants expressed poorly via insect cells and with reduced heme incorporation, creating significant hurdles to structural and biochemical analysis. Indeed, we hypothesize that the leucine zipper variant's particularly poor expression may be because its constitutive cyclase activity is toxic to insect cells. However, the design principles used for these activity variants can be extended to sGCs from other organisms and expression systems, creating an opportunity for future work utilizing engineered activity variant orthologs to better understand sGC structure and activation.

This work represents an important structure-based investigation of allostery in sGC and suggests that straightening of the CC domains is necessary and sufficient for full enzyme activation. Additionally, the lack of activation by YC-1 in any of the variants supports the hypothesis that YC-1 binds to and stabilizes the straightened conformation of the α CC domain, a finding that may aid in the development of new sGC-targeted drugs.

Acknowledgements

This work is based upon research conducted at the Center for High Energy X-ray Sciences (CHEXS), which is supported by the National Science Foundation under Award DMR-1829070, and the Macromolecular Diffraction at CHESS (MacCHESS) facility, which is supported by Award 1-P30-GM124166-01A1 from the National Institute of General Medical Sciences, National Institutes of Health, and by New York State's Empire State Development Corporation (NYSTAR).

References

(1) Bohlen, H. G. Nitric Oxide and the Cardiovascular System. *Comprehensive Physiology* **2015**, *5*, 803–828. https://doi.org/10.1002/cphy.c140052.

(2) Steinert, J. R.; Chernova, T.; Forsythe, I. D. Nitric Oxide Signaling in Brain Function, Dysfunction, and Dementia. *The Neuroscientist* **2010**, *16* (4), 435–452. https://doi.org/10.1177/1073858410366481.

(3) Buys, E.; Sips, P. New Insights into the Role of Soluble Guanylate Cyclase in Blood Pressure Regulation. *Current Opinion in Nephrology and Hypertension* **2014**, *23* (2), 135–142. https://doi.org/10.1097/01.mnh.0000441048.91041.3a.

(4) Stasch Johannes-Peter; Pacher Pál; Evgenov Oleg V. Soluble Guanylate Cyclase as an Emerging Therapeutic Target in Cardiopulmonary Disease. *Circulation* **2011**, *123* (20), 2263–2273. https://doi.org/10.1161/CIRCULATIONAHA.110.981738.

(5) Ben Aissa, M.; H. Lee, S.; M. Bennett, B.; R.J. Thatcher, G. Targeting NO/cGMP Signaling in the CNS for Neurodegeneration and Alzheimer's Disease. *Current Medicinal Chemistry* **2016**, *23* (24), 2770–2788. https://doi.org/10.2174/0929867323666160812145454.

(6) Ghosh, A.; Koziol-White, C. J.; Asosingh, K.; Cheng, G.; Ruple, L.; Groneberg, D.; Friebe, A.; Comhair, S. A. A.; Stasch, J.-P.; Panettieri, R. A.; Aronica, M. A.; Erzurum, S. C.; Stuehr, D. J. Soluble Guanylate Cyclase as an Alternative Target for Bronchodilator Therapy in Asthma. *Proc Natl Acad Sci USA* **2016**, *113* (17), E2355–E2362. https://doi.org/10.1073/pnas.1524398113.

(7) Papapetropoulos, A.; Simoes, D. C. M.; Xanthou, G.; Roussos, C.; Gratziou, C. Soluble Guanylyl Cyclase Expression Is Reduced in Allergic Asthma. *American Journal of Physiology-Lung Cellular and Molecular Physiology* **2006**, *290* (1), L179–L184. https://doi.org/10.1152/ajplung.00330.2005.

(8) Arnold, W. P.; Mittal, C. K.; Katsuki, S.; Murad, F. Nitric Oxide Activates Guanylate Cyclase and Increases Guanosine 3':5'-Cyclic Monophosphate Levels in Various Tissue Preparations. *Proceedings of the National Academy of Sciences* **1977**, *74* (8), 3203–3207. https://doi.org/10.1073/pnas.74.8.3203.

(9) Conole, D.; Scott, L. J. Riociguat: First Global Approval. *Drugs* **2013**, *73* (17), 1967–1975. https://doi.org/10.1007/s40265-013-0149-5.

(10) Russwurm, M.; Koesling, D. NO Activation of Guanylyl Cyclase. *EMBO J* **2004**, *23* (22), 4443–4450. https://doi.org/10.1038/sj.emboj.7600422.

(11) Cary, S. P. L.; Winger, J. A.; Marletta, M. A. Tonic and Acute Nitric Oxide Signaling through Soluble Guanylate Cyclase Is Mediated by Nonheme Nitric Oxide, ATP, and GTP. *PNAS* **2005**, *102* (37), 13064–13069. https://doi.org/10.1073/pnas.0506289102.

(12) Fernhoff, N. B.; Derbyshire, E. R.; Marletta, M. A. A Nitric Oxide/Cysteine Interaction Mediates the Activation of Soluble Guanylate Cyclase. *Proceedings of the National Academy of Sciences* **2009**, *106* (51), 21602–21607. https://doi.org/10.1073/pnas.0911083106.

(13) Emmons, T. L.; Mathis, K. J.; Shuck, M. E.; Reitz, B. A.; Curran, D. F.; Walker, M. C.; Leone, J. W.; Day, J. E.; Bienkowski, M. J.; Fischer, H. D.; Tomasselli, A. G. Purification and Characterization of Recombinant Human Soluble Guanylate Cyclase Produced from Baculovirus-Infected Insect Cells. *Protein Expression and Purification* **2009**, *65* (2), 133–139. https://doi.org/10.1016/j.pep.2009.01.001.

(14) Gerzer, R.; Böhme, E.; Hofmann, F.; Schultz, G. Soluble Guanylate Cyclase Purified from Bovine Lung Contains Heme and Copper. *FEBS Letters* **1981**, *132* (1), 71–74. https://doi.org/10.1016/0014-5793(81)80429-2.

(15) Stone, J. R.; Marletta, M. A. Soluble Guanylate Cyclase from Bovine Lung: Activation with Nitric Oxide and Carbon Monoxide and Spectral Characterization of the Ferrous and Ferric States. *Biochemistry* **1994**, *33* (18), 5636–5640. https://doi.org/10.1021/bi00184a036.

(16) Alapa, M.; Cui, C.; Shu, P.; Li, H.; Kholodovych, V.; Beuve, A. Selective Cysteines Oxidation in Soluble Guanylyl Cyclase Catalytic Domain Is Involved in NO Activation. *Free Radical Biology and Medicine* **2021**, *162*, 450–460. https://doi.org/10.1016/j.freeradbiomed.2020.11.001.

(17) Zhao, Y.; Brandish, P. E.; Ballou, D. P.; Marletta, M. A. A Molecular Basis for Nitric Oxide Sensing by Soluble Guanylate Cyclase. *Proceedings of the National Academy of Sciences* **1999**, *96* (26), 14753–14758. https://doi.org/10.1073/pnas.96.26.14753.

(18) Hall, C. N.; Garthwaite, J. What Is the Real Physiological NO Concentration in Vivo? *Nitric Oxide* **2009**, *21* (2), 92–103. https://doi.org/10.1016/j.niox.2009.07.002.

(19) Ko, F.-N.; Wu, C.-C.; Kuo, S.-C.; Lee, F.-Y.; Teng, C.-M. YC-1, a Novel Activator of Platelet Guanylate Cyclase. *Blood* **1994**, *84* (12), 4226–4233. https://doi.org/10.1182/blood.V84.12.4226.

(20) Friebe, A.; Schultz, G.; Koesling, D. Sensitizing Soluble Guanylyl Cyclase to Become a Highly CO-Sensitive Enzyme. *The EMBO Journal* **1996**, *15* (24), 6863–6868. https://doi.org/10.1002/j.1460-2075.1996.tb01078.x.
(21) Stasch, J.-P.; Becker, E. M.; Alonso-Alija, C.; Apeler, H.; Dembowsky, K.; Feurer, A.; Gerzer, R.; Minuth, T.; Perzborn, E.; Pleiß, U.; Schröder, H.; Schroeder, W.; Stahl, E.; Steinke, W.; Straub, A.; Schramm, M. NO-Independent Regulatory Site on Soluble Guanylate Cyclase. *Nature* **2001**, *410* (6825), 212–215. https://doi.org/10.1038/35065611.
(22) Nakai, T.; Perl, N. R.; Barden, T. C.; Carvalho, A.; Fretzen, A.; Germano, P.; Im, G.-Y. J.; Jin, H.; Kim, C.; Lee, T. W.-H.; Long, K.; Moore, J.; Rohde, J. M.; Sarno, R.; Segal, C.; Solberg, E. O.; Tobin, J.; Zimmer, D. P.; Currie, M. G. Discovery of IWP-051, a Novel Orally Bioavailable sGC Stimulator with Once-Daily Dosing Potential in Humans. *ACS Med. Chem. Lett.* **2016**, *7* (5), 465–469. https://doi.org/10.1021/acsmedchemlett.5b00479.
(23) Tobin, J. V.; Zimmer, D. P.; Shea, C.; Germano, P.; Bernier, S. G.; Liu, G.; Long, K.; Miyashiro, J.; Ranganath, S.; Jacobson, S.; Tang, K.; Im, G.-Y. J.; Sheppeck, J.; Moore, J. D.; Sykes, K.; Wakefield, J.; Sarno, R.; Banijamali, A. R.; Profy, A. T.; Milne, G. T.; Currie, M. G.; Masferrer, J. L. Pharmacological Characterization of IW-1973, a Novel Soluble Guanylate Cyclase Stimulator with Extensive Tissue Distribution, Antihypertensive, Anti-Inflammatory, and Antifibrotic Effects in Preclinical Models of Disease. *J Pharmacol Exp Ther* **2018**, *365* (3), 664–675. https://doi.org/10.1124/jpet.117.247429.
(24) Buys, E. S.; Zimmer, D. P.; Chickering, J.; Graul, R.; Chien, Y. T.; Profy, A.; Hadcock, J. R.; Masferrer, J. L.; Milne, G. T. Discovery and Development of next Generation sGC Stimulators with Diverse Multidimensional Pharmacology and Broad Therapeutic Potential. *Nitric Oxide* **2018**, *78*, 72–80. https://doi.org/10.1016/j.niox.2018.05.009.
(25) Wedel, B.; Humbert, P.; Harteneck, C.; Foerster, J.; Malkewitz, J.; Bohme, E.; Schultz, G.; Koesling, D. Mutation of His-105 in the B1 Subunit Yields a Nitric Oxide-Insensitive Form of Soluble Guanylyl Cyclase. *Proceedings of the National Academy of Sciences* **1994**, *91*, 2592–2596.
(26) Zhao, Y.; Marletta, M. A. Localization of the Heme Binding Region in Soluble Guanylate Cyclase. *Biochemistry* **1997**, *36* (50), 15959–15964. https://doi.org/10.1021/bi971825x.
(27) Zhao, Y.; Schelvis, J. P. M.; Babcock, G. T.; Marletta, M. A. Identification of Histidine 105 in the B1 Subunit of Soluble Guanylate Cyclase as the Heme Proximal Ligand. *Biochemistry* **1998**, *37* (13), 4502–4509. https://doi.org/10.1021/bi972686m.
(28) Koglin, M.; Behrends, S. A Functional Domain of the A1 Subunit of Soluble Guanylyl Cyclase Is Necessary for Activation of the Enzyme by Nitric Oxide and YC-1 but Is Not Involved in Heme Binding. *Journal of Biological Chemistry* **2003**, *278* (14), 12590–12597. https://doi.org/10.1074/jbc.M212740200.
(29) Kang, Y.; Liu, R.; Wu, J.-X.; Chen, L. Structural Insights into the Mechanism of Human Soluble Guanylate Cyclase. *Nature* **2019**, *574* (7777), 206–210. https://doi.org/10.1038/s41586-019-1584-6.
(30) Horst, B. G.; Yokom, A. L.; Rosenberg, D. J.; Morris, K. L.; Hammel, M.; Hurley, J. H.; Marletta, M. A. Allosteric Activation of the Nitric Oxide Receptor Soluble Guanylate Cyclase Mapped by Cryo-Electron Microscopy. *eLife* **2019**, *8*, e50634. https://doi.org/10.7554/eLife.50634.
(31) Campbell, M. G.; Underbakke, E. S.; Potter, C. S.; Carragher, B.; Marletta, M. A. Single-Particle EM Reveals the Higher-Order Domain Architecture of Soluble Guanylate Cyclase.

Proceedings of the National Academy of Sciences **2014**, *111* (8), 2960–2965. https://doi.org/10.1073/pnas.1400711111.

(32) Weichsel, A.; Kievenaar, J. A.; Curry, R.; Croft, J. T.; Montfort, W. R. Instability in a Coiled-coil Signaling Helix Is Conserved for Signal Transduction in Soluble Guanylyl Cyclase. *Protein Sci* **2019**, *28* (10), 1830–1839. https://doi.org/10.1002/pro.3707.

(33) Childers, K. C.; Yao, X.-Q.; Giannakoulias, S.; Amason, J.; Hamelberg, D.; Garcin, E. D. Synergistic Mutations in Soluble Guanylyl Cyclase (sGC) Reveal a Key Role for Interfacial Regions in the sGC Activation Mechanism. *Journal of Biological Chemistry* **2019**, *294* (48), 18451–18464. https://doi.org/10.1074/jbc.RA119.011010.

(34) Liu, R.; Kang, Y.; Chen, L. Activation Mechanism of Human Soluble Guanylate Cyclase by Stimulators and Activators. *Nat Commun* **2021**, *12* (1), 5492. https://doi.org/10.1038/s41467-021-25617-0.

(35) Wittenborn, E. C.; Marletta, M. A. Structural Perspectives on the Mechanism of Soluble Guanylate Cyclase Activation. *IJMS* **2021**, *22* (11), 5439. https://doi.org/10.3390/ijms22115439.

(36) Jumper, J.; Evans, R.; Pritzel, A.; Green, T.; Figurnov, M.; Ronneberger, O.; Tunyasuvunakool, K.; Bates, R.; Žídek, A.; Potapenko, A.; Bridgland, A.; Meyer, C.; Kohl, S. A. A.; Ballard, A. J.; Cowie, A.; Romera-Paredes, B.; Nikolov, S.; Jain, R.; Adler, J.; Back, T.; Petersen, S.; Reiman, D.; Clancy, E.; Zielinski, M.; Steinegger, M.; Pacholska, M.; Berghammer, T.; Bodenstein, S.; Silver, D.; Vinyals, O.; Senior, A. W.; Kavukcuoglu, K.; Kohli, P.; Hassabis, D. Highly Accurate Protein Structure Prediction with AlphaFold. *Nature* **2021**, *596* (7873), 583–589. https://doi.org/10.1038/s41586-021-03819-2.

(37) Mirdita, M.; Schütze, K.; Moriwaki, Y.; Heo, L.; Ovchinnikov, S.; Steinegger, M. ColabFold: Making Protein Folding Accessible to All. *Nat Methods* **2022**, *19* (6), 679–682. https://doi.org/10.1038/s41592-022-01488-1.

(38) Hu, X.; Murata, L. B.; Weichsel, A.; Brailey, J. L.; Roberts, S. A.; Nighorn, A.; Montfort, W. R. Allostery in Recombinant Soluble Guanylyl Cyclase from *Manduca Sexta*. *Journal of Biological Chemistry* **2008**, *283* (30), 20968–20977. https://doi.org/10.1074/jbc.M801501200.

(39) Acerbo, A. S.; Cook, M. J.; Gillilan, R. E. Upgrade of MacCHESS Facility for X-Ray Scattering of Biological Macromolecules in Solution. *J Synchrotron Radiat* **2015**, *22* (Pt 1), 180–186. https://doi.org/10.1107/S1600577514020360.

(40) Skou, S.; Gillilan, R. E.; Ando, N. Synchrotron-Based Small-Angle X-Ray Scattering of Proteins in Solution. *Nat Protoc* **2014**, *9* (7), 1727–1739. https://doi.org/10.1038/nprot.2014.116.

(41) Hopkins, J. B.; Gillilan, R. E.; Skou, S. BioXTAS RAW: Improvements to a Free Open-Source Program for Small-Angle X-Ray Scattering Data Reduction and Analysis. *J Appl Cryst* **2017**, *50* (5), 1545–1553. https://doi.org/10.1107/S1600576717011438.

(42) Svergun, D. I. Determination of the Regularization Parameter in Indirect-Transform Methods Using Perceptual Criteria. *J Appl Cryst* **1992**, *25* (4), 495–503. https://doi.org/10.1107/S0021889892001663.

(43) Evers, T. H.; van Dongen, E. M. W. M.; Faesen, A. C.; Meijer, E. W.; Merkx, M. Quantitative Understanding of the Energy Transfer between Fluorescent Proteins Connected via Flexible Peptide Linkers. *Biochemistry* **2006**, *45* (44), 13183–13192. https://doi.org/10.1021/bi061288t.

(44) van Rosmalen, M.; Krom, M.; Merkx, M. Tuning the Flexibility of Glycine-Serine Linkers To Allow Rational Design of Multidomain Proteins. *Biochemistry* **2017**, *56* (50), 6565–6574. https://doi.org/10.1021/acs.biochem.7b00902.
(45) Reddy Chichili, V. P.; Kumar, V.; Sivaraman, J. Linkers in the Structural Biology of Protein–Protein Interactions. *Protein Science* **2013**, *22* (2), 153–167. https://doi.org/10.1002/pro.2206.
(46) Buel, G. R.; Walters, K. J. Can AlphaFold2 Predict the Impact of Missense Mutations on Structure? *Nat Struct Mol Biol* **2022**, *29* (1), 1–2. https://doi.org/10.1038/s41594-021-00714-2.
(47) Martin, E.; Sharina, I.; Kots, A.; Murad, F. A Constitutively Activated Mutant of Human Soluble Guanylyl Cyclase (sGC): Implication for the Mechanism of sGC Activation. *Proceedings of the National Academy of Sciences* **2003**, *100* (16), 9208–9213. https://doi.org/10.1073/pnas.1633590100.
(48) Truebestein, L.; Leonard, T. A. Coiled-coils: The Long and Short of It. *BioEssays* **2016**, *38* (9), 903–916. https://doi.org/10.1002/bies.201600062.
(49) Mason, J. M.; Arndt, K. M. Coiled Coil Domains: Stability, Specificity, and Biological Implications. *ChemBioChem* **2004**, *5* (2), 170–176. https://doi.org/10.1002/cbic.200300781.
(50) Fritz, B. G.; Hu, X.; Brailey, J. L.; Berry, R. E.; Walker, F. A.; Montfort, W. R. Oxidation and Loss of Heme in Soluble Guanylyl Cyclase from *Manduca Sexta*. *Biochemistry* **2011**, *50* (26), 5813–5815. https://doi.org/10.1021/bi200794c.
(51) Surmeli, N. B.; Marletta, M. A. Insight into the Rescue of Oxidized Soluble Guanylate Cyclase by the Activator Cinaciguat. *ChemBioChem* **2012**, *13* (7), 977–981. https://doi.org/10.1002/cbic.201100809.

Chapter 3

Molecular Aspects of Soluble Guanylate Cyclase Activation and Stimulator Function

Summary

Soluble guanylate cyclases (sGCs) are heme-containing, gas-sensing proteins which catalyze the formation of cGMP from GTP. In humans, sGCs are highly selective sensors of nitric oxide (NO) and play a critical role in NO-based regulation of cardiovascular and pulmonary function. The physiological importance of sGC signaling has led to the development of drugs, known as stimulators and activators, which increase sGC catalytic function. Here we characterize a newly developed stimulator, CYR715, which is a particularly potent stimulator of *Manduca sexta* (*Ms*) sGC catalytic function even in the absence of NO, increasing activity of the NO-free enzyme to 45% of full catalytic activity. CYR715 also increased the catalytic activity of *Ms* sGC βC122A and βC122S variants, with a marked stimulation of the NO-free βC122S variant to 74% of maximum. High-resolution cryo-electron microscopy structures were solved for CYR715 bound to *Ms* sGC βC122S revealing that CYR715 occupies the same binding site as the characterized sGC stimulators YC-1 and riociguat. Additionally, the core scaffold of CYR715 makes a binding interaction with βC78 while the flexible tail can interact with αR429 or βY7 and E361. Conformational extension of sGC following NO, YC-1, or CYR715 binding was characterized using small-angle X-ray scattering, revealing that while ligand binding results in sGC extension this extension does not directly correlate to observed activity. This suggests that not all conformational extensions of sGC result in increased catalytic activity, and that effective stimulators assist in converting extension into catalytic function.

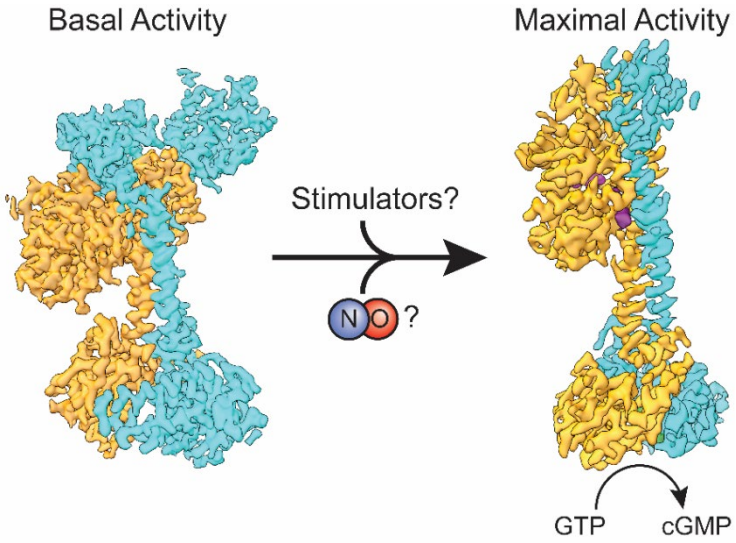

This work was carried out in collaboration with Dr. William C. Thomas in the lab of Prof. Michael A. Marletta. K.A.H. wrote the manuscript. K.A.H., W.C.T., and M.A.M designed research and edited the manuscript. K.A.H. and W.C.T. conducted research and analyzed data.

Introduction

Nitric oxide (NO) is a membrane diffusible diatomic gas which plays a crucial role in endogenous signaling in humans and other eukaryotes[1–4], regulating processes such as vasodilation, platelet aggregation, mitochondrial respiration, and neuronal development.[5–9] Soluble guanylate cyclase (sGC) is a physiological receptor for NO, and NO-binding stimulates sGC-catalyzed cyclization of guanosine triphosphate (GTP) to the secondary messenger molecule cyclic guanosine monophosphate (cGMP). Thus, sGC is responsible for converting the short-lived NO signal into the physiological responses noted above.[10] Dysregulation of NO-signaling has been linked to several human pathologies, particularly those involving cardiovascular function[11], leading to robust research towards small molecule therapeutics capable of increasing sGC catalytic function.

sGCs are heme-containing dimeric proteins found throughout many domains of life. The best characterized sGCs are α/β-type, consisting of two heterodimeric subunits, denoted α and β. Each subunit shares the same domain architecture: a regulatory N-terminal heme nitric oxide/oxygen binding (H-NOX) domain, Per/Arnt/Sim (PAS) and coiled-coil (CC) signal transduction domains, and a catalytic (CAT) domain.[12,13] Each sGC heterodimer binds one heme cofactor in the β H-NOX subunit via a highly conserved histidine residue, which binds to the heme iron, and a YxSxR motif, which coordinates with the heme propionate chains.[14–17] The PAS and CC domains promote dimerization[14], participate in signal transduction[18], and facilitate the conformational changes responsible for sGC activation.[19,20] Each CAT subunit contributes some residues necessary for catalysis, forming a singular active site.[21]

The mechanisms of sGC activation by NO have been the subject of decades of research. When NO is absent (also referred to as the unliganded state, U, or ligand-free), sGC exhibits a low, basal level of activity. When NO is added to sGC, the first equivalent of NO binds tightly to the distal face of the heme cofactor, leading to the rupture of the proximal iron-histidine bond and propagation of the NO-activation signal.[22–25] When NO is present at stoichiometric equivalence to the heme within sGC (the 1-NO state), sGC is activated to approximately 15% of maximal activity.[26,27] sGC can be fully activated by excess NO relative to the heme (the xsNO state), and physiological concentrations of NO in the nM range bring about full activation.[28,29] Recently solved full-length cryo-electron microscopy (cryo-EM) structures of sGCs from *Homo sapiens* (*Hs*, human)[20,30] and *Manduca sexta* (*Ms*, tobacco hawk moth)[19] have provided insight into the mechanisms of allosteric communication in sGC. In the NO-free state, sGC adopts a contracted conformation via a bend in the CC domain. Under activating conditions, the CC domain straightens resulting in an extension of the enzyme and opening of the catalytic basket.

sGC activity is targeted therapeutically via two types of small molecules, activators and stimulators, which utilize different mechanisms of action to increase sGC activity. Oxidative stress can lead to heme oxidation and loss, forming apo-sGC which no longer responds to NO.[31–35] Activators bind to the empty heme-binding pocket of apo-sGC, restoring partial activity without

restoring sensitivity to NO.[36–38] Stimulators, however, are heme-dependent effectors of sGC activity.[37,39,40] When endogenous NO is low and sGC is NO-free, stimulators increase sGC activity to approximately the 1-NO level.[19,37,41] In conditions where endogenous NO is present in sufficient concentrations to form 1-NO sGC, stimulators increase sGC activity to the xsNO level.[19,30,37,41] YC-1, a benzyl indazole derivative, was the first characterized sGC stimulator[42] and served as the lead structure for optimization screens for more potent and specific sGC stimulators.[37,43] Two stimulators, both YC-1 derivatives, have received FDA approval: Bayer's riociguat (Adempas®)[43–45] in 2013 and vericiguat (VERQUVO®) in 2021.[46–48] Full-length cryo-EM structures have revealed the mechanism of action for small molecule sGC stimulators. Solved structures for *Ms* sGC[19] bound to YC-1 and *Hs* sGC[30] bound to YC-1 or riociguat found that these stimulators bind in the same pocket for both *Ms* and *Hs* sGC and revealed that stimulators engage with sGC at positions which facilitate straightening of the CC domain and thus stabilize sGC in the extended, active conformation.

While research continues into the development of sGC stimulators, only two such compounds have received FDA approval, and both utilize fused ring structures derived from the initial YC-1 scaffold (Figure 3.1). In fact, a recent sGC stimulator patent review[39] found that most stimulator designs, while incorporating a diverse array of chemical functionalization, still utilize a fused ring scaffold. In this work, we have characterized the interactions between *Ms* sGC and CYR715[49], a potent sGC stimulator representing a new class of chemically novel sGC stimulators featuring a biaryl pyrazole scaffold.

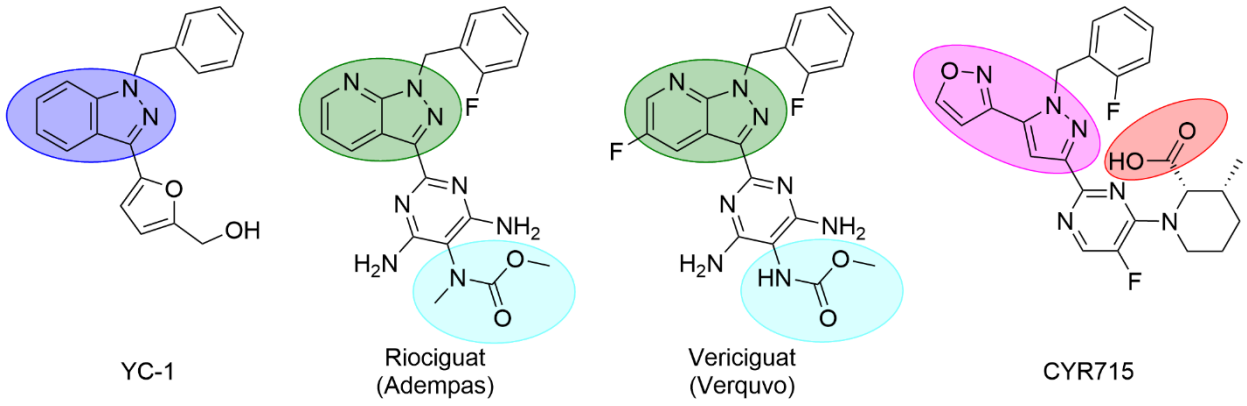

Figure 3.1. Structural comparisons of sGC stimulators YC-1, riociguat, vericiguat, and CYR715. Core molecular scaffolds for each stimulator are indicated: benzyl indazole for YC-1 (dark blue), pyrazolo[3,4-b]pyridine for both riociguat and vericiguat (green), and biaryl pyrazole for CYR715 (pink). The activity enhancing carbamate[43,46,48] of riociguat and vericiguat is shown light blue, and the carboxylic acid of CYR715 is shown in red.

To better understand the interplay of stimulator binding with sGC conformation, we have studied these interactions using wild type (WT) and single point variants of *Ms* sGC at position βC122. This highly conserved cysteine has been previously implicated in sGC desensitization via nitrosation and is suspected to play a role in the regulation of sGC activity.[50,51] Thus, we hypothesized that slight perturbations of structure or polarity at this highly conserved position near

the heme binding pocket could impact stimulator binding site accessibility or activation-conformation response following stimulator or NO binding. In this work, we present biochemical and structural studies of the ligand-induced activation and conformational responses of sGC, advancing our understanding of the sGC activation-conformation landscape.

Materials and Methods

Materials

All chemicals were purchased from commercial vendors and used without further purification. Primers were purchased from Integrated DNA Technologies (Coralville, IA). Gibson-like Master Mix was purchased from the QB3 MacroLab (Berkeley, CA). PrimeSTAR Max Premix was purchased from Takara Bio USA (Mountain View, CA). DNA purification kits were purchased from Qiagen (Germantown, MD). Sf9 cells were purchased from Novagen (Madison, WI). ExCell-420 media, DNAase 1 from bovine pancreas, β-mercaptoethanol, sodium phosphate dibasic (Na_2HPO_4), potassium phosphate (K_2HPO_4), sodium dithionite ($Na_2S_2O_4$), guanosine triphosphate sodium salt (GTP) (>95%, HPLC), sodium carbonate (Na_2CO_3), and zinc acetate ($Zn(CH_3CO_2)_2$) were purchased from Merck (Darmstadt, Germany). 4-(2-hydroxyethyl)piperazine-1-ethanesulfonic acid (HEPES) and Zeba spin desalting columns were purchased from ThermoFisher Scientific (Waltham, MA). 4-(2-aminoethyl)benzenesulfonyl fluoride hydrochloride (AEBSF) and tris(2-carboxyethyl)phosphine hydrochloride (TCEP) were purchased from Research Products International (Mount Prospect, IL). Benzamidine, glycerol, sodium chloride (NaCl), and magnesium chloride ($MgCl_2$) were purchased from VWR Life Science (Visalia, CA). Dithiothreitol (DTT) was purchased from Bachem (Bubendorf, Switzerland). Imidazole was purchased from Oakwood Chemical (West Columbia, SC). Triethanolamine (TEA) was purchased from Spectrum Chemical (Gardena, CA). TALON Superflow resin was purchased from Cytiva (Marlborough, MA). PROLI NONOate, DEA-NONOate, and YC-1 were purchased from Cayman Chemical Company (Ann Arbor, MI). CYR715 was provided by Cyclerion Therapeutics (Cambridge, MA). Guanosine-5'-[(α,β)-methyleno]triphosphate (GpCpp) was purchased from Jena Bioscience (Thuringia, Germany). Fluorinated octyl maltoside (FOM) was purchased from Anatrace (Maumee, Ohio).

Generation of Expression Constructs

Constructs of WT *Ms* sGC α and β subunits were previously generated in the pFastBac (Bac-to-Bac Baculovirus Expression system) vector and designated as pFastBac_Ms_sGC_α1_His6 and pFastBac_Ms_sGC_β1, respectively.[19] A C-terminal hexahistidine tag was added to the α subunit to aid in purification. For this work, variant β subunit fragments were generated through PCR which were then cloned into linearized pFastBac vectors by Gibson assembly (Table S1). Sequences were verified by Sanger Sequencing at the UC Berkeley DNA Sequencing Facility.

Generation of Bacmid DNA

Recombinant baculovirus bacmid DNA was generated via transformation of plasmids and gene transposition in DH10Bac-GFP *E. coli* cells. Recombinant bacmids were isolated from successful

transformants, and sequences were verified by PCR amplification and sequencing. Recombinant baculoviruses were obtained by transfection of bacmids into Sf9 cells.

Protein Expression and Purification

Sf9 cells were grown in suspension in ExCell-420 media at 27 °C, with shaking at 130 rpm. Recombinant baculovirus for each subunit was amplified until viral titer was greater than 1 x 10^8 pfu/mL. Sf9 cultures at a density of 4 x 10^6 cells/mL were co-infected with 50 mL of α and β amplified virus, for a total of 100 mL of virus per liter. Infected cells were grown for 72 hours before harvesting by centrifugation at 3,280 g for 20 minutes. Pellets were flash frozen in liquid nitrogen and stored at -80 °C.

Protein was purified as previously published,[19] with the following changes. The crude cell lysate was clarified by ultracentrifugation at 158,000 g for 90 minutes. Lysate was applied to a 2.5 mL TALON Superflow column at 0.5 mL/min, and the protein-loaded column was washed with 10 column volumes (CV) of Buffer A (50 mM Na_2HPO_4, 200 mM NaCl, 1 mM imidazole, 1 mM benzamidine, 5% (v/v) glycerol, pH 8.0, 0.22 μm filtered), 15 CV of Buffer A supplemented with 1.2 M NaCl, and again with 10 CV of Buffer A at 1 mL/min before elution with Buffer B (50 mM Na_2HPO_4, 200 mM NaCl, 150 mM imidazole, 1 mM benzamidine, 5% (v/v) glycerol, pH 8.0, 0.22 μm filtered). Protein-containing fractions were concentrated to < 1 mL, supplemented with 5 mM DTT and 1 mM EDTA, diluted to 9 mL with Buffer C (25 mM TEA, 25 mM NaCl, 5 mM DTT, 5% (v/v) glycerol, pH 7.4, 0.22 μm filtered) and immediately applied to a POROS HQ2 anion exchange column at 0.25 mL/min before elution with Buffer D (25 mM TEA, 750 mM NaCl, 5 mM DTT, 5% (v/v) glycerol, pH 7.4, 0.22 μm filtered). Protein-containing fractions were concentrated, flash frozen in liquid nitrogen, and stored at -80 °C. The typical yield for this expression and purification procedure was 250 μg per liter of insect cells.

Activity Assays and cGMP Quantification

Samples were prepared and assayed in an anaerobic chamber at RT, unless otherwise noted. Protein was thawed at 4 °C, reduced using 10 mM $Na_2S_2O_4$ for 15 minutes at RT and desalted using a Zeba spin column equilibrated with Buffer E (50 mM HEPES, 150 mM NaCl, 5% (v/v) glycerol, pH 7.5, 0.22 μm filtered). UV-Vis spectra were collected, and protein concentration was determined using the reduced heme Soret peak at 433 nm (149,000 M^{-1} cm^{-1}).[19,52] An aliquot of ligand-free protein was reserved for activity assays. The remaining protein was brought to the xsNO state by the addition of 50 μM PROLI NONOate, for an NO concentration of 100 μM, and allowed to incubate for 15 minutes. Protein was then desalted using a Zeba spin column to generate 1-NO protein. UV-Vis spectra were collected using a Nanodrop 2000c spectrophotometer, and the concentration of the 1-NO protein was determined by comparing the ratio of A_{280} peaks for the ligand-free and 1-NO protein.

Activity assays were performed at 25 °C in Buffer E supplemented with 5 mM DTT and 5 mM $MgCl_2$ using a final protein concentration of 20 nM. Samples containing either CYR715 or YC-1 were brought to a final stimulator concentration of 150 μM (final DMSO concentration 1%) and

allowed to equilibrate for 15 minutes. DMSO (final concentration 1%) was added to all other samples. To generate xsNO protein, PROLI NONOate (50 μM) was added to the 1-NO protein and allowed to incubate for 5 minutes. Reactions were initiated by the addition of 2 mM GTP, and time points were quenched 1:4 (v:v) using 125 mM $Zn(CH_3CO_2)_2$. Sample pH was adjusted by the addition of an equal volume of 125 mM Na_2CO_3. Samples were stored at -80 °C. Quenched assays were thawed and centrifuged for 10 minutes at 21,130 g to remove zinc precipitate. Samples were diluted, and cGMP formation was quantified in duplicate using a cGMP Enzyme Linked Immunosorbent Assay (ELISA) following manufacturer protocols (Enzo Life Sciences). Initial rates were calculated from the linear phase of the time course where < 10% of the GTP substrate was consumed.

Cryo-EM Sample Preparation and Data Collection

Samples were prepared in a Coy anaerobic chamber at RT, unless otherwise noted. Protein was thawed at 4 °C, reduced with 10 mM $Na_2S_2O_4$ for 15 minutes at RT, and desalted using a Zeba spin column equilibrated with Buffer F (25 mM TEA, 25 mM NaCl, 5 mM DTT, 5 mM $MgCl_2$, pH 7.5, 0.22 μm filtered). Protein was concentrated before dilution to 10 μM in equivalent buffer with the addition of 0.5 mM FOM, a detergent that can aid in particle distribution. The CYR715 plus GpCpp treated sample was prepared similarly, but 250 μM CYR715 and 1 mM GpCpp were added to the sample before freezing.

Cryo-EM samples were prepared by applying 3 μl to a glow-discharged Quantifoil R1.2/1.3 holey-carbon cryo-EM grid. The grid was blotted for 4 s with Whatman #1 filter paper and then plunge-frozen in liquid ethane with a Mark IV Vitrobot (ThermoFisher) at 4° C and 100% humidity. Both datasets were collected on Titan Krios 300 keV electron microscopes (ThermoFisher) at the Stanford-SLAC Center for Cryo-EM.

Cryo-EM Data Collection and Processing for Ms sGC βC122S with No Ligands

11,872 movies were collected in total using a ThermoFisher Falcon 4i direct electron detector in counting mode. Images were recorded at a pixel size of 0.954 Å, frame duration of 0.2195 sec/frame, dose per frame of 1.25 e/Å^2, and total dose of 50 e/Å^2. Defocus was set at -2.5 to -1.5 μm. Initial data processing was performed in cryoSPARC. Movies were aligned and motion corrected, then manual curation was used to remove poor micrographs, leaving a total of 7,721 micrographs. A sample micrograph can be seen in Figure B.1A. After CTF estimation, autopicking was used to produce a stack of 1,226,641 particles. Particles showing poor alignment or broken complexes were removed using a series of 2D classification steps, leaving a particle stack of 368,563 particles that resembled sGC dimers (Figure B.1B). Subsequent processing workflow steps are summarized in Figure B.1D-E. The particle stack was subjected to 2-class *ab initio* reconstruction followed by heterogeneous refinement in cryoSPARC. 264,227 particles sorted into a higher resolution 3D class, on which Non-Uniform (NU) refinement was performed. The resulting 3.3 Å global map strongly resembled previous sGC structures in the ligand-free, contracted state, and the map was used for initial model building. Other refinement strategies were

attempted but did not lead to higher resolution global map densities. Refinement statistics are summarized in Table S2.

In addition, the larger 368,563 particle stack was also imported to Relion for focused 3D classification to investigate potential alternative sGC conformations in the particle stack. Six classes were used with the NU-refinement density from cryoSPARC as an initial seed. Three classes (classes 2, 3, and 4) were of the highest quality and mostly match the same 264,227 particles used in the NU refinement. The sixth class, constituting 49,358 particles (13.7%), was found to resemble an extended sGC conformation as seen in *Hs* sGC (Figure B.1E, PDB: 8HBF[53]). However, attempts at improving the resolution of this class were unsuccessful, likely due to its relatively small number of particles.

During refinement it became clear that there was interdomain flexibility within the main 264,227-particle stack. In particular, the catalytic domain was at lower resolution and had considerable missing density. Separate masks were created for each domain, and local refinement as implemented in cryoSPARC was used to separately improve the resolution of the catalytic and H-NOX domains of the global map. The subsequent local refinements resulted in 3.0 Å and 3.4 Å maps for the H-NOX and catalytic domains respectively, which were then recombined into a composite global map. This composite map has improved density for outer regions of the map and improved local resolution relative to the consensus map (Figure B.2).

Cryo-EM Data Collection and Processing for Ms sGC βC122S with CYR715

8,433 movies were collected in total using a Gatan K3 direct electron detector in counting mode. Images were recorded at a pixel size of 0.86 Å, frame duration of 0.0354 sec/frame, dose per frame of 1.25 e/Å^2, and total dose of 50 e/Å^2. Defocus was set at -2.5 to -1.5 µm. Initial data processing was performed in cryoSPARC. Movies were aligned and motion corrected, then manual curation was used to remove poor micrographs, leaving a total of 8,081 micrographs. A sample micrograph can be seen in Figure B.3A. After CTF estimation, autopicking was used to produce a stack of 2,299,895 particles. Particles showing poor alignment or broken complexes were removed using a series of 2D classification steps, leaving a particle stack of 902,997 particles that resembled sGC dimers (Figure B.3B). Subsequent processing workflow steps are summarized in Figure B.3D-E. The stack was subjected to 2-class *ab initio* refinement followed by heterogeneous refinement in cryoSPARC. 598,571 particles sorted into a higher resolution 3D class, on which NU refinement was performed. The resulting 3.7 Å consensus density resembled previous sGC structures in the extended, NO-bound state. Other refinement strategies were attempted but did not lead to higher resolution global map densities. Unlike the ligand-free *Ms* βC122S sGC map, there is minor orientation bias in the orientation distribution that may contribute to lower resolution (Figure B.3C).

Relion 3D focused classification was also used to investigate potential alternative conformations in the dataset. Due to computational limitations, only the 304,316-particle stack constituting the second heterogeneous 3D class from cryoSPARC was imported into Relion for focused 3D

classification. Six classes were used with the NU-refinement density from cryoSPARC as an initial seed. Most classes were of insufficient quality or resolution to differentiate active from inactive sGC conformations. Class 3, constituting ~29% of the smaller particle stack (~8% of all sGC dimer particles used), was found to contain density for a lobe positioned near the catalytic domain as seen only in the inactive form of sGC (Figure B.3E, PDB: 8HBE[53]). As with the alternative conformation subclass for ligand-free sGC, attempts at improving the quality and resolution of this class were unsuccessful. Refinement statistics are summarized in Table S2.

To improve local resolution of the domains of CYR715-bound sGC, local refinement was performed similarly to ligand-free sGC. Separate masks were created for each domain, and local refinement as implemented in cryoSPARC was used to improve the resolution of the catalytic and H-NOX domains of the global map. The subsequent local refinements resulted in 3.6 Å and 3.4 Å maps for the H-NOX and catalytic domains, respectively. The density for the catalytic domain improved substantially in both resolution and visibility of outer regions (Figure B.4). Even with local refinement, the α H-NOX domain could not be resolved at the N-terminal side of the active sGC. This may contribute to the overall lower resolution of the local refinement for the H-NOX domain relative to that of the ligand-free EM map.

Model Building of Ligand-free sGC

The initial model of *Ms* sGC βC122S was built using ModelAngelo[54,55] in known sequence mode and with the consensus global 3.3 Å map as a starting point. Subsequent refinement was performed using iterative rounds of Phenix real space refinement[56] and manual modeling in Coot.[57] Phenix refinement was performed for separate domains of the model using the higher-resolution local maps of those domains. The central coiled-coil domain was refined using the consensus map. Real space refinement was performed principally with default settings. Manual model-building was performed using both global and local maps in both unsharpened and sharpened forms. Heme was modeled into the structure based on previous cryo-EM structures of sGC. No density for other ligands was observed.

Model Building of CYR715-bound sGC

A homology model for extended *Ms* sGC βC122S was generated using Swiss-Model[58–62] based on the structure of NO and YC-1 activated *Hs* $\alpha_1\beta_1$ sGC (PDB: 7D9S[30]). The model was then placed into the global consensus and composite maps using UCSF ChimeraX[63–65] and manually rebuilt in Coot.[57] CYR715 was modeled into the corresponding density using eLBOW[66] as implemented in Phenix and by comparison with prior structures of sGC with bound stimulator (PDB: 8HBF[30]). The resolution of the cryo-EM map for sGC in the CYR715-bound state was insufficient to explicitly determine the conformation of the terminal piperidine and was modeled and evaluated in several conformations.

For both the ligand-free and the CYR715-bound structures, geometry and model statistics were evaluated with MolProbity[67] and the wwPDB validation server. Data refinement and model statistics are provided in Supplementary Table 2. Local resolution maps were calculated using

cryoSPARC. Model resolution was determined where the map-model FSC = 0.5. The atomic coordinates and composite maps of both structures have been deposited to the Protein Data Bank and EM Data Bank under accession codes 9OXN/EMD-70990 (ligand-free) and 9P2R/EMD-71204 (CYR715-bound). Additionally, consensus and local refinement maps can be found in the EM Data Bank under accession codes EMD-71045 (ligand-free consensus), EMD-71030 (ligand-free H-NOX local), EMD-71036 (ligand-free catalytic local), EMD-71150 (CYR715-bound consensus), EMD-71151 (CYR715-bound H-NOX local), and EMD-71152 (CYR715-bound catalytic local). Figures were made in UCSF ChimeraX.[63–65]

Small-angle X-ray Scattering (SAXS) Sample Preparation and Data Collection

SAXS experiments on *Ms* sGC WT, βC122S, and βC122A were performed under anaerobic conditions at the MacChess BioSAXS beamline (Sector 7A) at the Cornell High-Energy Synchrotron Source, Ithaca, New York on two occasions in June and October 2024.[68–70] Protein samples were thawed, reduced using 10 mM $Na_2S_2O_4$, and buffer exchanged in a Coy anaerobic chamber using a Zeba spin column equilibrated with SAXS assay buffer (50 mM HEPES, 150 mM NaCl, 1 mM TCEP, 5 mM $MgCl_2$, 1% (v/v) glycerol, pH 7.5, 0.22 μM filtered). After confirming heme reduction using UV-Vis spectroscopy, protein samples were prepared through the addition of one or more of the following ligands: 150 μM YC-1, 375 μM CYR715, or 1 mM GpCpp. NO equivalents were added to a final concentration of 200 μM NO via addition of 100 μM PROLI NONOate (half-life = 2 seconds) and 100 μM DEA NONOate (half-life = 16 min). For some samples, low but visible absorption at 415 nm was still observed after buffer exchange, indicating incomplete removal of $Na_2S_2O_4$ which could react with added NO and reduce the effective NO concentration. For samples with observed $Na_2S_2O_4$ absorption, 400 μM of effective NO equivalents were added to ensure xsNO conditions. 40 μL of 6 – 8 μM sample were directly injected into an anaerobic cell operating in batch mode. For experiments performed in October 2024, in-line UV/vis spectra were collected using a fiber optic spectrophotometer located after the SAXS flow cell (AvaSpec-ULS2048, Avantes).

Data were collected using a Dectris EIGER 4M detector in a flow cell held at 4 °C. 20 x 2s X-ray exposures were collected for each sample, discarding frames displaying X-ray-induced sample aggregation. Scattering images were integrated about the beam center and normalized by transmitted intensities measured on a photodiode beamstop. The integrated protein scattering profile, $I(q)$, was produced by subtraction of background buffer scattering from the protein solution scattering using an exact buffer match. The X-ray wavelength of the experiment was λ = 1.104 – 1.1061 Å and the sample to detector distance was 1,725 – 1,748.0 mm, as determined by silver behenate calibration. Scattering was collected over a range of q = 0.01 Å^{-1} to 0.45 Å^{-1}, where q is the scattering vector $q = 4\pi\sin\theta/\lambda$ and 2θ is the scattering angle. Data processing, analysis, and comparison to published WT *Ms* sGC[19] were performed in BioXTAS RAW using established protocol.[71] Radii of gyration (R_g) were estimated with Guinier analysis, and pair distance distribution analysis was performed using GNOM.[72] To address variance in sample aggregation, pair distance distribution values were calculated assuming a D_{max} of 135 Å for all samples, which is the calculated D_{max} of both extended and contracted sGC cryo-EM structures.[19,20,30,53] However,

we note that this assumption may introduce bias into the pair distance distribution estimation. Error bars associated with R_g values are curve-fitting uncertainties from Guinier analysis. The predicted scattering of contracted *Ms* sGC was calculated from our *Ms* sGC βC122S ligand-free contracted structure using Crysol[72]. The scattering of extended *Ms* sGC was calculated from our *Ms* sGC βC122S CYR715-bound extended structure. Both predicted scatterings were cross-validated with predictions from previously published structures.[19,20,30,53] Difference scattering was calculated in Primus after first normalizing Kratky plots by their maximum value between 0 – 0.3 $Å^{-1}$.[72]

Results

Activity of WT and Variant Ms sGCs

Ms sGC WT, βC122A, and βC122S were purified (Figure B.5), and all three proteins exhibited UV-Vis ligand-binding characteristics matching previous WT *Ms* sGC characterizations. Soret maxima were observed at 433 nm for protein in the Fe^{2+} ligand-free state[19,52] with a shift to 399 nm after NO binding, indicating the formation of a five-coordinate Fe^{2+}-NO species (Figure 3.2).[19,22,52,73,74] Since βC122 is positioned near the heme binding pocket, there were concerns that mutagenesis at this site could impact heme binding. Heme incorporation was estimated using a ratio of the absorbances at 280 and 433 nm. For fully heme-loaded WT *Ms* sGC, $A_{433}/A_{280} = 0.85$.[19] In this study, this ratio for the WT, βC122A, and βC122S proteins was 0.71, 0.83, and 0.61 indicating 84%, 97%, and 73% holoprotein, respectively. While heme incorporation of the βC122S variant was lower than that of the WT protein used in this study, it is within our observed range of heme incorporation for purified WT *Ms* sGC.

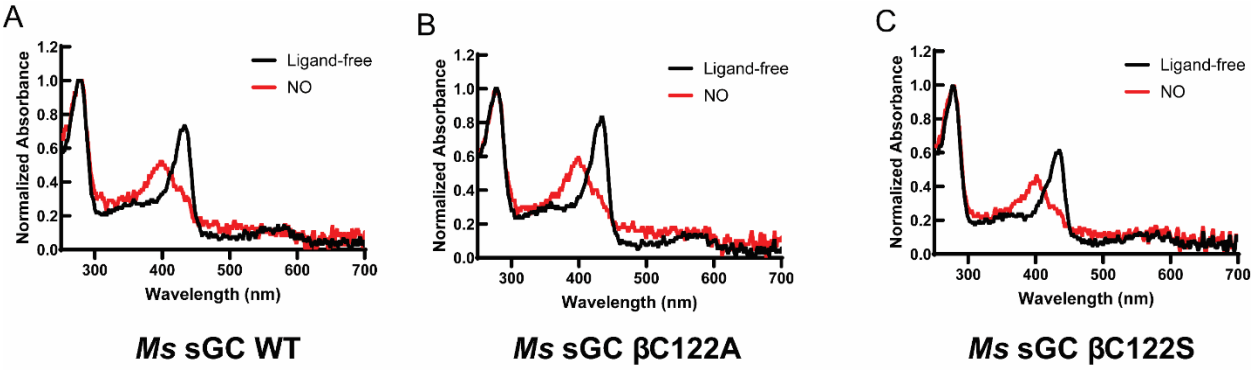

Figure 3.2. UV-Vis characterization of *Ms* sGC WT, βC122A, and βC122S sGCs when ferrous, ligand-free (black) and NO-bound (red). (A) UV-Vis absorption spectra of *Ms* sGC WT. $A_{433}/A_{280} = 0.71$, ~84% holoprotein. (B) UV-Vis absorption spectra of *Ms* sGC βC122A. $A_{433}/A_{280} = 0.83$, ~97% holoprotein. (C) UV-Vis absorption spectra of *Ms* sGC βC122S. $A_{433}/A_{280} = 0.62$, ~73% holoprotein.

As previously observed[19], *Ms* sGC WT displayed a low level of activity in the ligand-free state, partial activation in the 1-NO state, and full activity in xsNO state. Addition of YC-1 to the ligand-free protein resulted in partial activation (17% of xsNO activity), similar to protein in the 1-NO state (14% of xsNO activity). Addition of CYR715 to the ligand-free protein resulted in much greater sGC activation compared to YC-1, with CYR715-stimulated activity reaching 45%

of that observed for the fully activated protein in the presence of xsNO (Figure 3.3A). This high activity stands in contrast to previous observations of stimulator-induced activity for ligand-free sGC, where addition of stimulators to the ligand-free protein results in partial activation to approximately that seen in the 1-NO state.[19,27,75,76]

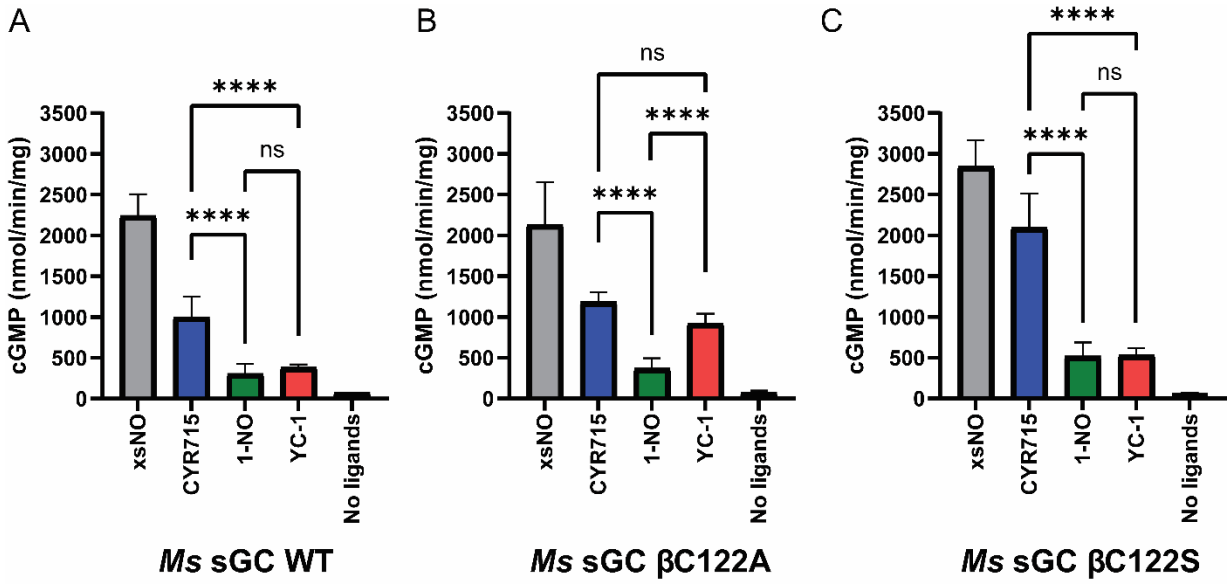

Figure 3.3. Activity profiles of *Ms* sGC WT, βC122A, and βC122S sGCs under various activation conditions: excess NO (xsNO, gray), 150 μM CYR715 (CYR715, blue), stoichiometric NO (1-NO, green), 150 μM YC-1 (YC-1, red), and without any ligands (No ligands, black). All reactions contained 20 nM sGC, 5 mM $MgCl_2$, and 2 mM GTP. Average specific activities were calculated per mg of holoprotein, and error bars represent 1 standard deviation. For WT *Ms* sGC, n = 5 for No ligand and YC-1, n = 10 for xsNO, and n = 15 for CYR715 and 1-NO samples. For βC122A *Ms* sGC, n=10 for all samples. For βC122S *Ms* sGC, n = 5 for 1-NO and n = 9 for all other samples. Rates of cGMP formation under different activation conditions were analyzed by ANOVA. ns = not significant. **** = $p < 0.0001$.

Both βC122 variants of *Ms* sGC displayed similar NO-based activation profiles to WT, showing low activity in the ligand-free state, partial activation in the 1-NO state, and full activation with xsNO. The βC122A variant showed enhanced activation by both stimulators, with the addition of YC-1 increasing activity to 43% and CYR715 reaching 55% of xsNO activity (Figure 3.3B). The βC122S variant was only moderately stimulated by the addition of YC-1 (19% of xsNO activity); however, addition of CYR715 resulted in significant stimulation of the enzyme, reaching 74% of xsNO activity (Figure 3.3C).

The differences in activities between *Ms* sGC WT and the βC122 variants following stimulator binding were unexpected, as was the ability of CYR715 to stimulate NO-free sGC activity to levels significantly above that of 1-NO protein. Thus, cryo-EM investigations were carried out using *Ms* sGC βC122S, which showed the greatest activation in response to CYR715 in the NO-free state, to characterize CYR715 binding. Likewise, SAXS was used to explore the ligand-induced conformational changes of WT and variant *Ms* sGCs.

Contracted Conformation of Ligand-free Ms sGC βC122S

Cryo-EM was used to solve the structure of *Ms* sGC βC122S in the ligand-free state. A final reconstruction of the main conformational component (86% of intact particles) observed on micrographs was solved to a consensus resolution of 3.3 Å (Figure 3.4A). Local refinement further improved the resolution of the H-NOX and catalytic domains to 3.0 and 3.4 Å, respectively (Figure B.2). As previously observed for *Ms* and *Hs* sGCs, the electron density for the inactive structure displays two large lobes, connected by a linker region, with the N-terminal domain bent towards the C-terminal lobe.[19,20,30] The structure overlays very closely with a previously published cryo-EM structure of WT *Ms* sGC in the contracted conformation (PDB: 6PAS)[19], suggesting that mutagenesis at βC122S does not cause major perturbation of the contracted state structure. However, the resolution of the βC122S map is a significant improvement that allows for improved accuracy in modeling, including the identification of the residues responsible for the bend in the coiled-coil region of the contracted conformation of *Ms* sGC as residues α420 – 426 and β346 – 350 (Figure 3.4B). Density is observed for βS122, which takes on a conformation similar to the corresponding cysteine residue in WT *Hs* sGC (Figure B.6C).

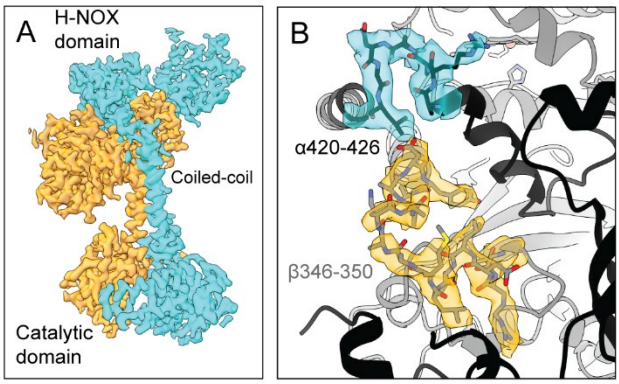

Figure 3.4. Cryo-EM structure of ligand-free *Ms* sGC βC122S in the contracted state. (A) A composite EM map of local refinements shows a contracted conformation sGC. The α subunit is shown in cyan and the β subunit in orange. Density is shown at threshold 0.783. (B) Visible density allowed for improved modeling of α420-426 and β346-350. Density is shown at threshold 0.448.

During focused classification of ligand-free *Ms* sGC βC122S, a small but significant subpopulation of particles (14%) was found to take on a more extended conformation than previously observed for WT ligand-free *Ms* sGC (Figure B.1E). Due to technical improvements in data collection and processing between the datasets, it is difficult to directly assess if this is unique to the βC122S variant or if WT *Ms* sGC also contains an extended, ligand-free population that existed below detection in the prior dataset.

Extended Conformation of NO-free CYR715-bound Ms sGC βC122S

To better understand the effect of CYR715 on *Ms* sGC, a cryo-EM structure was also solved for *Ms* sGC βC122S in the presence of CYR715 and the non-hydrolyzable GTP substrate analog GpCpp. NO was not present in this sample. A small fraction of particles (~9%) were found to more resemble a contracted conformation by focused classification, but further details could not be

resolved. The majority of particles were used for a final consensus reconstruction that was solved to a consensus resolution of 3.7 Å (Figure 3.5A), and local refinement of the H-NOX and catalytic domains further improved the resolution to 3.6 Å and 3.4 Å, respectively (Figure B.4). The core regions of the density are of sufficient quality for atomic modeling (Figure B.7). A significant portion of the α H-NOX domain is unresolved, which has previously been observed for WT *Ms* sGC.[19] The observed electron density matches previously solved structures for WT *Ms* and *Hs* sGCs in either NO, NO + YC-1, or NO + riociguat conditions[19,20,30,53], with the coiled-coil domain fully extended leading to separation of the N- and C-terminal lobes. Mutagenesis at βC122S does not appear to induce significant perturbations to the global structure of the protein in the extended conformation. Density was clearly observed for GpCpp in the catalytic basket as previously observed in other sGC structures (Figure B.7B). Clear density for the heme cofactor is also visible in the β H-NOX subunit, and there is evident electron density between βH105 and the central Fe atom in the heme (Figure B.7C). This density has previously been observed in cryo-EM structures of *Hs* sGC in the NO-free state. Density is again observed for βS122, which does not make any unique interactions relative to the corresponding βC122 in *Hs* sGC (Figure B.7D).

The CYR715 Binding Site

Unassigned density was observed in a pocket adjacent to the coiled-coil and β H-NOX domains, a location where stimulators YC-1 and riociguat have previously been observed to bind.[19,30] CYR715 was modeled into this density (Figure 3.5B, Figure B.7E-G). While the resolution is insufficient to positively identify the exact binding conformation (Figure B.7I-J), we found that a plausible conformation maintains similar binding interactions to those observed between *Hs* sGC and riociguat (Figure 3.5C). The fluorophenyl ring of CYR715 stacks with βY112 while making additional hydrophobic interactions with the heme and βY2 and F4 (Figure B.7E). The core biaryl pyrazole interacts with the β H-NOX domain at F4, F77, Y83, and E361 (β370 in *Hs* sGC) (Figure B.7F). The fluoropyrimidine interacts at αL426 (αL425 in *Hs* sGC) and βV39, R40, and S81 (Figure B.7G). In addition, CYR715 has two binding interactions which differ from those observed with riociguat in previous structures. First, the oxygen of the biaryl pyrazole is positioned to engage in hydrogen bonding with βC78 (Figure B.7H). The terminal piperidine and its substituents can sample several conformations, which can access an electrostatic interaction with αR429 (αL428 in *Hs* sGC) (Figure B.7I) or hydrogen bonding interactions with βY7 and E361 (Figure B.7J).

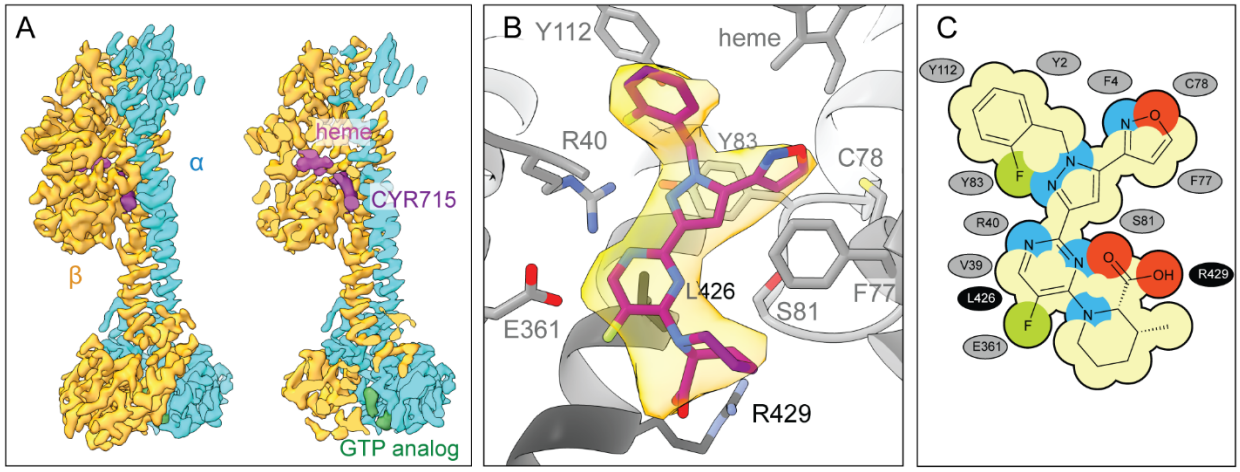

Figure 3.5. Cryo-EM structure of CYR715-bound *Ms* sGC βC122S in the extended state. (A) (Left) A composite EM map of local refinements shows an extended conformation sGC. The α subunit is shown in cyan and β subunit in orange. (Right) A cut-away reveals density for heme, GTP substrate analog (GpCpp), and CYR715. (B) A zoomed in view of the CYR715 binding site, with EM density in orange and CYR715 modeled in purple. Interacting residues from α are shown in in black and β in gray. (C) A schematic of interactions between CYR715 and sGC. Residues in the α or β subunits are shown in black or gray, respectively. All maps are shown at threshold = 0.906.

SAXS Studies of WT and Variant Ms sGCs

Cryo-EM structures of sGCs solved in this and prior work reflect extreme end-states under either ligand-free or excess effector conditions with particles computationally "purified" through selection and averaging. However, our focused classification of both ligand-free and CYR715-bound *Ms* sGC βC122S provide evidence that these solutions are not as homogeneous as the highest resolution end-state structures would suggest. Prior SAXS and negative-stain EM experiments also support that WT *Ms* and *Rattus norvegicus* (*Rn*) sGC exist in a mixture of conformations.[19,77] We hypothesized that differences in activation by different stimulators or in different *Ms* sGC variants may be due to an enrichment of one conformation over another. Thus, SAXS was used to study the conformational states of WT and variant *Ms* sGCs under different ligand conditions to better understand potential differences in their conformational landscapes. SAXS experiments on *Ms* sGC variants were performed under ligand-free conditions as well as conditions including the addition of NO, YC-1, CYR715, and GpCpp. Time and sample constraints limited the conditions that were studied with each variant. Because NO is oxygen-sensitive, these experiments were performed using an anaerobic-SAXS setup in which an anaerobic chamber is positioned in-line with an in-vacuum flow cell.[70]

For all experiments, *Ms* sGC variants show similar overall scattering curve shapes indicative of an sGC dimer (Figure B.8A-C) with a radius of gyration (R_g) between 47 – 53 Å (Table S3). These values are slightly higher than previously observed for WT *Ms* sGC, but this is likely caused by minor aggregation in samples that were not further purified by size-exclusion chromatography-coupled SAXS. The most notable difference observable in SAXS experiments between liganded and ligand-free sGC has previously been shown to be a change in scattering at $q \sim 0.078$ Å^{-1}. When sGC extends, this motion causes scattering in the mid-q region to increase.[19,74]

Thus, scattering at 0.078 Å^{-1} was used as a proxy for the degree of extension and/or the fraction of the population that are extended. It is important to note that because SAXS is a technique that averages information over bulk-phase molecules, it can be difficult to differentiate a solution with a single homogeneous intermediate conformation from a mixture of multiple, more extreme conformations.

SAXS profiles for each condition were normalized by maximum I(q)*q^2 and compared as Kratky plots, a transformation that helps emphasize mid-q features (Figure B.8D-F). Difference Kratky plots were then determined for each variant by subtracting the WT ligand-free scattering from previously published *Ms* sGC SEC-SAXS data[19], thus making a "difference Kratky" plot (Figure 3.6, top row). The difference at 0.078 Å^{-1} is also plotted as a bar graph for each variant (Figure 3.6, bottom row). Comparison of the previously performed ligand-free WT *Ms* sGC SEC-SAXS experiment with the current experiment suggests that there is variability between different samples of the same sGC variant. The most recent ligand-free WT experiment appears to have more extended sGC compared to the previous study.[19] Ligand-free *Ms* sGC βC122S and βC122A better match the conformationally contracted scattering measured previously. Despite sample variability, qualitative comparisons can still be made.

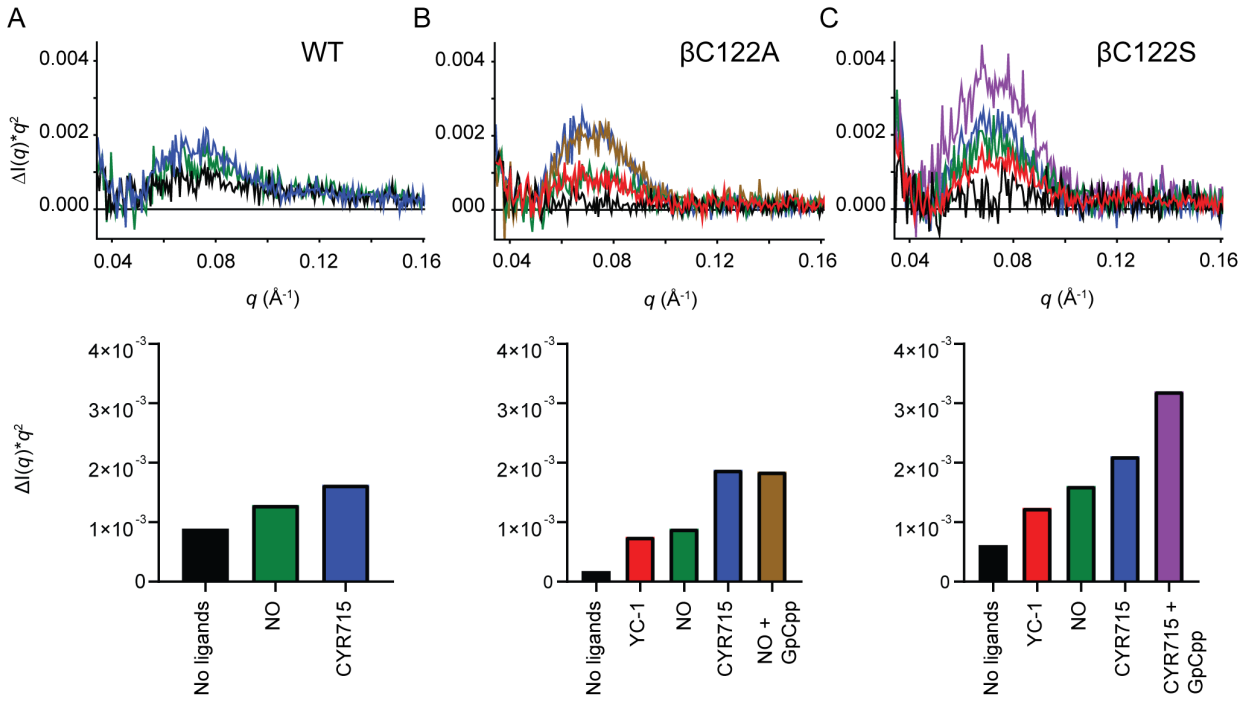

Figure 3.6. SAXS experiments reveal conformational extension with addition of ligands. (A-C, Top row): Normalized difference Kratky plots for *Ms* sGC with different ligands. Kratky plots use a y-axis transformation to emphasize mid-q scattering features. Difference plots were calculated by first normalizing the Kratky plots, then subtracting the previously published scattering of WT ligand-free *Ms* sGC determined in an SEC-SAXS experiment[19] (A-C, Bottom row): Differences in normalized Kratky peak height plotted as bar charts. Peak heights were determined by averaging intensity across q = 0.074 – 0.082 Å^{-1}. (A) WT *Ms* sGC with no ligands (black), NO (green), and CYR715 (blue) included in the SAXS flow cell. (B) βC122A *Ms* sGC with no ligands (black), YC-1 (red), NO (green), CYR715

(blue), and NO and GpCpp (brown). (C) βC122S *Ms* sGC with no ligands (black), YC-1 (red), NO (green), CYR715 (blue), and CYR715 and GpCpp (purple).

In all cases, the scattering at $q = 0.078$ Å^{-1} increases upon addition of ligands. The general trend observed for WT, βC122S, and βC122A variants is that addition of ligands leads to sGC extension from least to most in the order of YC-1, NO, and CYR715. Samples under ligand-free conditions mostly match the SAXS scattering expected for the cryo-EM ligand-free state (Figure B.8G). On the other hand, the predicted scattering of the CYR715-bound sGC cryo-EM structure does not match any of the experimental SAXS profiles. Thus, this structure represents a more extended conformation than observed in SAXS. This has been previously observed in prior SAXS experiments for WT *Ms* sGC in the presence of xsNO.[19] Further, samples including substrate analog GpCpp suggest that bound substrate is partially responsible for full conformational extension. However, even the most extended condition, *Ms* sGC βC122S with CYR715 and GpCpp, does not match the expected scattering predicted from for the extended EM structure.

Discussion

CYR715 is a recently developed sGC stimulator capable of increasing sGC activity both *in vitro* and *in vivo*.[49] CYR715 belongs to a family of sGC stimulators which contains a biaryl pyrazole core, deviating from the benzyl indazole core found in YC-1 and the derivative fused ring pyrazolo[3,4-b]pyridine core found in FDA-approved sGC stimulators riociguat and vericiguat.[49,42,43,46] Additionally, CYR715 substitutes a carboxylic acid moiety for the carbamate of riociguat[43] and vericiguat.[46,48] However, several interaction sites for both YC-1 and riociguat occur via either the core scaffold or carbamate[30], with the latter having been implicated for its importance in stimulating sGC activity.[43,46,48] In this work, we sought to better characterize and compare sGC stimulation by CYR715 *in vitro* while also determining the effects and binding interactions of CYR715 with *Ms* sGC.

CYR715 was found to be a potent stimulator of NO-free *Ms* sGC *in vitro*, and mutagenesis at βC122 resulted in varying degrees of activation response for each protein variant and stimulator assayed (Figure 3.3). This variety of responses in stimulator effect on protein variants was unexpected, and several explanations for these effects were considered. The two cryo-EM structures of *Ms* sGC βC122S solved in this work were found to mostly match previous cryo-EM structures of WT *Ms* sGC, albeit at a higher resolution which allowed for improved modeling and correction of mismodeled areas. Mutagenesis of *Ms* sGC at βC122 resulted in no major structural differences compared to WT *Ms* sGC or *Hs* sGC. The most notable difference is the presence of a subpopulation of extended conformation sGC even without NO or stimulators present. It has been suggested that activity in ligand-free sGC arises from a small population of the enzyme randomly sampling the active, fully extended conformation.[77,78] Thus, this population is consistent with a hypothesis that the variants are more easily stimulated because they more readily sample an extended conformation, increasing access to stimulator binding sites. Some interdomain flexibility, reported in all cryo-EM structures to date, is likely a requisite for sGC activity and stimulator binding in the ligand-free state. *Ms* sGC βC122S and βC122A may be more susceptible to

stimulation because they have a higher fraction in an extended conformation that readily binds stimulator molecules. Unfortunately, without access to and direct reanalysis of the particles from previous cryo-EM experiments, we cannot conclusively state that similar subpopulations exist at lower concentrations in WT *Ms* or *Hs* sGC.

The structure of CYR715-bound *Ms* sGC revealed that the protein can adopt the extended conformation without any NO bound at the heme. Previous structural investigations which have produced structures of extended conformation heme-containing sGCs have done so using NO or NO in combination with various stimulators.[19,20,30] This work presents the first structural example of an sGC in the extended conformation with an intact His-Fe bond. We hypothesize that the activating ability of CYR715 stems from the additional binding interactions observed with residues αR429 and βC78 which provide sufficient stabilization to trap some of the population of NO-free sGC randomly sampling the extended conformation in the extended state.

We previously reported using coiled-coil variants of *Ms* sGC to show that the protein could be rendered constitutively active or inactive through mutations which trapped the protein in either a straightened or bent conformation of the linker coiled-coil region, respectively.[74] In that work, we observed that a protein which could not sample the extended conformation was not stimulated by the addition of YC-1. We hypothesized that small molecules such as YC-1 stimulate sGC activity by stabilizing the straightened conformation of the coiled-coil domains. Previous work[30] on *Hs sGC* and our structure of CYR715-bound *Ms* sGC reveal that stimulators engage sGCs via the β H-NOX and coiled-coil domains of the protein and serve to straighten the bend in the CC domain, much like a molecular splint. Crucially, potent sGC stimulators such as riociguat and CYR715 feature terminal moieties which engage sGC just beyond the C-terminal side of the bent region of the α subunit coiled-coil. Riociguat achieves this interaction via a terminal methylcarbamate; however, the steric bulk from the methyl group at the end of this moiety decreases the potential potency of this interaction. Indeed, sGC variants with reduced steric bulk at positions αL425 or R428 are more potently affected by riociguat, even though these mutations likely decrease the extent of binding interactions between sGC and riociguat.[30] This suggests that stimulator potency can be improved by increasing the quantity or quality of stabilizing interactions with the extended conformation while minimizing steric bulk in the region between the β H-NOX and CC domains. CYR715 engages position αR429 of *Ms* sGC via the carboxylate of the terminal piperidine ring, introducing a stabilizing electrostatic interaction while occupying a sterically compact space to facilitate straightening of the CC domains.

The structural changes observed in SAXS experiments performed in this work support the main conclusions made from the biochemical assays. Addition of stimulators or NO leads to a conformational extension of the average sGC molecule in solution. This change is more pronounced with CYR715 compared to YC-1, reflective of the stronger effect CYR715 has on the activity of sGC under NO-free conditions. βC122S sGC is both the most activated and the most extended variant with CYR715. However, the conformational information provided by SAXS and the activity data are not completely consistent.

First, the SAXS data reveal a lesser conformational extension of sGC with excess NO than would be expected based on activity data. sGC is highly active under excess NO conditions, and so we expected to capture sGC in solution in a highly extended conformation. Instead, while the NO SAXS experiments were designed to ensure the presence of excess NO in solution, the conformations seen in SAXS for NO conditions appear to match an intermediate extension that instead aligns with the activity observed in the 1-NO state. A potential explanation is that there is X-ray induced loss of NO in the sample cell during data collection. In-line UV-Vis measurements positioned directly after the SAXS flow cell showed that NO was still bound to heme in our xsNO conditions (Figure B.9). Under xsNO conditions, NO is thought to form a transient adduct at a second and unknown non-heme site.[27,79,80] While the heme-bound NO remained, the second-site NO interaction may have been lost, leading to rapid equilibration back to a 1-NO-like conformational landscape.

A second inconsistency between SAXS data and activity assays lies in the nuances of the activity profile of βC122S versus βC122A variants. In activity assays, βC122A was more readily activated by YC-1 than WT and βC122S. By contrast, the SAXS data showed very similar incremental increases in conformational extension, with YC-1-bound variants slightly extended and CYR715-bound variants more extended. We hypothesize that this is due to the incomplete information SAXS can provide on protein flexibility. The SAXS data are not high enough resolution or sensitivity to differentiate subtle differences in the extended conformation, such as the precise conformation of the catalytic basket. Furthermore, as bulk averages, these data are unable to fully differentiate changes in conformational landscape or conformational flexibility.

The above points suggest that an interpretation of sGC particles as homogeneous and static structures in solution is inadequate. Indeed, this "end-state" homogeneity has never been supported by SAXS experiments nor any EM experiments on sGCs to date. Both cryo-EM studies reported here and prior studies on *Hs* sGC involve "local" or "multi-body" refinement techniques to correct for interdomain flexibility between the H-NOX and catalytic domains[20,30,53], and earlier negative stain EM work suggested a continuum of states between the fully contracted and extended extremes.[77] The *Ms* sGC βC122S cryo-EM datasets provide further support for conformational heterogeneity, including the observation of an extended subpopulation of βC122S sGC even under NO and other ligand-free conditions.

One potential explanation for the differential activity profiles of βC122S and βC122A variants compared to WT *Ms* sGC lies in differences in flexibility and conformational landscapes. While βC122 does not directly interact with stimulator ligands, its position on the beta sheet adjacent to the alpha helix coordinating the NO-binding heme may play a role in stabilization of the contracted conformation of sGC. The increased ability of βC122S to be activated by CYR715 may be due to increased dynamics in the β H-NOX domain or a propensity to sample a more extended state more readily. The increased activity of βC122A with YC-1 is harder to interpret, but conformational landscapes may not be 1-dimensional. There may be subtleties to the different conformations that are not visible by our SAXS profiles or cryo-EM end-state structures. Future

experiments could entail collection of complementary high-resolution datasets on WT *Ms* sGC and *Ms* sGC βC122A and subsequent conformational landscape analysis as previously described in other work on conformationally dynamic proteins.[81]

Conclusions

Development of small molecule sGC stimulators for the treatment of cardiovascular and NO-signaling related disorders remains an area of intense research and development. All currently FDA approved sGC stimulators were developed before high-resolution full-length structures of sGC were available. While CYR715 differs from these sGC stimulators in several structural aspects, it still accesses the same binding pocket and maintains the same interaction sites observed with riociguat and *Hs* sGC[30] while adding an additional hydrogen bonding interaction at βC78 and new interactions via the terminal piperidine-carboxylic acid moiety. Understanding sGC-stimulator interactions and their role in stabilizing the CC domain to the extended, active conformation can direct rational design of more potent and specific sGC stimulators.

In the past 10 years, our understanding of the structural states of sGCs has grown tremendously. We have gone from zero structures to ten (including the contributions of this work), depicting sGCs in conformations matching both basal and full activity states. And yet, our continued work reveals sGCs are not limited to conformational end states. Here, we have shown that subtle mutations can have major effects on activation profiles without affecting the structures of these end states. We have also shown that the stimulator and activator paradigm of sGC is far from a true dichotomy. Next steps should address how sGC dynamics and conformational landscape lead to catalytic activity.

Acknowledgements

Molecular graphics and analyses performed with UCSF ChimeraX, developed by the Resource for Biocomputing, Visualization, and Informatics at the University of California, San Francisco, with support from National Institutes of Health R01-GM129325 and the Office of Cyber Infrastructure and Computational Biology, National Institute of Allergy and Infectious Diseases. Some of this work was performed at the Stanford-SLAC Cryo-EM Center (S^2C^2), which is supported by the National Institute of General Medical Sciences (1R24GM154186). This work is based on research conducted at the Center for High-Energy X-ray Sciences (CHEXS), which is supported by the National Science Foundation (BIO, ENG and MPS Directorates) under award DMR-2342336, and the Macromolecular Diffraction at CHESS (MacCHESS) facility, which is supported by award 1-P30-GM124166 from the National Institute of General Medical Sciences and the National Institutes of Health.

References

(1) Furchgott, R. F.; Zawadzki, J. V. The Obligatory Role of Endothelial Cells in the Relaxation of Arterial Smooth Muscle by Acetylcholine. *Nature* **1980**, *288* (5789), 373–376. https://doi.org/10.1038/288373a0.

(2) Palmer, R. M. J.; Ferrige, A. G.; Moncada, S. Nitric Oxide Release Accounts for the Biological Activity of Endothelium-Derived Relaxing Factor. *Nature* **1987**, *327* (6122), 524–526. https://doi.org/10.1038/327524a0.

(3) Ignarro, L. J.; Byrns, R. E.; Buga, G. M.; Wood, K. S. Endothelium-Derived Relaxing Factor from Pulmonary Artery and Vein Possesses Pharmacologic and Chemical Properties Identical to Those of Nitric Oxide Radical. **1987**. https://doi.org/10.1161/01.RES.61.6.866.

(4) Knowles, R. G.; Palacios, M.; Palmer, R. M.; Moncada, S. Formation of Nitric Oxide from L-Arginine in the Central Nervous System: A Transduction Mechanism for Stimulation of the Soluble Guanylate Cyclase. *Proc. Natl. Acad. Sci.* **1989**, *86* (13), 5159–5162. https://doi.org/10.1073/pnas.86.13.5159.

(5) Bredt, D. S. Endogenous Nitric Oxide Synthesis: Biological Functions and Pathophysiology. *Free Radic. Res.* **1999**, *31* (6), 577–596. https://doi.org/10.1080/10715769900301161.

(6) Steinert, J. R.; Chernova, T.; Forsythe, I. D. Nitric Oxide Signaling in Brain Function, Dysfunction, and Dementia. *Neurosci. Rev. J. Bringing Neurobiol. Neurol. Psychiatry* **2010**, *16* (4), 435–452. https://doi.org/10.1177/1073858410366481.

(7) Moncada, S.; Palmer, R. M.; Higgs, E. A. Nitric Oxide: Physiology, Pathophysiology, and Pharmacology. *Pharmacol. Rev.* **1991**, *43* (2), 109–142.

(8) Brown, G. C.; Cooper, Chris. E. Nanomolar Concentrations of Nitric Oxide Reversibly Inhibit Synaptosomal Respiration by Competing with Oxygen at Cytochrome Oxidase. *FEBS Lett.* **1994**, *356* (2), 295–298. https://doi.org/10.1016/0014-5793(94)01290-3.

(9) Cleeter, M. W. J.; Cooper, J. M.; Darley-Usmar, V. M.; Moncada, S.; Schapira, A. H. V. Reversible Inhibition of Cytochrome c Oxidase, the Terminal Enzyme of the Mitochondrial Respiratory Chain, by Nitric Oxide: Implications for Neurodegenerative Diseases. *FEBS Lett.* **1994**, *345* (1), 50–54. https://doi.org/10.1016/0014-5793(94)00424-2.

(10) Arnold, W. P.; Mittal, C. K.; Katsuki, S.; Murad, F. Nitric Oxide Activates Guanylate Cyclase and Increases Guanosine 3':5'-Cyclic Monophosphate Levels in Various Tissue Preparations. *Proc. Natl. Acad. Sci. U. S. A.* **1977**, *74* (8), 3203–3207. https://doi.org/10.1073/pnas.74.8.3203.

(11) Lundberg, J. O.; Weitzberg, E. Nitric Oxide Signaling in Health and Disease. *Cell* **2022**, *185* (16), 2853–2878. https://doi.org/10.1016/j.cell.2022.06.010.

(12) Derbyshire, E. R.; Marletta, M. A. Structure and Regulation of Soluble Guanylate Cyclase. *Annu. Rev. Biochem.* **2012**, *81* (Volume 81, 2012), 533–559. https://doi.org/10.1146/annurev-biochem-050410-100030.

(13) Montfort, W. R.; Wales, J. A.; Weichsel, A. Structure and Activation of Soluble Guanylyl Cyclase, the Nitric Oxide Sensor. *Antioxid. Redox Signal.* **2017**, *26* (3), 107–121. https://doi.org/10.1089/ars.2016.6693.

(14) Zhao, Y.; Marletta, M. A. Localization of the Heme Binding Region in Soluble Guanylate Cyclase†. *Biochemistry* **1997**, *36* (50), 15959–15964. https://doi.org/10.1021/bi971825x.

(15) Zhao, Y.; Schelvis, J. P. M.; Babcock, G. T.; Marletta, M. A. Identification of Histidine 105 in the B1 Subunit of Soluble Guanylate Cyclase as the Heme Proximal Ligand. *Biochemistry* **1998**, *37* (13), 4502–4509. https://doi.org/10.1021/bi972686m.
(16) Wedel, B.; Humbert, P.; Harteneck, C.; Foerster, J.; Malkewitz, J.; Böhme, E.; Schultz, G.; Koesling, D. Mutation of His-105 in the Beta 1 Subunit Yields a Nitric Oxide-Insensitive Form of Soluble Guanylyl Cyclase. *Proc. Natl. Acad. Sci. U. S. A.* **1994**, *91* (7), 2592–2596. https://doi.org/10.1073/pnas.91.7.2592.
(17) Boon, E. M.; Huang, S. H.; Marletta, M. A. A Molecular Basis for NO Selectivity in Soluble Guanylate Cyclase. *Nat. Chem. Biol.* **2005**, *1* (1), 53–59. https://doi.org/10.1038/nchembio704.
(18) Möglich, A.; Ayers, R. A.; Moffat, K. Structure and Signaling Mechanism of Per-ARNT-Sim Domains. *Struct. Lond. Engl. 1993* **2009**, *17* (10), 1282–1294. https://doi.org/10.1016/j.str.2009.08.011.
(19) Horst, B. G.; Yokom, A. L.; Rosenberg, D. J.; Morris, K. L.; Hammel, M.; Hurley, J. H.; Marletta, M. A. Allosteric Activation of the Nitric Oxide Receptor Soluble Guanylate Cyclase Mapped by Cryo-Electron Microscopy. *eLife* **2019**, *8*, e50634. https://doi.org/10.7554/eLife.50634.
(20) Kang, Y.; Liu, R.; Wu, J.-X.; Chen, L. Structural Insights into the Mechanism of Human Soluble Guanylate Cyclase. *Nature* **2019**, *574* (7777), 206–210. https://doi.org/10.1038/s41586-019-1584-6.
(21) Allerston, C. K.; von Delft, F.; Gileadi, O. Crystal Structures of the Catalytic Domain of Human Soluble Guanylate Cyclase. *PLoS ONE* **2013**, *8* (3), e57644. https://doi.org/10.1371/journal.pone.0057644.
(22) Stone, J. R.; Marletta, M. A. Soluble Guanylate Cyclase from Bovine Lung: Activation with Nitric Oxide and Carbon Monoxide and Spectral Characterization of the Ferrous and Ferric States. *Biochemistry* **1994**, *33* (18), 5636–5640. https://doi.org/10.1021/bi00184a036.
(23) Ignarro, L. J.; Degnan, J. N.; Baricos, W. H.; Kadowitz, P. J.; Wolin, M. S. Activation of Purified Guanylate Cyclase by Nitric Oxide Requires Heme Comparison of Heme-Deficient, Heme-Reconstituted and Heme-Containing Forms of Soluble Enzyme from Bovine Lung. *Biochim. Biophys. Acta BBA - Gen. Subj.* **1982**, *718* (1), 49–59. https://doi.org/10.1016/0304-4165(82)90008-3.
(24) Ignarro, L. J.; Wood, K. S.; Wolin, M. S. Regulation of Purified Soluble Guanylate Cyclase by Porphyrins and Metalloporphyrins: A Unifying Concept. *Adv. Cyclic Nucleotide Protein Phosphorylation Res.* **1984**, *17*, 267–274.
(25) Herzik, M. A.; Jonnalagadda, R.; Kuriyan, J.; Marletta, M. A. Structural Insights into the Role of Iron-Histidine Bond Cleavage in Nitric Oxide-Induced Activation of H-NOX Gas Sensor Proteins. *Proc. Natl. Acad. Sci. U. S. A.* **2014**, *111* (40), E4156-4164. https://doi.org/10.1073/pnas.1416936111.
(26) Russwurm, M.; Koesling, D. NO Activation of Guanylyl Cyclase. *EMBO J.* **2004**, *23* (22), 4443–4450. https://doi.org/10.1038/sj.emboj.7600422.
(27) Fernhoff, N. B.; Derbyshire, E. R.; Marletta, M. A. A Nitric Oxide/Cysteine Interaction Mediates the Activation of Soluble Guanylate Cyclase. *Proc. Natl. Acad. Sci.* **2009**, *106* (51), 21602–21607. https://doi.org/10.1073/pnas.0911083106.
(28) Stone, J. R.; Marletta, M. A. Spectral and Kinetic Studies on the Activation of Soluble Guanylate Cyclase by Nitric Oxide. *Biochemistry* **1996**, *35* (4), 1093–1099. https://doi.org/10.1021/bi9519718.

(29) Schrammel, A.; Behrends, S.; Schmidt, K.; Koesling, D.; Mayer, B. Characterization of 1H-[1,2,4]Oxadiazolo[4,3-a]Quinoxalin-1-One as a Heme-Site Inhibitor of Nitric Oxide-Sensitive Guanylyl Cyclase. *Mol. Pharmacol.* **1996**, *50* (1), 1–5.
(30) Liu, R.; Kang, Y.; Chen, L. Activation Mechanism of Human Soluble Guanylate Cyclase by Stimulators and Activators. *Nat. Commun.* **2021**, *12* (1), 5492. https://doi.org/10.1038/s41467-021-25617-0.
(31) Fritz, B. G.; Hu, X.; Brailey, J. L.; Berry, R. E.; Walker, F. A.; Montfort, W. R. Oxidation and Loss of Heme in Soluble Guanylyl Cyclase from Manduca Sexta. *Biochemistry* **2011**, *50* (26), 5813–5815. https://doi.org/10.1021/bi200794c.
(32) Hoffmann, L. S.; Schmidt, P. M.; Keim, Y.; Hoffmann, C.; Schmidt, H. H. H. W.; Stasch, J.-P. Fluorescence Dequenching Makes Haem-Free Soluble Guanylate Cyclase Detectable in Living Cells. *PLOS ONE* **2011**, *6* (8), e23596. https://doi.org/10.1371/journal.pone.0023596.
(33) Pan, J.; Zhang, X.; Yuan, H.; Xu, Q.; Zhang, H.; Zhou, Y.; Huang, Z.-X.; Tan, X. The Molecular Mechanism of Heme Loss from Oxidized Soluble Guanylate Cyclase Induced by Conformational Change. *Biochim. Biophys. Acta BBA - Proteins Proteomics* **2016**, *1864* (5), 488–500. https://doi.org/10.1016/j.bbapap.2016.02.012.
(34) Dubois-Deruy, E.; Peugnet, V.; Turkieh, A.; Pinet, F. Oxidative Stress in Cardiovascular Diseases. *Antioxidants* **2020**, *9* (9), 864. https://doi.org/10.3390/antiox9090864.
(35) Stuehr, D. J.; Misra, S.; Dai, Y.; Ghosh, A. Maturation, Inactivation, and Recovery Mechanisms of Soluble Guanylyl Cyclase. *J. Biol. Chem.* **2021**, *296*, 100336. https://doi.org/10.1016/j.jbc.2021.100336.
(36) Martin, F.; Baskaran, P.; Ma, X.; Dunten, P. W.; Schaefer, M.; Stasch, J.-P.; Beuve, A.; van den Akker, F. Structure of Cinaciguat (BAY 58–2667) Bound to *Nostoc* H-NOX Domain Reveals Insights into Heme-Mimetic Activation of the Soluble Guanylyl Cyclase*. *J. Biol. Chem.* **2010**, *285* (29), 22651–22657. https://doi.org/10.1074/jbc.M110.111559.
(37) Follmann, M.; Griebenow, N.; Hahn, M. G.; Hartung, I.; Mais, F.; Mittendorf, J.; Schäfer, M.; Schirok, H.; Stasch, J.; Stoll, F.; Straub, A. The Chemistry and Biology of Soluble Guanylate Cyclase Stimulators and Activators. *Angew. Chem. Int. Ed.* **2013**, *52* (36), 9442–9462. https://doi.org/10.1002/anie.201302588.
(38) Stasch, J.-P.; Schlossmann, J.; Hocher, B. Renal Effects of Soluble Guanylate Cyclase Stimulators and Activators: A Review of the Preclinical Evidence. *Curr. Opin. Pharmacol.* **2015**, *21*, 95–104. https://doi.org/10.1016/j.coph.2014.12.014.
(39) Sandner, P.; Vakalopoulos, A.; Hahn, M. G.; Stasch, J.-P.; Follmann, M. Soluble Guanylate Cyclase Stimulators and Their Potential Use: A Patent Review. *Expert Opin. Ther. Pat.* **2021**, *31* (3), 203–222. https://doi.org/10.1080/13543776.2021.1866538.
(40) Stasch, J.-P.; Hobbs, A. J. NO-Independent, Haem-Dependent Soluble Guanylate Cyclase Stimulators. In *cGMP: Generators, Effectors and Therapeutic Implications*; Schmidt, H. H. H. W., Hofmann, F., Stasch, J.-P., Eds.; Springer: Berlin, Heidelberg, **2009**; pp 277–308. https://doi.org/10.1007/978-3-540-68964-5_13.
(41) Sandner, P.; Follmann, M.; Becker-Pelster, E.; Hahn, M. G.; Meier, C.; Freitas, C.; Roessig, L.; Stasch, J.-P. Soluble GC Stimulators and Activators: Past, Present and Future. *Br. J. Pharmacol.* **2024**, *181* (21), 4130–4151. https://doi.org/10.1111/bph.15698.
(42) Ko, F.-N.; Wu, C.-C.; Kuo, S.-C.; Lee, F.-Y.; Teng, C.-M. YC-1, a Novel Activator of Platelet Guanylate Cyclase. *Blood* **1994**, *84* (12), 4226–4233. https://doi.org/10.1182/blood.V84.12.4226.bloodjournal84124226.

(43) Mittendorf, J.; Weigand, S.; Alonso-Alija, C.; Bischoff, E.; Feurer, A.; Gerisch, M.; Kern, A.; Knorr, A.; Lang, D.; Muenter, K.; Radtke, M.; Schirok, H.; Schlemmer, K.-H.; Stahl, E.; Straub, A.; Wunder, F.; Stasch, J.-P. Discovery of Riociguat (BAY 63-2521): A Potent, Oral Stimulator of Soluble Guanylate Cyclase for the Treatment of Pulmonary Hypertension. *ChemMedChem* **2009**, *4* (5), 853–865. https://doi.org/10.1002/cmdc.200900014.

(44) Conole, D.; Scott, L. J. Riociguat: First Global Approval. *Drugs* **2013**, *73* (17), 1967–1975. https://doi.org/10.1007/s40265-013-0149-5.

(45) Ghofrani, H.-A.; Galiè, N.; Grimminger, F.; Grünig, E.; Humbert, M.; Jing, Z.-C.; Keogh, A. M.; Langleben, D.; Kilama, M. O.; Fritsch, A.; Neuser, D.; Rubin, L. J. Riociguat for the Treatment of Pulmonary Arterial Hypertension. *N. Engl. J. Med.* **2013**, *369* (4), 330–340. https://doi.org/10.1056/NEJMoa1209655.

(46) Follmann, M.; Ackerstaff, J.; Redlich, G.; Wunder, F.; Lang, D.; Kern, A.; Fey, P.; Griebenow, N.; Kroh, W.; Becker-Pelster, E.-M.; Kretschmer, A.; Geiss, V.; Li, V.; Straub, A.; Mittendorf, J.; Jautelat, R.; Schirok, H.; Schlemmer, K.-H.; Lustig, K.; Gerisch, M.; Knorr, A.; Tinel, H.; Mondritzki, T.; Trübel, H.; Sandner, P.; Stasch, J.-P. Discovery of the Soluble Guanylate Cyclase Stimulator Vericiguat (BAY 1021189) for the Treatment of Chronic Heart Failure. *J. Med. Chem.* **2017**, *60* (12), 5146–5161. https://doi.org/10.1021/acs.jmedchem.7b00449.

(47) Armstrong, P. W.; Pieske, B.; Anstrom, K. J.; Ezekowitz, J.; Hernandez, A. F.; Butler, J.; Lam, C. S. P.; Ponikowski, P.; Voors, A. A.; Jia, G.; McNulty, S. E.; Patel, M. J.; Roessig, L.; Koglin, J.; O'Connor, C. M. Vericiguat in Patients with Heart Failure and Reduced Ejection Fraction. *N. Engl. J. Med.* **2020**, *382* (20), 1883–1893. https://doi.org/10.1056/NEJMoa1915928.

(48) Xia, J.; Hui, N.; Tian, L.; Liang, C.; Zhang, J.; Liu, J.; Wang, J.; Ren, X.; Xie, X.; Wang, K. Development of Vericiguat: The First Soluble Guanylate Cyclase (sGC) Stimulator Launched for Heart Failure with Reduced Ejection Fraction (HFrEF). *Biomed. Pharmacother.* **2022**, *149*, 112894. https://doi.org/10.1016/j.biopha.2022.112894.

(49) Rennie, G. R.; Barden, T. C.; Bernier, S. G.; Carvalho, A.; Deming, R.; Germano, P.; Hudson, C.; Im, G.-Y. J.; Iyengar, R. R.; Jia, L.; Jung, J.; Kim, E.; Lee, T. W.-H.; Mermerian, A.; Moore, J.; Nakai, T.; Perl, N. R.; Tobin, J.; Zimmer, D. P.; Renhowe, P. A. Discovery of CYR715: A Novel Carboxylic Acid-Containing Soluble Guanylate Cyclase Stimulator. *Bioorg. Med. Chem. Lett.* **2021**, *40*, 127886. https://doi.org/10.1016/j.bmcl.2021.127886.

(50) Sayed, N.; Baskaran, P.; Ma, X.; van den Akker, F.; Beuve, A. Desensitization of Soluble Guanylyl Cyclase, the NO Receptor, by S-Nitrosylation. *Proc. Natl. Acad. Sci.* **2007**, *104* (30), 12312–12317. https://doi.org/10.1073/pnas.0703944104.

(51) Fernhoff, N. B.; Derbyshire, E. R.; Underbakke, E. S.; Marletta, M. A. Heme-Assisted *S*-Nitrosation Desensitizes Ferric Soluble Guanylate Cyclase to Nitric Oxide*. *J. Biol. Chem.* **2012**, *287* (51), 43053–43062. https://doi.org/10.1074/jbc.M112.393892.

(52) Hu, X.; Murata, L. B.; Weichsel, A.; Brailey, J. L.; Roberts, S. A.; Nighorn, A.; Montfort, W. R. Allostery in Recombinant Soluble Guanylyl Cyclase from *Manduca Sexta**. *J. Biol. Chem.* **2008**, *283* (30), 20968–20977. https://doi.org/10.1074/jbc.M801501200.

(53) Liu, R.; Kang, Y.; Chen, L. NO Binds to the Distal Site of Haem in the Fully Activated Soluble Guanylate Cyclase. *Nitric Oxide* **2023**, *134–135*, 17–22. https://doi.org/10.1016/j.niox.2023.03.002.

(54) Cianfrocco, M. A.; Wong-Barnum, M.; Youn, C.; Wagner, R.; Leschziner, A. COSMIC2: A Science Gateway for Cryo-Electron Microscopy Structure Determination. In *Practice and*

Experience in Advanced Research Computing 2017: Sustainability, Success and Impact; PEARC '17; Association for Computing Machinery: New York, NY, USA, **2017**; pp 1–5. https://doi.org/10.1145/3093338.3093390.

(55) Jamali, K.; Käll, L.; Zhang, R.; Brown, A.; Kimanius, D.; Scheres, S. H. W. Automated Model Building and Protein Identification in Cryo-EM Maps. *Nature* **2024**, *628* (8007), 450–457. https://doi.org/10.1038/s41586-024-07215-4.

(56) Liebschner, D.; Afonine, P. V.; Baker, M. L.; Bunkóczi, G.; Chen, V. B.; Croll, T. I.; Hintze, B.; Hung, L.-W.; Jain, S.; McCoy, A. J.; Moriarty, N. W.; Oeffner, R. D.; Poon, B. K.; Prisant, M. G.; Read, R. J.; Richardson, J. S.; Richardson, D. C.; Sammito, M. D.; Sobolev, O. V.; Stockwell, D. H.; Terwilliger, T. C.; Urzhumtsev, A. G.; Videau, L. L.; Williams, C. J.; Adams, P. D. Macromolecular Structure Determination Using X-Rays, Neutrons and Electrons: Recent Developments in Phenix. *Acta Crystallogr. Sect. Struct. Biol.* **2019**, *75* (10), 861–877. https://doi.org/10.1107/S2059798319011471.

(57) Emsley, P.; Lohkamp, B.; Scott, W. G.; Cowtan, K. Features and Development of Coot. *Acta Crystallogr. D Biol. Crystallogr.* **2010**, *66* (Pt 4), 486–501. https://doi.org/10.1107/S0907444910007493.

(58) Guex, N.; Peitsch, M. C.; Schwede, T. Automated Comparative Protein Structure Modeling with SWISS-MODEL and Swiss-PdbViewer: A Historical Perspective. *ELECTROPHORESIS* **2009**, *30* (S1), S162–S173. https://doi.org/10.1002/elps.200900140.

(59) Bienert, S.; Waterhouse, A.; de Beer, T. A. P.; Tauriello, G.; Studer, G.; Bordoli, L.; Schwede, T. The SWISS-MODEL Repository—New Features and Functionality. *Nucleic Acids Res.* **2017**, *45* (D1), D313–D319. https://doi.org/10.1093/nar/gkw1132.

(60) Bertoni, M.; Kiefer, F.; Biasini, M.; Bordoli, L.; Schwede, T. Modeling Protein Quaternary Structure of Homo- and Hetero-Oligomers beyond Binary Interactions by Homology. *Sci. Rep.* **2017**, *7* (1), 10480. https://doi.org/10.1038/s41598-017-09654-8.

(61) Waterhouse, A.; Bertoni, M.; Bienert, S.; Studer, G.; Tauriello, G.; Gumienny, R.; Heer, F. T.; de Beer, T. A. P.; Rempfer, C.; Bordoli, L.; Lepore, R.; Schwede, T. SWISS-MODEL: Homology Modelling of Protein Structures and Complexes. *Nucleic Acids Res.* **2018**, *46* (W1), W296–W303. https://doi.org/10.1093/nar/gky427.

(62) Studer, G.; Rempfer, C.; Waterhouse, A. M.; Gumienny, R.; Haas, J.; Schwede, T. QMEANDisCo—Distance Constraints Applied on Model Quality Estimation. *Bioinformatics* **2020**, *36* (6), 1765–1771. https://doi.org/10.1093/bioinformatics/btz828.

(63) Goddard, T. D.; Huang, C. C.; Meng, E. C.; Pettersen, E. F.; Couch, G. S.; Morris, J. H.; Ferrin, T. E. UCSF ChimeraX: Meeting Modern Challenges in Visualization and Analysis. *Protein Sci. Publ. Protein Soc.* **2018**, *27* (1), 14–25. https://doi.org/10.1002/pro.3235.

(64) Pettersen, E. F.; Goddard, T. D.; Huang, C. C.; Meng, E. C.; Couch, G. S.; Croll, T. I.; Morris, J. H.; Ferrin, T. E. UCSF ChimeraX: Structure Visualization for Researchers, Educators, and Developers. *Protein Sci. Publ. Protein Soc.* **2021**, *30* (1), 70–82. https://doi.org/10.1002/pro.3943.

(65) Meng, E. C.; Goddard, T. D.; Pettersen, E. F.; Couch, G. S.; Pearson, Z. J.; Morris, J. H.; Ferrin, T. E. UCSF ChimeraX: Tools for Structure Building and Analysis. *Protein Sci.* **2023**, *32* (11), e4792. https://doi.org/10.1002/pro.4792.

(66) Moriarty, N. W.; Grosse-Kunstleve, R. W.; Adams, P. D. Electronic Ligand Builder and Optimization Workbench (eLBOW): A Tool for Ligand Coordinate and Restraint Generation. *Acta Crystallogr. D Biol. Crystallogr.* **2009**, *65* (Pt 10), 1074–1080. https://doi.org/10.1107/S0907444909029436.

(67) Williams, C. J.; Headd, J. J.; Moriarty, N. W.; Prisant, M. G.; Videau, L. L.; Deis, L. N.; Verma, V.; Keedy, D. A.; Hintze, B. J.; Chen, V. B.; Jain, S.; Lewis, S. M.; Arendall, W. B.; Snoeyink, J.; Adams, P. D.; Lovell, S. C.; Richardson, J. S.; Richardson, D. C. MolProbity: More and Better Reference Data for Improved All-Atom Structure Validation. *Protein Sci. Publ. Protein Soc.* **2018**, *27* (1), 293–315. https://doi.org/10.1002/pro.3330.

(68) Acerbo, A. S.; Cook, M. J.; Gillilan, R. E. Upgrade of MacCHESS Facility for X-Ray Scattering of Biological Macromolecules in Solution. *J. Synchrotron Radiat.* **2015**, *22* (1), 180–186. https://doi.org/10.1107/S1600577514020360.

(69) Skou, S.; Gillilan, R. E.; Ando, N. Synchrotron-Based Small-Angle X-Ray Scattering of Proteins in Solution. *Nat. Protoc.* **2014**, *9* (7), 1727–1739. https://doi.org/10.1038/nprot.2014.116.

(70) Illava, G.; Gillilan, R.; Ando, N. Development of In-Line Anoxic Small-Angle X-Ray Scattering and Structural Characterization of an Oxygen-Sensing Transcriptional Regulator. *J. Biol. Chem.* **2023**, *299* (8), 105039. https://doi.org/10.1016/j.jbc.2023.105039.

(71) Hopkins, J. B.; Gillilan, R. E.; Skou, S. BioXTAS RAW: Improvements to a Free Open-Source Program for Small-Angle X-Ray Scattering Data Reduction and Analysis. *J. Appl. Crystallogr.* **2017**, *50* (5), 1545–1553. https://doi.org/10.1107/S1600576717011438.

(72) Svergun, D. I. Determination of the Regularization Parameter in Indirect-Transform Methods Using Perceptual Criteria. *J. Appl. Crystallogr.* **1992**, *25* (4), 495–503. https://doi.org/10.1107/S0021889892001663.

(73) Gerzer, R.; Böhme, E.; Hofmann, F.; Schultz, G. Soluble Guanylate Cyclase Purified from Bovine Lung Contains Heme and Copper. *FEBS Lett.* **1981**, *132* (1), 71–74. https://doi.org/10.1016/0014-5793(81)80429-2.

(74) Wittenborn, E. C.; Thomas, W. C.; Houghton, K. A.; Wirachman, E. S.; Wu, Y.; Marletta, M. A. Role of the Coiled-Coil Domain in Allosteric Activity Regulation in Soluble Guanylate Cyclase. *Biochemistry* **2023**, *62* (10), 1568–1576. https://doi.org/10.1021/acs.biochem.3c00052.

(75) Stone, J. R.; Marletta, M. A. Synergistic Activation of Soluble Guanylate Cyclase by YC-1 and Carbon Monoxide: Implications for the Role of Cleavage of the Iron-Histidine Bond during Activation by Nitric Oxide. *Chem. Biol.* **1998**, *5* (5), 255–261. https://doi.org/10.1016/S1074-5521(98)90618-4.

(76) Horst, B. G.; Marletta, M. A. Physiological Activation and Deactivation of Soluble Guanylate Cyclase. *Nitric Oxide* **2018**, *77*, 65–74. https://doi.org/10.1016/j.niox.2018.04.011.

(77) Campbell, M. G.; Underbakke, E. S.; Potter, C. S.; Carragher, B.; Marletta, M. A. Single-Particle EM Reveals the Higher-Order Domain Architecture of Soluble Guanylate Cyclase. *Proc. Natl. Acad. Sci.* **2014**, *111* (8), 2960–2965. https://doi.org/10.1073/pnas.1400711111.

(78) Wittenborn, E. C.; Marletta, M. A. Structural Perspectives on the Mechanism of Soluble Guanylate Cyclase Activation. *Int. J. Mol. Sci.* **2021**, *22* (11), 5439. https://doi.org/10.3390/ijms22115439.

(79) Cary, S. P. L.; Winger, J. A.; Marletta, M. A. Tonic and Acute Nitric Oxide Signaling through Soluble Guanylate Cyclase Is Mediated by Nonheme Nitric Oxide, ATP, and GTP. *Proc. Natl. Acad. Sci.* **2005**, *102* (37), 13064–13069. https://doi.org/10.1073/pnas.0506289102.

(80) Derbyshire, E. R.; Marletta, M. A. Butyl Isocyanide as a Probe of the Activation Mechanism of Soluble Guanylate Cyclase: INVESTIGATING THE ROLE OF NON-HEME NITRIC

OXIDE. *J. Biol. Chem.* **2007**, *282* (49), 35741–35748. https://doi.org/10.1074/jbc.M705557200.

(81) Xu, D.; Thomas, W. C.; Burnim, A. A.; Ando, N. Conformational Landscapes of a Class I Ribonucleotide Reductase Complex during Turnover Reveal Intrinsic Dynamics and Asymmetry. *Nat. Commun.* **2025**, *16* (1), 2458. https://doi.org/10.1038/s41467-025-57735-4.

Chapter 4

Investigating the Non-Heme NO Activation of Pathway of Soluble Guanylate Cyclase

Summary

The nitric oxide (NO) receptor protein soluble guanylate cyclase (sGC) displays a two-step activation profile in response to NO binding. From basal activity in the NO-free (unliganded, U) state, sub-stoichiometric concentrations of NO result in a non-linear increase of sGC catalytic activity which reaches approximately 15% of maximal activity when concentrations of NO are equal to the concentration of enzyme-bound heme (1-NO) in sGC. When NO concentrations are in stoichiometric excess over the heme concentration (xsNO), sGC activity increases to its maximal level. Upon removal of excess NO from solution, sGC activity rapidly returns to approximately 15% of maximum, matching the activity observed for sGC in the 1-NO state, while NO remains bound to the heme. These observations suggest that NO increases sGC activity via two different interactions: the first is the well-characterized interaction between NO and the heme cofactor while evidence suggests that the second activation site involves a reversible NO-cysteine interaction at conserved positions in NO-responsive sGCs. This chapter discusses investigations of this potential NO-cysteine interaction using the cysteine labeling reagents *S*-methyl methanethiosulfonate (MMTS) and iodoacetamide (IAM), trypsinized mass spectrometry (MS) of MMTS-labeled protein, and bioinformatic approaches to determine important, conserved regulatory positions in sGC. Both MMTS and IAM label cysteine residues in sGC, however labeling by IAM alone does not prevent xsNO activation of sGC while labeling with MMTS alone or in tandem with IAM prevents xsNO activation of sGC. Trypsin MS results revealed that labeling with low concentrations of MMTS resulted in partial modification of a substrate coordinating cysteine in the β catalytic subunit, providing potential explanation for the partial activity of the MMTS-labeled protein. Bioinformatic analysis of the H-NOX domains of β or β-like subunits of various sGCs was performed, revealing cysteines which are not conserved between NO- and O_2-sensing sGCs which could be involved in the xsNO response.

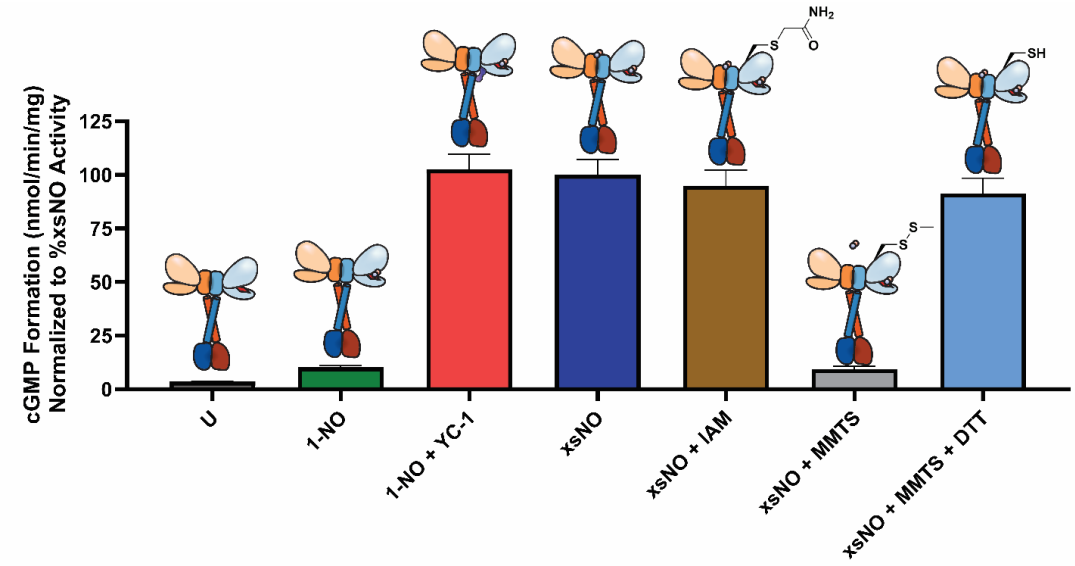

Introduction

Nitric oxide plays a significant role in endogenous signaling in many organisms with well-studied roles in cardiovascular regulation, neuronal development, and platelet function.[1–5] Soluble guanylate cyclase (sGC) is a physiological receptor for NO which increases its cyclization of guanosine 5'triphosphate (GTP) into guanosine 3',5'-cyclic monophosphate (cGMP) in response to NO binding.[6] Broadly, the first step of sGC activation occurs via NO binding at the heme of the β subunit of the N-terminal regulatory heme nitric oxide oxygen binding (H-NOX) domain.[7,8] Full activation of sGC requires additional NO, and maximal activity is achieved through conformational toggling in the coiled-coil (CC) and Per/Arnt/Sim (PAS) signal transduction domains which leads to an opening of the C-terminal catalytic (CAT) domains which facilitates catalysis.[9,10] NO concentrations in the picomolar to nanomolar range are sufficient to stimulate sGC activity[11], however the exact mechanisms behind this activation are not fully understood.

When isolated and in the absence of NO, sGC exhibits a low, basal level of activity.[12] The first equivalent of NO binds to sGC via the heme cofactor in the β H-NOX domain with a $K_d < 1.2 \times 10^{-12}$ M.[13] Given that physiological NO concentrations range from 20 pM to 5 nM and the off-rate for heme NO is 3×10^{-4} s^{-1}, the NO-heme interaction is effectively irreversible in physiological conditions.[11,12,14–18] Biochemical characterization of sGC in the presence of stoichiometric equivalents of NO to heme revealed that sGC was only activated to approximately 15% of maximal activity.[12,19] The addition of stoichiometric excess NO relative to the heme fully activates sGC, while removal of non-heme NO via gel filtration or an NO trap rapidly returns the enzyme to 15% of maximal activity while maintaining the NO bound at the heme.[12] Additionally, the ultra violet visible (UV-Vis) characteristics of sGC in the stoichiometric NO state are indistinguishable from sGC in the stoichiometric excess NO state, suggesting that the heme remains in a 5-coordinate (5c) heme-NO state in the presence of excess NO and that NO is interacting with the protein at a non-heme site.[12] Experiments utilizing n-butyl isocyanide (BIC) as an alternative heme ligand found that excess NO was still capable of stimulating sGC activity even when unable to bind directly to the heme.[20] These observations suggest that sGC exhibits three activity states, with a two-step activation profile, in conditions with an absence of NO (U), a stoichiometric equivalent of NO (1-NO), or a stoichiometric excess of NO (xsNO). The 1-NO state is the most likely physiological resting state for sGC, and *in vivo* stimulation of activity from the 1-NO and xsNO states is likely driven by a non-heme sGC-NO interaction.

NO has been shown to regulate protein activity via interactions with cysteine residues.[21–26] These interactions can occur via oxidative addition yielding a covalent, relatively long-lived RSNO nitrosothiol complex, or via nucleophilic addition resulting in a transient RSNO●⁻ species. Activation of sGC via NO occurs in both anaerobic and aerobic environments and is reversible on the order of seconds, indicating that the interactions which increase sGC activity proceed via a non-oxidative, non-nitrosothiol pathway.[27] The potential of a cysteine-NO interaction as the basis for the xsNO activity of sGC was investigated through experiments which modified the cysteines of rat (*Rn*) sGC using the labeling reagent *S*-methyl methanethiosulfonate (MMTS).[27] Researchers found that protein which had been modified by MMTS was unable to fully activate in the presence of excess NO and instead exhibited activity close to that of 1-NO protein. The excess NO sensitivity of MMTS-labeled sGC could be restored after reduction with dithiothreitol (DTT) which removed the *S*-methyl adduct from labeled cysteines.

Protein which had been labeled with MMTS could be partially stimulated by the addition of the sGC stimulator YC-1 along with NO, which was interpreted as evidence that the *S*-methyl adduct introduced by MMTS was not introducing a steric block that prevented conformational change necessary for full catalytic activity.[27] Even so, the addition of YC-1 only led to approximately 30% of the activity observed for unlabeled protein in the same conditions, suggesting that MMTS labeling, while not fully limiting conformational change in sGC, could be introducing steric bulk which limited the total range of conformational flexibility for the enzyme. Previous work investigating the role of cysteines in sGC activation was performed before high-resolution, full-length structures were solved for sGC. These structures revealed that sGC undergoes significant changes in global conformation when excess NO is present while highlighting additional, subtle conformational changes in the H-NOX and CAT domains when comparing the basal and maximal activity states. These structures refocused attention on the significance of conformational change during the activation of sGC and have provided new routes to explore the role of conserved residues in sGC.

This chapter discusses further attempts to probe potential NO-cysteine activation of sGC using the cysteine labeling reagents *S*-methyl methanethiosulfonate (MMTS) and iodoacetamide (IAM). MMTS-labeled trypsinized protein was analyzed by mass spectrometry, and peptide coverage was mapped to determine which conserved cysteines had been modified. Results were also interpreted utilizing structural context provided by newly solved full-length structures for sGC. Conserved cysteines between NO- and O_2-sensing sGCs were investigated using a bioinformatics approach.

Materials and Methods

Materials

All chemicals were purchased from commercial vendors and used without further purification. Primers were purchased from Integrated DNA Technologies (Coralville, IA). Gibson-like Master Mix was purchased from the QB3 MacroLab (Berkeley, CA). PrimeSTAR Max Premix was purchased from Takara Bio USA (Mountain View, CA). DNA purification kits were purchased from Qiagen (Germantown, MD). Sf9 cells were purchased from Novagen (Madison, WI). ExCell-420 media, DNAase 1 from bovine pancreas, β-mercaptoethanol, sodium phosphate dibasic (Na_2HPO_4), potassium phosphate (K_2HPO_4), sodium dithionite ($Na_2S_2O_4$), guanosine 5'-triphosphate sodium salt (GTP) (>95%, HPLC), sodium carbonate (Na_2CO_3), zinc acetate ($Zn(CH_3CO_2)_2$), *S*-methyl methanethiosulfonate (MMTS, 97%), iodoacetamide (IAM), and trifluoroacetic acid (TFA) were purchased from Merck (Darmstadt, Germany). Trypsin/Lys-C Mix was purchased from Promega (Madison, WI). 4-(2-hydroxyethyl)piperazine-1-ethanesulfonic acid (HEPES), urea, and Zeba spin desalting columns were purchased from ThermoFisher Scientific (Waltham, MA). 4-(2-aminoethyl)benzenesulfonyl fluoride hydrochloride (AEBSF) was purchased from Research Products International (Mount Prospect, IL). Benzamidine, glycerol, sodium chloride (NaCl), and magnesium chloride ($MgCl_2$) were purchased from VWR Life Science (Visalia, CA). Dithiothreitol (DTT) was purchased from Bachem (Bubendorf, Switzerland). Imidazole was purchased from Oakwood Chemical (West Columbia, SC). Triethanolamine (TEA) was purchased from Spectrum Chemical (Gardena, CA). TALON Superflow resin was purchased from Cytiva (Marlborough, MA). Vivaspin 500 (30,000 MWCO)

spin concentrators were purchased from Sartorius (Fremont, CA). PROLI NONOate was purchased from Cayman Chemical Company (Ann Arbor, MI).

Generation of Expression Constructs

Constructs of *Ms* sGC α1 (Uniprot: O77105) and β1(Uniprot: O77106) were cloned into pFastBac vectors generating pFastBac_Ms_sGC_α1_His6 and pFastBac_Ms_sGC_β1, respectively.[9] Genes were transposed into baculovirus bacmid DNA in DH10Bac-GFP *E. coli* cells. Bacmid was isolated, and gene sequences were validated by PCR amplification and Sanger sequencing (UC Berkeley DNA Sequencing Facility). Individual recombinant baculovirus for the α and β subunits were generated via transfection of bacmids into Sf9 cells.

Protein Expression and Purification

Sf9 cells were grown in suspension at 27 °C, with shaking at 130 rpm. Recombinant baculovirus for each subunit was amplified until viral titer was greater than 1 x 10^8 pfu/mL. Sf9 cultures at a density of 4 x 10^6 cells/mL were co-infected with 50 mL of α and β amplified virus, for a total of 100 mL virus per liter. Infected cells were grown for 72 hours before harvesting by centrifugation at 3,280 g for 20 minutes. Pellets were snap frozen in liquid nitrogen and stored at -80 °C.

Protein purification was performed at 4 °C unless otherwise indicated. Cell pellets were thawed on ice and resuspended in Buffer A (50 mM K_2HPO_4, 200 mM NaCl, 1 mM imidazole, 5 mM β-mercaptoethanol, 1 mM benzamidine, 5% (v/v) glycerol, pH 8.0, 0.22 μm filtered), supplemented with 10 mM benzamidine, 0.25 mM AEBSF, 0.5 mg/mL DNase I, and 5 mM β-mercaptoethanol. Cells were lysed by bead beating with 0.5 mm glass beads for 3 pulses of 15 s, with 60 s rests in between. Beads were removed by centrifugation at 1,800 g for 5 minutes. The crude cell lysate was clarified by ultracentrifugation at 158,000 g for 90 minutes. Lysate was applied to a 2.5 mL TALON Superflow column at 0.5 mL/min. The column was washed with 10 column volumes (CV) of Buffer A, 15 CV of Buffer A supplemented with 1.2 M NaCl, and again with 10 CV of Buffer A, all at 1 mL/min, before elution. Protein was eluted with 10 CV of Buffer B (50 mM K_2HPO_4, 200 mM NaCl, 125 mM imidazole, 5 mM β-mercaptoethanol, 1 mM benzamidine, 5% (v/v) glycerol, pH 8.0, 0.22 μm filtered). Yellow-colored fractions were concentrated to < 1 mL, supplemented with 5 mM DTT and 1 mM EDTA, diluted to 9 mL with Buffer C (25 mM TEA, 25 mM NaCl, 5 mM DTT, 5% (v/v) glycerol, pH 7.4, 0.22 μm filtered) and immediately applied to a POROS HQ2 anion exchange column at 0.25 mL/min. The column was washed with 3 CV of Buffer C, followed by a gradient up to 50% Buffer D (25 mM triethanolamine, 750 mM NaCl, 5 mM DTT, 5% (v/v) glycerol, pH 7.4, 0.22 μm filtered) developed over 17 CV running at 1 mL/min. Fractions containing sGC were concentrated, snap frozen in liquid nitrogen, and stored at -80 °C.

Sample Preparation and Labeling for Activity Assays and Trypsinized Mass Spectrometry

Samples were prepared in an anaerobic chamber at RT, unless otherwise noted. Protein was thawed at 4 °C, reduced using 10 mM $Na_2S_2O_4$ for 15 minutes at RT, and desalted using a Zeba spin column equilibrated with Buffer E (50 mM HEPES, 150 mM NaCl, 5% (v/v) glycerol, pH 7.5, 0.22 μm filtered). Residual DTT from protein purification was removed by five rounds of dilution to 500 μL with Buffer E and concentration to 50 μL using a Vivaspin 500 (30,000 MWCO) spin concentrator. UV-Vis spectra were collected using a Nanodrop 2000c spectrophotometer, and protein concentration was determined using the reduced heme Soret peak at 433 nm (149,000 M^{-1} cm^{-1}).[9,28] 1-NO and xsNO protein was first brought to the xsNO state by the addition of 50 μm

PROLI NONOate, for an NO concentration of 100 μM. Protein was then desalted using a Zeba spin column to generate 1-NO protein. UV-Vis spectra were collected, and the concentration of the 1-NO protein was determined by comparing the ratio of A_{280} peaks for the U and 1-NO protein. To generate xsNO protein, 50 μM PROLI NONOate was added to the 1-NO protein and allowed to incubate for 5 minutes. When needed, MMTS or IAM were diluted from 1 mM stock solutions to final concentrations between 50 and 200 μM. Proteins were incubated for 30 minutes after each addition of labeling reagent. For assays where MMTS labeling was reversed, 10 mM DTT was added to samples and allowed to incubate for 5 minutes.

Activity Assays and cGMP Quantification

Activity assays were performed in an anaerobic chamber at 25 °C in Buffer E. For reactions without labeling agents, Buffer E was supplemented with 5 mM DTT and 5 mM $MgCl_2$, while for reactions using labeling agents only 5 mM $MgCl_2$ was added. Final protein concentrations ranged between 20 and 50 nM. Reactions were initiated by the addition of 2 mM GTP and were quenched 1:4 (v:v) using 125 mM $Zn(CH_3CO_2)_2$. Sample pH was adjusted to pH 7 by the addition of an equal volume of 125 mM Na_2CO_3. Samples were stored at -80 °C. Quenched assays were thawed and centrifuged for 10 minutes at 21,130 g to remove the zinc precipitate. Samples were diluted, and cGMP formation was quantified in duplicate using a cGMP Enzyme Linked Immunosorbent Assay (ELISA) following manufacturer protocols (Enzo Life Sciences). Initial rates were calculated from the linear phase of the time course where < 10% of the GTP substrate was consumed.

Mass Spec of Trypsinized MMTS-labeled Protein

Protein samples were prepared as described in the Sample Preparation section. MMTS-labeled protein was removed from the anaerobic chamber and solubilized in 7 M urea in 50 mM Tris-HCl (pH 8). Protein denaturation was monitored by observing sample color loss due to unfolding of the heme-containing β H-NOX domain. After denaturation, samples were alkylated using 15 mM IAM and incubated for 30 minutes at RT. Samples were then diluted 7-fold to reduce urea concentrations to 1 M using 50 mM Tris-HCl (pH 8). Trypsin/Lys-C Mix was added to a final ratio of 25:1 sGC:Trypsin (w/w), mixed, and incubated overnight at 37 °C. Digestion was terminated using TFA at a final concentration of 1%. Samples were snap frozen in liquid nitrogen and stored at -80 °C until analysis. Samples were analyzed at the QB3/Chemistry Mass Spectrometry Facility at the University of California, Berkeley by Dr. Anthony Iavarone using a Synapt G2-Si mass spectrometer connected in-line with an Acquity M-class liquid chromatography system (Waters, Milford, MA) using previously published methodology.[29] Data analysis was performed using MassLynx and Progenesis QI for Proteomics software (Waters).

Results and Discussion

Heterodimeric NO-sensitive α/β-type sGCs from animals including human (*Hs*), rat (*Rn*), and moth (*Ms)* have been characterized, and these enzymes all show a two-step activation response to NO binding. If the non-heme second site NO interaction leading to xsNO activity proceeds via a cysteine-NO interaction, then the participating cysteine residue is likely conserved across similarly activated NO-sensitive sGCs. To date, no reproducible method for heterologous expression of these heterodimeric sGCs in *E. coli* has been determined, necessitating the use of insect cell expression and purification to obtain even small yields of pure protein. The labor-

intensive nature of insect cell expression has led to previous cysteine-variant screens being performed only on small volume cultures using enriched cell lysate assays. Thus, cysteine labeling reagents, mass spectrometry, structural biology, and bioinformatics of wild type (WT) sGC proteins were used to facilitate the search for which cysteine(s) could serve as potential second NO sites.

Conserved cysteines in α/β-types sGCs

Sequences from three NO-sensitive α/β-types sGCs (*Hs*, *Rn*, *Ms*) were compared to determine which cysteines were conserved in both the α and β subunits (Figure 4.1). Significant sequence identity is shared in *Hs* and *Rn* sGCs subunits (89.2% in α and 98.9% in β), with 34 of the 38 cysteines of *Hs* sGC being conserved in *Rn* sGC (20 conserved cysteines in the α subunit and 10 in the β subunit). When expanding sequence analysis to include conserved cysteines from *Ms* sGC (41.0% identity in the α and 60.3% in the β subunits with *Hs* sGC), only 16 total cysteines (8 from each subunit) are conserved between these three sGCs which have been characterized with a two-step activation profile in response to NO. Thus, *Ms* sGC offers a more concise representation of potential cysteines which have been conserved in NO-sensitive sGCs.

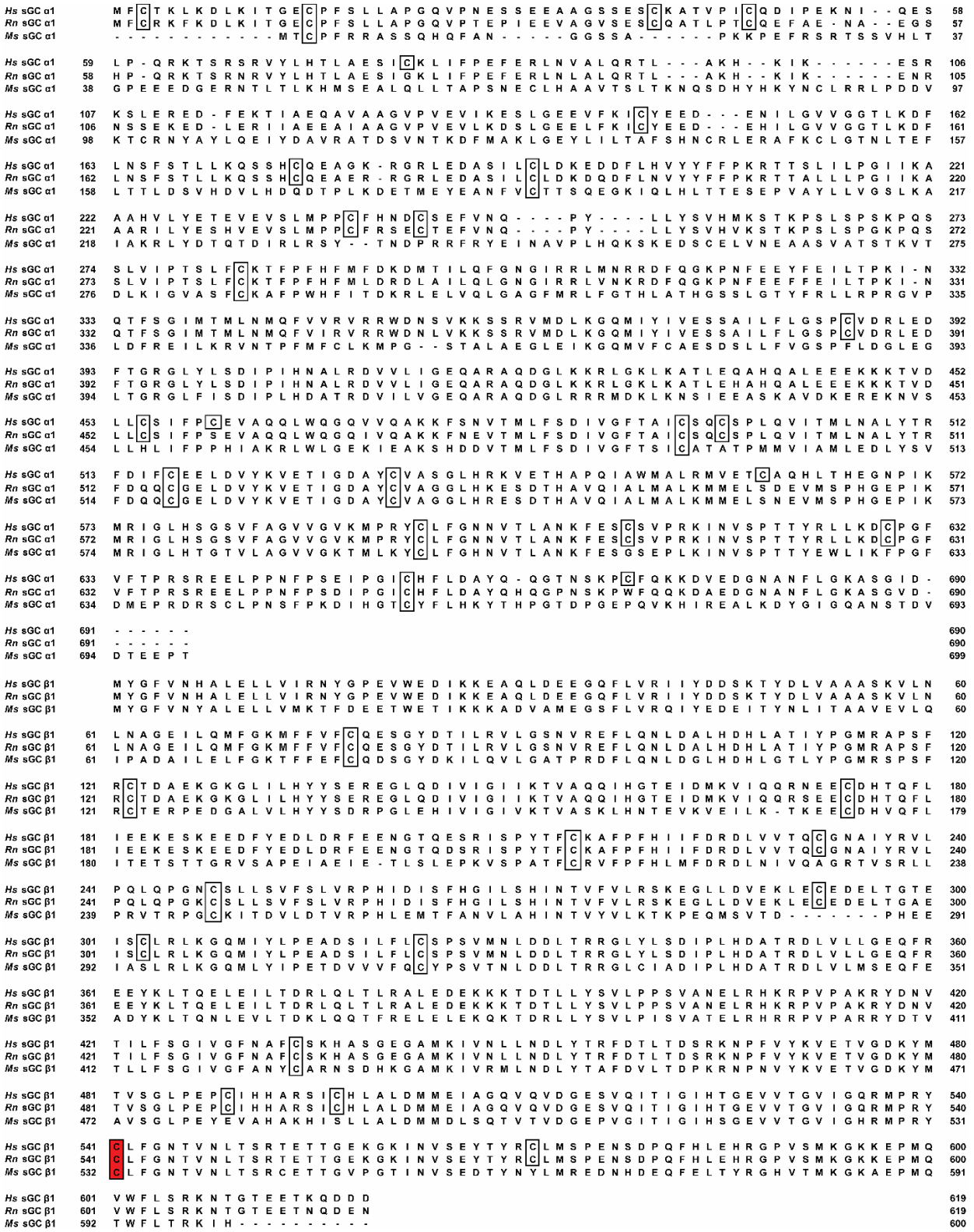

Figure 4.1. Sequence alignments of *Hs*, *Rn*, and *Ms* sGCs. Sequences of the α and β subunits are aligned and displayed separately. Cysteines which are conserved between *Hs*, *Rn*, and *Ms* sGC are boxed, and the catalytic cysteine residue involved in substrate coordination (βC541 in *Hs*[30] and *Rn* sGC, βC532 in *Ms* sGC) is also highlighted in red.

If the cysteine involved in a second site NO interaction critical for maximal sGC activity were mutated to a residue which was not capable of NO interaction, the variant sGC would be expected to display only two activity states *in vitro*: a low, basal activity when NO is absent, and a small increase in activity when NO is present in either stoichiometric equivalence or excess. Previous unpublished work[31] utilized point variants of either *Rn* or *Ms* sGC to determine potential second site cysteine residues. First, cysteines which had shown decreases in exchange rates in hydrogen deuterium exchange mass spectrometry experiments[32,33] following the addition of NO (*Rn* αC532 and βC248) were mutated to serine. The individual αC532S and βC248S variants were purified to homogeneity and found to retain sensitivity to excess concentrations of NO. A subsequent effort involved mutating 14 of the 16 conserved cysteines in *Ms* sGC. These variants were not purified to homogeneity and were instead characterized via enriched cell lysate assays utilizing xsNO, MMTS, and YC-1. Results from these assays were inconclusive and suggested that a different approach was necessary to screen for potential second sites in sGC.

Activity Assays Using Cysteine Labeling Agents

In physiological conditions, sGCs are activated by concentrations of NO in the nM range, suggesting that a cysteine residue involved in such interactions must be highly reactive. If these reactive cysteines were first labeled with cysteine labeling regents, the labeled sGC would then be expected to be insensitive to excess NO concentrations. Two such labeling reagents, IAM and MMTS, were used to label reactive cysteines in *Ms* sGC before treated proteins were characterized in activity assays (Figure 4.2). IAM is a polar molecule capable of forming an irreversible covalent bond with cysteines in sGC. MMTS is a small, non-polar molecule which can access cysteines within hydrophobic pockets yielding an adduct which can be reversed using reducing agents such as DTT. These labeling agents were then used in sequential labeling assays to investigate both the differential reactivity and accessibility of cysteines in *Ms* sGC.

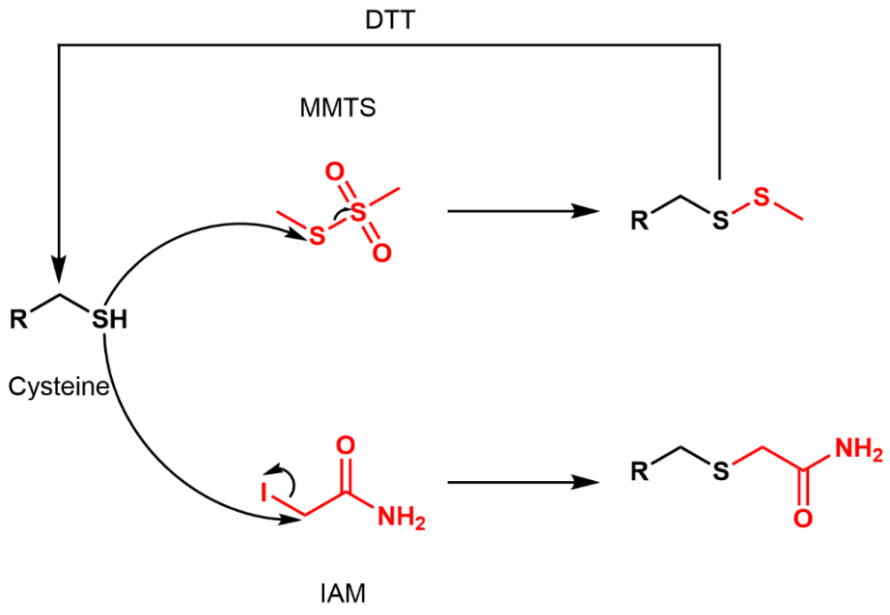

Figure 4.2. Comparison of cysteine labeling reagents MMTS and IAM. Labeling with MMTS results in the formation of an *S*-methyl adduct which can be readily reversed by the addition of reducing agents such as DTT. Labeling with IAM yields a non-reversible, polar acetamide adduct.

Ms sGC at 1 μM (28 μM cysteine), in the absence of NO, was first labeled with either 50 μM MMTS or IAM. After incubation, an additional 50 μM of MMTS or IAM was added to each sample. This resulted in four final labeling states, by order of addition: MMTS|MMTS, MMTS|IAM, IAM|IAM, and IAM|MMTS. Excess NO was added to a portion of these labeled proteins, and activation by excess NO was compared for proteins in the unliganded and xsNO states (Figure 4.3). These results revealed that IAM labeling of sGC, even at 100 μM, did not affect sGC sensitivity to excess NO. Successful labeling of *Ms* sGC by IAM was verified by tandem mass spectrometry.[31] *Ms* sGC which was labeled by MMTS either exclusively or before or after labeling with IAM was insensitive to excess NO. This suggests that the cysteine involved in xsNO activation of sGC is not labeled by IAM, possibly due to chemical environment or accessibility. It was also observed, however, that protein labeled with 50 μM or higher concentrations of MMTS, in these sample preparation conditions, displayed activity below that of sGC in non-labeled, NO-free conditions. This represented a concerning loss of catalytic activity, introducing concerns that labeling with higher concentrations of MMTS might be causing denaturation of the protein.

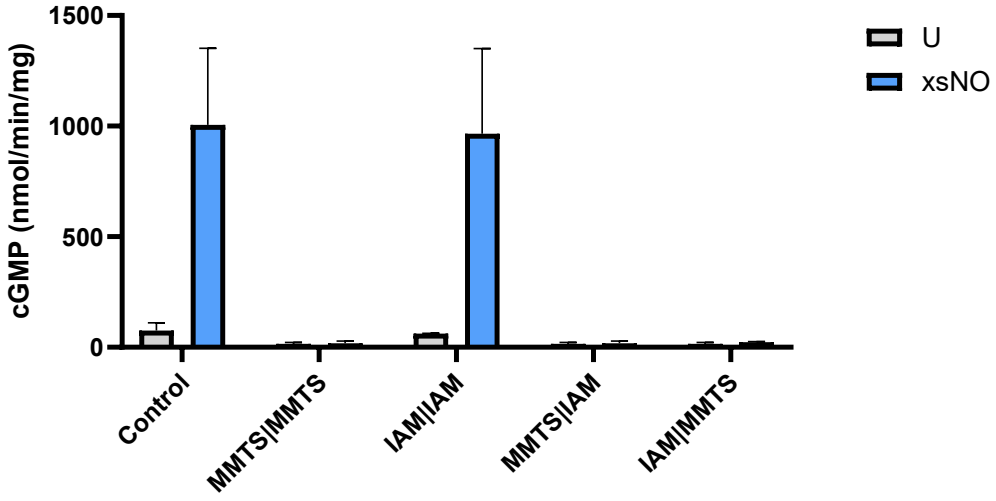

Figure 4.3. Sequential labeling activity assays of *Ms* sGC. Endpoint activity assay data showing the effects of labeling with cysteine labeling reagents. All reactions contained 20 – 50 nM sGC, 5 mM $MgCl_2$, and 2 mM GTP. In all non-control samples, the final total concentration for labeling agents was 100 μM, added in 50 μM increments with the first addition at 0 minutes and the second addition at 30 minutes.

MS Analysis of MMTS-labeled Protein

Since labeling with IAM did not impact the excess NO sensitivity of *Ms* sGC, MMTS was used to label protein for further characterization in trypsinized MS experiments, with the intent to determine which cysteines were labeled in proteins which had been rendered insensitive to excess NO. To address concerns that MMTS could be denaturing *Ms* sGC, a series of experiments were first performed to determine an effective, minimal concentration of MMTS which would successfully eliminate xsNO activity while minimizing excess cysteine labeling. *Ms* sGC at 1 μM (28 μM cysteine) was treated with varying concentrations of MMTS (from 7.5 to 50 μM) to determine which concentrations yielded protein that reached approximately 1-NO activity when excess NO was added and was restored to full catalytic activity when the label was removed by reduction with DTT (Figure 4.4). MMTS concentrations of 7.5 μM per 1 μM sGC (28 μM cysteine)

were found sufficient to inhibit excess NO sensitivity in labeled protein without evident denaturation of the protein as full activity was restored upon reduction and label removal.

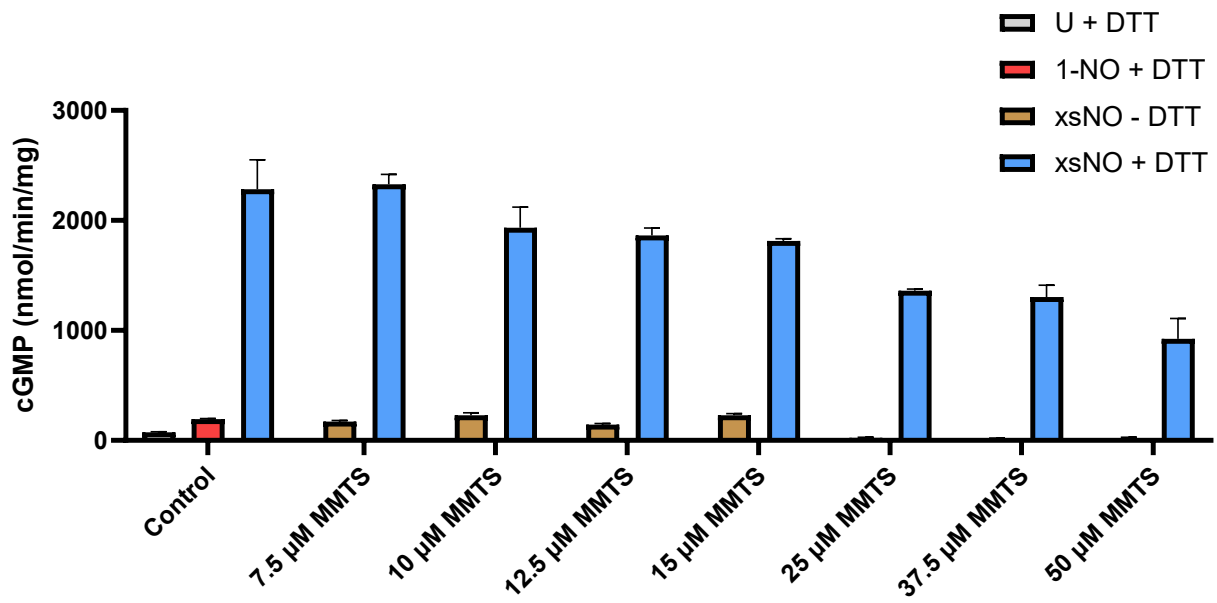

Figure 4.4. *Ms* sGC activity in MMTS titration-style assays. NO-free sGC was prepared for labeling with different concentrations of MMTS. Labeled protein was then split, with one fraction undergoing reduction and label removal via incubation with 5 mM DTT. All reactions contained 20 – 50 nM sGC, 5 mM $MgCl_2$, and 2 mM GTP.

Samples of *Ms* sGC were then labeled at 7.5 µM MMTS, verified by activity assay, and prepared for and analyzed via trypsinized MS. Observed peptide coverage was mapped to the primary amino acid sequence for both the α and β subunits of *Ms* sGC. Cysteines with an *S*-methyl adduct were then mapped to the sequence of *Ms* sGC (Figure 4.5). In the α subunit, peptide coverage was observed for 9 of 18 cysteine residues. For conserved α subunit cysteines in *Hs*, *Rn*, and *Ms* sGCs, only 3 were observed in peptide fragments and all 3 were modified by MMTS. In the β subunit, peptide coverage was observed for 5 of 10 cysteine residues. For conserved β subunit cysteines in *Hs*, *Rn*, and *Ms* sGCs, only 4 were observed in peptide fragments and all 4 were modified by MMTS. Of the 14 cysteine residues observed via mass spec, 13 were modified by MMTS. These results were insufficient to narrow the list of potential cysteine second sites involved in sGC activation by excess NO.

Figure 4.5. Trypsinized MS results for MMTS-labeled *Ms* sGC. The alpha (A) and beta (B) subunits are mapped separately. Regions of peptide coverage are highlighted in yellow. Observed lysine or arginine cleavage sites are underlined. Cysteines which are conserved in *Hs*, *Rn*, and *Ms* sGCs are colored in blue. Cysteines which are not conserved are colored in gray. Cysteines which were observed to have been modified by MMTS are boxed.

These results, however, did offer a potential alternative explanation for the decreased catalytic activity observed in MMTS-labeled sGC. Peptide coverage for the β subunit included peptide fragments containing βC532 in both a modified and unmodified state. βC532 (βC541 in *Hs* sGC) is involved in GTP coordination in the catalytic active site.[30,34] Recent high-resolution structures solved for *Ms* sGC (discussed in Chapter 3) using the substrate analog guanosine-5'-[(α,β)-methyleno]triphosphate (GpCpp), reveal that the sulfur of βC532 is positioned 5 Å from O6 in GpCpp. Introduction of an *S*-methyl to the cysteine at βC532 reduces that distance to approximately 2 Å between the methyl carbon and O6 of GpCpp (Figure 4.6). Given the importance of βC532 for coordinating substrate within the catalytic pocket[30,34], it is likely that labeling at this position is sufficient to decrease the activity of *Ms* sGC through reduced hydrogen bonding with the substrate or though the introduction of steric bulk into the binding pocket which prevents or reduces substrate binding. Previous work[27] which utilized MMTS labeling to suggest an NO/cysteine interaction in the activation of sGC did not report peptide coverage for any fragments containing *Rn* βC541, so potential labeling of the catalytic cysteine in those experiments cannot be determined. Unpublished work[35] with a homodimeric NO-activated sGC from *Choanoeca flexa* (*Cf*), which does not contain this substrate-coordinating cysteine, determined that MMTS labeling decreased the catalytic activity of the WT enzyme. Intact protein MS indicated

that *Cf* sGC was labeled either singly or doubly when labeled with 5 μM MMTS. Unfortunately, no MS digest experiments were performed to determine which sites had been modified.

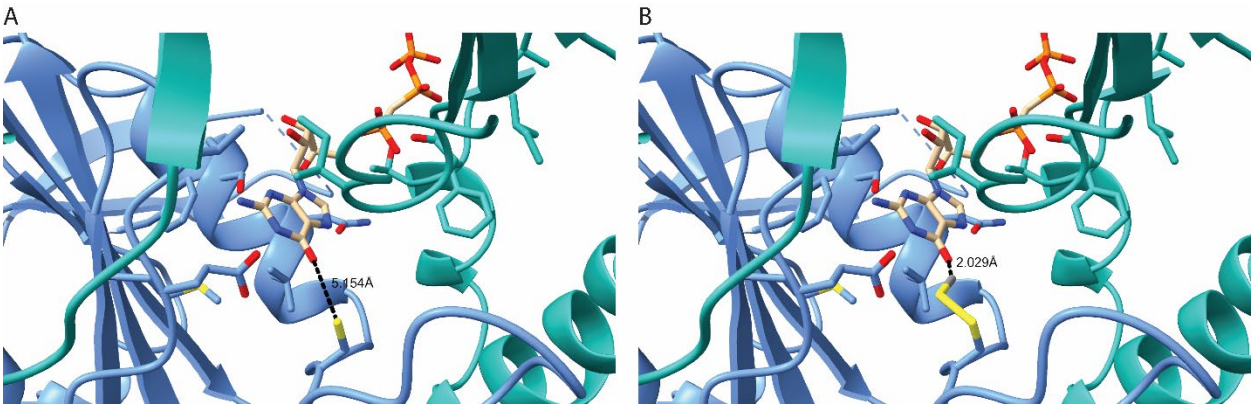

Figure 4.6. Catalytic pocket of *Ms* sGC in the extended conformation (PDB ID: 9P2R, Chapter 3) with GTP substrate analog GpCpp bound. (A) The O6 of GpCpp is positioned approximately 5 Å from the sulfur atom of βC532. (B) Addition of an *S*-methyl adduct to the sulfur of βC532 decreases the distance to the O6 atom to approximately 2 Å.

Bioinformatic Analysis of Conserved Cysteine Residues in sGC

Full-length structures for *Ms* and *Hs* sGC have opened new routes for investigating the activation of sGC. Comparison of sGC structures solved in NO-free and excess NO conditions reveals that the protein adopts a contracted conformation in the absence of NO and rearranges to an extended conformation in the presence of excess NO.[9,10] The H-NOX domains, particularly the heme-containing β H-NOX domain, have long been considered the regulatory domains for sGC activity. The α H-NOX domain does not bind heme, and its potential role in NO regulation is largely unknown. When truncations deleting either the α or β H-NOX domains were characterized, proteins missing the α H-NOX domain could be stimulated by NO while those missing the β H-NOX domain were insensitive to NO.[10,36] This suggests that the α H-NOX domain is not involved in NO sensing and likely serves a role in structural stabilization, especially when considering that the α H-NOX subunit undergoes only minor translational changes between the contracted and extended conformations. This is also supported by generally lower conservation across species in the α H-NOX domain compared to conservation in the β H-NOX domain.

By comparison, the β H-NOX domain has well characterized roles in NO sensing. It contains the crucial heme cofactor needed for the first steps in activation by NO and undergoes conformational changes during activation by NO which results in both the disruption and formation of stabilizing hydrogen bonding networks.[37] Desensitization of sGC when treated with excess NO has been observed and involves oxidative *S*-nitrosation in β H-NOX domains at positions C78 and C122.[38] Mutagenesis at position βC78 to serine reduced heme binding in sGC.[39] Mutagenesis at position βC122 to either alanine or serine (discussed in Chapter 3) yielded proteins which, even in the absence of NO, were highly stimulated following the addition of small molecule stimulators YC-1 or CYR715. These results reveal that even small perturbations in sGC structure at key conserved positions result in significant changes in heme incorporation and activation response. Further, such sensitivity to structural changes in the β H-NOX domain suggest that the

β H-NOX domain could contain the cysteine residues involved in the excess NO response for two-step activated sGCs.

A sequence similarity network (SSN) was generated to investigate conserved cystine residues within sGCs from a wide array of species (Figure 4.7).[40] In an SSN, individual or highly similar sequences are represented by nodes, and if those nodes have sufficient alignment scores, they are connected by an edge. Nodes which are connected through sufficient similarity are then grouped into distinct clusters, such that sequences within the same cluster likely serve similar biochemical functions. The SSN was generated using the sequence from the β_1 H-NOX domain (residues 1 – 194) of *Rn* sGC (UniProtKB: P20595). Sequence outputs were restricted to sequences between 500 and 900 amino acids in length using an alignment score threshold of 130. Using these parameters, several large clusters were observed. Two large clusters were generated for β_1 and β_2 type sGCs which represent NO-sensing sGCs from numerous multicellular organisms. A diverging cluster containing β_1 type sGCs from flies and mosquitoes was observed, suggesting functional drift for this class of insect sGCs. A large cluster of putative oxygen (O_2)-sensing sGCs from aquatic organisms such as fish and mollusks was also observed. Several other clusters containing sGCs from nematodes were also present. 2,400 unique sequences from these clusters were then aligned to the sequence of *Hs* sGC β_1 (UniProtKB: Q02153). Each cluster was aligned separately using ClustalOmega.[41–43] Sequence alignments were then analyzed for variation in residue identities between clusters and *Hs* sGC β_1, with special focus on differences in cysteine conservation between NO- and O_2-sensing sGCs in the β H-NOX and PAS domains.

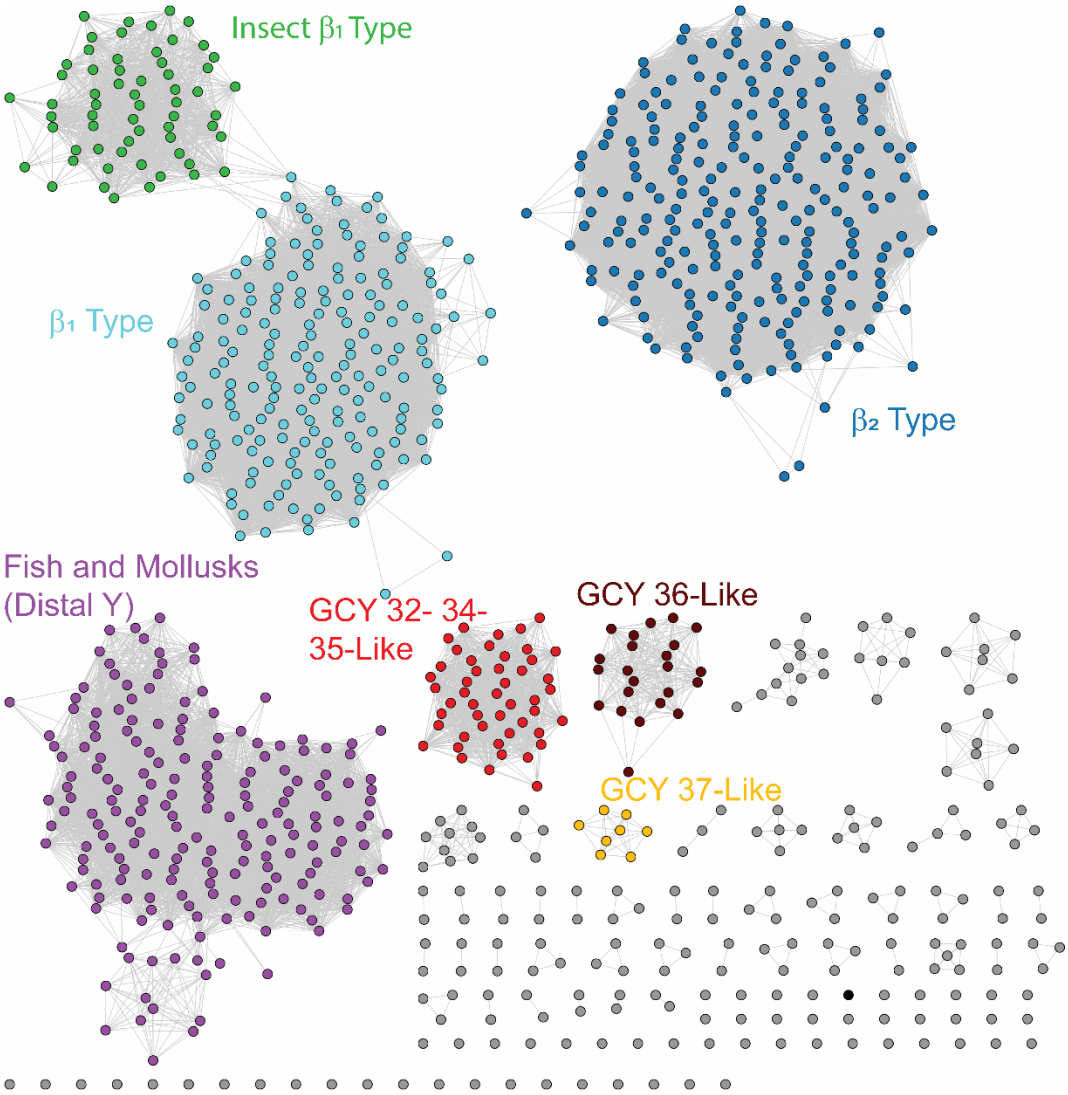

Figure 4.7. Sequence Similarity Network (SSN) generated from a BLAST of the β_1 H-NOX domain of *Rn* sGC with an alignment score threshold of 130. Sequences included in the SSN were from 500 – 900 amino acids in length. Edges indicate sequences sharing > 45% sequence identity. Two large clusters containing β_1 and β_2 type subunits are shown in light and dark blue, respectively. Additional sequences representing β_1 type sGCs from flies and mosquitoes (light green), and distal tyrosine sGCs from fish and mollusks (purple), and GCY-like O_2-sensing[44] sGCs from nematodes (red, dark brown, and yellow) are also shown. The input sequence (residues 1 – 194 of *Rn* sGC β_1) is shown in black. The SSN was calculated using the EFI Enzyme Similarity Tool[45,46] and visualized using Cytoscape 3.10.2.[47]

Three cysteines in the β H-NOX domain and one cysteine at the beginning of the PAS domain are conserved across *Hs*, *Rn*, and *Ms* sGCs at positions 78, 122, and 174, and 214 (*Hs* numbering). βC78 and C214 in the PAS domain have been shown to be play a role in heme incorporation[39], while βC78 and C122 have both been shown to play a role in NO desensitization following S-nitrosation.[38] Less is known about βC174, but full-length structures indicate that this residue occupies a disordered region on the surface of the protein in both the contracted or extended states.[48] Conservation of these four cysteines was compared for the NO- and O_2-sensing sGCs (Table 4.1).

Table 4.1. Conservation of selected cysteines in β H-NOX and PAS domains of sGCs

Cluster ID	Total Sequences	Characterized† or Putative‡ Ligand	Cys at 78 # (%)	Cys at 122 # (%)	Cys at 174 # (%)	Cys at 214 # (%)
β_1 Type	1123	NO†	1076 **(96%)**	1079 **(96%)**	1036 **(92%)**	1106 **(98%)**
β_2 Type	781	NO†	770 **(96%)**	11 **(1%)**	0 **(0%)**	767 **(98%)**
Insect β_1 Type	83	NO‡	81 **(98%)**	83 **(100%)**	10 **(12%)**	83 **(100%)**
Fish and Mollusks	319	O2‡	0 **(0%)**	213 **(67%)**	0 **(0%)**	0 **(0%)**
GCY 32- 34- 35-Like	79	O2†	0 **(0%)**	78 **(99%)**	0 **(0%)**	7 **(9%)**
GCY 36-Like	35	O2†	0 **(0%)**	35 **(100%)**	0 **(0%)**	10 **(29%)**
GCY 37-Like	13	O2‡	12 **(92%)**	13 **(100%)**	0 **(0%)**	0 **(0%)**

†Indicates clusters which contain sGCs which have been characterized to respond to the indicated gaseous ligand. ‡Indicates clusters which contain a distal pocket tyrosine (Fish and Mollusks) or are found in organisms without NO biosynthetic pathways[44] (GCY 37-Like).

Analysis of these conserved cysteines between NO- and O_2-sensing sGCs reveals several patterns. sGCs which sense NO maintain significant (>95%) conservation of cysteines at positions βC78 and βC214, while most O_2-sensing sGCs do not. βC78S and C214S variants initially showed low NO-sensitivity due to low heme incorporation; however the βC214S variant regained excess NO sensitivity when the protein was reconstituted with heme, suggesting that this position was not responsible for excess NO sensitivity.[39] The heme reconstituted βC78 variant regained some NO sensitivity, but not to WT levels of maximal activity.[39] βC122 is inconsistently conserved between NO- and O_2- sensing sGCs, but purified point variants for βC122A and C122S (Chapter 3) still displayed sensitivity to excess NO, indicating this position is not singly responsible for excess NO sensitivity. βC174, however, was uniquely conserved at 92% by only NO-sensing β_1 type sGCs. Further consideration of βC174 will be discussed in greater detail in Chapter 5.

Conclusions

sGC-mediated cGMP signaling plays a critical role in numerous regulatory processes, yet our understanding of the physiological regulation of this enzyme by non-heme NO remains poorly understood. The 1-NO and excess NO activities of sGC differ by an order of magnitude, yet these two activity states can be accessed and reversed in mere seconds by nM concentrations of NO. Determining the mechanism of this activation process could lead to improved understanding of the rapid regulation of proteins with no well-characterized or apparent regulatory interaction sites.

This work sought to build upon previous observations of potential cysteine sites being responsible for the excess NO activity observed in NO-sensitive sGCs. Labeling of sGCs with MMTS and IAM revealed that potential second site cysteines could be selectively labeled with MMTS. However, labeling with even substoichiometric concentrations of MMTS (to cysteines in sGC) led to multiple cysteines being labeled by MMTS, including a key catalytic cysteine responsible for substrate coordination in the active site. These results highlight that any additional attempts to use thiol labeling agents in pursuit of NO-reactive cysteines must be carefully analyzed to eliminate potential confounding effects on observed enzyme activity.

Ever-growing repositories of genetic information and improvements in bioinformatic techniques provide powerful tools for exploring sequence variance across thousands of species. This work utilized an SSN to visualize 2,400 sGC sequences from the UniProt database. Even though the SSN was built on a query sequence from the NO-sensing β_1 subunit of *Rn* sGC, distinct clusters for oxygen-sensing sGCs were obtained, allowing for detailed analysis of cysteine conservation between these protein clusters. Four cysteines from the β H-NOX and PAS domains were considered, and βC174 was found to be uniquely conserved in NO-sensing sGCs, some of which have characterized two-step activation profiles. Similar analysis for the full-length α and β subunits of NO-sensing sGCs could reveal additional cysteines with unique conservation patterns among sGCs.

Acknowledgements

The mass spectrometer used in this study was purchased with NIH support (grant 1S10OD020062-01).

References

(1) Bredt, D. S. Endogenous Nitric Oxide Synthesis: Biological Functions and Pathophysiology. *Free Radic. Res.* **1999**, *31* (6), 577–596. https://doi.org/10.1080/10715769900301161.

(2) Steinert, J. R.; Chernova, T.; Forsythe, I. D. Nitric Oxide Signaling in Brain Function, Dysfunction, and Dementia. *Neurosci. Rev. J. Bringing Neurobiol. Neurol. Psychiatry* **2010**, *16* (4), 435–452. https://doi.org/10.1177/1073858410366481.

(3) Moncada, S.; Palmer, R. M.; Higgs, E. A. Nitric Oxide: Physiology, Pathophysiology, and Pharmacology. *Pharmacol. Rev.* **1991**, *43* (2), 109–142.

(4) Brown, G. C.; Cooper, Chris. E. Nanomolar Concentrations of Nitric Oxide Reversibly Inhibit Synaptosomal Respiration by Competing with Oxygen at Cytochrome Oxidase. *FEBS Lett.* **1994**, *356* (2), 295–298. https://doi.org/10.1016/0014-5793(94)01290-3.

(5) Cleeter, M. W. J.; Cooper, J. M.; Darley-Usmar, V. M.; Moncada, S.; Schapira, A. H. V. Reversible Inhibition of Cytochrome c Oxidase, the Terminal Enzyme of the Mitochondrial Respiratory Chain, by Nitric Oxide: Implications for Neurodegenerative Diseases. *FEBS Lett.* **1994**, *345* (1), 50–54. https://doi.org/10.1016/0014-5793(94)00424-2.

(6) Arnold, W. P.; Mittal, C. K.; Katsuki, S.; Murad, F. Nitric Oxide Activates Guanylate Cyclase and Increases Guanosine 3':5'-Cyclic Monophosphate Levels in Various Tissue Preparations. *Proc. Natl. Acad. Sci. U. S. A.* **1977**, *74* (8), 3203–3207. https://doi.org/10.1073/pnas.74.8.3203.

(7) Pellicena, P.; Karow, D. S.; Boon, E. M.; Marletta, M. A.; Kuriyan, J. Crystal Structure of an Oxygen-Binding Heme Domain Related to Soluble Guanylate Cyclases. *Proc. Natl. Acad. Sci.* **2004**, *101* (35), 12854–12859. https://doi.org/10.1073/pnas.0405188101.
(8) Zhao, Y.; Marletta, M. A. Localization of the Heme Binding Region in Soluble Guanylate Cyclase†. *Biochemistry* **1997**, *36* (50), 15959–15964. https://doi.org/10.1021/bi971825x.
(9) Horst, B. G.; Yokom, A. L.; Rosenberg, D. J.; Morris, K. L.; Hammel, M.; Hurley, J. H.; Marletta, M. A. Allosteric Activation of the Nitric Oxide Receptor Soluble Guanylate Cyclase Mapped by Cryo-Electron Microscopy. *eLife* **2019**, *8*, e50634. https://doi.org/10.7554/eLife.50634.
(10) Kang, Y.; Liu, R.; Wu, J.-X.; Chen, L. Structural Insights into the Mechanism of Human Soluble Guanylate Cyclase. *Nature* **2019**, *574* (7777), 206–210. https://doi.org/10.1038/s41586-019-1584-6.
(11) Batchelor, A. M.; Bartus, K.; Reynell, C.; Constantinou, S.; Halvey, E. J.; Held, K. F.; Dostmann, W. R.; Vernon, J.; Garthwaite, J. Exquisite Sensitivity to Subsecond, Picomolar Nitric Oxide Transients Conferred on Cells by Guanylyl Cyclase-Coupled Receptors. *Proc. Natl. Acad. Sci. U. S. A.* **2010**, *107* (51), 22060–22065. https://doi.org/10.1073/pnas.1013147107.
(12) Cary, S. P. L.; Winger, J. A.; Marletta, M. A. Tonic and Acute Nitric Oxide Signaling through Soluble Guanylate Cyclase Is Mediated by Nonheme Nitric Oxide, ATP, and GTP. *Proc. Natl. Acad. Sci.* **2005**, *102* (37), 13064–13069. https://doi.org/10.1073/pnas.0506289102.
(13) Zhao, Y.; Brandish, P. E.; Ballou, D. P.; Marletta, M. A. A Molecular Basis for Nitric Oxide Sensing by Soluble Guanylate Cyclase. *Proc. Natl. Acad. Sci.* **1999**, *96* (26), 14753–14758. https://doi.org/10.1073/pnas.96.26.14753.
(14) Roy, B.; Garthwaite, J. Nitric Oxide Activation of Guanylyl Cyclase in Cells Revisited. *Proc. Natl. Acad. Sci. U. S. A.* **2006**, *103* (32), 12185–12190. https://doi.org/10.1073/pnas.0602544103.
(15) Roy, B.; Halvey, E. J.; Garthwaite, J. An Enzyme-Linked Receptor Mechanism for Nitric Oxide-Activated Guanylyl Cyclase. *J. Biol. Chem.* **2008**, *283* (27), 18841–18851. https://doi.org/10.1074/jbc.M801712200.
(16) Hall, C. N.; Garthwaite, J. What Is the Real Physiological NO Concentration in Vivo? *Nitric Oxide* **2009**, *21* (2), 92–103. https://doi.org/10.1016/j.niox.2009.07.002.
(17) Wood, K. C.; Batchelor, A. M.; Bartus, K.; Harris, K. L.; Garthwaite, G.; Vernon, J.; Garthwaite, J. Picomolar Nitric Oxide Signals from Central Neurons Recorded Using Ultrasensitive Detector Cells. *J. Biol. Chem.* **2011**, *286* (50), 43172–43181. https://doi.org/10.1074/jbc.M111.289777.
(18) Stone, J. R.; Marletta, M. A. Spectral and Kinetic Studies on the Activation of Soluble Guanylate Cyclase by Nitric Oxide. *Biochemistry* **1996**, *35* (4), 1093–1099. https://doi.org/10.1021/bi9519718.
(19) Russwurm, M.; Koesling, D. NO Activation of Guanylyl Cyclase. *EMBO J.* **2004**, *23* (22), 4443–4450. https://doi.org/10.1038/sj.emboj.7600422.
(20) Derbyshire, E. R.; Marletta, M. A. Butyl Isocyanide as a Probe of the Activation Mechanism of Soluble Guanylate Cyclase: INVESTIGATING THE ROLE OF NON-HEME NITRIC OXIDE. *J. Biol. Chem.* **2007**, *282* (49), 35741–35748. https://doi.org/10.1074/jbc.M705557200.

(21) Gow, A. J.; Chen, Q.; Hess, D. T.; Day, B. J.; Ischiropoulos, H.; Stamler, J. S. Basal and Stimulated Protein S-Nitrosylation in Multiple Cell Types and Tissues. *J. Biol. Chem.* **2002**, *277* (12), 9637–9640. https://doi.org/10.1074/jbc.C100746200.
(22) Gaston, B.; Singel, D.; Doctor, A.; Stamler, J. S. S-Nitrosothiol Signaling in Respiratory Biology. *Am. J. Respir. Crit. Care Med.* **2006**, *173* (11), 1186–1193. https://doi.org/10.1164/rccm.200510-1584PP.
(23) Paige, J. S.; Xu, G.; Stancevic, B.; Jaffrey, S. R. Nitrosothiol Reactivity Profiling Identifies S-Nitrosylated Proteins with Unexpected Stability. *Chem. Biol.* **2008**, *15* (12), 1307–1316. https://doi.org/10.1016/j.chembiol.2008.10.013.
(24) Foster, M. W.; Hess, D. T.; Stamler, J. S. Protein S-Nitrosylation in Health and Disease: A Current Perspective. *Trends Mol. Med.* **2009**, *15* (9), 391–404. https://doi.org/10.1016/j.molmed.2009.06.007.
(25) Marozkina, N. V.; Gaston, B. S-Nitrosylation Signaling Regulates Cellular Protein Interactions. *Biochim. Biophys. Acta* **2012**, *1820* (6), 722–729. https://doi.org/10.1016/j.bbagen.2011.06.017.
(26) Dent, M. R.; DeMartino, A. W. Nitric Oxide and Thiols: Chemical Biology, Signalling Paradigms and Vascular Therapeutic Potential. *Br. J. Pharmacol.* **2023**, 10.1111/bph.16274. https://doi.org/10.1111/bph.16274.
(27) Fernhoff, N. B.; Derbyshire, E. R.; Marletta, M. A. A Nitric Oxide/Cysteine Interaction Mediates the Activation of Soluble Guanylate Cyclase. *Proc. Natl. Acad. Sci.* **2009**, *106* (51), 21602–21607. https://doi.org/10.1073/pnas.0911083106.
(28) Hu, X.; Murata, L. B.; Weichsel, A.; Brailey, J. L.; Roberts, S. A.; Nighorn, A.; Montfort, W. R. Allostery in Recombinant Soluble Guanylyl Cyclase from *Manduca Sexta**. *J. Biol. Chem.* **2008**, *283* (30), 20968–20977. https://doi.org/10.1074/jbc.M801501200.
(29) Light, S. H.; Su, L.; Rivera-Lugo, R.; Cornejo, J. A.; Louie, A.; Iavarone, A. T.; Ajo-Franklin, C. M.; Portnoy, D. A. A Flavin-Based Extracellular Electron Transfer Mechanism in Diverse Gram-Positive Bacteria. *Nature* **2018**, *562* (7725), 140–144. https://doi.org/10.1038/s41586-018-0498-z.
(30) Allerston, C. K.; von Delft, F.; Gileadi, O. Crystal Structures of the Catalytic Domain of Human Soluble Guanylate Cyclase. *PLoS ONE* **2013**, *8* (3), e57644. https://doi.org/10.1371/journal.pone.0057644.
(31) Horst, B. G. The Structure and Activation of Soluble Guanylate Cyclase. Ph.D., University of California, Berkeley, United States -- California, 2019. https://www.proquest.com/dissertations/docview/2385781355/abstract/5C8FCA03E5254BEBPQ/1 (accessed 2025-06-03).
(32) Underbakke, E. S.; Iavarone, A. T.; Marletta, M. A. Higher-Order Interactions Bridge the Nitric Oxide Receptor and Catalytic Domains of Soluble Guanylate Cyclase. *Proc. Natl. Acad. Sci.* **2013**, *110* (17), 6777–6782. https://doi.org/10.1073/pnas.1301934110.
(33) Underbakke, E. S.; Iavarone, A. T.; Chalmers, M. J.; Pascal, B. D.; Novick, S.; Griffin, P. R.; Marletta, M. A. Nitric Oxide-Induced Conformational Changes in Soluble Guanylate Cyclase. *Structure* **2014**, *22* (4), 602–611. https://doi.org/10.1016/j.str.2014.01.008.
(34) Sunahara, R. K.; Beuve, A.; Tesmer, J. J.; Sprang, S. R.; Garbers, D. L.; Gilman, A. G. Exchange of Substrate and Inhibitor Specificities between Adenylyl and Guanylyl Cyclases. *J. Biol. Chem.* **1998**, *273* (26), 16332–16338. https://doi.org/10.1074/jbc.273.26.16332.
(35) Wu, Y. The Study of Soluble Guanylate Cyclases From Choanoeca Flexa. Ph.D., University of California, Berkeley, United States -- California, 2024.

https://www.proquest.com/dissertations/docview/3176103326/abstract/DC61B65012434FF3PQ/5 (accessed 2025-06-04).
(36) Koglin, M.; Behrends, S. A Functional Domain of the A1 Subunit of Soluble Guanylyl Cyclase Is Necessary for Activation of the Enzyme by Nitric Oxide and YC-1 but Is Not Involved in Heme Binding*. *J. Biol. Chem.* **2003**, *278* (14), 12590–12597. https://doi.org/10.1074/jbc.M212740200.
(37) Wittenborn, E. C.; Marletta, M. A. Structural Perspectives on the Mechanism of Soluble Guanylate Cyclase Activation. *Int. J. Mol. Sci.* **2021**, *22* (11), 5439. https://doi.org/10.3390/ijms22115439.
(38) Fernhoff, N. B.; Derbyshire, E. R.; Underbakke, E. S.; Marletta, M. A. Heme-Assisted *S*-Nitrosation Desensitizes Ferric Soluble Guanylate Cyclase to Nitric Oxide*. *J. Biol. Chem.* **2012**, *287* (51), 43053–43062. https://doi.org/10.1074/jbc.M112.393892.
(39) Friebe, A.; Wedel, B.; Harteneck, C.; Foerster, J.; Schultz, G.; Koesling, D. Functions of Conserved Cysteines of Soluble Guanylyl Cyclase. *Biochemistry* **1997**, *36* (6), 1194–1198. https://doi.org/10.1021/bi962047w.
(40) Atkinson, H. J.; Morris, J. H.; Ferrin, T. E.; Babbitt, P. C. Using Sequence Similarity Networks for Visualization of Relationships across Diverse Protein Superfamilies. *PloS One* **2009**, *4* (2), e4345. https://doi.org/10.1371/journal.pone.0004345.
(41) Goujon, M.; McWilliam, H.; Li, W.; Valentin, F.; Squizzato, S.; Paern, J.; Lopez, R. A New Bioinformatics Analysis Tools Framework at EMBL–EBI. *Nucleic Acids Res.* **2010**, *38* (suppl_2), W695–W699. https://doi.org/10.1093/nar/gkq313.
(42) Sievers, F.; Wilm, A.; Dineen, D.; Gibson, T. J.; Karplus, K.; Li, W.; Lopez, R.; McWilliam, H.; Remmert, M.; Söding, J.; Thompson, J. D.; Higgins, D. G. Fast, Scalable Generation of High-quality Protein Multiple Sequence Alignments Using Clustal Omega. *Mol. Syst. Biol.* **2011**, *7* (1), 539. https://doi.org/10.1038/msb.2011.75.
(43) Madeira, F.; Madhusoodanan, N.; Lee, J.; Eusebi, A.; Niewielska, A.; Tivey, A. R. N.; Lopez, R.; Butcher, S. The EMBL-EBI Job Dispatcher Sequence Analysis Tools Framework in 2024. *Nucleic Acids Res.* **2024**, *52* (W1), W521–W525. https://doi.org/10.1093/nar/gkae241.
(44) Derbyshire, E. R.; Marletta, M. A. Structure and Regulation of Soluble Guanylate Cyclase. *Annu. Rev. Biochem.* 2012, *81* (Volume 81, **2012**), 533–559. https://doi.org/10.1146/annurev-biochem-050410-100030.
(45) Zallot, R.; Oberg, N.; Gerlt, J. A. The EFI Web Resource for Genomic Enzymology Tools: Leveraging Protein, Genome, and Metagenome Databases to Discover Novel Enzymes and Metabolic Pathways. *Biochemistry* **2019**, *58* (41), 4169–4182. https://doi.org/10.1021/acs.biochem.9b00735.
(46) Oberg, N.; Zallot, R.; Gerlt, J. A. EFI-EST, EFI-GNT, and EFI-CGFP: Enzyme Function Initiative (EFI) Web Resource for Genomic Enzymology Tools. *J. Mol. Biol.* **2023**, *435* (14), 168018. https://doi.org/10.1016/j.jmb.2023.168018.
(47) Shannon, P.; Markiel, A.; Ozier, O.; Baliga, N. S.; Wang, J. T.; Ramage, D.; Amin, N.; Schwikowski, B.; Ideker, T. Cytoscape: A Software Environment for Integrated Models of Biomolecular Interaction Networks. *Genome Res.* **2003**, *13* (11), 2498–2504. https://doi.org/10.1101/gr.1239303.
(48) Liu, R.; Kang, Y.; Chen, L. NO Binds to the Distal Site of Haem in the Fully Activated Soluble Guanylate Cyclase. *Nitric Oxide* **2023**, *134–135*, 17–22. https://doi.org/10.1016/j.niox.2023.03.002.

Chapter 5

Remaining Questions and Future Directions for Understanding sGC Activation

Summary

The work discussed in this dissertation has advanced our understanding of how conformational change in sGC is linked to catalytic activity. In Chapter 2, coiled-coil domain variants were generated for *Ms* sGC, and those variants revealed that sGC catalytic activity could be controlled through the elimination or introduction of a coiled-coil structure within a conformationally flexible region in the coiled-coil domains of the protein. Chapter 3 discussed characterization of a novel sGC stimulator, CYR715, which was able to highly stimulate catalytic activity for sGC even in the complete absence of gaseous ligands, highlighting the importance of the conformational flexibility and landscape of sGC. Chapter 4 presented work which attempted to determine potential non-heme interaction sites for NO activation of sGCs, providing new guidance for further investigations of sGC activation by non-heme NO. This final chapter will discuss a new model of the conformation-activity landscape in sGC while proposing future directions for exploring the roles of NO and stimulators in changing this landscape.

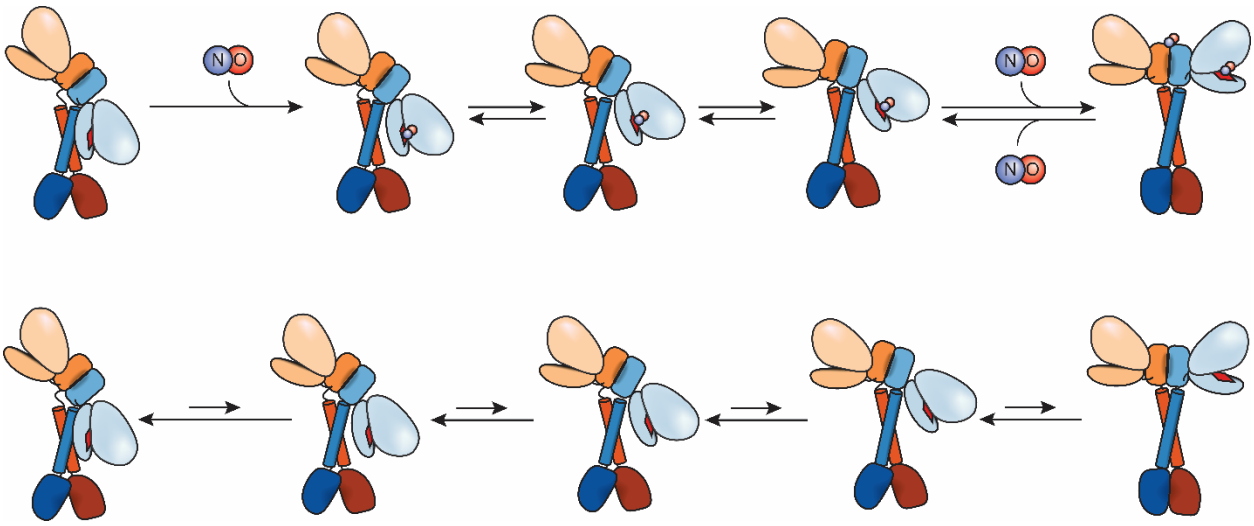

Introduction

Soluble guanylate cyclases (sGCs) are conformationally flexible heme-containing, gas-sensing proteins which catalyze the formation of cyclic guanosine monophosphate (cGMP) from guanosine 5'-triphosphate (GTP).[1] Many sGCs are sensors of physiological nitric oxide (NO) which increase their catalytic function in response to NO binding.[2] Three activity states have been characterized for sGCs *in vitro*. sGCs exhibit basal activity in the complete absence of NO[3] (U), moderately increased activity when one equivalent of NO is bound to the heme in sGC (1-NO)[4], and full activity when NO concentrations are in excess of the heme in sGC (xsNO).[5]

Full-length cryo-electron microscopy (cryo-EM) structures have been solved for *Homo sapiens* (*Hs*, human) and *Manduca sexta* (*Ms*, tobacco hawk moth) sGCs in both contracted and extended conformations.[6–8] Contracted conformations of sGC were observed in conditions where NO was absent, and extended conformations were observed when excess NO or small molecules capable of increasing sGC activity, known as stimulators, were present. These structures likely represent the extremes of sGC conformational flexibility, where the contracted state represents sGC conformation in the basal activity state and the extended state corresponds to sGC conformation in the maximal activity state. These conclusions were further supported by the work in Chapter 2, which demonstrated that sGC variants which could only sample the contracted or extended conformation exhibited only basal or maximal catalytic activities, respectively.

These two conformational end states, however, do not provide a full picture of the conformational landscape of sGC. Structural and conformational dynamics have long been known to play a role in protein regulation and catalytic function[9], yet detailed characterizations of such motions have remained elusive. As discussed in Chapter 1, negative stain electron microscopy results using *Rattus norvegicus* (*Rn*, brown rat) sGC revealed that sGC samples a full range of conformations both in the presence and absence of NO.[10] Unfortunately, these 25 – 40 Å structures were of insufficient resolution to determine any molecular level changes in the structure of sGC in the observed conformations.

Published work[6] using wild type (WT) *Ms* sGC and additional experiments detailed in Chapter 3 used small-angle X-ray scattering (SAXS) to further probe the conformational response of sGC following the addition of NO or small molecule stimulators. These studies found that sGC extends, to varying degrees, upon the addition of NO, stimulators, and/or substrate. However, as discussed in Chapter 3, comparison of the SAXS scattering profiles of WT and βC122 variants of *Ms* sGC to the catalytic activities of these sGCs in the same ligation states revealed that the observed extensions of sGC did not clearly correlate to catalytic activity.

No sGC structures have been solved in the 1-NO state. While the previously mentioned SAXS experiments indicate that sGC undergoes some conformational extension following the addition of stoichiometric concentrations of NO, they did not provide information on the conformational details of this extension or how it contributes to sGC activity. Excess concentrations of NO, through a currently uncharacterized mechanism, interact with sGC in the 1-NO state and bring the enzyme to full activity. Whether this interaction stabilizes the extended state or impedes a return to the contracted state is unknown.

The poorly understood conformational landscape of sGC presents significant challenges to the development of small molecule sGC stimulators. While it is unlikely that stimulators engage with sGC in the contracted conformation, where the stimulator binding site is occupied by the β H-NOX domain, it is unknown if stimulators bind to an intermediate or fully extended conformation of sGC. This is a distinction of importance, as stimulator binding to the extended conformation would need to keep the enzyme in that conformation, while stimulators binding to a partially extended conformation would need sufficient affinity to bind to a partially extended state while possessing a higher affinity for the extended conformation to facilitate the eventual full extension of the enzyme. The cryo-EM structure for the *Ms* sGC βC122S variant with CYR715 bound (Chapter 3) was solved in the extended conformation without a ligand bound at the heme and with the His-Fe bond intact, revealing that the paradigms of physiological sGC activation (discussed in Chapter 1) can be bypassed if stimulators are able to stabilize certain conformations of sGC.

The activation-conformation landscape of sGC is complicated, and significant gaps in our understanding of this landscape remain. sGCs undergo conformational extension upon ligand binding, but those extensions do not directly correlate to increases in catalytic activity. Thus, some conformational flexibility in sGC is unproductive (no increase in catalytic activity), and excess NO and stimulators must function in manner that either minimizes unproductive movements or converts those movements into productive motions which increase catalytic activity. This chapter explores the sGC activation-conformation landscape in greater detail, while exploring potential future directions to better understand the roles of NO and small molecule stimulators in facilitating productive conformational changes in sGC.

Proposed Models of Conformational Sampling in sGC Activation

The presence of excess NO leads to large conformational changes in sGC. Conformational landscapes, using only the previously solved contracted and extended conformations for sGC, lead to three simple landscapes to consider. In the first, the contracted and extended conformational states of sGC have roughly equivalent free energies but are separated by an energy barrier between those conformations (Figure 5.1A). In the second landscape, the contracted conformation of sGC is at a lower free energy and the addition of NO drives the contracted conformation to a higher energy, extended conformation either by destabilizing the contracted conformation or stabilizing the extended conformation (Figure 5.1B). In the third proposed landscape, the contracted conformation of sGC has a higher energy state which is then converted to a lower energy extended conformation following interactions with NO (Figure 5.1C).

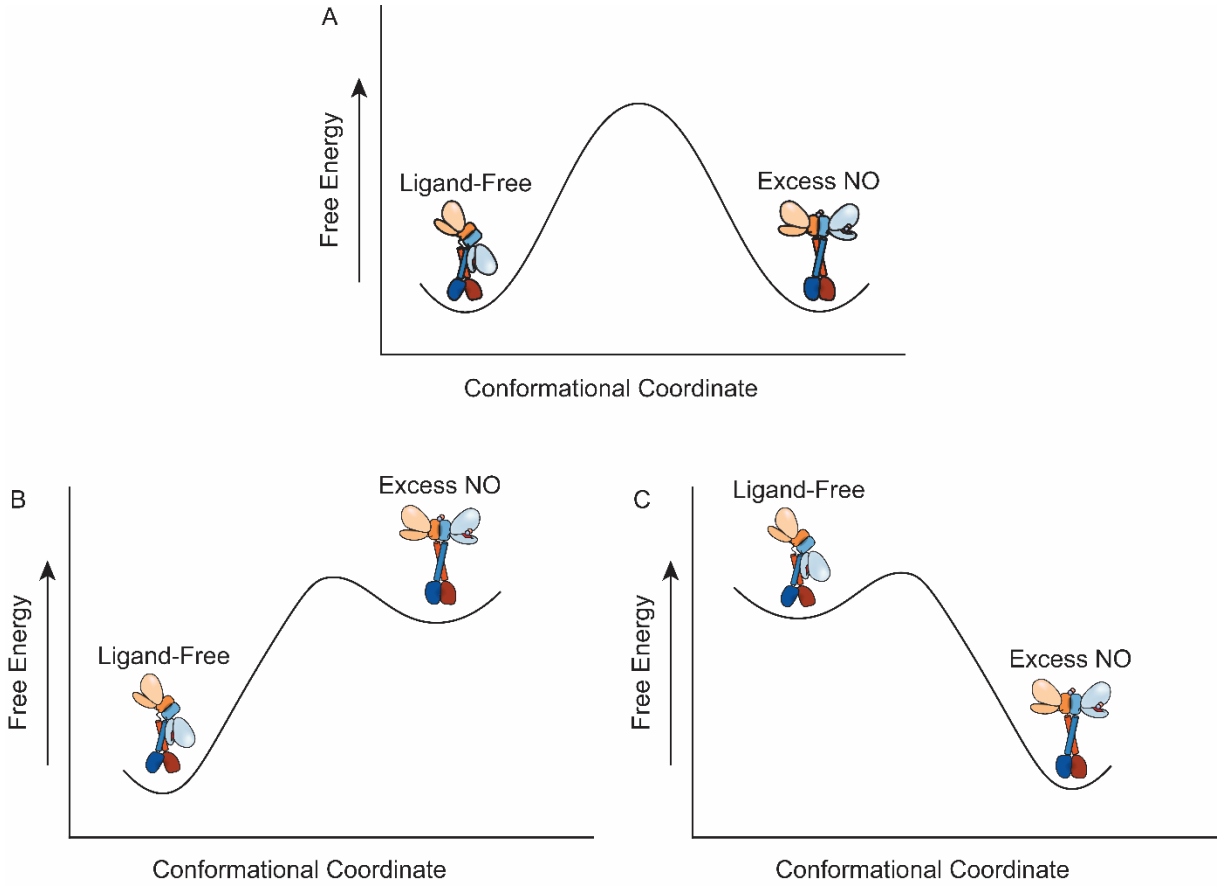

Figure 5.1. Simple conformational landscapes for sGC conformational change upon NO binding. (A) Both the contracted and extended conformations of sGC are at similar relative free energies but are separated by a high energy barrier. (B) The NO-free contracted conformation is the low energy resting state for sGC; and the addition of NO shifts sGC conformation to a less stable, higher energy state. (C) The NO-free contracted conformation is the high energy state for sGC, and the addition of NO allows for the transition to a lower energy extended conformation.

Three-dimensional structures of sGC reveal numerous interactions which stabilize either the contracted or extended conformations of sGC, supporting a hypothesis that NO binding serves to lower the energy needed to transition between these separate, stabilized conformations. Simple landscapes that consider only the contracted and extended conformations ignore potential implications of the 1-NO state on the conformational landscape of sGC. This state, described in detail in Chapter 1, is long-lived due to the high affinity of NO for the heme iron in sGC and exhibits activity between the basal and maximal levels. Addition of NO to the 1-NO state leads to a rapid extension of the enzyme, as evidenced by increased catalytic activity.[11] Removal of excess NO results in a rapid return to the 1-NO activity state[4], likely accomplished through a return to the 1-NO conformational state.

For simplicity and since we do not have information on the relative free energies of the contracted and extended states, we only consider the case where those relative free energies are the same. The 1-NO state could exist as a distinct, and thus far uncharacterized, partially extended conformation. This single conformation would present a uniform opportunity for ligands to interact with accessible regions of the protein. Alternatively, the 1-NO state could exist as a continuum of

intermediate states, across which conformational sampling is energetically allowed. In this model, conformational sampling in the 1-NO state could expose or occlude different regions of the protein over time, restricting opportunities for NO or small molecule stimulators to interact with critical amino acids in the protein. If the 1-NO state exists as a continuum of states, then activity for sGC in that state would represent an average of the catalytic activities for those populations. However, those average activities are significantly below that of maximal activity, in agreement with previous SAXS findings that conformational extension following ligand binding for *Ms* sGC WT and βC122 variants (Chapter 3) does not always lead to increased catalytic activity. If this concept is then applied to the first landscape discussed earlier, the 1-NO state could serve as an alternative, lower energy pathway between the contracted and extended conformations (Figure 5.2A,B).

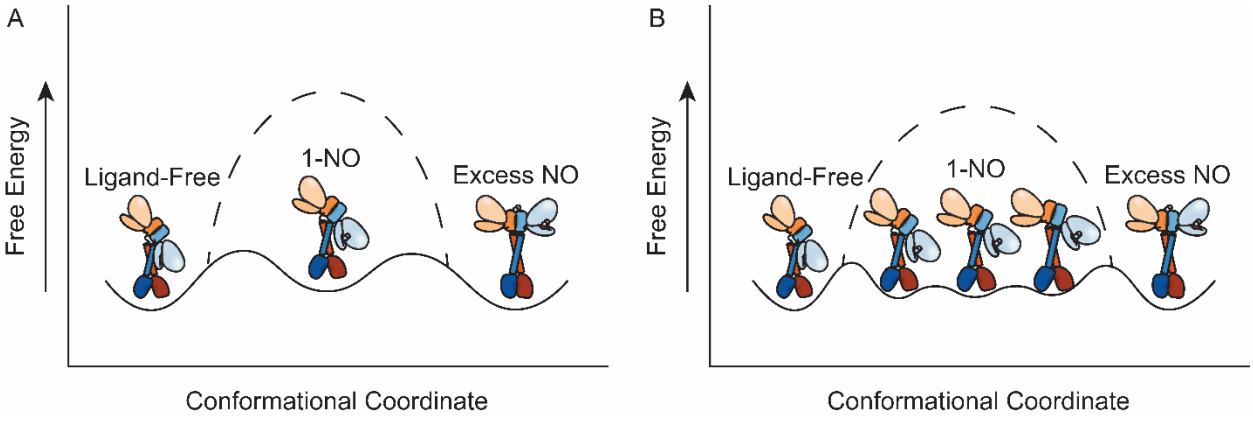

Figure 5.2. Conformational landscapes for sGC which consider the role of the 1-NO state. In both panels, the dotted path represents the free energy needed for conformational change directly between the ligand free, contracted conformation and the excess NO, extended conformation. (A) The 1-NO state is a singular conformation which lowers the necessary total energy to sample between the contracted and extended conformations. (B) The 1-NO state is a continuum of conformations which lowers the total energy needed to sample between the contracted and extended conformations.

Prior work (Chapter 2) has shown that sGC extension via straightening of the CC domains leads to full catalytic activity. However, data processing for high-resolution cryo-EM structures for both the contracted and extended states of sGC have required that the H-NOX and CAT domains be masked, or hidden, during processing due to flexibility between the two domains. This suggests that both domains still exhibit some conformational flexibility even when they are occupying one of the extreme conformations. Additionally, cryo-EM analysis of the *Ms* sGC βC122S variant (Chapter 3) revealed a significant population of sGC in a conformation which, at low resolution, better fit an extended conformation of sGC. Catalytic activity for the ligand-free *Ms* sGC βC122S variant, however, was statistically equivalent to that of WT *Ms* sGC where no partially extended protein was reported for the contracted protein sample data set.[6]

It has been suggested that allosteric communication in sGC can proceed bidirectionally between the H-NOX and CAT domains.[13–15] Evaluation of the potential for independent conformational sampling by the H-NOX and CAT domains, and the role of the CC domain in syncing those movements, could provide insight into sGC activation by NO and small molecule

stimulators. The fully extended structures for sGC reveal that the CC domains have both straightened and rotated about themselves during extension[6,7] leading to full activity. Conformational sampling in the H-NOX domain might result in an opening of the H-NOX and PAS domain bundle (Figure 5.3A). Meanwhile, sampling from the CAT domain might lead to rotation of CC domains (Figure 5.3B). When this sampling from the H-NOX and CAT domains occurs in sync, both the CC and H-NOX domains are positioned to stabilize the extended, maximally active conformation of sGC.

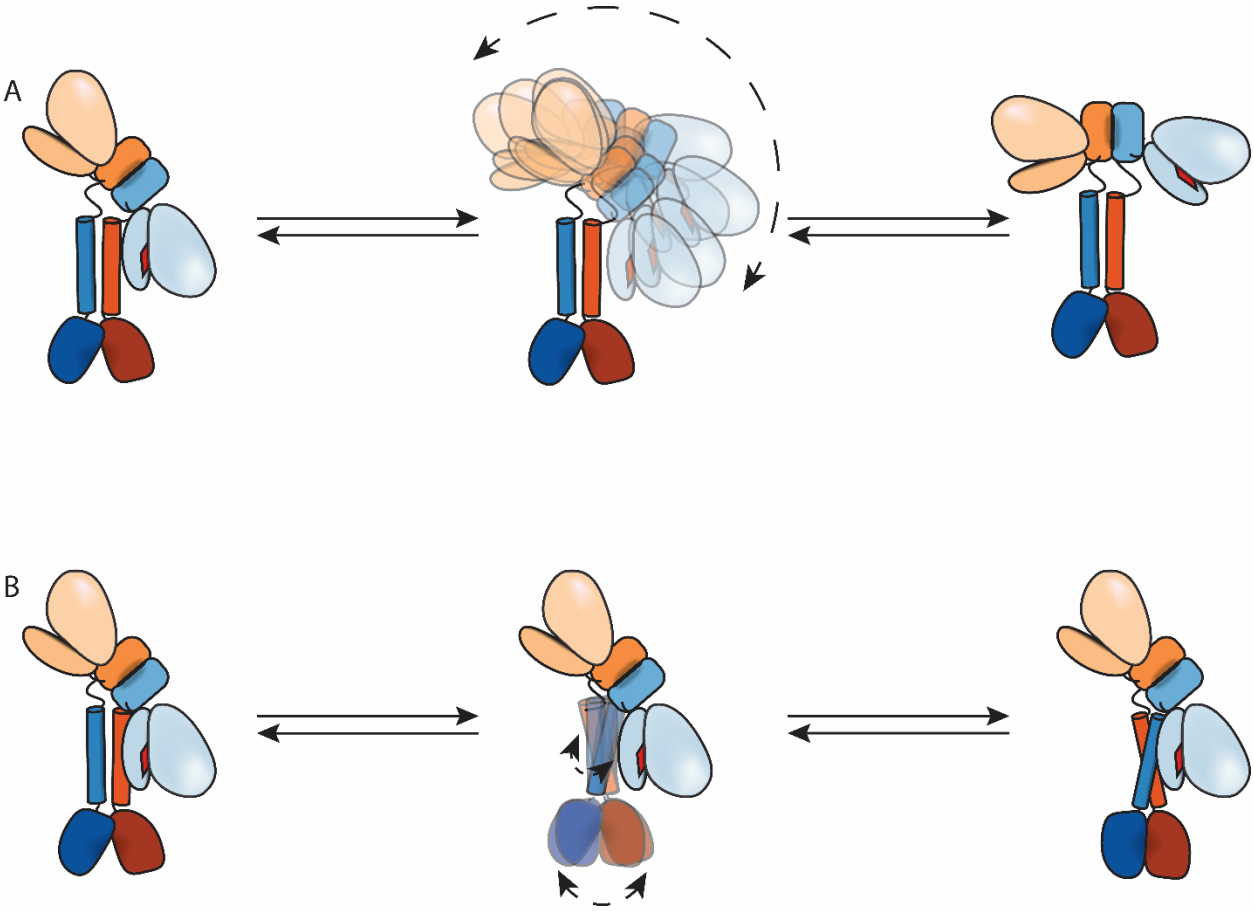

Figure 5.3. Desynchronized conformational sampling in sGC. (A) The H-NOX and PAS domain bundle sampling the full range of conformational flexibility without subsequent rotation of the CC domains. (B) Conformational sampling in the CAT domain driving rotation of the CC domains without altering the conformation of the H-HOX and PAS domains.

Independent conformational sampling by the H-NOX and CAT domains is supported by the known mechanisms of *in vivo* regulation of sGC activity by NO and the nucleotides GTP and adenosine 5'-triphosphate (ATP). Conformational sampling in the H-NOX and PAS domains is likely under the regulatory control of heme occupancy and NO binding to the heme. When NO is absent, conformational sampling of the H-NOX domain would be restricted due to rigidity imposed by the heme cofactor and the His-Fe bond. Binding of NO at the heme and rupture of the

His-Fe bond would relax this restriction, allowing the H-NOX and PAS domains to sample the full range of conformations more freely. Conformational sampling by the CAT domains is likely responsible for the minimal catalytic activity observed in the ligand free state. This is supported by cryo-EM structures for contracted sGC which revealed that substrate access to the catalytic site is sterically blocked in the contracted conformation, indicating that the CAT domains must be able to access an open conformation even in the absence of NO. Regulation at the catalytic domain is likely coordinated by the purine nucleotides ATP and GTP. ATP is able to bind at a pseudosymmetric site in the CAT domains of sGC and inhibits sGC activity in an NO-dependent manner.[13,14,16–18] Biochemical characterization of sGCs which, in the absence of ATP, were preincubated with GTP[4] or the substrate analog guanosine-5'-[(α,β)-methyleno]triphosphate (GpCpp)[14] before the addition of NO found that these substrate-primed sGCs were fully active in the 1-NO state. Together, these results suggest that nucleotide binding to the CAT domains of sGC can shift the conformation-activity response of sGC to NO, potentially through shifting the equilibrium of the open or closed conformations of the CAT domains.

Biochemical[7,19] and structural[7] investigations of the *Hs* sGC variant βH105C provide additional insight towards how this independent conformational sampling may relate towards sGC function. This variant was purified as a heme-deficient heterodimer. In activity assays, this variant was found to be constitutively active and showed no increase in catalytic activity in response to NO.[7,19] Interestingly, one study[19] of βH105C sGC found that the basal activity of heme-deficient βH105C *Hs* sGC was well above the basal activity of WT *Hs* sGC but below that of maximally active WT protein, while a more recent study[7] reported that this variant had the same activity as maximally active xsNO WT *Hs* sGC. When the variant from the first study was reconstituted with heme, this constitutive activity was largely lost and NO sensitivity was restored.[19] In the second study, a 6.8 Å cryo-EM map was solved for the *Hs* sGC βH105C variant in the presence of 1 mM GpCpp. While no atomic modeling was done for this variant, the model of NO-activated sGC fits into this map more accurately than a map of ligand-free sGC. Together, these studies of this variant suggest that removing conformational restriction imposed by heme occupancy in the β H-NOX domain at the N-terminus of sGC increases productive conformational sampling at the CAT domains resulting in increased catalytic rates.

As mentioned in Chapter 4, research suggests that the β H-NOX domain likely plays a significant role in the regulation of catalytic activity in sGC. Comparisons of contracted and extended structures from *Hs* sGC reveal that several key stabilizing interactions between the β H-NOX and α CC domains are disrupted or formed in the two conformations.[20] In the contracted conformation, αR428 engages in hydrogen bonding with αQ418 and βT110 which serves to stabilize the contracted conformation by preventing rotation of the α CC domain into the extended conformation. Biochemical characterization of a βT110A variant revealed that the variant displayed high basal activity, suggesting a role for βT110 in stabilizing the basal activity, contracted structure for sGC.[21] The potential role of αR428 in stabilizing the contracted conformation of sGC is of particular interest. αR428 is located at the C-terminus of the bent region

of the α CC domain and thus would serve a crucial role in allosteric communication towards the N-terminus from the CAT domains.

Particularly potent stimulators such as riociguat and CYR715 (see Chapter 3) engage with sGCs at position αR428[8] (αR429, *Ms* sGC), while less potent stimulators such as YC-1 do not. Interaction with αR428 is facilitated by the terminal moieties of each stimulator (a carbamate in riociguat and a carboxylic acid in CYR715), with stronger binding interactions with αR428 leading to greater stimulation of the enzyme. Chapter 3 presented strong evidence for the importance of this interaction, as an electrostatic interaction between CYR715 and αR429 of *Ms* sGC resulted in high activity for the NO-free enzyme and yielded structures of NO-free, heme-containing sGC in the extended conformation. Thus, it is plausible that stimulators capable of interacting with αR428 contribute to sGC activity by engaging in a stabilizing interaction which captures the catalytically active conformation of the CAT domain propagated through the CC domains.

These observations can be synthesized into a single model for sGC conformational sampling and catalytic activity. In the absence of NO, conformational sampling of the H-NOX domains is restricted due to rigidity imposed by the heme cofactor and the Fe-His bond. What sampling does occur is disconnected from the CAT domains due to the bent region of the CC domains. Meanwhile, the CAT domains undergo conformational sampling under regulation by ATP or GTP binding, where ATP binding stabilizes the closed conformation and GTP binding promotes the open conformation of the CAT domains. This conformational sampling propagates towards the N-terminus of the protein along the CC domains, with the open conformation of the CAT domains promoting rotation of the α CC domain. When NO binds to the heme, the rigidity imposed by the β H-NOX domain is relaxed; and the H-NOX domains can sample open conformations more freely. This shifts conformational equilibrium such that rotation of the α CC domain is allowed due to movement in the β H-NOX domain and results in the increased catalytic activity observed in the 1-NO state. Under highly activating conditions of excess NO, the equilibrium of this sampling shifts such that the H-NOX and CAT domains more frequently sample their open conformations leading to a higher probability that interactions stabilizing the fully extended conformation of the protein can occur. The mechanism of interaction which leads to these equilibrium shifts in the xsNO state remains unknown.

Stimulators increase sGC activity by shifting the conformational landscape of sGC. For sGC without NO bound at the heme, stimulators result in only slightly increased activity, likely due to the small population of sGC with an open conformation of the H-NOX domains or an inability remain in the stimulator binding pocket due to the strong interactions driving the H-NOX domains towards the closed conformation. In moderately activating conditions like the 1-NO state, stimulators bind the β H-NOX domain in the more frequently sampled open conformation, shifting the conformational equilibrium of the H-NOX domains towards the open state and preventing bonding interactions between βT110, αQ418, and αR428 which stabilize the closed conformation. Stimulators thus increase the activity of 1-NO protein to maximum by freeing rotation of the α CC domains. Stimulators increase the activity of xsNO sGC only slightly[6,8], suggesting that sufficient

NO concentrations can shift most of the sGC population to the fully extended state. As observed with riociguat[8] and CYR715 (Chapter 3), stimulators which can engage αR429 shift the equilibrium of the CAT domains towards the open state through via direct interaction which stabilizes the rotated conformation of the α CC domain. As observed with CYR715, it is also possible that additional interactions within the β H-NOX domain, such as with βC78 (discussed as an important residue for heme incorporation in sGC in Chapter 4), can provide sufficient disruption to the closed conformation of the H-NOX domains that stimulators can lead to significant increases in activity for even NO-free protein.

Investigating Conformational Sampling in sGC

Investigating this potential model for conformational sampling of sGC, as well as the effects of ligands on this equilibrium, is a complicated task. Previous attempts using SAXS to characterize conformational change in sGC have been complicated by the difficulty in maintaining anerobic conditions during experiments[6] or by the seeming loss of excess NO interactions in sGC during X-ray exposure (Chapter 3). Additionally, since SAXS data represent bulk averages for proteins in solution, this method is unable to identify unique conformational populations within this average that might exist in the 1-NO state. Furthermore, structural data obtained through SAXS is of limited resolution, so while electron density maps can be generated from these data using algorithms such as DENSS[22], such data may not be of sufficient resolution to determine regions undergoing only slight degrees of conformational change.

Full-length structures for sGC could not be solved using X-ray crystallography, likely due to the independent conformational flexibility of the H-NOX and CAT domains rendering it poorly amenable to crystallization. Cryo-EM, due to its use of samples frozen in vitreous ice, was able to provide high resolution maps of sGC, yet this technique still has limitations. Advances in software-based analytical tools, such as motion correction[23] and real-time contrast transfer function determination[24], coupled with hardware improvements such as direct electron detectors[25] have allowed maps constructed from single-particle analysis of cryo-EM samples to reach near atomic-level resolution. Unfortunately, the data analysis necessary to produce these cryo-EM maps is computationally challenging, thus several assumptions and limitations are often imposed on the data. Conformational flexibility is assumed to arise from independent, distinct states and, through a process known as "3D classification"[26], particle classes are fit to initial models for refinement. However, since the number of potential structural conformations are unknown, refinement can be biased by which models are chosen, yielding maps which best fit the initial models. Additionally, restricting refinement to a finite number of initial models will result in the loss of conformational changes within the particle population, effectively "purifying" only certain conformations out from the data set.

Recent efforts have been made toward improving data processing and map generation for heterogenous protein populations. Masked or focused refinement is an analysis technique which assumes that isolated domains of proteins will largely retain their own internal structure but may

change their orientations relative to other regions of the protein.[27] In this technique, electron densities from certain regions of the protein are masked or hidden during analysis, allowing a different region of the map to be processed to a higher resolution.[27] Thus, conformational flexibility between domains is ignored to facilitate higher resolution maps of isolated domains. The assumptions underlying focused refinement are problematic when aspects of conformational flexibility between domains are not isolated, as is the case in sGC where conformational sampling in the H-NOX or CAT domains is propagated along the protein via conformational changes in the CC domains. Additionally, changes in stabilizing contacts between the β H-NOX and CC domains of sGC likely play a crucial role in shifting the conformational equilibrium between the contracted and extended states of the enzyme.

To address some of these limitations, the cryo-EM processing package RELION[26] has incorporated Multibody Refinement as a tool to better investigate conformational variance in cryo-EM data sets.[27] This approach is an improvement on focused refinement which allows researchers to separate a consensus refinement into a finite number of classes of independently moving regions. These classes are then used to fit particles to the discrete class which they best match, and signals from non-matching classes are subtracted. This processing allows the data set to capture large conformational motions while being able to recover high resolution information from relevant portions of the data set.

For proteins which are not best described as homogeneous, rigid particles, a technique known as non-uniform refinement (NU), implemented in cryoSPARC, facilitates the reconstruction of higher resolution maps for particles with significant heterogeneity.[28] Unlike the previously described methods, NU refinement generates particle classes from an initial low resolution map and uses fundamental principles of protein structure to generate structural classes without user input. This eliminates the bias inherent in focused or multibody refinement techniques. This process, as utilized in Chapter 3, revealed that an extended population of *Ms* sGC βC122S existed in a sample without any ligands to facilitate such conformational change.

Combinations of these methods have been used to solve the currently known structures[6–8,29] for sGC in both contracted and extended conformations. Except for the work presented in Chapter 3, none have mentioned the presence of unexpected conformations of sGC in analyzed samples. This is likely not due to a lack of heterogeneity in the sample sets, but likely a limitation of the processing techniques used and/or computational power available to analyze the collected data. A new processing tool for cryo-EM data sets, cryoDRGN[30], uses deep neural networks to build a continuous distribution of electron density maps, allowing for per particle mapping of conformational heterogeneity in single-particle cryo-EM data. This facilitates the detection of conformational states which contain as few as 1,000 particles, allowing for structural information to be determined for even low population conformations. Recent work[31] utilized cryoDRGN to investigate the conformational landscape of a class I ribonucleotide reductase (RNR) and found that the RNR complex undergoes significant conformational sampling during turnover while maintaining the global asymmetry necessary for regulating this turnover. Researchers were able to

solve 24 unique classes for various stages of the catalytic cycle, leading to the determination of a unique conformational class which is enriched in the later stages of catalytic turnover.

Tools such as cryoDRGN provide a unique opportunity to fully investigate the conformational landscape of sGC. Chapter 3 detailed SAXS experiments which revealed a global extension of sGC following ligand binding to either the N- or C-termini of the protein. These extensions, however, did not directly correlate to observed activity in biochemical assays suggesting that some extensions can be decoupled from catalysis. To better understand the scope of sGC activation, particularly how conformational sampling results in the extension of the CC domains, cryo-EM samples should be prepared for sGC in various partially activating conditions which are not associated with the basal or maximal activity states of sGC. N-terminal conformational sampling of sGC can be investigated using heme ligands such as NO, carbon monoxide[32], n-butyl isocyanide[33], or stimulators which have been shown to result in partial activation of sGC. C-terminal conformational sampling can be investigated through the addition of ATP or GTP nucleotides or analogs to sGC without any other activating ligands. Conformational analysis of these partially activated or inhibited states could provide crucial information towards the identity of intermediate 1-NO state(s) in sGC while better understanding the dynamic interplay in the bidirectional regulation of sGC activity.

Elucidation of this conformational landscape would greatly facilitate the rational design of sGC stimulators. If the greatest regulatory control of sGC is exerted by conformational sampling of the H-NOX domains, then stimulators should be targeted towards binding the largest population of sGC with a partially or fully extended H-NOX domain. Understanding the molecular motions of sGC contraction would allow for the design of stimulators which effectively resist these motions to prevent expulsion from the binding site. If inhibition or activation from the CAT domains can drive sGC activity, then new classes of stimulators could be designed to increase sGC activity, perhaps in a manner independent of regulation from the H-NOX domains.

Evolutionary Perspectives on Excess NO Activation of sGC

Significant effort, explained in detail in Chapter 1 and continued in Chapter 4, has been invested towards understanding where excess NO interacts with sGC to facilitate full catalytic activity. The hypothesis with greatest experimental support is that excess NO interacts with sGC at a non-heme site[33,34] which mostly likely involves reactive cysteine(s) in the protein.[35] Experiments discussed in Chapter 4 of this work attempted to use thiol labeling reagents to determine the identity of potential second-site cysteines in *Ms* sGC, but the results were confounded by labeling of a catalytic cysteine.

As discussed in Chapter 4, analysis of a sequence similarity network (SSN) generated from the *Rn* sGC β_1 H-NOX domain (residues 1 – 194) revealed that cysteine residues are differentially conserved between oxygen- (O_2) and NO-sensing sGCs. Highly conserved cysteines in NO-sensing sGCs at position βC78, C122, and C214 were not conserved in O_2-sensing sGCs, highlighting their potential involvement in second-site activation by NO. Direct characterizations

of variants at these positions either yielded a heme-deficient sGC[36] (βC78S and C214S) or an sGC which still responded to excess NO (βC122A and C122S, Chapter 3). While βC78, C122, and αC517 have been shown to undergo *S*-nitrosation leading to desensitization of sGC[37,38], none of these residues were found to exhibit extended electron density due to NO binding in cryo-EM structures solved under excess NO conditions.[29] βC174 was found to be uniquely conserved in β_1-type NO-sensitive sGCs. This contrasts with βC78 and C214 which are conserved in all NO-sensing sGC clusters. Thus, better understanding differences in the activation pathways between β_1- and β_2-containing sGCs could provide insight into NO-activation of sGCs.

In humans, the α_1/β_1 heterodimer is the most prevalent form of sGC, with both the α_1 and β_1 subunits being expressed in most tissues[39]; and similar α/β-type heterodimers have been well characterized for sGCs from numerous organisms. The β_2 subunit, however, is less understood. The human β_2 subunit shares only 28.03% and 34.03% identity with the α_1 and β_1 subunits, respectively. In rats, the sequence identity is roughly similar, at 27.85% and 34.89% identity with the α_1 and β_1 subunits, respectively. In rats, the β_2 isoform is primarily expressed in the kidney[40] with RNA transcription levels that are developmentally regulated.[41] The *Rn* β_2 isoform does not form functional heterodimers with α sGC subunits, but does exhibit cyclase activity in the absence of α subunits, suggesting that β_2 could serve as a functional homodimer.[42] β_2 sGC increases catalytic activity in response to NO binding, but these homodimers were not stimulated by the addition of YC-1[42] likely due to missing YC-1 interacting residues at the N-terminus of the β_2 subunit (Figure 5.4).

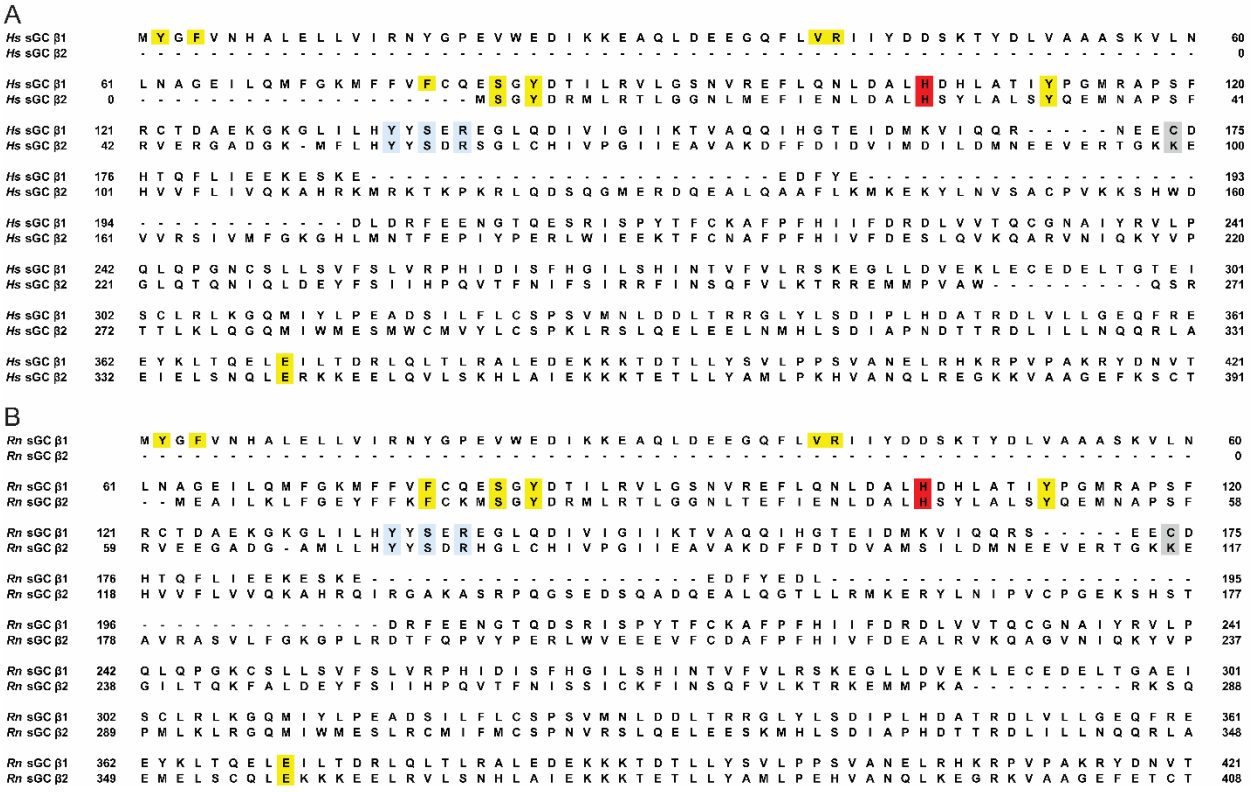

Figure 5.4. Sequence alignments for the β_1 and β_2 subunits for (A) human (*Hs*) and (B) rat (*Rn*) sGCs. Residues which bind YC-1[8] are shown in yellow. The heme ligating histidine is shown in red. The YxSxR motif is shown in blue. βC174 in the β_1 subunit is shown in gray.

Rn β_2 sGC increases activity in response to NO, but activity is only increased by ~4.5-fold over basal in the presence of 100 μM DEA NONOate[42] which is similar to the increase in activity observed for α_1/β_1 sGCs in the 1-NO state. The addition of NO to the β_2 homodimer results in both a decrease in K_M and an increase in V_{max}[42], similar to what was observed for the basal to 1-NO activation of α_1/β_1 *Rn* sGG.[35] There was no change to K_M following stimulation from the 1-NO to the xsNO state for α_1/β_1 *Rn* sGG.[35] Unfortunately, no UV-Vis data were collected for the β_2 homodimeric sGC to determine if the basal sGC sample was NO-free, nor were experiments performed to characterize the activity of this enzyme in the presence of stoichiometric NO.

Studies of choanoflagellates, the closest evolutionary relative of unicellular animals, provide unique opportunities to investigate the evolution of sGC function and NO signaling. α/β type sGCs are proposed to have evolved their heterodimeric structure following duplication of a β-type subunit and eventual differentiation towards an α-type subunit.[43] Recent work[44] characterized an NO-sensitive homodimeric sGC from the choanoflagellate *Choanoeca flexa* (*Cf*) which shows a two-step activation profile in response to NO-binding. The sequence of *Cf* sGC1 shares greater identity with the β-type subunits of *Rn* sGC (31.58% with β_1, 34.40% with β_2) than with the α_1 subunit (28.55%), supporting a hypothesis that *Cf* sGC1 represents a potential evolutionary neighbor of NO-sensing heterodimeric sGCs. Thus, cysteines which are conserved in this homodimeric sGC with a two-step activation in response to NO-binding are ideal candidates for residues involved in excess NO-sensing in α/β type sGCs.

Four cysteines are conserved between *Cf* sGC1 and the β_1 subunits of *Hs*, *Rn*, and *Ms* sGC at positions 123, 177, 355, and 489 (122, 174, 309, and 407, *Rn* sGC β_1). *Cf* sGC1 cysteines at positions 123 and 489 are conserved with the α_1 subunits of *Hs*, *Rn*, and *Ms* sGC (192 and 516, *Rn* sGC α_1). Three cysteines are conserved between *Cf* sGC1 and the β_2 subunit of *Rn* sGC at positions 271, 355, and 452 (266, 310, and 407, *Rn* sGC β_2). These data are presented for greater clarity in Table 5.1. Of these conserved cysteines, three were mutated to non-cysteine residues (C123S, C355G, and C489A) to test for excess NO sensitivity in *Cf* sGC1.[45] The triple cysteine variant sGC was found to still possess two-step activation with distinct activity states for basal, 1-NO, and excess NO activity, suggesting that these residues were not solely responsible for excess NO sensitivity in *Cf* sGC1.

Table 5.1. Conservation of selected cysteines between *Cf* sGC1 and *Rn* sGC subunits

Cf sGC Position	*Rn* sGC Position		
	α_1	β_1	β_2
123†	192	122	
177		174	
271			266
355†		309	310
452			407
489†	516	407	

†Indicates residues which were mutagenized to non-cysteines to characterize excess NO response in *Cf* sGC1.[45]

Interestingly, C177 (βC174 *Rn* sGC) was excluded from this characterization due to poor sequence consensus in the surrounding region (Figure 5.5A).[45] However, there still is some degree of similarity in the surrounding sequences, with a large number of charged and polar residues flanking this position in all four sequences. Additionally, structural prediction for a *Cf* sGC homodimer using AlphaFold[46] predicts that this residue occupies a similar position to the equivalent βC174 in solved structures of *Hs* sGC. *Hs* sGC βC174 occupies a position on the disordered loop connecting strands 3 and 4 of the β sheet which is adjacent to the αF helix which contains the heme-ligating histidine. In the contracted conformation, βC174 appears to share visible electron density with βQ178 (Figure 5.5B). In the NO-activated state, however, this shared electron density is no longer evident between these residues (Figure 5.5C). The *Cf* sGC1 sequence contains a glutamine at Q183 which could plausibly participate in a similar interaction with C177 in *Cf* sGC.

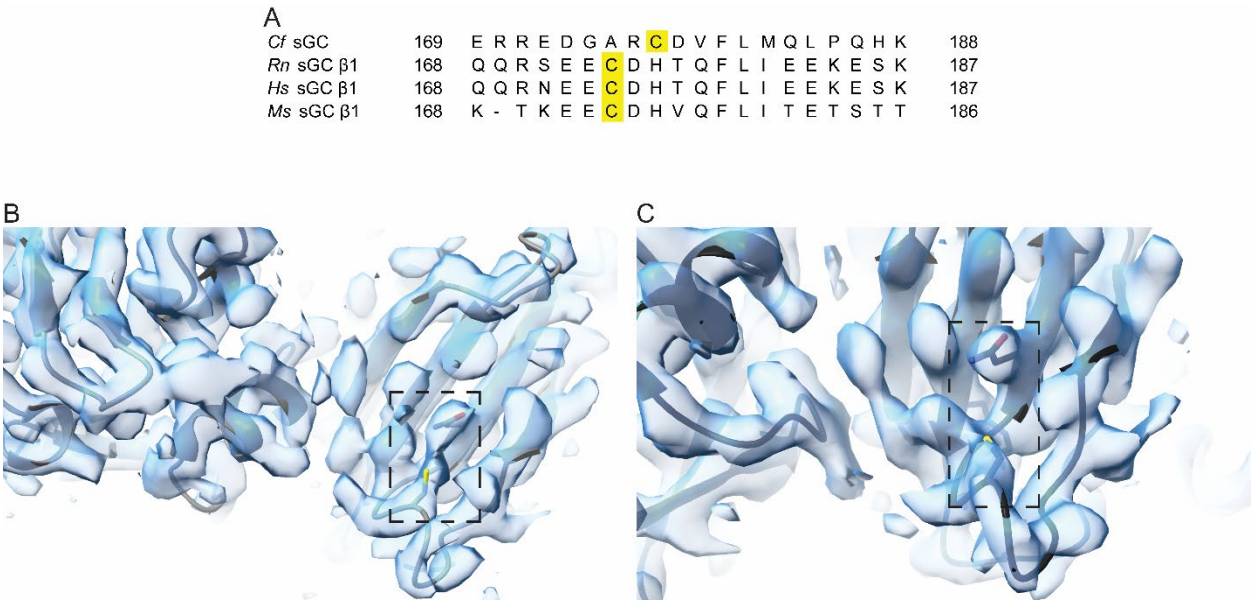

Figure 5.5. Surrounding sequence and structure for a conserved sGC cysteine. A) Sequence alignment of equivalent cystines (yellow) in *Cf, Hs*, *Rn*, and *Ms* sGC. B) Structure and electron density map for NO-free *Hs* sGC (PDB ID: 8HBE[29]). Observed electron density between βC174 and βQ178 is shown in the dotted box. C) Structure and electron density map for NO-activated *Hs* sGC (PDB ID: 8HBH[29]). βC174 and βQ178 are shown in the dotted box, and no shared electron density is evident.

As discussed at the beginning of this chapter, the most likely free energy landscape for sGC activation by NO involves destabilization of a contracted NO-free or partially extended 1-NO sGC into the extended conformation. In the NO-free structure of an NO-sensing sGC, βC174 appears to share electron density with βQ178 in the β sheet flanking the heme in the β H-NOX domain. This interaction likely serves to stabilize this region of the protein. As discussed in Chapter 3, slight perturbations of this β sheet at position βC122 resulted in an sGC which was highly activated by small molecule stimulators even in the absence of NO. This suggested that even slight changes to the structure or stability of this β sheet can lead to increased sGC activity. NO binding to βC174 could result in disruption of this stabilizing interaction with βQ178, potentially facilitating full conformational change to the active, extended conformation of sGC.

Conclusions

Understanding of sGC activation has increased dramatically since the first full-length structures of sGC were solved. For each question these structures answered, however, more questions remain. Structural information for the 1-NO state, thus far only characterized biochemically, remains elusive. Continued improvements in data collection and processing for cryo-EM data sets, however, provide powerful avenues for investigating this difficult and likely conformationally heterogeneous state. These tools can also provide opportunities for characterizing the conformational landscape of sGC, allowing for the design of stimulators which can bind the most populated or productive conformations of sGC.

The second site involved in the activation of sGC by excess NO remains unknown. Bioinformatic approaches allow for the screening of thousands of characterized and putative sGCs from diverse organisms in pursuit of the evolutionary breadcrumbs of NO signaling and sGC regulation. These tools can be used to determine cysteines with unique conservation patterns in NO-sensitive sGCs, such as βC174. Characterization of so-called atypical sGCs, such as β_2 homodimers, could provide information on the evolution in function and regulation of NO-sensing sGCs in eukaryotes. Determining the identity of the NO second site in sGC, and subsequently characterizing the mechanism of conformational change following NO interaction, will provide valuable insight into the NO activation and regulation of proteins via non-nitrosative methods.

References

(1) Arnold, W. P.; Mittal, C. K.; Katsuki, S.; Murad, F. Nitric Oxide Activates Guanylate Cyclase and Increases Guanosine 3':5'-Cyclic Monophosphate Levels in Various Tissue Preparations. *Proc Natl Acad Sci U S A* **1977**, *74* (8), 3203–3207. https://doi.org/10.1073/pnas.74.8.3203.

(2) Stone, J. R.; Marletta, M. A. Spectral and Kinetic Studies on the Activation of Soluble Guanylate Cyclase by Nitric Oxide. *Biochemistry* **1996**, *35* (4), 1093–1099. https://doi.org/10.1021/bi9519718.

(3) Marletta, M. A.; Underbakke, E. S.; Fernhoff, N. B. Molecular Aspects of sGC Regulation. *BMC Pharmacol* **2011**, *11* (Suppl 1), O10. https://doi.org/10.1186/1471-2210-11-S1-O10.

(4) Russwurm, M.; Koesling, D. NO Activation of Guanylyl Cyclase. *The EMBO Journal* **2004**, *23* (22), 4443–4450. https://doi.org/10.1038/sj.emboj.7600422.

(5) Ignarro, L. J.; Wood, K. S.; Wolin, M. S. Regulation of Purified Soluble Guanylate Cyclase by Porphyrins and Metalloporphyrins: A Unifying Concept. *Advances in cyclic nucleotide and protein phosphorylation research* **1984**, *17*, 267–274.

(6) Horst, B. G.; Yokom, A. L.; Rosenberg, D. J.; Morris, K. L.; Hammel, M.; Hurley, J. H.; Marletta, M. A. Allosteric Activation of the Nitric Oxide Receptor Soluble Guanylate Cyclase Mapped by Cryo-Electron Microscopy. *eLife* **2019**, *8*, e50634. https://doi.org/10.7554/eLife.50634.

(7) Kang, Y.; Liu, R.; Wu, J.-X.; Chen, L. Structural Insights into the Mechanism of Human Soluble Guanylate Cyclase. *Nature* **2019**, *574* (7777), 206–210. https://doi.org/10.1038/s41586-019-1584-6.

(8) Liu, R.; Kang, Y.; Chen, L. Activation Mechanism of Human Soluble Guanylate Cyclase by Stimulators and Activators. *Nat Commun* **2021**, *12* (1), 5492. https://doi.org/10.1038/s41467-021-25617-0.

(9) Frauenfelder, H.; Sligar, S. G.; Wolynes, P. G. The Energy Landscapes and Motions of Proteins. *Science* **1991**, *254* (5038), 1598–1603. https://doi.org/10.1126/science.1749933.

(10) Campbell, M. G.; Underbakke, E. S.; Potter, C. S.; Carragher, B.; Marletta, M. A. Single-Particle EM Reveals the Higher-Order Domain Architecture of Soluble Guanylate Cyclase. *Proceedings of the National Academy of Sciences* **2014**, *111* (8), 2960–2965. https://doi.org/10.1073/pnas.1400711111.

(11) Zhao, Y.; Brandish, P. E.; Ballou, D. P.; Marletta, M. A. A Molecular Basis for Nitric Oxide Sensing by Soluble Guanylate Cyclase. *Proceedings of the National Academy of Sciences* **1999**, *96* (26), 14753–14758. https://doi.org/10.1073/pnas.96.26.14753.

(12) Wittenborn, E. C.; Thomas, W. C.; Houghton, K. A.; Wirachman, E. S.; Wu, Y.; Marletta, M. A. Role of the Coiled-Coil Domain in Allosteric Activity Regulation in Soluble Guanylate Cyclase. *Biochemistry* **2023**, *62* (10), 1568–1576. https://doi.org/10.1021/acs.biochem.3c00052.
(13) Ruiz-Stewart, I.; Tiyyagura, S. R.; Lin, J. E.; Kazerounian, S.; Pitari, G. M.; Schulz, S.; Martin, E.; Murad, F.; Waldman, S. A. Guanylyl Cyclase Is an ATP Sensor Coupling Nitric Oxide Signaling to Cell Metabolism. *Proc Natl Acad Sci U S A* **2004**, *101* (1), 37–42. https://doi.org/10.1073/pnas.0305080101.
(14) Cary, S. P. L.; Winger, J. A.; Marletta, M. A. Tonic and Acute Nitric Oxide Signaling through Soluble Guanylate Cyclase Is Mediated by Nonheme Nitric Oxide, ATP, and GTP. *Proceedings of the National Academy of Sciences* **2005**, *102* (37), 13064–13069. https://doi.org/10.1073/pnas.0506289102.
(15) Tsai, A.-L.; Berka, V.; Sharina, I.; Martin, E. Dynamic Ligand Exchange in Soluble Guanylyl Cyclase (sGC): Implications for sGC Regulation and Desensitization. *J Biol Chem* **2011**, *286* (50), 43182–43192. https://doi.org/10.1074/jbc.M111.290304.
(16) Yazawa, S.; Tsuchiya, H.; Hori, H.; Makino, R. Functional Characterization of Two Nucleotide-Binding Sites in Soluble Guanylate Cyclase. *Journal of Biological Chemistry* **2006**, *281* (31), 21763–21770. https://doi.org/10.1074/jbc.M508983200.
(17) Derbyshire, E. R.; Fernhoff, N. B.; Deng, S.; Marletta, M. A. Nucleotide Regulation of Soluble Guanylate Cyclase Substrate Specificity. *Biochemistry* **2009**, *48* (31), 7519–7524. https://doi.org/10.1021/bi900696x.
(18) Sürmeli, N. B.; Müskens, F. M.; Marletta, M. A. The Influence of Nitric Oxide on Soluble Guanylate Cyclase Regulation by Nucleotides. *J Biol Chem* **2015**, *290* (25), 15570–15580. https://doi.org/10.1074/jbc.M115.641431.
(19) Martin, E.; Sharina, I.; Kots, A.; Murad, F. A Constitutively Activated Mutant of Human Soluble Guanylyl Cyclase (sGC): Implication for the Mechanism of sGC Activation. *Proceedings of the National Academy of Sciences* **2003**, *100* (16), 9208–9213. https://doi.org/10.1073/pnas.1633590100.
(20) Wittenborn, E. C.; Marletta, M. A. Structural Perspectives on the Mechanism of Soluble Guanylate Cyclase Activation. *Int J Mol Sci* **2021**, *22* (11), 5439. https://doi.org/10.3390/ijms22115439.
(21) Baskaran, P.; Heckler, E. J.; Akker, F. van den; Beuve, A. Identification of Residues in the Heme Domain of Soluble Guanylyl Cyclase That Are Important for Basal and Stimulated Catalytic Activity. *PLOS ONE* **2011**, *6* (11), e26976. https://doi.org/10.1371/journal.pone.0026976.
(22) Grant, T. D. Ab Initio Electron Density Determination Directly from Solution Scattering Data. *Nat Methods* **2018**, *15* (3), 191–193. https://doi.org/10.1038/nmeth.4581.
(23) Li, X.; Mooney, P.; Zheng, S.; Booth, C. R.; Braunfeld, M. B.; Gubbens, S.; Agard, D. A.; Cheng, Y. Electron Counting and Beam-Induced Motion Correction Enable near-Atomic-Resolution Single-Particle Cryo-EM. *Nat Methods* **2013**, *10* (6), 584–590. https://doi.org/10.1038/nmeth.2472.
(24) Zhang, K. Gctf: Real-Time CTF Determination and Correction. *J Struct Biol* **2016**, *193* (1), 1–12. https://doi.org/10.1016/j.jsb.2015.11.003.
(25) Bammes, B. E.; Rochat, R. H.; Jakana, J.; Chen, D.-H.; Chiu, W. Direct Electron Detection Yields Cryo-EM Reconstructions at Resolutions beyond ¾ Nyquist Frequency. *J Struct Biol* **2012**, *177* (3), 589–601. https://doi.org/10.1016/j.jsb.2012.01.008.

(26) Scheres, S. H. W. RELION: Implementation of a Bayesian Approach to Cryo-EM Structure Determination. *Journal of Structural Biology* **2012**, *180* (3), 519–530. https://doi.org/10.1016/j.jsb.2012.09.006.
(27) Nakane, T.; Kimanius, D.; Lindahl, E.; Scheres, S. H. Characterisation of Molecular Motions in Cryo-EM Single-Particle Data by Multi-Body Refinement in RELION. *eLife* **2018**, *7*, e36861. https://doi.org/10.7554/eLife.36861.
(28) Punjani, A.; Zhang, H.; Fleet, D. J. Non-Uniform Refinement: Adaptive Regularization Improves Single-Particle Cryo-EM Reconstruction. *Nat Methods* **2020**, *17* (12), 1214–1221. https://doi.org/10.1038/s41592-020-00990-8.
(29) Liu, R.; Kang, Y.; Chen, L. NO Binds to the Distal Site of Haem in the Fully Activated Soluble Guanylate Cyclase. *Nitric Oxide* **2023**, *134–135*, 17–22. https://doi.org/10.1016/j.niox.2023.03.002.
(30) Zhong, E. D.; Bepler, T.; Berger, B.; Davis, J. H. CryoDRGN: Reconstruction of Heterogeneous Cryo-EM Structures Using Neural Networks. *Nat Methods* **2021**, *18* (2), 176–185. https://doi.org/10.1038/s41592-020-01049-4.
(31) Xu, D.; Thomas, W. C.; Burnim, A. A.; Ando, N. Conformational Landscapes of a Class I Ribonucleotide Reductase Complex during Turnover Reveal Intrinsic Dynamics and Asymmetry. *Nat Commun* **2025**, *16* (1), 2458. https://doi.org/10.1038/s41467-025-57735-4.
(32) Stone, J. R.; Marletta, M. A. Synergistic Activation of Soluble Guanylate Cyclase by YC-1 and Carbon Monoxide: Implications for the Role of Cleavage of the Iron-Histidine Bond during Activation by Nitric Oxide. *Chemistry & Biology* **1998**, *5* (5), 255–261. https://doi.org/10.1016/S1074-5521(98)90618-4.
(33) Derbyshire, E. R.; Marletta, M. A. Butyl Isocyanide as a Probe of the Activation Mechanism of Soluble Guanylate Cyclase: INVESTIGATING THE ROLE OF NON-HEME NITRIC OXIDE. *Journal of Biological Chemistry* **2007**, *282* (49), 35741–35748. https://doi.org/10.1074/jbc.M705557200.
(34) Guo, Y.; Suess, D. L. M.; Herzik, M. A.; Iavarone, A. T.; Britt, R. D.; Marletta, M. A. Regulation of Nitric Oxide Signaling by Formation of a Distal Receptor–Ligand Complex. *Nat Chem Biol* **2017**, *13* (12), 1216–1221. https://doi.org/10.1038/nchembio.2488.
(35) Fernhoff, N. B.; Derbyshire, E. R.; Marletta, M. A. A Nitric Oxide/Cysteine Interaction Mediates the Activation of Soluble Guanylate Cyclase. *Proceedings of the National Academy of Sciences* **2009**, *106* (51), 21602–21607. https://doi.org/10.1073/pnas.0911083106.
(36) Friebe, A.; Wedel, B.; Harteneck, C.; Foerster, J.; Schultz, G.; Koesling, D. Functions of Conserved Cysteines of Soluble Guanylyl Cyclase. *Biochemistry* **1997**, *36* (6), 1194–1198. https://doi.org/10.1021/bi962047w.
(37) Sayed, N.; Baskaran, P.; Ma, X.; van den Akker, F.; Beuve, A. Desensitization of Soluble Guanylyl Cyclase, the NO Receptor, by S-Nitrosylation. *Proceedings of the National Academy of Sciences* **2007**, *104* (30), 12312–12317. https://doi.org/10.1073/pnas.0703944104.
(38) Fernhoff, N. B.; Derbyshire, E. R.; Underbakke, E. S.; Marletta, M. A. Heme-Assisted *S*-Nitrosation Desensitizes Ferric Soluble Guanylate Cyclase to Nitric Oxide*. *Journal of Biological Chemistry* **2012**, *287* (51), 43053–43062. https://doi.org/10.1074/jbc.M112.393892.

(39) Budworth, J.; Meillerais, S.; Charles, I.; Powell, K. Tissue Distribution of the Human Soluble Guanylate Cyclases. *Biochemical and Biophysical Research Communications* **1999**, *263* (3), 696–701. https://doi.org/10.1006/bbrc.1999.1444.

(40) Yuen, P. S. T.; Potter, L. R.; Garbers, D. L. A New Form of Guanylyl Cyclase Is Preferentially Expressed in Rat Kidney. *Biochemistry* **1990**, *29* (49), 10872–10878. https://doi.org/10.1021/bi00501a002.

(41) Behrends, S.; Budaeus, L.; Kempfert, J.; Scholz, H.; Starbatty, J.; Vehse, K. The Beta 2 Subunit of Nitric Oxide-Sensitive Guanylyl Cyclase Is Developmentally Regulated in Rat Kidney. *Naunyn Schmiedebergs Arch Pharmacol* **2001**, *364* (6), 573–576. https://doi.org/10.1007/s00210-001-0499-5.

(42) Koglin, M.; Vehse, K.; Budaeus, L.; Scholz, H.; Behrends, S. Nitric Oxide Activates the Beta 2 Subunit of Soluble Guanylyl Cyclase in the Absence of a Second Subunit. *J Biol Chem* **2001**, *276* (33), 30737–30743. https://doi.org/10.1074/jbc.M102549200.

(43) Montfort, W. R.; Wales, J. A.; Weichsel, A. Structure and Activation of Soluble Guanylyl Cyclase, the Nitric Oxide Sensor. *Antioxidants & Redox Signaling* **2017**, *26* (3), 107–121. https://doi.org/10.1089/ars.2016.6693.

(44) Wu, Y.; Thomas, W. C.; Green, Z.; Marletta, M. Characterization of a NO-Activated Homodimeric Soluble Guanylate Cyclase from a Choanoflagellate. *Biochemistry* **2025**. https://doi.org/10.1021/acs.biochem.5c00228.

(45) Wu, Y. The Study of Soluble Guanylate Cyclases From Choanoeca Flexa. Ph.D., University of California, Berkeley, United States -- California, **2024**. https://www.proquest.com/dissertations/docview/3176103326/abstract/DC61B65012434FF3PQ/5 (accessed 2025-06-04).

(46) Jumper, J.; Evans, R.; Pritzel, A.; Green, T.; Figurnov, M.; Ronneberger, O.; Tunyasuvunakool, K.; Bates, R.; Žídek, A.; Potapenko, A.; Bridgland, A.; Meyer, C.; Kohl, S. A. A.; Ballard, A. J.; Cowie, A.; Romera-Paredes, B.; Nikolov, S.; Jain, R.; Adler, J.; Back, T.; Petersen, S.; Reiman, D.; Clancy, E.; Zielinski, M.; Steinegger, M.; Pacholska, M.; Berghammer, T.; Bodenstein, S.; Silver, D.; Vinyals, O.; Senior, A. W.; Kavukcuoglu, K.; Kohli, P.; Hassabis, D. Highly Accurate Protein Structure Prediction with AlphaFold. *Nature* **2021**, *596* (7873), 583–589. https://doi.org/10.1038/s41586-021-03819-2.

APPENDICES

Appendix A

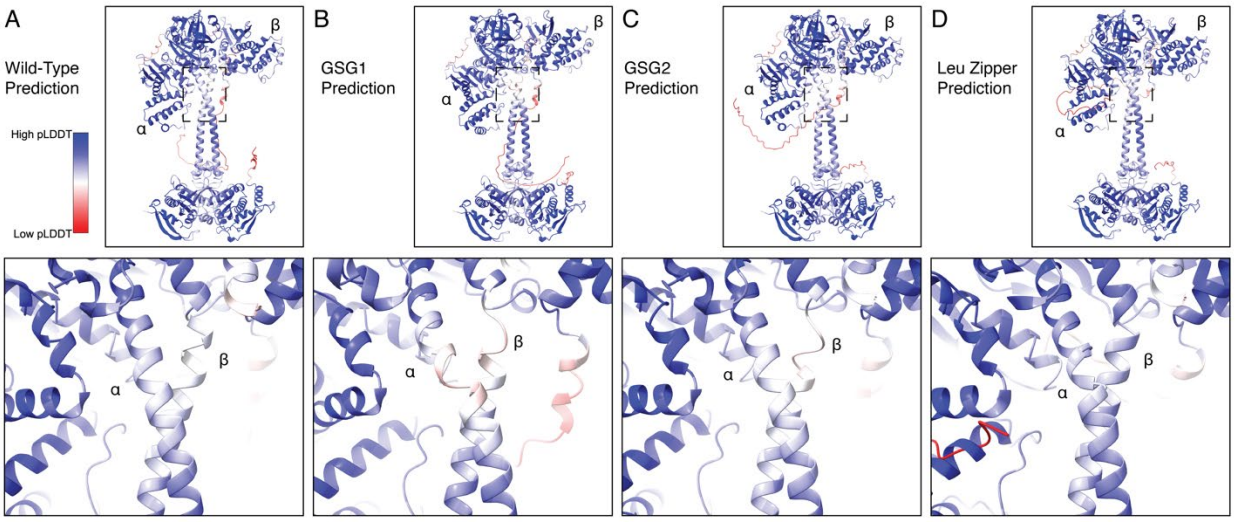

Figure A.1. AlphaFold2 structures for *Ms* sGC αβ dimers predicted using ColabFold.[1,2] (Top) AlphaFold2 predicts all structures in the active, straightened CC conformation. Predictions are shown for (A) WT, (B) *Ms* sGC(GSG1), (C) *Ms* sGC(GSG2), and (D) *Ms* sGC(Leu zipper). A WT experimental structure exists, but a prediction was produced for comparative purposes. The structures are shown as cartoons with colors representing prediction confidence scores (pLDDT) from 0 (red) to 100 (blue). A high score indicates higher prediction confidence. (Bottom) A zoomed in view of the mutated region of the CC for each variant.

Table A.1. AlphaFold2 prediction confidence (pLDDT) for mutated regions of *Ms* sGC

Residue Number	WT Residue	WT pLDDT	GSG1 Residue	GSG1 pLDDT	GSG2 Residue	GSG2 pLDDT	Leu Zipper Residue	Leu Zipper pLDDT
419A	Gln	69.76	Gln	60.89	Gln	69.47	Gln	73.1
420A	Ala	67.23	Gly	54.46	Ala	67.1	Leu	71.53
421A	Arg	68.86	Ser	50.21	Arg	65.9	Arg	70.44
422A	Ala	66.4	Gly	48.26	Gly	62.98	Ala	66.3
423A	Gln	65.04	Gly	49.19	Ser	62.73	Leu	68.11
424A	Asp	65.52	Ser	50.6	Gly	59.65	Asp	63.73
425A	Gly	66.79	Gly	58.2	Gly	63.65	Gly	69.59
426A	Leu	66.73	Ser	62.93	Leu	66.75	Leu	71.7
427A	Arg	67.1	Arg	60.54	Arg	65.75	Leu	72.61
428A	Arg	68.11	Arg	63.26	Arg	65.36	Arg	71.71
345B	Leu	75.17	Leu	78	Leu	80.55	Leu	77.22
346B	Met	70.98	Gly	64.68	Gly	67.65	Met	76.21
347B	Ser	61.71	Ser	54.86	Ser	56	Ser	69.68
348B	Glu	59.06	Gly	51.12	Gly	53.22	Glu	67.06
349B	Gln	60.84	Ser	49.08	Ser	50.4	Gln	70.46
350B	Phe	56.94	Gly	50.78	Gly	47.66	Leu	67.92
351B	Glu	57.14	Glu	52.8	Glu	47.96	Glu	65.17
352B	Ala	60	Ala	58.04	Ala	54.19	Ala	66.98
353B	Asp	60.55	Asp	61.14	Asp	57.5	Leu	69.12
354B	Tyr	58.13	Tyr	59.74	Tyr	53.61	Tyr	62.6
355B	Lys	63.92	Lys	64.35	Lys	62.22	Lys	67.48
356B	Leu	64.51	Leu	66.19	Leu	66.77	Leu	72.33
357B	Thr	62.25	Thr	66.1	Thr	63.65	Thr	66.9

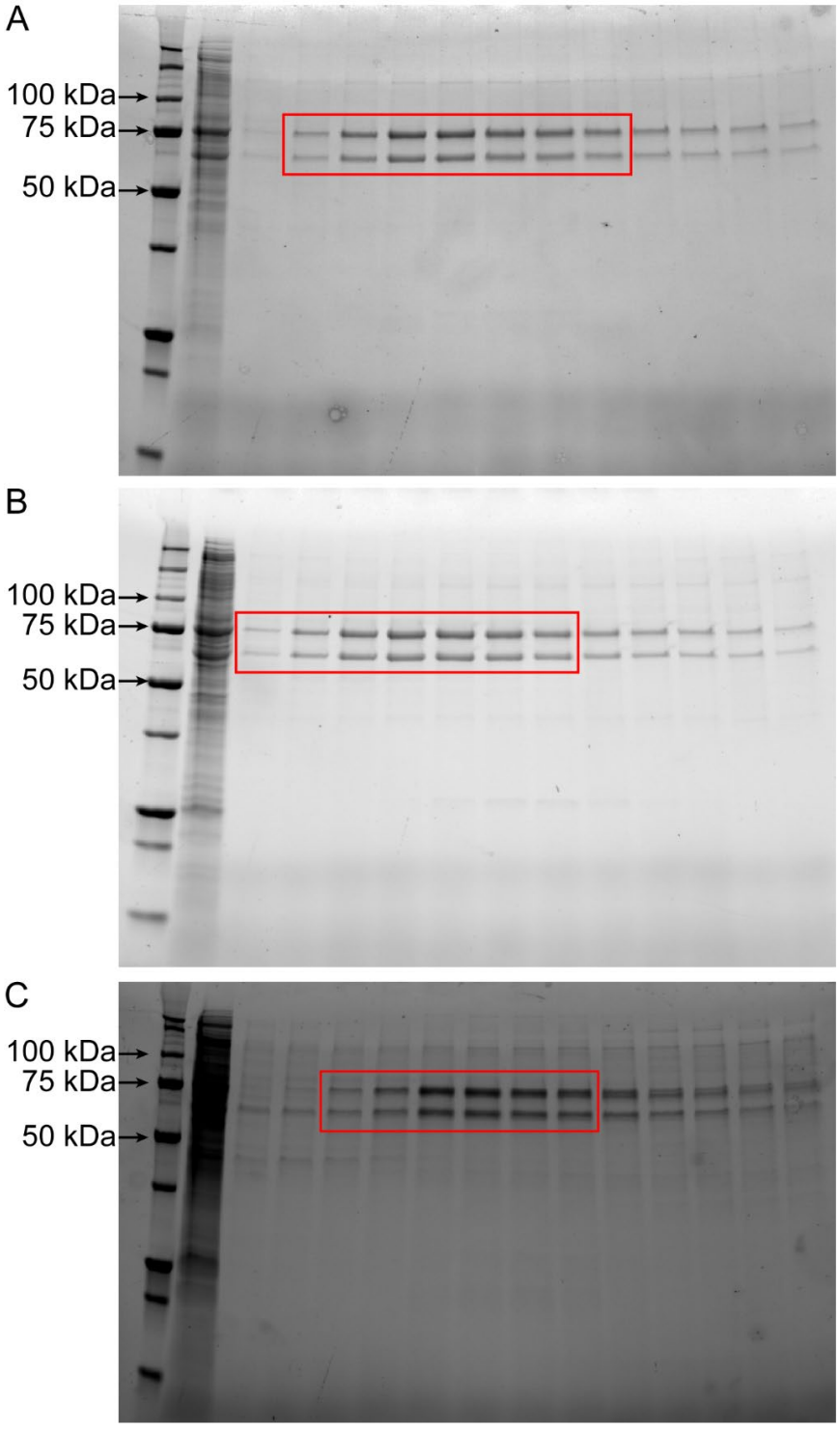

Figure A.2. Representative SDS-PAGE gels from anion exchange (POROS HQ2) columns for (A) *Ms* sGC(GSG1), (B) *Ms* sGC(GSG2), and (C) *Ms* sGC(Leu zipper). The first lane next to the molecular weight marker in each gel is the sample before anion exchange. Red boxes indicate fractions that were pooled.

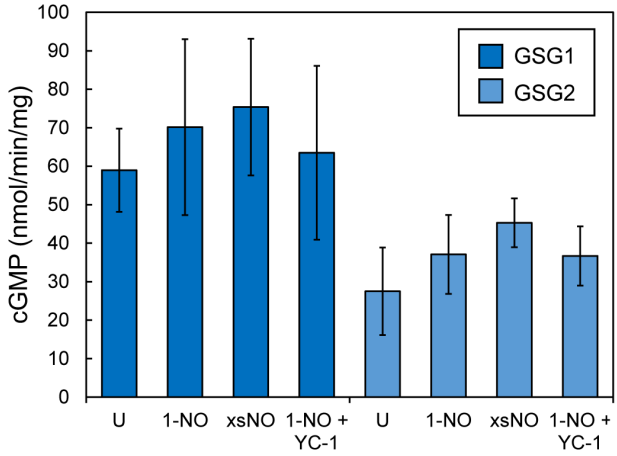

Figure A.3. Activity profiles of *Ms* sGC(GSG1) and *Ms* sGC(GSG2). Activities are plotted as in Figure 2.2C of Chapter 2.

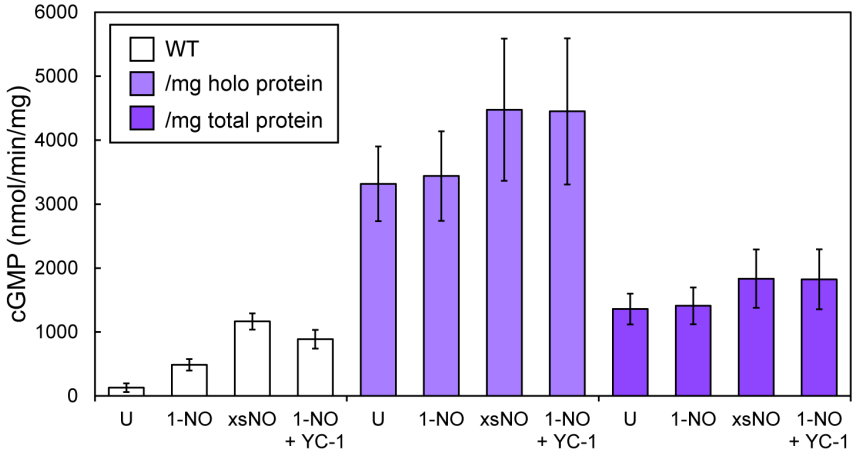

Figure A.4. Activity profile of *Ms* sGC(Leu zipper) compared to WT. Calculation of specific activities with respect to the amount of holo protein in the sample (lighter purple bars) leads to higher values than for typical WT preparations (white bars).

Appendix B

Table B.1. Primers used in this study

Sequence (5' → 3')	Target	Purpose
GGAGATAATTAAAATGATAACCATCTCGC	pFastBac	Sequencing
TTTATTTGTGAAATTTGTGATGCTATTGC	pFastBac	Sequencing
CTGTTGCCACCTCGACCAAAGTG	Ms α	Sequencing
GCCTGCACGATCATCTCGGGAC	Ms β	Sequencing
CTGGTTCCTCACCAGGAAGATCCATTAAATGGCAGCCTTTGTGGGG	pFastBac (F)	Cloning
GGGCATAGTTCACAAACCCGTACATGGTGTCCGCTCCCGGAGC	pFastBac (R)	Cloning
CCCCTCGTTCCGATCCACCGAGCGTCCTG	βC122S (F)	Cloning
CAGGACGCTCGGTGGATCGGAACGAGGGG	βC122S (R)	Cloning
CCCCTCGTTCCGAGCCACCGAGCGTCCTG	βC122A (F)	Cloning
CAGGACGCTCGGTGGCTCGGAACGAGGGG	βC122A (R)	Cloning

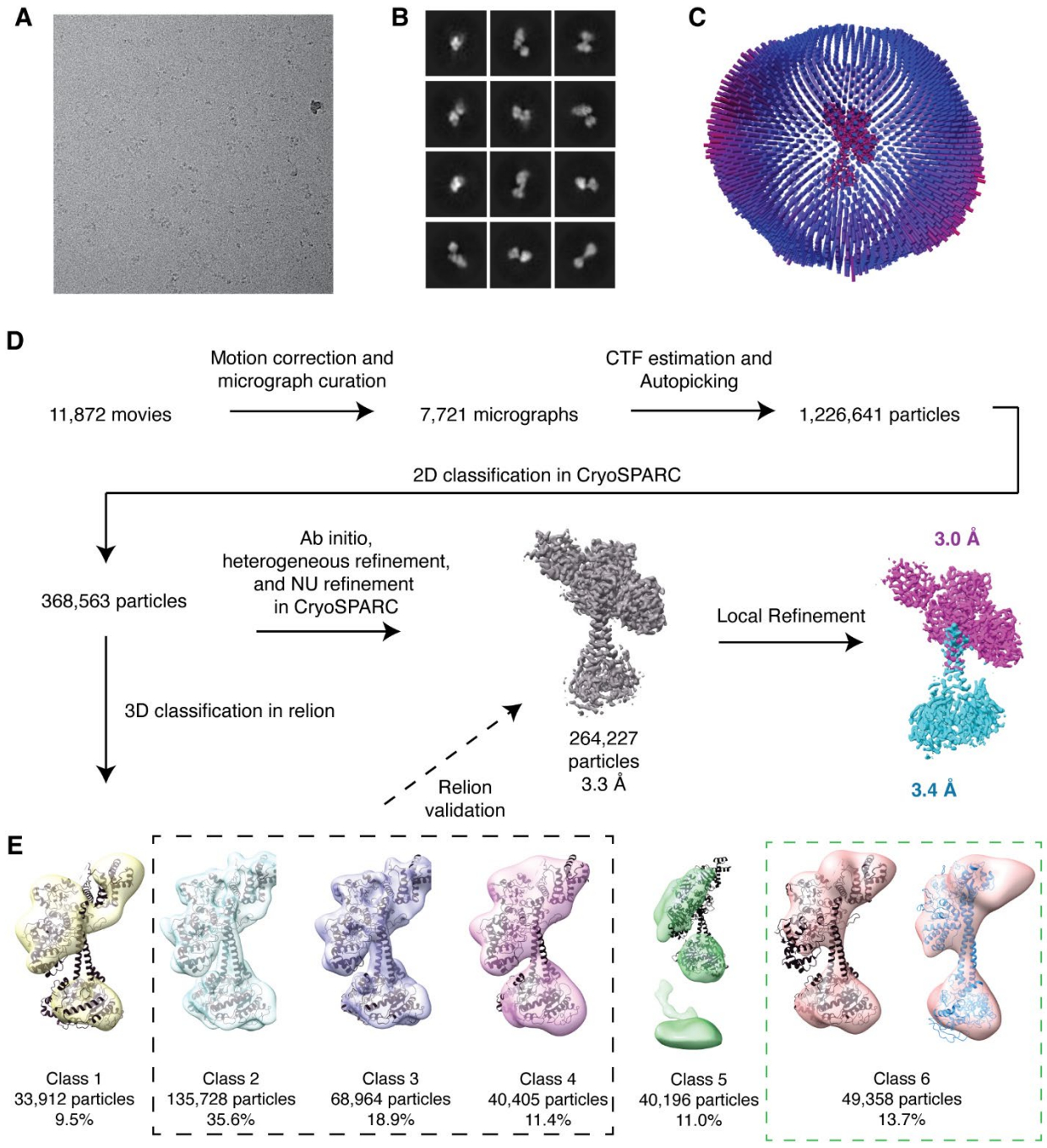

Figure B.1. Cryo-EM processing of ligand-free βC122S *Ms* sGC. (A) A representative raw micrograph of the ligand-free sGC dataset. (B) Representative 2D classes showing sGC dimers. (C) Projection orientation map showing angular distribution for the consensus refinement map of ligand-free sGC. (D) The cryo-EM data processing workflow for ligand-free sGC. This process led to a consensus 3.3 Å map and local refinement maps at 3.0 Å and 3.4 Å for the H-NOX and catalytic domains respectively. (E) 3D classification of sGC dimer 2D classes. Class 6 was found to more closely resemble extended sGC. Shown in black are contracted ligand-free human sGC (PDB: 8HBE[1]), and in blue is extended xsNO-bound human sGC (PDB: 8HBH[1]).

Table B.2. Cryo-EM collection and refinement

	Contracted βC122S *Ms* sGC (ligand-free)	Extended βC122S *Ms* sGC (CYR715)
Accession Codes	9OXN / EMD-70990	9P2R / EMD-71204
Data Collection and Processing		
Voltage (keV)	300	300
Electron Exposure (e- Å-2)	50	50
Defocus range (μm)	- 2.5 to -1.5	-2.5 to -1.5
Pixel size (Å)	0.942	0.85
Symmetry imposed	none	none
Initial particle images (no.)	1,226,641	2,299,895
Final particle images (no.)	264,227	598,571
Map resolution (Å)	3.3 Å (global), 3.0 Å (HNOX), 3.4 Å (CAT)	3.7 Å (global), 3.6 Å (HNOX), 3.4 Å (CAT)
FSC threshold	0.143	0.143
Map resolution range (Å)	2.5 - 4.5	3.0 - 4.5
Refinement		
Initial model	ModelAngelo	7D9S, SwissModel
Model resolution (Å)	3	3.7
FSC threshold	0.5	0.5
CC (mask)	0.74	0.77
Map sharpening B factor (Å2)		
Model composition	18142	13561
Non-hydrogen atoms (per ASU)	9107	6877
Protein residues (per ASU)	1158	878
Ligands	Heme	Heme, GpCpp, CYR715
B factors (A2)		
Protein	77.8	45.07
Ligand	34.91	42.62
R.m.s. deviations		
Bond lengths (Å)	0.002 (0)	0.003 (0)
Bond angles (°)	0.499 (0)	0.558 (0)
Validation		
MolProbity score	1.37	1.82
Clashscore	5.4	9.16
Poor rotamers (%)	0.1	0.7
Ramachandran plot		
Favored (%)	97.62	95.29
Allowed (%)	2.38	4.59
Disallowed (%)	0	0.12

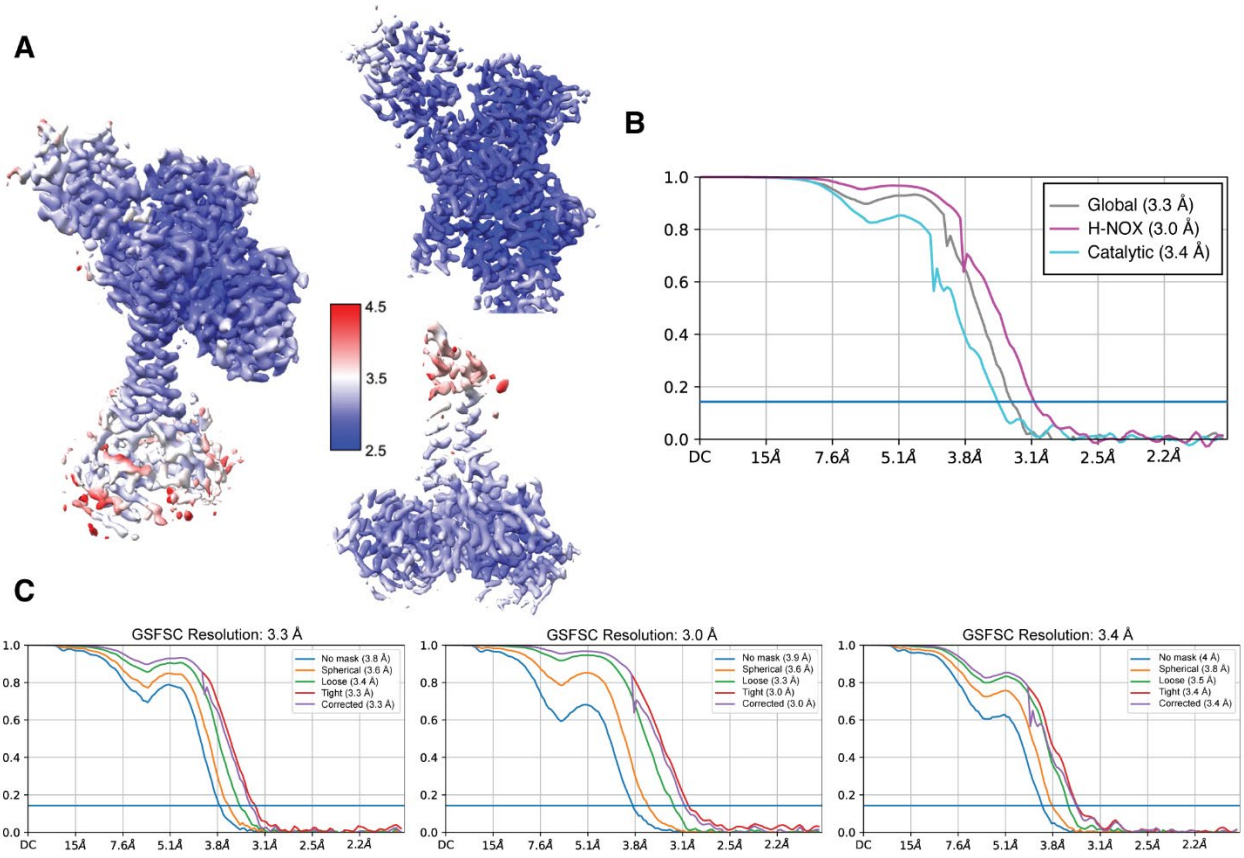

Figure B.2. Resolution cut-offs for ligand-free βC122S *Ms* sGC. (A) Local resolution distribution maps of consensus global refinement (left), local refinement of H-NOX domain (top-right), and local refinement of catalytic domain (bottom-right). (B) Gold-standard Fourier Shell Correlation (FSC) after correction for masking effects. (C) FSC Curves for all maps with and without masking with (left) consensus global, (middle) H-NOX domain, and (right) catalytic domain.

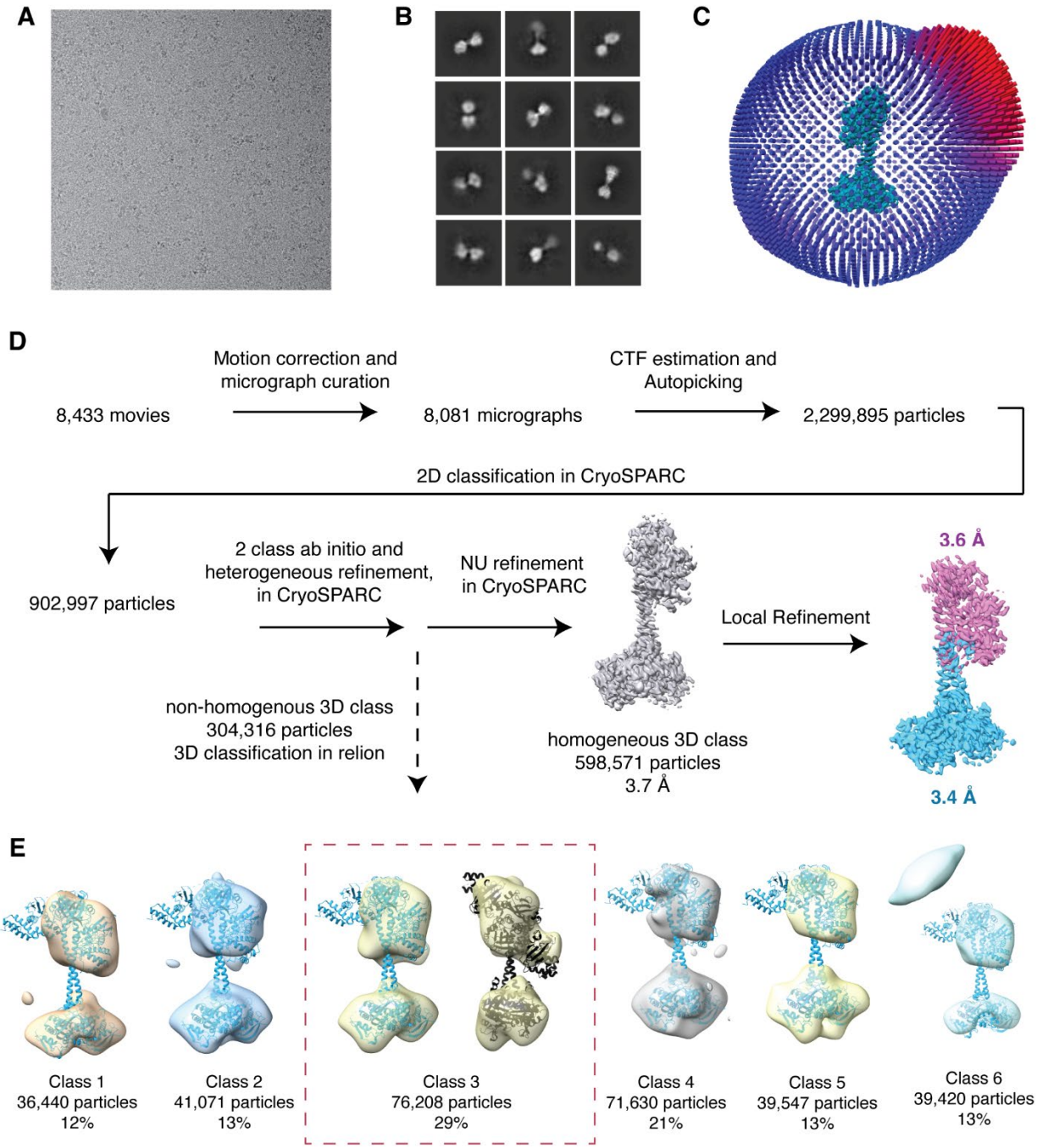

Figure B.3. Cryo-EM processing of CYR715-bound βC122S *Ms* sGC. (A) A representative raw micrograph of the CYR715-bound sGC dataset. (B) Representative 2D classes showing sGC dimers. (C) Projection orientation map showing angular distribution for the consensus refinement map of CYR715-bound sGC. (D) The cryo-EM data processing workflow for CYR715-bound sGC. This process led to a consensus 3.7 Å map and local refinement maps at 3.6 Å and 3.4 Å for the H-NOX and catalytic domains respectively. (E) 3D classification of sGC dimer 2D classes. Class 3 was found to more closely resemble contracted sGC. Shown in black is contracted ligand-free human sGC (PDB: 8HBE[1]) and in blue is extended xsNO-bound human sGC (PDB: 8HBH[1]).

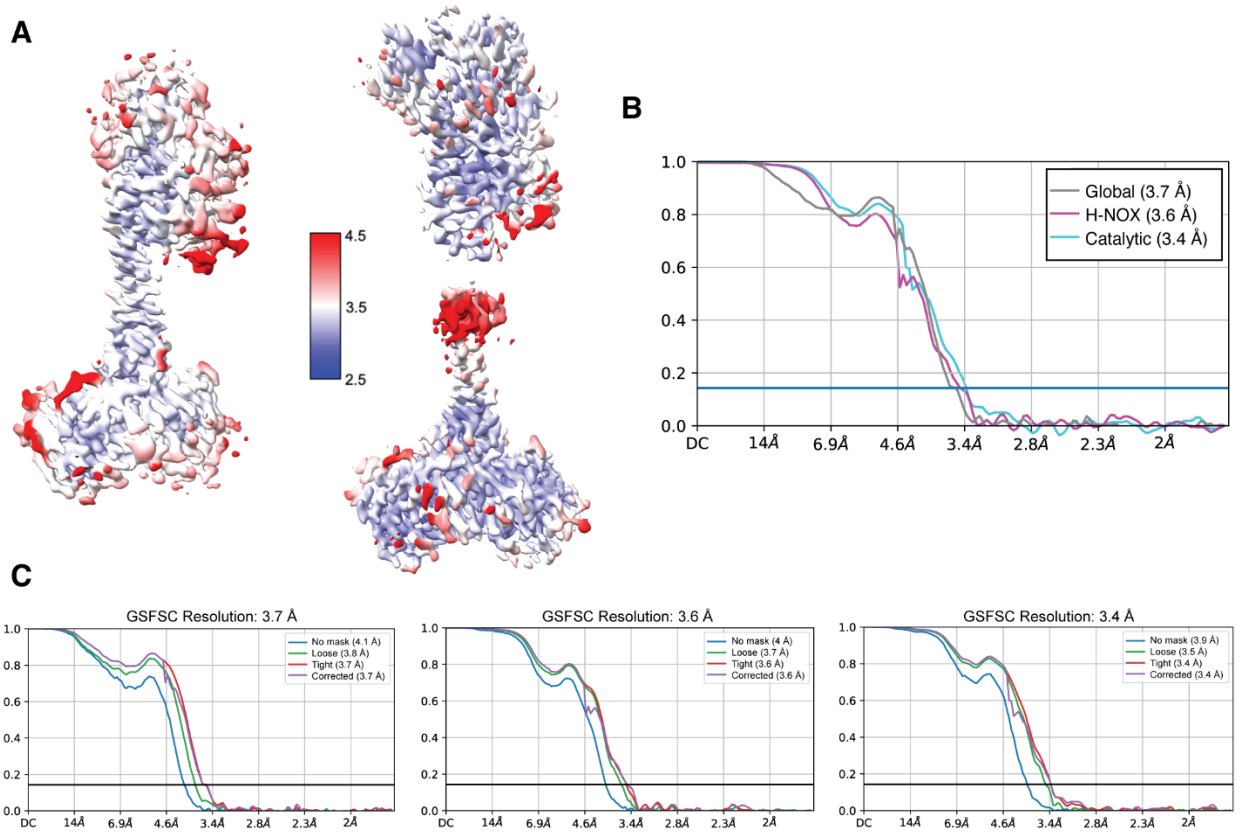

Figure B.4. Resolution cut-offs for CYR715 βC122S *Ms* sGC. (A) Local resolution distribution maps of consensus global refinement (left), local refinement of H-NOX domain (top-right), and local refinement of catalytic domain (bottom-right). (B) Gold-standard Fourier Shell Correlation (FSC) after correction for masking effects. (C) FSC Curves for all maps with and without masking, with (left) consensus global, (middle) H-NOX domain, and (right) catalytic domain.

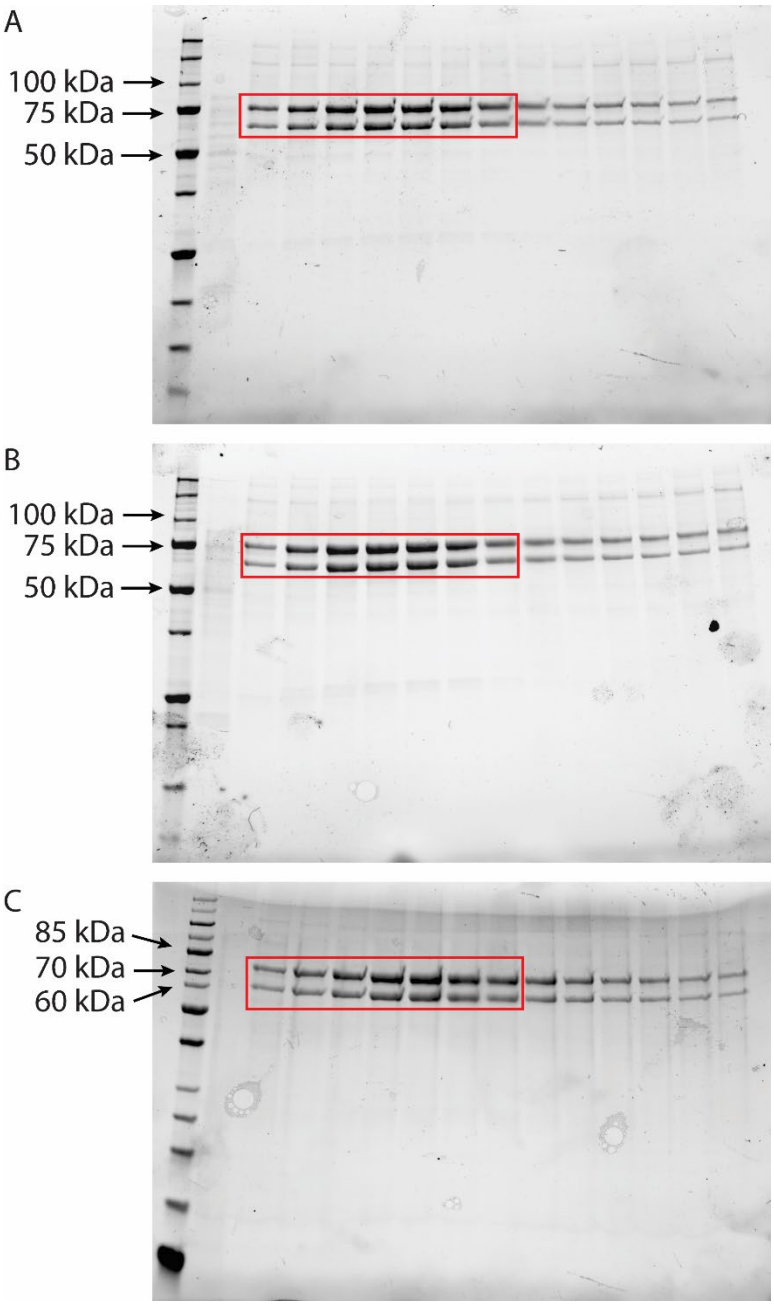

Figure B.5. Representative SDS-PAGE gels. Gels following anion exchange (POROS HQ2) chromatography for (A) *Ms* sGC WT, (B) *Ms* sGC βC122A, and (C) *Ms* sGC βC122S. The first lane next to the molecular weight marker in each gel is the flowthrough from the anion exchange column. Red boxes indicate fractions that were pooled.

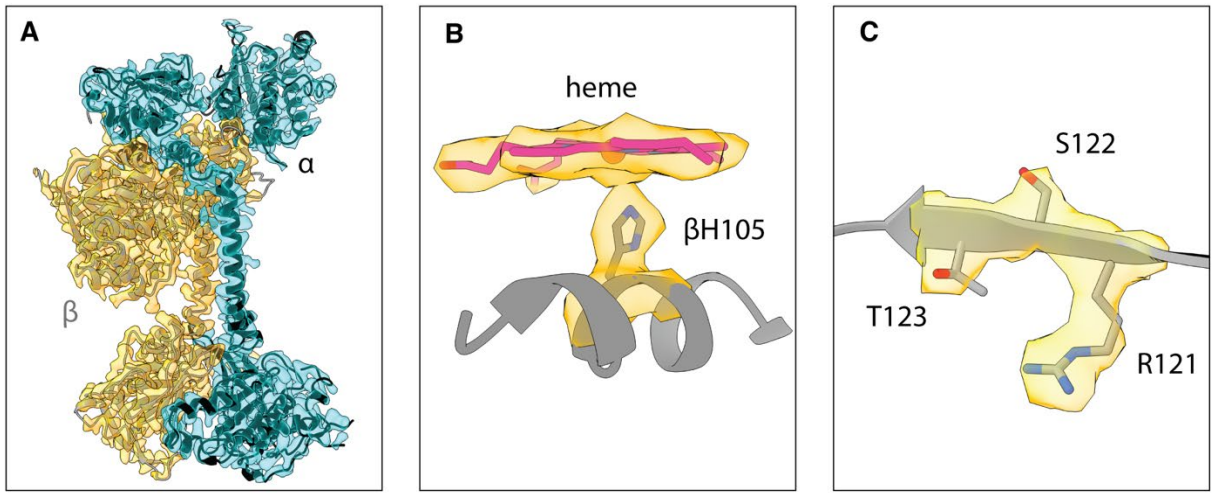

Figure B.6. EM structure of ligand-free βC122S *Ms* sGC. (A) A model of ligand-free sGC fit into the cryo-EM density, with the α subunit in black and cyan and the β subunit in grey and orange. (B) The electron density of the heme site is contiguous with βH105. (C) Map and model of mutant βS122. No major differences in conformation are observed at this residue between this and βC122 (WT) *Hs* structures. All density is shown at threshold 0.783.

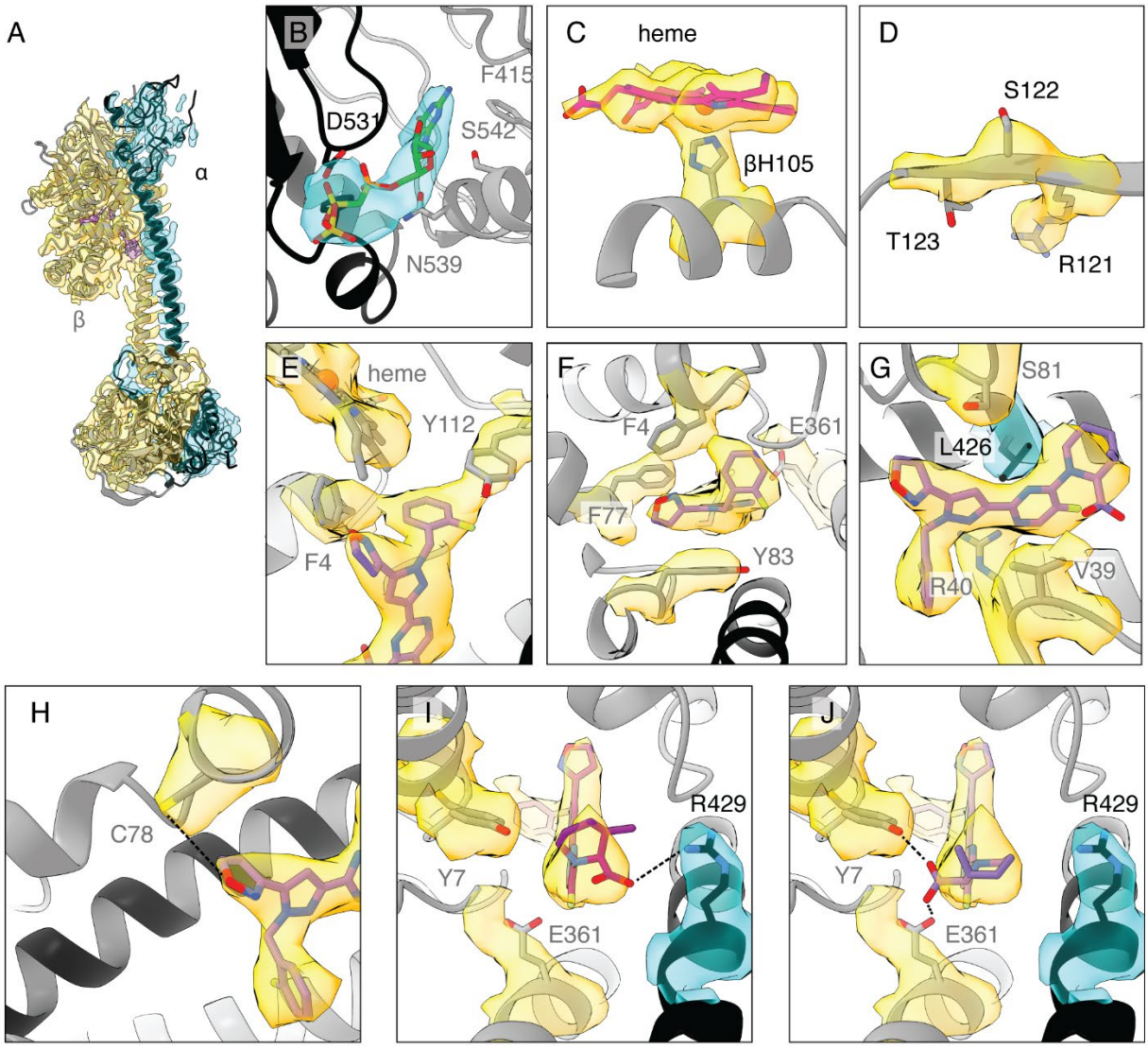

Figure B.7. EM structure of CYR715-bound βC122S *Ms* sGC. (A) A model of CYR715-bound sGC fit into the cryo-EM density, with the α subunit in black and cyan and the β subunit in grey and orange. (B) GTP analog (GpCpp) bound at the enzyme active site is shown in green, with map density in cyan at threshold 0.669. (C) The density of the heme is contiguous with βH105. Density is shown at threshold 0.695. (D) Map and model of variant βS122. Density is shown at threshold 0.785. (E-H) Various views of CYR715 showing different binding interactions. EM density is shown in cyan and orange for α and β, respectively, at threshold 0.906. (I-J) Two alternative conformations of the piperidine chair interact alternatively with αR429 or βY7 and E361. The conformation shown in (I) is used throughout this work.

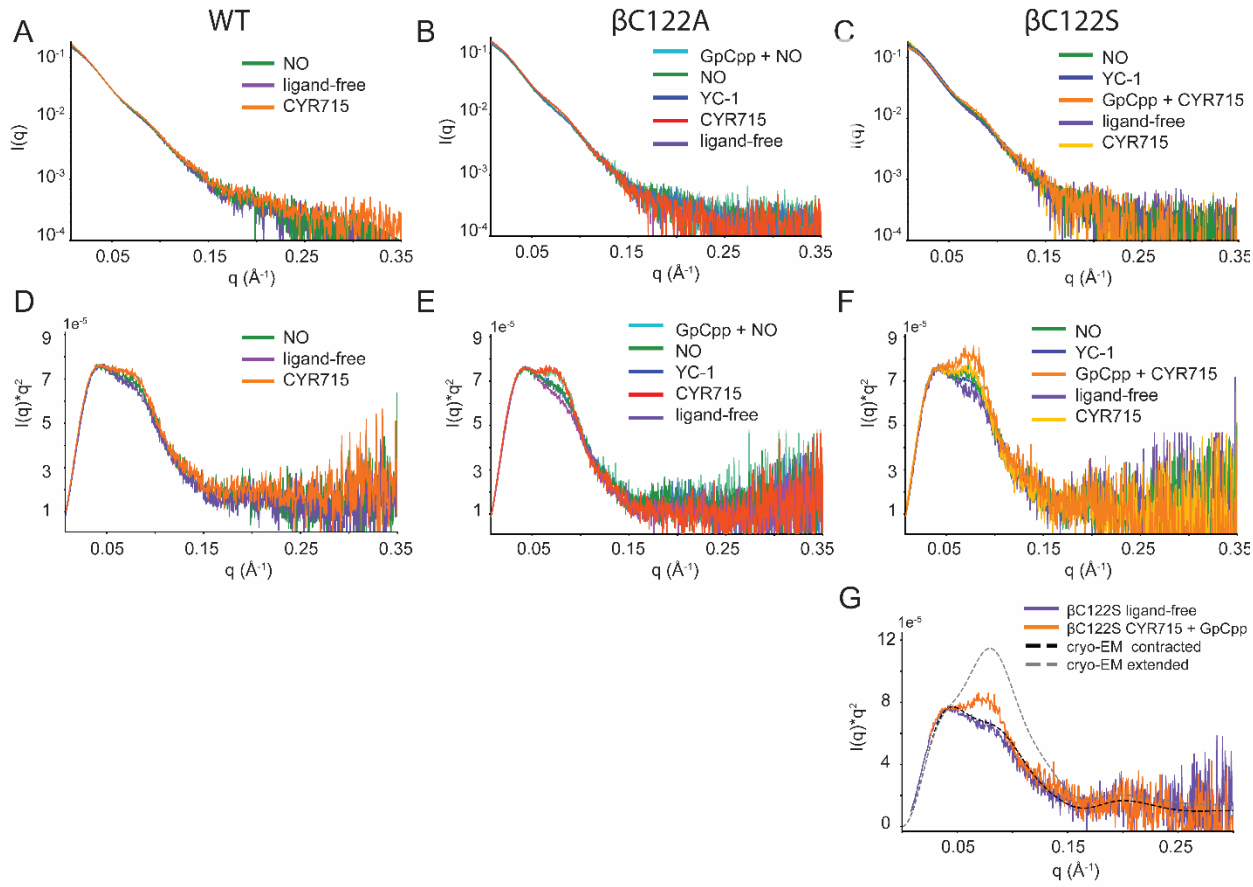

Figure B.8. Normalized SAXS scattering of *Ms* sGC. (A-C) Semilog plots of (A) WT, (B) βC122A, and (C) βC122S *Ms* sGC under different ligand conditions. (D-F) Kratky plots of the same datasets, (D) WT, (E) βC122A, and (F) βC122S *Ms* sGC. Conformational extension is visible with addition of ligand at q = 0.078. (G) Calculated scattering fits based on the contracted, unliganded cryo-EM structure (9OXN, black dotted line) and the extended CYR715-bound (9P2R, grey dotted line) are compared to unliganded βC122S *Ms* sGC (purple) and βC122S *Ms* sGC with CYR715 and GpCpp (orange). These samples represent the least and most extended states observed by SAXS, respectively.

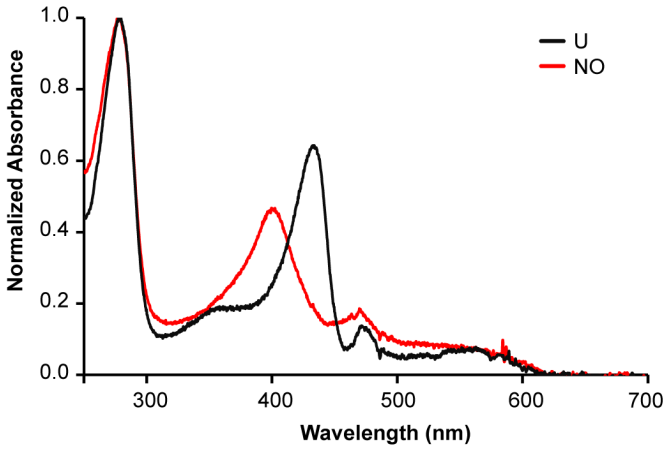

Figure B.9. In-line UV-vis absorption spectra for *Ms* sGC. Spectra show NO bound to heme under xsNO conditions (red) for βC122S in anaerobic SAXS experiments. UV-vis measurements were taken using a UV-vis cell placed in-line after the X-ray flow cell.

Table B.3. SAXS analysis statistics

		Pair Distance Distribution				Guinier				
Variant	Sample	Radius of gyration (Å)	Rg Error	I0	Dmax (Å)	Radius of gyration (Å)	Rg Error	I0	Fit to contracted EM structure χ^2	Fit to extended EM structure χ^2
WT	Ligand-free	46.7	0.3	0.14	135	49.9	0.3	0.15	2.917	15.54
	NO	47.9	0.3	0.14	135	51.2	0.5	0.15	4.247	13.83
	CYR715	48.7	0.3	0.15	135	54.3	0.4	0.16	5.616	14.4
C122S	Ligand-free	47.2	0.5	0.14	135	48.1	0.4	0.15	2.169	5.831
	YC1	49.4	0.2	0.16	135	53.5	0.2	0.17	12.04	25.84
	NO	49.2	0.4	0.16	135	53.7	0.4	0.17	5.099	9.482
	CYR715	50.1	0.4	0.16	135	53.9	0.6	0.18	5.076	7.105
	CYR715+ GpCPP	48.8	0.5	0.15	135	49.8	0.4	0.15	4.117	4.149
C122A	Ligand-free	46.5	0.27	0.14	135	48.6	0.2	0.14	3.7	19.9
	YC1	47.2	0.3	0.14	135	48.9	0.3	0.15	4.484	15.54
	NO	47.9	0.3	0.14	135	50.8	0.2	0.15	5.675	17.06
	CYR715	48.5	0.3	0.15	135	49.6	0.3	0.15	8.536	12.66
	NO + GpCPP	48.8	0.5	0.15	135	50.7	0.3	0.15	6.448	11.32
Contracted EM calculated scattering (9OXN)		42.3	0.05		135	41.9	0.002			
Extended EM calculated scattering (9P2R)		45.6	0.06			44.75	0.002			

References

(1) Jumper, J.; Evans, R.; Pritzel, A.; Green, T.; Figurnov, M.; Ronneberger, O.; Tunyasuvunakool, K.; Bates, R.; Žídek, A.; Potapenko, A.; Bridgland, A.; Meyer, C.; Kohl, S. A. A.; Ballard, A. J.; Cowie, A.; Romera-Paredes, B.; Nikolov, S.; Jain, R.; Adler, J.; Back, T.; Petersen, S.; Reiman, D.; Clancy, E.; Zielinski, M.; Steinegger, M.; Pacholska, M.; Berghammer, T.; Bodenstein, S.; Silver, D.; Vinyals, O.; Senior, A. W.; Kavukcuoglu, K.; Kohli, P.; Hassabis, D. Highly Accurate Protein Structure Prediction with AlphaFold. *Nature* **2021**, *596* (7873), 583–589. https://doi.org/10.1038/s41586-021-03819-2.

(2) Mirdita, M.; Schütze, K.; Moriwaki, Y.; Heo, L.; Ovchinnikov, S.; Steinegger, M. ColabFold: Making Protein Folding Accessible to All. *Nat. Methods* **2022**, *19* (6), 679–682. https://doi.org/10.1038/s41592-022-01488-1.
(3) Liu, R.; Kang, Y.; Chen, L. NO Binds to the Distal Site of Haem in the Fully Activated Soluble Guanylate Cyclase. *Nitric Oxide* **2023**, *134–135*, 17–22. https://doi.org/10.1016/j.niox.2023.03.002.